9TH MIDDLE EASTERN SIMULATION MULTICONFERENCE

MESM'2008

EDITED BY

Professor
Marwan Al-Akaidi

AUGUST 26-28, 2008

Amman, Jordan

A Publication of

EUROSIS-ETI

Printed in Ghent, Belgium

9TH MIDDLE EASTERN SIMULATION MULTICONFERENCE

AUGUST 26-28, 2008

Organised by

ETI

Sponsored by

EUROSIS

De Montfort University

IEEE UKRI - SPC

Ghent University

Hosted by

Philadelphia University

Amman, Jordan

EXECUTIVE EDITOR

PHILIPPE GERIL
(BELGIUM)

EDITORS

General Conference and Programme Chair

Professor Dr M. Al-Akaidi
De Montfort University,
Leicester, United Kingdom

Local Chair

Prof. Mahmoud Kishta, Dean, Academic Research & Graduate Studies, Philadelphia University, Jordan

Local Co-Chair

Dr. Kasim M. Al-Aubidy, Dean, Faculty of Engineering, Philadelphia University, Jordan.

Local Committee

Dr. Riyad Jabri, Dean, Faculty of Science, Philadelphia University, Jordan
Dr. Mohammed Mohafza, Dean, Information Technology Faculty, Philadelphia University, Jordan
Dr. Munzer Kreshan, Dean, Ma'an Technical College, Al'Balqaa University, Jordan
Dr. Mikhled Alfaouri, Philadelphia University, Jordan
Dr. Malik Tayseer, Philadelphia University, Jordan
Dr. Hazim Al-Otum, JUST, Jordan
Dr. Omar Badran, Al'Balqaa University, Jordan

INTERNATIONAL PROGRAMME COMMITTEE

Modelling Methodology and Modelling Tools
Jose Antonio Barata Oliveira, Universidade Nova de Lisboa, Caparica, Portugal
Fabrice Bernardi, Universite de Corse, Corte, France
Ana M. Camacho, UNED, Madrid, Spain
Frantisek Capkovic, Slovak Academy of Sciences, Bratislava , Slovak Republic
John Dalseng, Finnmark College, Alta, Norway
Juan de Lara, Universidad Autonama de Madrid, Madrid, Spain
Jesus Felez, Universidad Politecnica de Madrid, Madrid, Spain
Frederic Grimaud. Ecole Nat Superieure de Mines de St.Etienne, France
Helge Hagenauer, Universitaet Salzburg, Salzburg, Austria
Brian Hollocks, Bournemouth University, Bournemouth, United Kingdom
Bjoern Johansson, Chalmers University of Technology, Goeteborg, Sweden
Panajotis T. Katsaros, Aristotle University Thessaloniki, Thessaloniki, Greece
Yan Luo, NIST, Gaithersburg, USA
Thomas O Mathuna, Cork Institute of Technology, Cork, Ireland
Michel Minoux, Universite P. et M. Curie-CNRS, Paris cedex 05, France
Tudor Niculiu, University Politecnica Bucharest, Bucharest, Romania
Marc Parenthoen, CERV, Plouzane, France
Zdravko Terze, University of Zagreb, Zagreb, Croatia
Dmitry Zaitsev, Odessa National Telecommunications Academy, Odessa, Ukraine

Analysis Methodology
Abdel Aitouche, Hautes Etudes Industrielles, Lille Cedex, France
Bruno Ciciani, Universita di Roma "La Sapienza", Rome, Italy
John Dalton, University of Newcastle, Newcastle-upon-Tyne, United Kingdom
Julie Dugdale, Universite Paul Sabatier, Narbonne, France
Mauro Iacono, SUN - II Universita di Napoli, Aversa (CE) Italy
Jens Kohlmeyer, Universitaet Ulm, Ulm, Germany
Francesco Moscato, Seconda Universita di Napoli, Aversa, Italy
Jairo R. Montoya-Torres, Ecole Nationale Superieure des Mines de Saint-Etienne, Gardanne, France

Simulation of Networks and Communication
Salvatore D'Antonio, Consorzio Interuniversitario Nazionale per l'Informatica, Naples, Italy
Dirk Brade, FOI, Stockholm, Sweden
Eugen Dedu, LIFC, Montbelliard, France
Carlos Palau, UPV, Valencia, Spain
Rob Pooley, University of Edinburgh, Edinburgh, United Kingdom

INTERNATIONAL PROGRAMME COMMITTEE

Djamel Sadok, The Federal University of Pernambuco - Brazil
Ahmad A. Sharieh, University of Jordan, Amman, Jordan
Veronique Veque, Universite de Paris Sud LRI, Orsay, France

Complex Systems Simulation
Zdzislaw Bubnicki, Wroclaw University of Technology, Wroclaw, Poland
Marta Pla Castells, Universidad de Valencia, Valencia, Spain
Michele Colajanni, Unviersita di Modena, Modena, Italy
Krzysztof Fujarewicz, Silesian University of Technology, Gliwice, Poland
Tom Dhaene, University of Antwerp, Antwerp, Belgium
Alessandro Genco, University of Palermo, ICAR / CNR, Palermo, Italy
Jean-Christophe Guyot, EADS SPACE Transportation, Les Mureaux Cedex, France
Daniel Huber, Heinz Nixdorf Institute, University of Paderborn, Paderborn, Germany
Abder Koukam, Universite de Technologie de Belfort-Montbeliard, France
Jan Lemeire, VUB, Brussels, Belgium
Brian Mayoh, Aarhus University, Aarhus N, Denmark
Jorge M. Perez, ITP, S.Fernando de Hernares, Spain
Panos Periorellis, University of Newcastle Upon Tyne, Newcastle, United Kingdom
Fatima Rateb, University College London, London, United Kingdom
Marco Remondino, University of Turin, Turin, Italy
Marc Rouff, University of Caen Basse-Normandie, Caen, France
Jan Studzinski, Systems Research Institute of Polish Academy of Science

Simulation of Signal and Image Processing
Bruno Ciciani, Universita di Roma "La Sapienza", Rome, Italy
Tania Jimenez, Universidad de Los Andes, Merida, Venezuela
Viorel Nicolau, "Dunarea de Jos" University of Galati, Romania
Bogdan Raducanu, UAB, Cerdanyola, Spain
Renate Sitte, Griffith University, Gold Coast Mail Centre, Australia
Joao Manuel R. S. Tavares, University of Porto, Porto, Portugal
Hanene Trichili, University of Sfax, Sfax, Tunisia
Ahmed M. Zeki, International Islamic University Malaysia (IIUM), Kuala Lumpur, Malaysia

Energy Systems Simulation
Paulo Maciel, UFPE, Recife, Brazil
Janos Sebestyen Janosy, KFKI, Budapest, Hungary
Carlos Ramos, Polytechnic of Porto (ISEP/IPP), Porto, Portugal
Tzanko Tzanov, Technical University of Sofia, Sofia, Bulgaria
Patrick Waeger, EMPA, St. Gallen, Switzerland

Simulation in the Chemical and Petrochemical Industry
Ammar Al Khani, Espoo, Finland
Diganta Bhusan Das, University of Oxford, Oxford, United Kingdom
Eugenio Ferreira, Universidade do Minho, Braga Portugal
Vahid Nassehi, Loughborough University, Loughborough, United Kingdom
Cornel Resteanu, Research Institute of Informatics, Bucharest, Romania

Multimedia and Virtual Reality Systems
Ahmed Bin Subaih, University of Sheffield, Sheffield, United Kingdom
Christos Bouras, University of Patras, Rion, Patras, Greece
Eckhard C. Bollow, Software Technology and IT-Project Management, Lueneburg, Germany
Richard Chbeir, Universite de Bourgogne, Dijon Cedex, France
Paule Ruiz del Puerto, University of Oviedo, Oviedo, Spain
Zhisheng Huang, Vrije University Amsterdam, The Netherlands
Christoph Laroque, University of Paderborn, Paderborn, Germany
Ahmed Mostefaoui , Laboratoire d'Informatique de Franche-Comte Montbeliard Cedex, France
Dorin-Mircea Popovici, Centre Europeen de Realite Virtuelle, Plouzane, France
Christian Reimann, C-LAB, Paderborn, Germany
Marco Roccetti, University of Bologna, Bologna, Italy
Zasriati Azla Sabot, University Tun Abdul Razak (UNITAR) Selanngor, Malaysia
Mike Sips, University of Konstanz, Konstanz, Germany
Charles van der Mast, Delft University of Technology, Delft, The Netherlands

Decision Processing in Management
Hadhoum Boukachour, Le Havre University, Le Havre, France
Naoufel Cheikhrouhou, Ecole Polytechnique Federale de Lausanne, Lausanne, Switzerland
Joel Colloc, Le Havre University, Le Havre, France
Jeanne Schreurs, Universiteit Hasselt, Diepenbeek, Belgium
Christine Sybord, Lyon 2 Lumiere University, Lyon, France

Modelling and Simulation for Industrial Applications
Track Chair: Prof. David Stockton, de Montfort University, Leicester, United Kingdom
Luis Felipe Acebes Arconada, Universidad de Valladolid, Valladolid, Spain
Leopoldo Arnesto, UPV, Valencia, Spain
Andre Astolfi, Naval Academy Research Institute, Brest Naval, France
Michel Benne, Sucreries de Bois Rouge, Saint-Andre, France
Pascal Berruet, Universite Bretagne Sud, Lorient cedex, France
Christelle Bloch, Universite de Technologie de Belfort-Montbeliard, Belfort Cedex, France

INTERNATIONAL PROGRAMME COMMITTEE

PJ Byrne, Enterprise Research Centre, University of Limerick, Ireland
A. Chatzinikolaou, Bosch Rexroth SA, Athens, Greece
Olaf Diegel, Massey University, Albany Campus, North Shore Mail Centre, Auckland, New Zealand
S Collart Dutilleul, LAGIS-EC-LILLE, Villenneuve d'Ascq, France
Christoph Hartmann, The German University in Cairo, New Cairo City, Egypt
Sergej Kalaschnikow, VA TECH ELIN EBG Elektronik GmbH & Co, Vienna, Austria
Markus Koch, C-LAB, Paderborn, Germany
Habtom Mebrahtu, Anglia Polytechnica University, Chelmsford, United Kingdom
Pascal Meyer, Forschungszentrum Karlsruhe, Karlsruhe, Germany
Carlos E. Pereira, Universidad Federal do Rio Grande Do Sul, Porto Alegre, Brazil
Caterina Rizzi, Universita degli Studi di Bergama, Dalmine, Italy
Hans Veeke, TU Delft, Delft, The Netherlands
Ramiro Velazquez, Universite Paris 6 - CNRS, Fontenay aux Roses, France
Val Vitanov, Cranfield University, Cranfield, United Kingdom
Ursula Wellen, Deutsche Post AG, Bonn, Germany
Joao de Silva Wellington, UFPE, Recife, Brazil

Simulation in Logistics, Traffic, Transport and Harbour Simulation
Paul Davidsson, Blekinge Institute of Technology, Ronneby, Sweden
Isabel Garcia Gutierrez, Universidad Carlos III de Madrid, Leganes, Madrid, Spain
Thomas Hanne, Fraunhofer-Institut ITWM, Kaiserslautern, Germany
Daniel Krajzewicz, GermanAerospace Centre, Berlin, Germany
Herve Manier, Universite de Technologie de Belfort-Montbeliard (UTBM), Belfort Cedex, France
Vittorio Maniezzo, Universita di Bologna, Bologna, Italy
Rafael J. Martinez, Universitat de Valencia, Valencia, Spain
Philippe Mussi, INRIA Sophia Antipolis, France Frederic Serin, IUT du Havre, Le Havre, France

Web based Simulation
Victor Bassilious, University of Abertay Dundee, United Kingdom
Jorge Marx Gomez, Otto-von-Guericke-Universitaet Magdeburg, Magdeburg, Germany
Wolfgang Kuehn, University of Wuppertal Wuppertal, Germany
Jose Machado, Unviersidade do Minho, Braga Codex, Portugal
Mara Nikolaidou, University of Athens, Ilissia, Athens, Greece
Francesco Quaglia, Universita' di Roma "La Sapienza", Roma, Italy
Stefan Sarstedt, University of Ulm, Ulm, Germany
Jaroslav Sklenar, University of Malta, Msida, Malta
Alfonso Urquia, UNED, Madrid, Spain

Simulation in Information Processing
Julien Bourgeois, LIFC, Montbelliard, France
Christophe Claramunt, Naval Academy Research Institute, Brest Naval, France
Patrick De Causmaecker, University of Nottingham, Nottingham, United Kingdom
Khalil Drira, LAAS-CNRS, Toulouse Cedex 04, France
Laurent Guillon, Naval Academy Research Institute, Brest Naval, France
Jean-Claude Hochon, GFI Consulting, Toulouse, France
Peter Lawrence, Monash University, Clayton, Australia
Christophe Roche, Universite de Savoie, Le Bourget du Lac cedex, France
Christian Siemers, TU Clausthal, Clausthal-Zellerfeld, Germany
Jim Torresen, University of Oslo, Oslo, Norway

Simulation in Fuzzy Systems, Neural Networks and Genetic Algorithms
Chrissanthi Angeli, Technological Education Institute of Piraeus, Athens, Greece
Mokhtar Beldjehem, École Polytechnique de Montréal, Montréal, Canada
Ulrich Bodenhofer, Software Competence Center Hagenberg GmbH, Hagenberg, Austria
Sabine Bostelmann, TU Clausthal, Clausthal, Germany
Luc Boullart, Ghent University, Ghent, Belgium
Maroua Bouzid, University of Caen, Caen, France
Paulo Alexandre Ribeiro Cortez, University of Minho, Guimaraes, Portugal
Analicia Schiaffino Morales De Franceschi, ULBRA, Canoas - RS, Brazil
Seung Man Lee, NASA Ames Research Center, Moffett Field, USA
Antoni Ligeza, AGH - University of Science and Technology, Krakow, Poland
Marie-Ange Manier, Universite de Technologie de Belfort-Montbeliard (UTBM), Belfort Cedex, France
Paulo Moura Oliveira, UTAD-Universidade de Tres-os-Montes e Alto Douro, Vila Real, Portugal
Angus Wu, City University of Hong Kong, Hong Kong

Simulation in the Built Environment
Bernadette O'Regan, University of Limerick, Limerick, Ireland
Agustin Yague, Universidad Politicnica de Madrid, Madrid, Spain

Simulation in Archaeology
Jean Yves Blaise, UMR CNRS/MCC 694 MAP, Marseille, France
Anders Hast, University of Gavle, Gavle, Sweden
Wolfgang Kreutzer, University of Canterbury, Christchurch, New Zealand
Marcos A Rodrigues, Sheffield Hallam University, Sheffield ,United Kingdom

MESM’2008

EUROSIS is a Division of ETI Bvba, The European Technology Institute, Torhoutsesteenweg 162, Box 4, B-8400 Ostend, Belgium

Printed in Belgium by Reproduct NV, Ghent, Belgium
Cover Design by Grafisch Bedrijf Lammaing, Ostend, Belgium

EUROSIS-ETI Publication
ISBN: 978-90-77381-43-4
ISN: 978-90-77381-43-4

PREFACE

Dear conference delegate,

I have the pleasure to welcome you all to the 9th Middle East Modeling & Simulation Multiconference (MESM2006) Organized by the EUROSIS and hosted by Philadelphia University in Amman, Jordan. The MESM2008 is sponsored by the IEEE – UKRI SPC & De Montfort University (UK).

This year's event marks our return to Jordan with the MESM'2008 and we are doubly grateful for the fact that this year's event will again be opened by H.R.H. Crown Prince Al-Hassan Ben Talal of Jordan.

The MESM'2008 Conference highlights recent and significant advances in many research areas of modeling and simulation related to Methodology, Simulation Programming and Tools, Simulation and AI, Decision Making, Simulation in Electronics and Virtual Environments.

Your presence at this conference emphasizes an important fact: the challenge and opportunities that surrounding the Modeling and Simulation practice anywhere in the world. We in EUROSIS believe strongly that Modeling & Simulation make a powerful combination to improve the systems and organisation of the 21st century. It will continue to contribute to increase public awareness of the quality of life, and the growing need to improve this through better organizations and systems.

As a General Conference & Programme Chair, I would like to express my thanks to
De Montfort University (UK) for giving me the time to chair this conference and thanks also to the committee members for reviewing the papers and to our local chair Dr. Kasim Al-Aubidy The Dean, Faculty of Engineering, Philadelphia University, Jordan in organizing this event.

Special thanks to Cyrille Bertelle of the Université du Havre, Le Havre, France for giving the keynote speech and to Prof. Zamri Bin Yousif, Universiti Tenaga Nasional (UNITEN), Selangor, Malaysia for giving the invited speech. Furthermore, this year's event also features a tutorial by Gérard H.E. Duchamp, LIPN, Paris 13 University, France, whom we thank.

Thanks to my colleague Philippe Geril, executive director of EUROSIS office for supporting the event and for his time. Last but not least thanks to all authors without whom the conference would not be a successful conference.

Professor Dr Marwan Al-Akaidi
General Conference and Programme Chair
EUROSIS – M. East Chair
School of Engineering & Technology,
De Montfort University,
Leicester, LE 1 9BH, UK.
Email: mma@dmu.ac.uk

CONTENTS

CONTENTS

CONTENTS

SCIENTIFIC PROGRAMME

INVITED SPEAKER

NUMERICAL SIMULATIONS OF TRANSIENT FLOWS IN SHOCK TUBE AND VALIDATIONS WITH EXPERIMENTAL MEASUREMENTS

M. Z. Yusoff, A. Al-Falahi, N. H. Shuaib and T. Yusaf
Centre for Advance Computational Engineering,
Department of Mechanical Engineering, College of Engineering,
Universiti Tenaga Nasional (UNITEN),
Putrajaya Campus, 43009, Selangor, Malaysia
E-mail: zamri@uniten.edu.my

KEYWORDS
Shockwave, Shocktube, Transient high speed flows.

ABSTRACT

This paper describes the numerical simulations of transient flows in shock tube which involves multiple reflections of shockwaves, contact surface and expansion waves and their interactions. The numerical formulations solve the fully compressible Reynolds Averaged Navier Stokes (RANS) equations set using finite volume method. The numerical results are validated against analytical solutions and experimental measurements in the high speed flow test facility available at the Universiti Tenaga Nasional (UNITEN), Malaysia. Experimental tests for different operating conditions have been performed. High precision pressure transducers were used to measure the pressure history at two different locations within the shock tube. Experimental results were compared with the numerical results and good agreements were obtained. The numerical simulations also revealed that the flow tend to be very unstable in the region close to the diaphragm after the reflected shock wave interacts with the contact surface.

INTRODUCTION

There are many different ways to generate a source of air at a sufficiently high temperature and pressure to act as the working fluid of a hypersonic wind tunnel. This includes hotshot tunnels, plasma jets, shock tubes, shock tunnels, free-piston tunnels and light gas guns (Pope and Goin, 1965). Various hypersonic wind tunnels have been constructed at different universities and research centers all over the world such as at University of Oxford (Buttsworth et al., 2002), University of Southampton in the United Kingdom (East, 1960), University of Queensland (Jacobs, 1994) and University of Southern Queensland in Australia (Buttsworth, 2002). However, these facilities are very costly and very expensive to run and maintain. A low cost facility, which could show the various effects of hypersonic ionization and dissociation, along with experimental testing of hypersonic heat transfer effects has been developed in Universiti Tenaga Nasional (UNITEN). The hypersonic test facility has been designed so that it can be easily used as a shock-tube, shock tunnel and free piston tunnel interchangeably (Yusaf et al., 2008). The objective of building such facility is to generate gas flows or gas conditions of sufficiently high temperature and pressure that are difficult to achieve in other test devices. The facility is to be used to test a new fiber-optic pressure sensor for high speed flows in gas and steam turbines, which is being developed and to study the heat transfer phenomena associated with high speed flows.

In order to compliment the experimental work, a specialized CFD solver has been developed for simulations of transient flows in the facility. The CFD solver solves the time accurate Reynolds Averaged Navier Stokes (RANS) equations set using second order accurate cell-vertex finite volume spatial discretization and fourth order accurate Runge-Kutta temporal integration and it is designed to simulate the flow process for similar driver/driven gases (e.g. Air-Air as working fluids). The solver is applied to inviscid standard Sod problem, inviscid flows in real shock tube and viscous flows in real shock tube. In the real shock tube, a bush is placed in the diaphragm section in order to facilitate the rupture process. Therefore, the effective area of the diaphragm (throat) opening at rupture will be some what smaller than the bush opening area. There will be also a dead flow region behind the bush. The exact location of the reattachment point will be highly dependent on the flow speed. In the present work, since the two parameters are not known, the effective throat area and the wedge angle were calibrated and the values which give the closest agreement between experimental data and simulation results will be used.

Experimental tests for different operating conditions have been performed. High precision pressure transducers were used to measure the pressure history at two different locations within the shock tube. The analytical and experimental results were compared with the numerical results and good agreements were obtained.

NUMERICAL FORMULATION OF THE SOLVER

The two-dimensional continuity, x- and y-momentum and energy equations describing the turbulent flow of a compressible fluid expressed in strong conservation form in the x-, y-cartesian co-ordinate system may be written as

$$\frac{\partial \underline{w}}{\partial t} + \frac{\partial \underline{F}}{\partial x} + \frac{\partial \underline{G}}{\partial y} = \underline{J} \qquad (1)$$

where w represents the conserved variables. F and G are the
overall fluxes in x-, y-directions respectively:

$$\underline{F} = \underline{F_C} - \underline{F_V} - \underline{F_T}, \quad (2)$$

$$\underline{G} = \underline{G_C} - \underline{G_V} - \underline{G_T}, \quad (3)$$

and

$$\underline{w} = \begin{pmatrix} \rho \\ \rho u \\ \rho v \\ \rho e_0 \end{pmatrix}, \quad \underline{F_C} = \begin{pmatrix} \rho u \\ \rho u^2 + P \\ \rho uv \\ \rho u h_0 \end{pmatrix}, \quad \underline{G_C} = \begin{pmatrix} \rho v \\ \rho uv \\ \rho v^2 + P \\ \rho v h_0 \end{pmatrix},$$

$$\underline{F_V} = \begin{pmatrix} 0 \\ \frac{4}{3}\mu\frac{\partial u}{\partial x} - \frac{2}{3}\mu\frac{\partial v}{\partial y} \\ \mu\frac{\partial u}{\partial y} + \mu\frac{\partial v}{\partial x} \\ k\frac{\partial T}{\partial x} + \frac{4}{3}\mu u\frac{\partial u}{\partial x} - \frac{2}{3}\mu u\frac{\partial v}{\partial y} + \mu v\frac{\partial u}{\partial y} + \mu v\frac{\partial v}{\partial x} \end{pmatrix},$$

$$\underline{F_T} = \begin{pmatrix} 0 \\ -\rho\overline{u'^2} \\ -\rho\overline{u'v'} \\ -\rho C_v\overline{u'T'} - \frac{3}{2}\rho u\overline{u'^2} - \frac{\rho}{2}u\overline{v'^2} - \rho v\overline{u'v'} \end{pmatrix},$$

$$\underline{G_V} = \begin{pmatrix} 0 \\ \mu\frac{\partial u}{\partial y} + \mu\frac{\partial v}{\partial x} \\ \frac{4}{3}\mu\frac{\partial v}{\partial y} - \frac{2}{3}\mu\frac{\partial u}{\partial x} \\ k\frac{\partial T}{\partial y} + \frac{4}{3}\mu v\frac{\partial v}{\partial y} - \frac{2}{3}\mu v\frac{\partial u}{\partial x} + \mu u\frac{\partial u}{\partial y} + \mu u\frac{\partial v}{\partial x} \end{pmatrix},$$

$$\underline{G_T} = \begin{pmatrix} 0 \\ -\rho\overline{u'v'} \\ -\rho\overline{v'^2} \\ -\rho C_v\overline{v'T'} - \frac{3}{2}\rho v\overline{v'^2} - \frac{\rho}{2}v\overline{u'^2} - \rho u\overline{u'v'} \end{pmatrix}$$

The turbulence terms are calculated by using mixing length turbulence model. The numerical scheme was based on an earlier work by the author as described in Bakhtar et al. (2007) and Bakhtar et al. (2008). The earlier program was developed for two-dimensional transient flow of two-phase condensing steam in low pressure turbine. In the current work modifications were made so that the program can be applied for high speed viscous flow in shock tube.

The first part of the spatial discretization consists of setting up a mesh or grid by which the flow domain is replaced by a finite number of points where the numerical values of the variables will be determined. In the present work, the physical domain is divided into a set of grids consisting of pitch-wise lines and quasi-streamlines. A cell-vertex formulation is used in which the flow variables are stored at cell vertices. It has been shown by Martinelli (1987), Dick (1990) and Swanson and Radiespiel (1991) that cell-vertex formulation offers some advantages over the cell-centred one. Since the variables are piece-wise linear over the cell face, the formulation is second-order accurate in space irrespective of the irregularity of the grid. On the other hand, the cell-centred formulation will only be first-order accurate on an irregular grid since the representation of the solution is done in piece-wise constant way. For a uniform mesh, there would be no difference between the cell-centred and cell-vertex schemes, however, cell-vertex scheme does not require extrapolation to the solid boundary to obtain the wall static pressure which is necessary in solving the momentum equations for cells adjacent to the solid boundary .

Central-difference generates odd-even decoupling near a discontinuity. The scheme can be stabilised by introducing a small amount of artificial viscosity. The artificial viscosity used in the present work, is that proposed by Jameson et al. (1981) modified to suit the cell-vertex formulation. This is a blend of second and fourth-order terms with a pressure switch to detect changes in pressure gradient. The time integration is done by means of a four-stage Runge-Kutta time stepping scheme, as proposed by Jameson et al. (1981).

EXPERIMENTAL FACILITY

Figure 1 shows the schematic diagram and a photograph of the high speed test facility. The facility consists of the following components as listed in Figure 1(a) :

1. Driver section - A high-pressure compressed air section (driver), which contains high pressure driver gas.
2. Pressure gauge - The gauge is used to measure the pressure inside the driver section.
3. Discharge valve – A valve use to discharge the driver section after each run.
4. Primary diaphragm – A thin sheet of metal use to isolate the low-pressure test gas from the high-pressure driver gas until the compression process is initiated.
5. Piston compression section - A piston is placed in the barrel (driven tube) adjacent to the primary diaphragm so that when the diaphragm ruptures, the piston is propelled through the driven tube, compressing the gas ahead of it.
6. Discharge valve - A valve use to discharge the driven section after each run.
7. Vacuum gauge - The gauge is use to set the pressure inside the barrel section to the required vacuum pressure.
8. Barrel section - A shock tube section to be filled with the required test gas.
9. Barrel extension - The last half meter of the barrel on which the pressure transducers and thermocouples are attached.
10. Secondary diaphragm - A light plastic diaphragm which separates the low pressure test gas inside the barrel from the test section and dump tank which are initially at a vacuum prior to the run.
11. Test section – This section consists of a nozzle and test section. The nozzle allows the high temperature test gas to expand to the correct high enthalpy conditions needed to simulate hypersonic flow. A range of Mach numbers can be obtained by changing the diameter of the throat

insert. Model to be tested can be put inside the test section. The test section has a clear window made of high strength glass for flow visualization.

12. Vacuum vessel – The vessel is to be evacuated to about 0.1 mm Hg pressure prior to a test.

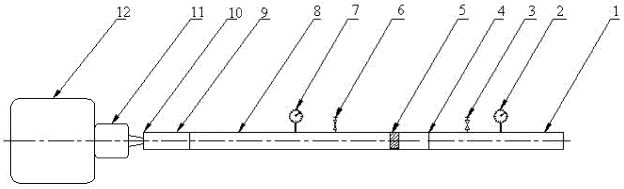

Figure 1(a) : Schematic Diagram of the Hypersonic Test Facility at UNITEN

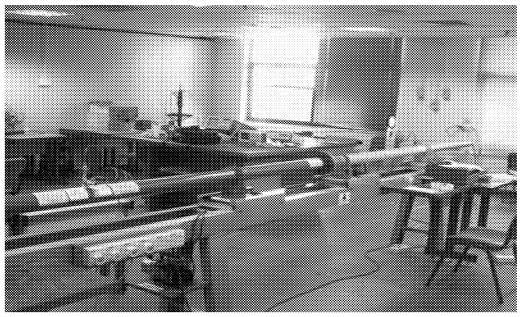

Figure 1(b) : Photograph of the hypersonic test facility at UNITEN

The facility consists of two major sections, the driver section and the driven section. These two sections are filled with gasses at 2 different pressures and are initially separated by a thin diaphragm. The diaphragm is designed to withstand a certain pressure ratio. When this ratio is exceeded, the high-pressure gas ruptures the diaphragm and expands into the low-pressure gas.

VALIDATION OF THE CFD CODE

In order to ensure the validity of the CFD code, in terms of the ability to capture shocks and contact discontinuity and to produce the correct pressure, density and speed profiles, two verification approaches have been used. The first one is the validation of the code against a standard analytical solution of the shock tube problem. The second is to compare the code solution with selected experimental measurements for a certain case of diaphragm pressure ratio.

Comparison with Exact Solution for Inviscid Flow in Shock Tube (Sod Problem)

The Sod problem (Sod, 1978) is an essentially one-dimensional flow discontinuity problem which provides a good test of a compressible code's ability to capture shocks and contact discontinuities with a small number of zones and to produce the correct density profile in a rarefaction. The problem spatial domain is $0 \leq x \leq 1$ as shown in Figure 2.

The initial solution of the problem consists of two uniform states, termed as left and right states, separated by a discontinuity at the origin, $x_o = 0.5$. The fluid is initially at rest on either side of the interface, and the density and pressure jumps are chosen so that all three types of flow discontinuity (shock, contact, and rarefaction) develop. To the ``left'' and ``right'' of the interface we have, $\rho_L = 1$, $\rho_R = 0.125$, $P_L = 1$, $P_R = 0.1$, $u_L = 0$, and $u_R = 0$. The ratio of specific heats γ is chosen to be 1.4 on both sides of the interface.

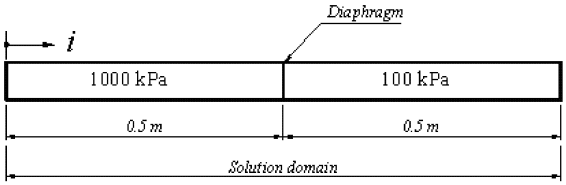

Figure 2: Solution domain for Sod's Problem

A uniform grid spacing with the number $N = 356$ is used. The boundary conditions of the problem are held fixed as a short time span of the unsteady flow is considered. The wave pattern of this problem consists of a rightward moving shock wave, a leftward moving rarefaction wave and a contact discontinuity separating the shock and rarefaction waves and moving rightward.

Figure 3 shows comparisons between the present results for the pressure, density and Mach number at a time $t = 0.2$ ms and the exact solutions. It can be observed that the present solver is capable of capturing the different types of discontinuities accurately.

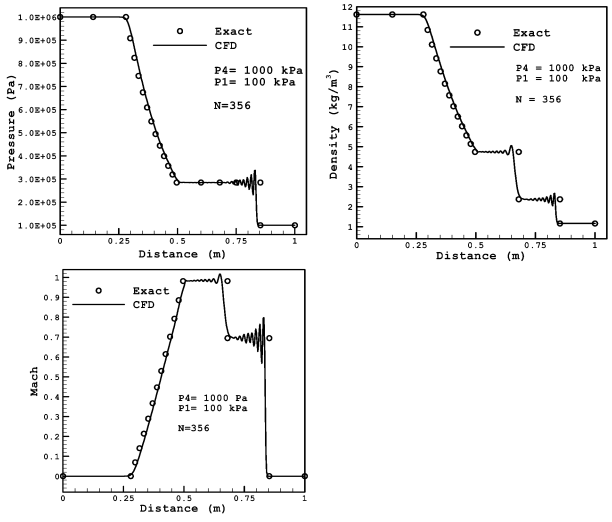

Figure 3: Results for the Sod's shock tube problem at $t = 0.2$ ms

Comparison with Experimental Data for Viscous Flow in Shock Tube

In order to validate the numerical formulation for the viscous terms, the solver was applied to transient shock wave motion in real shock tube. The results will be compared with the

experimental measurements done on the new short duration high speed flow test facility. In order to facilitate the process of diaphragm rupture and avoid any shear a small bush is designed with rounded edge and this bush is to be inserted in the driven section adjacent to the diaphragm, details of this bush is shown in Figure 4.

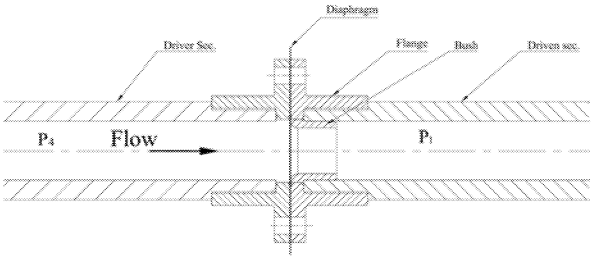

Figure 4: Diaphragm section of the shock tunnel

In order to represent the bush, in the solver, an artificial wedge was included. The CFD simulations are compared with experimental measurements at the test facility for air-air gas combination at diaphragm pressure ratio of 8.8. In the experiment, the transient pressure history at x = 6183 mm from the right hand side end wall was measured by using a highly sensitive piezoelectric pressure transducer. In the actual experiment, the effective area of the diaphragm (throat) opening at rupture is some what smaller than the bush opening area. There will be also a dead flow region (re-circulating flow) behind the bush as shown in Figure 5.

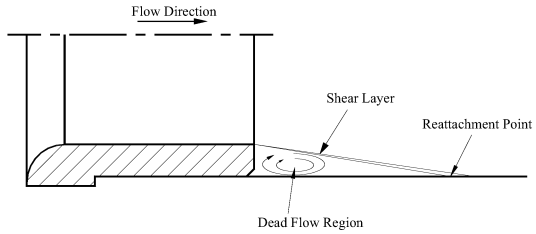

Figure 5: Re-circulating flow behind the bush

The exact location of the reattachment point is highly dependent on the flow speed. In the present work, since the two parameters are not known, the effective throat area and the wedge angle are calibrated and the values which give the closest agreement between experimental data and simulation results are used.

Figure 6 shows comparisons of predicted and measured pressure history with throat opening of 24 mm, 18 mm and 14 mm. All cases are able to predict the overall shock wave motion. The first pressure jump is the shock wave. This is followed by the second pressure jump due to the passing of the reflected shock wave. The pressure history after that also mimics the experimental measurement very well and shows the arrival of the contact discontinuity and subsequent interaction with shock wave. Comparing the three throat diameters, it can be seen that the shock wave strength reduces and get closer to the measured values as the diameter is reduced. The case with throat diameter of 14 mm gave the closet agreement with the experiment and therefore will be used in the subsequent investigation.

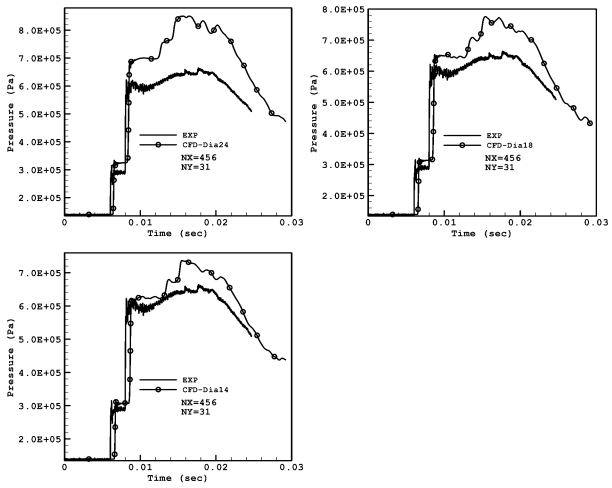

Figure 6: Experimental and CFD results of pressure history at different rupture area

Having fixed the throat diameter, the next parameter is the effect of wedge angle. Three wedge angles have been used; 3.5°, 5° and 6.5° and the results obtained are shown in Figure 7. It can be seen that as he wedge angle is increased the peak pressure reduced. The wedge angle that gave the closest agreement is 5° wedge.

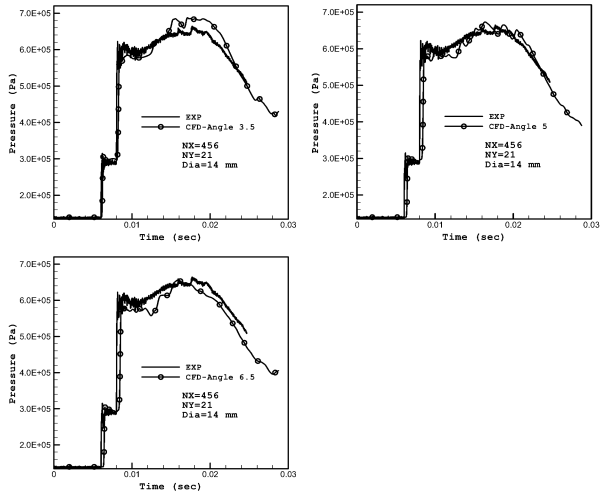

Figure 7: Experimental and CFD results of pressure history at different wedge angle

The x-t diagram is one of the important tools which give a good estimation for the maximum useful test time that can be obtained after removal of the diaphragm. Figure 8 shows the predicted x-t diagram for density profile along the whole length of the test facility obtained for diaphragm pressure ratio of (P_4/P_1) =10. It can been seen that the shock wave is followed by the contact surface. Then the reflected shock wave interacts with the contact surface and then the wave further reflects. It is interesting to note that after interaction with the reflected shock wave, the contact surface remains at about the same position, indicating achievement of the tailored condition. The presence of the bush is also seen to have prevented the rarefaction wave and the shock wave from passing to the other section. The rarefaction wave and the shock wave are reflected when they reach the bush.

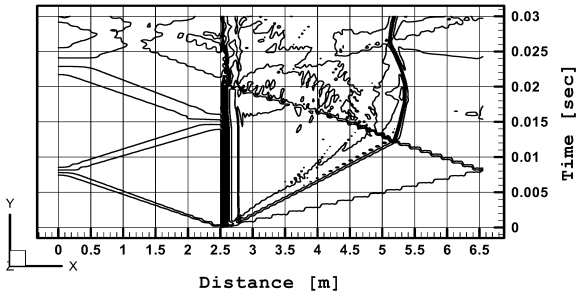

Figure 8: *x-t* diagram for the density history

It can be concluded, based on the agreement with the analytical results, that the numerical formulation of the solver is valid.

RESULTS AND DISCUSSION

Inviscid Transient Flow in Shock Tube

CFD solution for inviscid simulation for a diaphragm pressure ratio P_4/P_1 of 10 has been chosen for detail investigation. The pressure, temperature, density and Mach number of the flow were stored in two stations at the end of the barrel with an axial separation of 342 mm as shown in Figure 9.

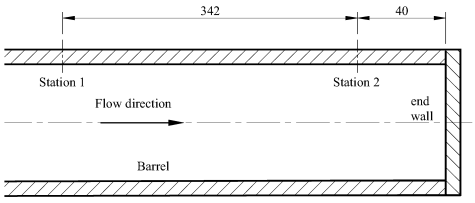

Figure 9: The two stations at the end of the facility

The pressure history for the above mentioned shot is depicted in Figure 10 from which one can follow the physics of the flow inside the shock tube. The first jump represents the shock wave, for which the pressure inside the barrel increases from 100 kPa to around 220 kPa. As the shock wave proceeds to the end of the tube it will reflects and moves in the opposite direction increasing the pressure to about 450 kPa. The shock wave will then interact with the contact surface which is following the shock wave and due to this interaction between the shock wave and the contact surface the pressure will be increased until it reaches its peak pressure value of 530 kPa.

The shock wave speed can be determined from the CFD data obtained from this simulation. As the distance between the two stations is known (0.342 m) and the time of shock travels from station 1 to station 2 can be obtained from the pressure history graph, as shown in Figure 10, the shock wave speed is determined for this shot is 518 m/s. Comparing to the theoretical value for this pressure ratio (558 m/s), the percentage difference is around 7% is reasonable. The difference is probably due to the two-dimensional effect which is not modeled by the theoretical solution. From experimental measurements the shock speed for the same pressure ratio is 450 m/s, which indicate percentage difference of about 13% from CFD results.

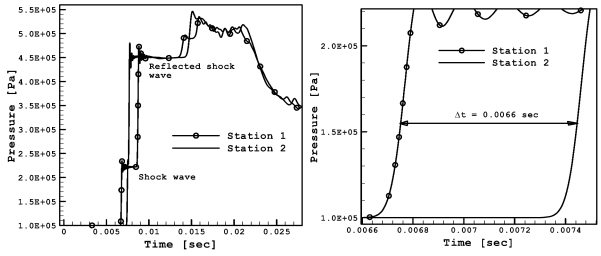

Figure 10: Pressure history for inviscid flow (P_4/P_1=10)

Using the same procedure, the reflected shock wave speed can be determined. As the wave reflects from the tube end and moves in the opposite direction (left direction), due to impact with the end wall the wave will lose some of its kinetic energy and consequently its speed decreases to about 342 m/s.

The same trend can be noted when the temperature history is investigated as shown in Figure 11. The first jump in the temperature profile represents the shock wave and the second jump is due to the reflected shock wave. The temperature is increased from the initial value 300 K to about 380 K due to shock wave effect and when the shock reflects from the tube end, the temperature rises to 475 K and after interaction between reflected shock wave and the contact surface; the flow temperature becomes about 490 K.

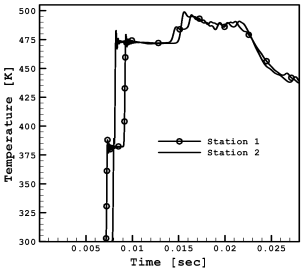

Figure 11: Temperature history inside the shock tube (inviscid flow)

Two-Dimensional Effects

The presence of the bush has caused the flow in the facility to be two-dimensional and this requires two-dimensional CFD simulations. The contour plots of the velocity in *x*-direction along the facility at selected times are shown in Figure 12.

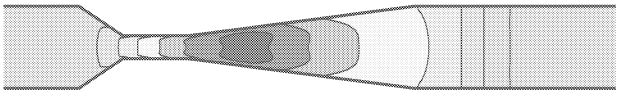

a: Velocity contour before shock reflection (t = 0.0007 sec)

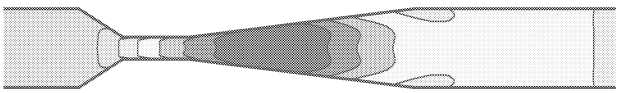

b: Velocity contour before shock reflection (t = 0.001 sec)

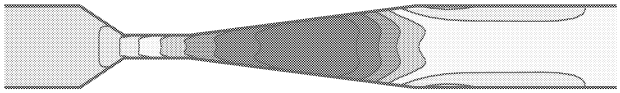

c: Velocity contour before shock reflection (t = 0.0015 sec)

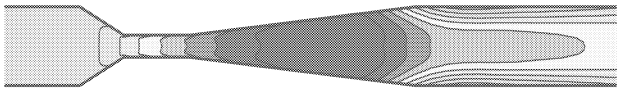

d: Velocity contour before shock reflection (t = 0.003 sec)

Figure 12: Velocity contour plots in x-direction at selected times

As the shock wave reflects from the tube end it will move to the left and interact with the contact surface and the flow no longer symmetry as shown in Figure 13.

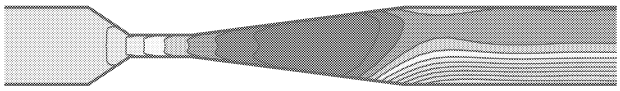

Figure 13: Velocity contour after shock reflection and interaction with contact surface (t = 0.0125 sec)

The velocity contours at 0.025s after diapraghm rupture are shown in Figure 14. It can be observed that the flow is highly two-dimensional especially in the region close to the bush in the driven section. It is interesting to note that after t = 0.0125 sec, the velocity in area close to the bush becomes asymmetric. The asymmetry becomes more and more obvious as time progress and creating recirculating region. However the extend of the recirculating region is of about 10 diameter of the bush.

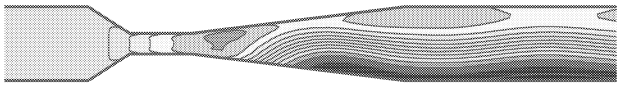

Figure 14: Velocity contour after shock reflection and interaction with contact surface (t = 0.02 sec)

To investigate further, the velocity profiles at x = 279 mm from the diaphragm are plotted in Figures 15 and 16 at different times. At time t = 0.001 sec the profile is perfectly symmetrical. However, the velocity profile contains inflexion part, which is according to Drazin and Reid (1993) is unstable and susceptible to disturbances. The asymmetry becomes more apparent as the process continues. The upper half of the tube has mainly positive velocity whereas the bottom half has negative velocity.

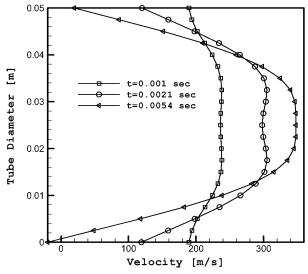

Figure 15: Velocity profile after diaphragm rupture at x = 279 mm from diaphragm

The formation of the recirculating region in this inviscid simulation is surprising especially considering that the tube is symmetrical. However, it has been reported in Xu and Xu (1992) that high speed flow tend to become unstable when shock wave interact with contact discontinuity.

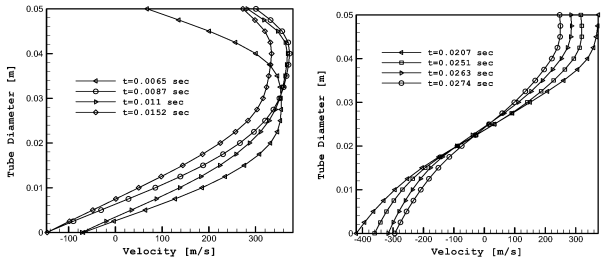

a)after shock reflection b) after interaction with contact surface

Figure 16: Flow after shock reflection

Figure 17 shows the velocity-time plot at selected points in radial direction along the facility which clearly shows oscillating flows.

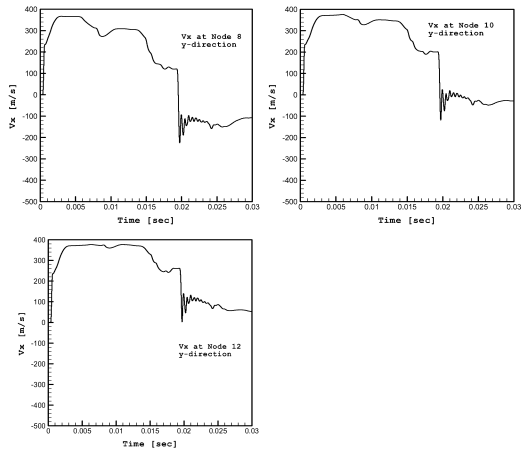

Figure 17: Velocity evolution at selected points in radial direction

Viscous Transient Flow in Shock Tube

In order to investigate the effect of viscosity on the transient flow in shock tube and how it affects the performance of the facility, a viscous simulation has been accomplished for the same boundary conditions of the inviscid simulation presented in the previous section. The pressure history for the above mentioned shot is depicted in Figure 18. The Figure shows similar trend as for the inviscid flow. The first jump represents the pressure rise due to shock wave, for which the pressure inside the barrel increases from 100 kPa to around 220 kPa. The shock wave then reflects as it hits the end of the tube and moves in the opposite direction subsequently the pressure increases to about 450 kPa.

The shock wave will then interact with the contact surface which is following the shock wave and due to this interaction between the shock wave and the contact surface the pressure will be increased until it reaches its peak pressure value which is in this case equal to around 530 kPa.

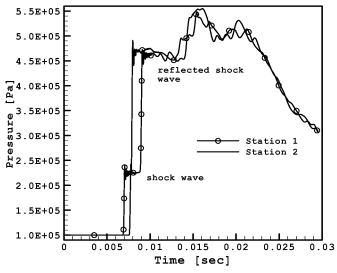

Figure 18: Pressure history for viscous flow (P_4/P_1=10)

The shock wave speed is determined for this shot is 456 m/s, comparing to inviscid value for the same pressure ratio (518 m/s) the effect of viscosity becomes obvious. It can be seen that viscosity decreases the shock wave speed to about 11% due to the boundary layer effects. From experimental measurements the shock speed for the same pressure ratio is 450 m/s, which indicate percentage difference of about 1.3% from CFD results. After it hits the tube end, shock wave will be reflected and it will move to the left with a slower velocity which can be determined using the same procedure. The wave speed decreases to about 311 m/s. Comparing with respect to the reflected shock wave speed for inviscid flow which is 342 m/s, it is apparent that viscosity resists the fluid motion causing slower speed of the shock wave by 9.1%.

Analyzing the temperature history for this simulation, it can be seen that the trend is quite similar to pressure history. The temperature results for this run have been displayed in Figure 19. The first jump represents the shock wave and the second jump is due to the reflected shock wave. The temperature is increased from the initial value 300 K to about 500 K.

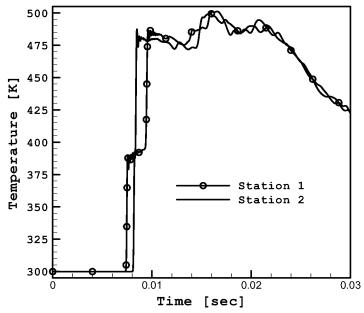

Figure 19: Temperature history inside the shock tube (viscous flow)

CONCLUSIONS

The paper described the use of the 2D-CFD solver designed for simulation of flow in shock tube. The program has been applied to a standard case of inviscid flow in shock tube and transient flow in real shock tube. The agreement with the analyzed solution is very good which proved the validity of the basic numerical scheme developed.

Experimental and CFD pressure data achieved from the above runs showed the effects of shock wave propagation through the barrel, as the shock wave travels from the burst diaphragm, it increases pressure and temperature of the driven gas. The shock reflects off the closed end of the barrel and passes back through the driven gas, further processing the gas causing further increase of the pressure and temperature. The shock strength of the experimental and that of CFD results are very much comparable.

REFERENCES

Bakhtar, F., Zamri, M.Y. and Rodriguez-Lelis, J.M., 2007, "A Comparative Study of Treatment of Two-Dimensional Two-Phase Flows of Steam by a Runge-Kutta and by Denton's Methods", Proceedings of the IMechE, Part C Journal of Mechanical Engineering Science, Volume 221, Number 6, pp. 689-706(18)

Bakhtar, F, Otto, S.R., Zamri, M.Y, Sarkier, J.M., 2008, "Instability in two-phase flows of steam", Proceedings of the Royal Society A: Mathematical, Physical and Engineering Sciences, Volume 464, Number 2091, pp 537–553, Royal Society Publishing, UK

Buttsworth, D.R, 2002, 'Heat transfer during transient compression: measurements and simulation', Shock Waves, 12 : 87-91.

Buttsworth, D.R, Jacobs, P.A, and Jones, T.V, 2002, 'Simulation of Oxford University Gun Tunnel performance using a quasi-0ne-dimensional model', Shock Waves, 11: 377–383

Dick, E., 1990, 'Introduction to Finite Volume Techniques', V.K.I Lecture Series

Drazin, P.G. and Reid, W.H., 1993, 'Hydrodynamic Stability', Cambridge Monographs on Mechanics and Applied Mathematics, Cambridge University Press.

East, R.A., 1960, 'The performance and operation of the University of Southampton hypersonic gun tunnel', Univ. of Southampton Aero. and Astro. Rep. no. 135.

Jacobs, P.A., 1994, 'Quasi-One-Dimensional Modeling of a Free-Piston Shock Tunnel', AIAA Journal, Vol.32, No. 1, January.

Jameson, A., Schmidt, W. and Turkel, E., 1981, 'Numerical Solutions of the Euler Equations by Finite Volume Methods using Runge-Kutta Time Stepping Schemes' AIAA Paper No. 81-1259

Martinelli, L., 1987, 'Calculations of Viscous Flows with a Multigrid Method', Ph.D Thesis, MAE Department, Princeton University

Pope, A. and Goin, K.L., 1965, 'High-Speed Wind Tunnel Testing', John Wiley, New York.

Sod, G.A. "A survey of several finite difference methods for systems of nonlinear hyperbolic conservation laws", J. Comput. Phys. 43 (1-31), 1978.

Swanson, R.C. and Radespiel, R., 1991, 'Cell Centred and Cell Vertex Multigrid Schemes for the Navier Stokes Equations.'AIAA Journal May 1991

Yusaf, T, Al-Falahi, A., Yusoff, M.Z., 2008, "Development of a Short Duration Hypersonic Test Facility and Universiti Tenaga Nasional", Journal Institute of Engineers, Malaysia, Vol. 69, No. 1, pg. 32-38

Xu Fu and Xu Cuiwei, 1992, "Instability theory of shock wave in a shock tube", Journal of Acta Mechanica Sinica, Volume 8, Number 2/May, Springer Berlin /Heidelberg.

SIMULATION PROGRAMMING AND TOOLS

OPTIMISTIC-PARALLEL, PROCESS-ORIENTED DES IN JAVA USING BYTECODE REWRITING

Andreas Kunert
Institut für Informatik, Humboldt-Universität zu Berlin, Germany
email: kunert@informatik.hu-berlin.de

KEYWORDS
Discrete simulation, Process-oriented, Parallel methods

Abstract

Since the very early beginnings of parallel discrete event-driven simulation (PDES) research, numerous general-purpose PDES frameworks have been implemented. These frameworks can be roughly classified by the utilized modelling view (process-oriented vs. event-oriented), kind of parallelism (conservative-parallel, optimistic-parallel), and implementation language.
Since the main motivation of parallel simulation is the acceleration of single simulation runs, most PDES frameworks have been written in rather low-level languages using the event-oriented modelling view. However, the drawbacks of this approach are modelling restrictions to the user and the impossibility to use concepts of higher-level programming languages or to interoperate directly with programs written in such languages.
In this paper, we review different approaches to implement general-purpose simulation processes in Java and discuss the appropriateness of them regarding optimistic-parallel simulations.
Afterwards, we present our current prototypical implementation of an optimistic-parallel simulation framework in Java providing simulation processes based on a bytecode rewriting approach.

INTRODUCTION

Combining optimistic-parallel simulation with the process-oriented modelling view is a task of combining two opposite design goals: While the main goal of (optimistic-) parallel simulation is the acceleration of simulation runs, the process-oriented modelling (i. e. building a simulation model based on simulation processes) focuses on the manageability of especially large and complex simulation models at the cost of simulation speed. However, there is a need for fast process-oriented simulation frameworks since especially the large and complex systems benefit most from simulation acceleration.
Unfortunately, simulation processes cannot be directly implemented in today's most used programming languages C++ and Java due to missing concepts like semi-coroutines and continuations. One workaround in low-level languages like C and C++ is the direct manipulation of the program stack using pointers and memory copy routines (8). In pure Java this approach can not be used due to the lack of possibilities to directly access the stack. However, there exist other promising approaches, which we will discuss in this paper.

The main goal of our research is the implementation of an optimistic-parallel simulation framework which utilizes a specific simulation process implementation approach based on bytecode rewriting. The bytecode rewriter itself was taken from a web application framework and enhanced to fit into our simulation scenario.

This paper is structured as follows: first, we present related work in the field of sequential and parallel, event- and process-oriented simulation. A discussion of simulation process implementation alternatives and their applicability to optimistic-parallel simulations is following. Then, a specific implementation approach is particularized and, finally, we present our simulation framework prototype.

RELATED WORK

Domain-specific simulation implementations

The work most related to our research is a simulator for large and complex telecommunication networks implemented at the Georgia Institute of Technology described in (15). The authors developed a compiler-based approach to implement simulation processes described in a domain-specific language.

Their approach and the one we propose share the same main idea: automatically adding program code to store/restore the program stack element by element (instead of copying the whole memory area the stack occupies) and to implement some semi-coroutine behaviour (discussed later). However, due to its compiler-based nature their domain-specific approach is not directly transferable to a general-purpose simulation framework in Java without having to implement a complete parser for Java which is undesirable for a number of reasons.

Table 1: Existing general-purpose simulation frameworks

DES framework	parallelism	modelling view
Desmo-J	sequential	process-oriented
jDisco	sequential	process-oriented
JiST	sequential	event-oriented
SPaDES/Java	conservative-parallel	process-oriented
FATWa	optimistic-parallel	event-oriented

General-purpose simulation frameworks

Up to today numerous general-purpose DES frameworks have been implemented in Java. However, most of them are based on sequential simulation kernels utilizing the event-oriented modelling view exclusively.
Two sequential DES frameworks supporting the process-oriented modelling view are Desmo-J (12) and jDisco (11), both implementing simulation processes as alternately running Java threads.
Another partially process-oriented sequential DES framework utilizing bytecode rewriting is JiST (5). Here bytecode rewriting is used to change the semantics of certain java methods to introduce a simulation time. The reached speed gain is impressive and an inclusion of parallelization was already considered in the design phase, however, the project has been discontinued after the departure of the main developer.
SPaDES/Java (16) is the only parallel DES framework known to us supporting a process-oriented modelling view. However, it has been implemented using a conservative-parallel approach and therefore the authors did not have to cope with the problems associated with the backward jumps in simulation time in optimistic simulation.
Finally there are optimistic-parallel DES implementations (e. g. FATWa (13)), usually utilizing the event-oriented modelling view.
Table 1 summarizes the mentioned general-purpose frameworks and their features. We are not aware of any general-purpose optimistic-parallel simulation framework providing the process-oriented modelling view.

SIMULATION PROCESSES IN JAVA

In (15), Perumalla and Fujimoto introduce five features of an ideal simulation process implementation shown in Table 2. While it is possible to ease implementation of the simulation kernel and/or increase simulation speed by not supporting some of the features, each missing one creates a restriction to the simulation modeller.
While the features F1 to F3 are standard features of any modern high-level programming language, the last two features, F4 and F5, are simulation specific ones. The mentioned primitives to advance simulation time are calls to simulation kernel methods interrupting the current event execution such as `suspend`, `sleep`, etc. We will revisit the feature list when discussing different simulation process implementation approaches.

Table 2: Main features of ideal simulation process implementations

F1	Procedures can declare and use local variables
F2	Procedure calls can be nested
F3	Procedures can be recursive and re-entrant
F4	Primitives to advance simulation time can be invoked in any procedure
F5	Primitives to advance simulation time can be invoked wherever conditional, looping or other statements can appear

Semi-Coroutines

The main concept needed to implement a simulation process is basically a method that can interrupt itself (e. g. by calling a "magical" method like `suspend()`) and resume from exactly this point of interruption on its next call. Such an interruptable method is called a *semi-coroutine* (7).
In the following code fragment an example method is shown. If this method behaves like a semi-coroutine, on each call it prints out the number of calls so far.

```
public void run() {
  int i=1;
  while (true) {
    System.out.println("#call:" + i++);
    suspend();
  }
}
```

One well-known way to realize semi-coroutines is to implement each semi-coroutine in a separate thread. When a semi-coroutine shall be started for the first time, the according thread is started. A interruption-call from the semi-coroutine leads to a suspension of the underlying thread and when the semi-coroutine is to be resumed, the underlying thread is resumed. Whenever the semi-coroutine thread is running, the main program (being a thread itself) waits and vice versa.
The implementation in Java is straight-forward. First the semi-coroutine-code has to be implemented in the `run()` method of a class implementing the `Runnable`-interface. Moreover, the class gets an attribute `Thread thread` that references the running semi-coroutine-thread.

```
public class MySemiCoroutine implements Runnable {

  // already discussed above
  private Thread thread;
  public void run() {...}

  // coming next
  public synchronized void resume() {...}
  public void suspend() { ... }

}
```

The implementation of the `resume` and the `suspend` methods are very similar. In each case the currently running thread sets itself into a waiting state immediately after notifying the other thread to continue working. It is important to notice, that even though both methods are implemented in the semi-coroutine class, `suspend` is exclusively called by the semi-coroutine thread, while `resume` is only called by the thread of the main program.

```
public synchronized void resume() {
  if (thread == null) {
    thread = new Thread(this);
    thread.setDaemon(true);
    thread.start();
  }
  else {
    synchronized (thread) {
      thread.notify();
    }
  }
  try {
    this.wait();
  } catch (InterruptedException e) {}
}

public void suspend() {
  synchronized (thread) {
    synchronized (this) {
      this.notify();
    }
    try {
      thread.wait();
    } catch (InterruptedException e) {}
  }
}
```

The threaded implementation approach including various implementation alternatives is particularized in (10). The approach is simple to implement and has been used in a couple of process-oriented DES frameworks (e. g. Desmo-J (12) and jDisco (11)).
Moreover, as already discussed in (15), the threaded simulation process implementation supports all features listed in Table 2.
However, the threading approach has one disadvantage: once a thread is resumed, its state before the interruption is lost. This is not a problem in sequential or even conservative-parallel simulation but becomes a huge problem when implementing an optimistic-parallel one.

Threaded simulation processes and the timewarp

In optimistic-parallel simulation, the simulation framework has to provide the necessary data structures and methods to undo all effects resulting from each event if the event becomes invalid due to a backward jump in simulation time (the timewarp). This "undo" is usually implemented by saving simulation model states after every event execution while the simulation time goes forward (9). If a timewarp occurs, the current state is set to the last valid state and all further saved states are deleted.
Once again introducing simulation processes, there is the problem that these process states also have to be saved at each event execution. However, this problem cannot be solved by the threading approach presented above.

Continuations

The abstract concept of storing and later resuming the current execution state of a program or a program part (including the option of reresuming the same stored state over and over again) is called *continuation*. It is obvious, that it is possible to implement a semi-coroutine behaviour using continuations. However, as with semi-coroutines, Java does not provide a direct support for continuations. Moreover, it is impossible to implement generic continuations using pure Java when one design goal is to keep the end-user unaware of the continuation implementation. This is the main reason why there is some work in progress on a Java specification request (JSR) to include continuations in future releases of the Java Development Kit (6).
There are two main problems to be solved when implementing continuations in a stack-based programming language (like Java): The first problem is how to store and restore (fragments of) the stack. This is important since it is the stack where the current local variable values as well as the complete procedure call hierarchy are stored. Once revisited Table 2, a stack backup automatically provides features F1 to F3. The second problem is the provision of entry points (the points in the program code where a continuation continues) to provide feature F4 and F5.
Both problems can be solved by hand when implementing a specific continuation. To solve the first problem, the continuation programmer has to assure that each local variable's value is stored on a global stack before calling another method. The second problem can be solved in a similar way as converting a process-oriented simulation to an event-oriented one: The method gets an additional parameter representing the point in the code where to continue and the method itself has to provide entry-points to be jumped to as dictated by the parameter (this is usually realized by an all-embracing switch-case statement).
As mentioned above, it is impossible to implement continuations using pure Java when the end-user does not provide some help solving the problems mentioned above. However, apart from the simulation community, Java-based continuations have been implemented utilizing bytecode rewriting, i. e. modifying the bytecode produced by the Java compiler prior to execution by the JVM.

CONTINUATION IMPLEMENTATION BY BYTECODE REWRITING

Continuation frameworks provide some "magic" methods (similar to semi-coroutine implementations) like `suspend` and `resume`, which end-users can use like any

other method. In a continuation framework based on bytecode rewriting, a bytecode rewriter analyzes the compiled Java code and adds additional bytecode statements that realizes the continuation behaviour.
The following code shows a simple continuation example using the later discussed continuation framework *Javaflow*.[1]

```
public void run() {
  while (true) {
    System.out.println("#call");
    Continuation.suspend();
  }
}
```

When compiling this code example using the java compiler *javac* the following bytecode is generated. Since bytecode is a binary code, we are using the according *jasmin* assembly representation introduced in (14) in the following code examples.[2]
The `while` loop is compiled into a backward jumping `goto` statement and an according Label (`Label0`). Moreover, the code example shows how the java compiler did not modify the `suspend` call, not knowing the additional behaviour it shall imply.

```
.method public run()V
  .limit stack 2
  .limit locals 1
Label0:
  getstatic System/out LPrintStream;
  ldc "#call"
  invokevirtual PrintStream/println(LString;)V
  invokestatic Continuation/suspend()V
  goto Label0
.end method
```

After Javaflow has modified the bytecode, the code looks as follows (the highlighted code was added by the bytecode rewriter):

```
.method public run()V
  .limit stack 5
  .limit locals 2
  invokestatic StkRec/get()LStkRec;
  dup
  astore_1
  ifnull Label70
  aload_1
  getfield StkRec/isRestoring Z
  ifeq Label70
  aload_1
  invokevirtual StkRec/popInt()I
  tableswitch 0 1
    Label40
    Label59
    default : Label70
Label40:
  aload_1
  invokevirtual StkRec/popObject()LObject;
  checkcast Test
  astore_0
  aload_1
  invokevirtual StkRec/popReference()LObject;
  checkcast PrintStream
  aconst_null
  goto Label75
Label59:
  aload_1
  invokevirtual StkRec/popObject()LObject;
  checkcast Test
  astore_0
  goto Label106
Label70:
  getstatic System/out LPrintStream;
  ldc "#call"
Label75:
  invokevirtual PrintStream/println(LString;)V
  aload_1
  ifnull Label106
  aload_1
  getfield StkRec/isCapturing Z
  ifeq Label106
  aload_1
  aload_0
  invokevirtual StkRec/pushReference(LObject;)V
  aload_1
  aload_0
  invokevirtual StkRec/pushObject(LObject;)V
  aload_1
  iconst_0
  invokevirtual StkRec/pushInt(I)V
  nop
  return
Label106:
  invokestatic Continuation/suspend()V
  aload_1
  ifnull Label137
  aload_1
  getfield StkRec/isCapturing Z
  ifeq Label137
  aload_1
  aload_0
  invokevirtual StkRec/pushReference(LObject;)V
  aload_1
  aload_0
  invokevirtual StkRec/pushObject(LObject;)V
  aload_1
  iconst_1
  invokevirtual StkRec/pushInt(I)V
  nop
  return
Label137:
  goto Label70
.end method
```

The new code in the first highlighted block combines the stack reconstruction and the jumping to specific entry points (stack reconstruction takes place after `Label40` and `Label59` while the entry points are the labels 70, 75 and 106). The last two highlighted code blocks (following the `println` and the `suspend`) do the stack backup.

Existing continuation frameworks

There are two well-known continuation frameworks for Java: Javaflow (3) and Rife/Continuations (4). Both have their origins in the field of web application development. The main use-case for continuations here is to simplify the implementation of user interactions: Typically, a web application starts showing the user a web page in the user's browser requesting some input. After the user responded, the application uses this input for some calculation and a new web page is created containing results, additional information and/or a new request for input. Again the user can respond and gets a new web page and so on.
This interaction between web application and user works quite well as long as the user keeps responding as expected. However, there is one browser-specific detail,

[1] We had to chose an even simpler example than the one used above since the bytecode added by the bytecode rewriter is quite lengthy.

[2] For a better readability the full qualified identifiers were shortened by the package names; `StkRec` is an abbreviation for `StackRecorder`.

that makes this approach complicated: the back-button. Since a browser (and sometimes a user as well) can not distinguish between static web pages and dynamically created pages from a web application, the user might press the back button and expect the last action to be undone.

The simple and actually used but unsatisfying approach to solve this problem is to programmatically disable the back button. A more sophisticated approach is to implement the user interaction using continuations and to save the continuation's state before each input request. When the user now hits the back button (even multiple times), the last valid continuation state will become the current one and all later ones will be deleted.

Rife/Continuations

Rife/Continuations is the continuation providing part of the open-source web application framework Rife (4). It was implemented using the bytecode rewriting library ASM (1) and has an additional convenient feature: it also saves and restores the attributes of the object a continuation is implemented in (i.e. information stored on the heap). In terms of simulation processes this means that automatically all simulation process variables are (re)stored, too.

However, up to the current version, Rife/Continuations has a drawback which disqualifies its usage for simulation purposes: since the added bytecode only saves the topmost stack segment, continuations implemented using Rife/Continuations are only allowed to suspend in their main method (in our example the `run` method), i. e. calls to `suspend` from subsequent methods are not allowed. This means that simulation processes based on the Rife/Continuations implementation would neither provide feature F4 nor F5 from Table 2. This is a serious drawback since process-oriented simulations based on such restricted simulation processes are in fact "process-wrapped" event-oriented simulations as shown in (15).

Javaflow

Javaflow is a subproject of the apache-commons-project and it is based on the Bytecode Engineering Library (BCEL) (2) which is an Apache project itself.

Unlike Rife/Continuations Javaflow allows calls to its `suspend` method also from nested and recursive called methods, thereby simulation processes based on Javaflow provide all desired features from Table 2.

Since Javaflow provides the semi-coroutine as well as the continuation behaviour which guarantees the provision of all desired features to a simulation process implementation, we chose Javaflow for our simulation framework implementation.

OUR JAVA PDES FRAMEWORK

We implemented a prototype of an optimistic-parallel simulation framework including simulation processes based on Javaflow continuations. As most process-oriented simulation frameworks, ours is built on top of an event-oriented one. The parallelism is directly based on Java threads, which makes synchronization very simple. Moreover, we do not have to deal with certain optimistic-parallel simulation problems arising from more distributed solutions such as delayed messages or messages arriving in a different order than sent.

End-user view

For the end-user, the continuation part is nearly invisible. The end-user implements a simulation process by deriving from an abstract class `SimProcess` which demands the definition of two methods: a `run` method which contains the behaviour of the simulation process and a `clone` method which is responsible for cloning all time variable attributes (regarding simulation time). The latter method is necessary since Javaflow does not contain the convenient feature of storing/restoring attributes. Moreover, it is a good idea to let the simulation modeller decide which attributes are time variable to avoid the time- and memory-consuming backup of time constant attributes (e. g. references to databases or files, fields filled with constant values, ...).

Simulation kernel implementation

Our simulation kernel consists of an arbitrary number of logical processes, which can send each other messages about future events by directly calling a target the `receive` method of a logical process. Each logical process runs in a separate Java thread and contains a message input queue where messages are sorted by the simulation times the according events shall occur.
It is also the `receive` method that detects causality errors and subsequently triggers timewarps. Since the `receive` method is marked `synchronized`, parallel access to the input queue of a logical process is automatically serialized.[3]
The following Java code example shows the main loop of a logical process:

```
public void run() {
  while (true) {
    synchronized (this) {
      if (timeWarpOccurred) {
        // restore already processed messages
      }
      if (!inputQueue.isEmpty()) {
        // remove first message from inputQueue
        // advance in simulation time
      }
    }
```

[3]All other methods accessing the input queue are also marked `synchronized`.

```
    if (currentMessage != null) {
      evaluateMessage(); // discussed later
    }
    yield();
    synchronized (this) {
      // backup processed message

      if (inputQueue.isEmpty() &&
            !timeWarpOccurred) {
        // wait
      }
    }
  }
}
```

As seen in the code example, timewarps are not handled asynchronously but in a `synchronized` block in the beginning part of the main loop. This guarantees that all external requests to the logical process are delayed until the timewarp has finished.
Another detail to point out is that the main loop does not differ between event-oriented and process-oriented simulation since the process specifics are dealt with in the `evaluateMessage` method. The following unabridged code shows the implementation of this method to demonstrate how Javaflow eases the implementation.

```
private void evaluateMessage() {
  if (currentMessage.target instanceof Event) {
    logger.trace("executing event");
    ((Event) currentMessage.target).eventRoutine();
  }
  else if (currentMessage.target
        instanceof SimProcess) {

    logger.trace("executing process");

    SimProcess p =
      (SimProcess) currentMessage.target;

    Continuation newState;
    SortedMap<SimTime, Continuation> t1;
    SortedMap<SimTime, SimProcess> t2;

    if (!processStackMap.containsKey(p)) {
      logger.trace("first call of process: " + p);
      t1 = new TreeMap<SimTime, Continuation>();
      t2 = new TreeMap<SimTime, SimProcess>();
      processStackMap.put(p, t1);
      processHeapMap.put(p, t2);
      newState = Continuation.startWith(p, p);
    }
    else {
      logger.trace("later call of process: " + p);
      t1 = processStackMap.get(p);
      t2 = processHeapMap.get(p);
      p = t2.get(t2.lastKey()).clone();

      newState = Continuation.continueWith(
        t1.get(t1.lastKey()), p
      );
    }
    t1.put(currentTime, newState);
    t2.put(currentTime, p);
  }
  else {
    logger.fatal("unknown target type");
  }
}
```

While the treatment of an event is straight-forward as the event's routine is directly being executed by a method call, the execution of a process needs some preparation.
Each logical process in our implementation contains two hash tables: While the `processStackMap` stores a sorted map for each simulation process containing continuation objects (preserving process state information stored on the stack), the `processHeapMap` stores a sorted map for each process containing process objects (preserving process state information stored on the heap).
When a process is to be started for the first time, two new sorted maps (`t1` and `t2` in the code example) are created and stored in the according hash tables, in either case using the process object itself as a hash key. Then the process (being a continuation as described above) is started. After the process execution has finished, the resulting continuation object (representing the state to continue with on the next call) is being stored as well as the process object (in its current state).
When a process is to be resumed, the last saved continuation object is restored to continue with. Moreover, the last saved process object is restored, but instead of directly resuming with this object, a cloned object is made to preserve the current process state for a potential later timewarp.[4] Then the process is resumed using the restored continuation object and the cloned process object. Afterwards continuation and process objects are stored as described above.

Experiences and future work

Our prototype already works with simple simulation models and the first simulation experiments reflect the expected behaviour: a large speed gain for simulation models consisting of encapsulated, non-interacting processes; a speed loss for strongly linked simulation models (in both cases compared to a sequential simulator).
However, up to now, we are restricted to small simulation models because we have not implemented a *fossil collection* yet. I. e. at the moment our implementation does not remove no longer used process states, which leads to a continuously growing memory consumption on each simulation run.
Our next step is the missing implementation of the fossil collection including the calculation of the *global virtual time*. Afterwards, we plan to implement some larger simulation models that shall demonstrate the speed gain by the parallelism as well as the convenience of the process-oriented modelling view.

CONCLUSION

In this paper we have discussed the two main concepts needed for an implementation of simulation processes in the field of optimistic-parallel simulation.
First, we have introduced the semi-coroutine concept (i. e. methods that can be suspended and resumed) that is needed to implement the behaviour of suspendable simulation processes and showed the typical semi-

[4] We do not have to clone the continuation object as well due to the semantics of Javaflow where a new continuation object is returned on each resumption.

coroutine implementation approach. Afterwards, we introduced the continuation concept which provides the ability to store and later resume the current execution state of a process (and can be used to implement semi-coroutine behaviour, too).
Using continuations, we can implement simulation processes that can go backward in simulation time by resuming from earlier saved process states as needed in optimistic-parallel simulations. We have shown a bytecode rewriting approach to implement continuations in Java and presented two existing continuation frameworks coming from the field of web application development.
Finally, we have presented our prototypical simulation framework using such a bytecode-rewriting continuation framework. The experiences with this prototype so far are promising as there is a speed gain compared to sequential simulation. Future implementation work will show how far this speed gain is affected by the completion of the simulation framework.
Once finished, a simulation modeller using our framework will benefit from the ability to build and execute optimistic-parallel simulation models using the process-oriented modelling view.

References

[1] ASM homepage. `asm.objectweb.org`.

[2] Byte code engineering library (BCEL) homepage. `jakarta.apache.org/bcel`.

[3] JavaFlow homepage. `commons.apache.org/sandbox/javaflow`.

[4] Rife homepage. `www.rifers.org`.

[5] R. Barr, Z. J. Haas, and R. van Renesse. Jist: an efficient approach to simulation using virtual machines: Research articles. *Softw. Pract. Exper.*, 35(6):539–576, 2005.

[6] G. Bevin. JSR continuations provider API – working draft. 2008.

[7] O. J. Dahl, E. W. Dijkstra, and C. A. R. Hoare, editors. *Structured programming*. Academic Press Ltd., London, UK, UK, 1972.

[8] J. Fischer and K. Ahrens. *Objektorientierte Prozeßsimulation in C++*. Addison-Wesley, Bonn, 1996.

[9] R. M. Fujimoto. *Parallel and Distribution Simulation Systems*. John Wiley & Sons, Inc., New York, NY, USA, 1999.

[10] K. Helsgaun. Discrete event simulation in Java. *DATALOGISKE SKRIFTER (Writings on Computer Science)*, 2001.

[11] K. Helsgaun. jDisco – a Java framework for combined discrete and continuous simulation. *DATALOGISKE SKRIFTER (Writings on Computer Science)*, 2001.

[12] T. Lechler and B. Page. Desmo-J: An object oriented discrete simulation framework in Java. In *Europäisches Simulations-Symposium 1999*, 1999.

[13] M. C. Lowry, P. J. Ashenden, and K. A. Hawick. Distributed high performance simulation using time warp and Java. Technical Report DHPC-084, Department of Computer Science, The University of Adelaide, South Australia, 2000.

[14] J. Meyer and T. Downing. *Java virtual machine*. O'Reilly & Associates, Inc., Sebastopol, CA, USA, 1997.

[15] K. S. Perumalla and R. M. Fujimoto. Efficient large-scale process-oriented parallel simulations. In *WSC '98: Proceedings of the 30th conference on Winter simulation*, pages 459–466, Los Alamitos, CA, USA, 1998. IEEE Computer Society Press.

[16] Y. M. Teo and Y. K. Ng. SPaDES/Java: Object-oriented parallel discrete-event simulation. In *SS '02: Proceedings of the 35th Annual Simulation Symposium*, page 245, Washington, DC, USA, 2002. IEEE Computer Society.

ANALYSIS OF A LINEAR INDUCTION MOTOR BY THE MEHTOD COUPLING MATLAB/SIMULINK AND VECTOR CONTROL APPROACH

SAMEER KHADER
College of Engineering and Technology
Palestine Polytechnic University
Hebron- West Bank
P.O.Box 198,Tel +970 22230068
Palestine
Email: sameer@ppu.edu

ABSTRACT

MATLAB/ Simulink is a very useful tool for analysis and design of control systems. Vector control method (VCM) is a powerful tool for the analysis of electromagnetic processes and optimized flux and current in order to realized optimized motor operation in general and linear induction motors as partial case.
Taking into account the Sinusoidal Pulse Width Modulation, six switching patterns used to control 6-switching transistors drives three-phase windings. This paper proposes a new method, where the MATLAB/ Simulink is coupled with VCM. We apply the proposed method to analyze a linear three-phase induction motor (LIM) behaviors, and to obtained optimized linear force with minimized ripples, low current ripples, and minimized losses. Prototype linear motor has been accomplished.

KEYWORDS

Computer Simulation, Linear Motor, Synchronous Motors, Induction Motor, Vector Control, and PWM.

INTRODUCTION

MATLAB/Simulink is well known as a very useful tool for the analysis and design of control systems [1,2]. We can analyze a motor drive system using MATLAB, where the motor is usually represented by a d-q model. Several control methods can be applied such as Field oriented control, and flux scalar control, but these method are characterized with drawbacks and consume much time in simulation . Therefore, a new method which called Vector Control, where both phase and magnitude of circuit flux is controlled. VCM is also well known as a powerful tool for the analysis of speed-torque control of electromagnetic devices. We can analyze the motor current, speed and electromagnetic flux in order to achieve optimized electromagnetic torque at reduced looses . When electrical motors are used in the control system, it is necessary to evaluate the whole system, which is composed the motor, the drive circuit, and the control system.

Several papers have been published to couple the MATLAB and the numerical calculation of the electromagnetic field and speed-torque calculations [3]. In this papers, the motor key performances is analyzed by using VCM and the results are sets as a data feedback file for the MATLAB, and then the MATLAB simulates the motor drive system using this input data with purpose to generate the inverter switching combinations and there durations, to calculate the electromagnetic torque and current, obtained speed. Some of the simulation subsystems have been designed and adapted with already exist in the MATLAB/ Simulink Library [4].
Application of linear induction and direct current motors for translation gives the possibility to diminish weight of drive moving parts, enlarges operating speeds and accelerations. In many cases a new construction of equipment is developed when the linear motor in two main types magnetic and reluctance becomes an incorporated part of the electromechanical systems [5,6,7,8] .
Linear motors are designed as single and multiphase motors, and can successfully be applied in the equipments where there are possibility to coincide the secondary with conductive parts of controlled equipment or in the systems where extra high speed is required.

The secondary (movable) part of the linear motor can be made from materials characterized with small specific weight, therefore every linear motor must be designed according to specific construction features, speeds and loads . The large airgap of linear motor in general determines the greater losses. Thus the main area where it is move expedient is to apply in electromechanical systems with short operation mode and intermediate operation mode [9,10]. During these operating modes a speed of secondary part usually does not reach steady state values and currents of stator winding also does not reach the steady operation.
Linear motors have nearly the same long history as rotary motors. The first linear motor was designed in 1883, but large airgap and low efficiency prevented linear motors from being widely used. Unlike rotary

electric motors, the linear motor has a start and end to it is travel [11]. Despite these restrictions, the main benefits of these motors are:
Lack of windings on either stator and rotor construction
Absence of mechanical gears.
Absence of significant heat source during secondary operation.
Simplicity in design .
Single phase Linear reluctance motor energized by AC and DC source has been discussed in details by Subbhadra Devicount [12] where comparison between both motor characteristics was realized. But the mentioned study does not use VCM in processing the system performances.

The present paper should describe the following tasks:
- Building the mathematical simulation model by using three to two axis transfer system, generating the sinusoidal PWM switching signals, PI controller, and torque-flux estimator.
- Forming the simulink subsystem taking into account the differences between rotary and linear movement motor.
- Linking the designed subsystem with already existed units in the simulink library.
- Estimating the designed model with respect to the motor mean torque, speed, and current

MATHEMATICAL MODELING

Principle Circuit

A principle control circuit of linear induction motor is illustrated on fig.1 where a three-phase linear motor is driven by electronic converter and two feedback signals with purpose to achieve continuous and stable torque operation with minimized ripples. The electrical circuit consists of three-phase uncontrolled rectifier, DC link circuit, three-phase inverter, and speed and current sensors realized the successful feedback. The inverter circuit consists of six switching devices such as MOSFET or IGBT connected each phase to the DC bus and controlled by sinusoidal Pulse Width Modulation approach (SPWM).

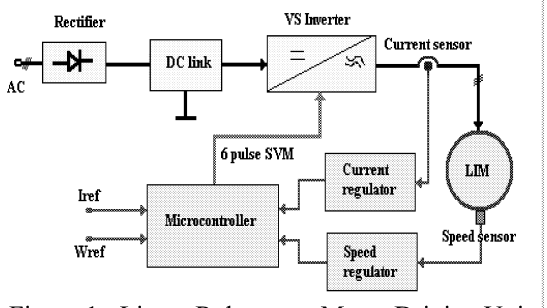

Figure 1 : Linear Reluctance Motor Driving Unit

The performance of LIM strongly depends on the applied control strategy. Figure2 shows a principle electronic converter energizing three-phase Wye connected windings, where a six space vector modulated pulses (SVM) controls the operation sequence of the motor phases. Each phase is energized throughout two switching IGBT transistors.

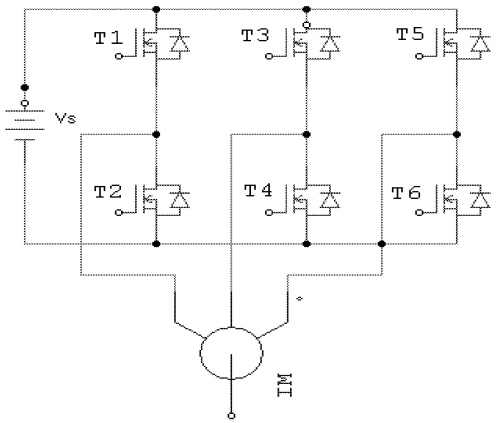

Figure 2 : Electronic Converter for Three-phase Linear Motor.

Proposed Construction

There are different versions of Linear motors for both reluctance and induction type depending on the proposed applications [3,8]. In this manner, there are short-stator linear induction motor and long-stator linear synchronous motor. Single side linear induction motor with flatted squirrel cage in the guide way consists of an double layer cage with aluminum bars as well shown on figure3.

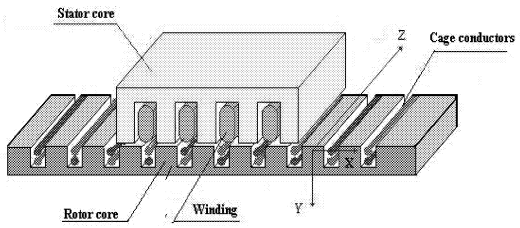

Figure 3 : Motor Electromechanical Construction

The primary winding is supplies by three-phase inverted voltage Vs at given frequency fs, which causes the current to flow, producing the magnetic flux that is closed through the path perpendicular to the direction of motion (axis x).
The produced total magnet flux yield tangential (linear or thrust) force and normal (perpendicular or attractive/repellent) forces.

The vector control is referring not only to the magnitude but also to the phase of motor input variables. Matrix and vectors are used to represent the control quantities.

This method takes into consideration not only successive steady-states but real mathematical equations that describe the motor itself, the control results

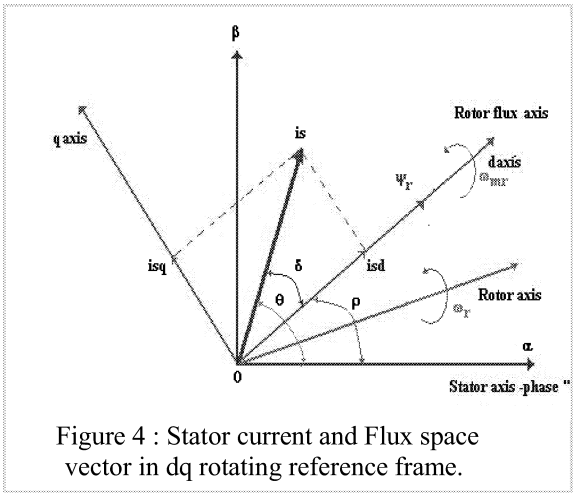

Figure 4 : Stator current and Flux space vector in dq rotating reference frame.

obtained have a better dynamic for torque variations in a wider speed range. Though the induction motor have a very simple structure, its mathematical model is complex due to the coupling factor between a large number of variables and the non-linearity's. The Field Oriented Control (FOC) offers a solution to circumvent the need to solve high order equations and achieve an efficient control with high dynamic. This approach needs more calculations than a standard V/f control scheme.

The FOC consists in controlling the components of the motor stator currents, represented by a vector, in a rotating reference frame d,q aligned with the rotor flux. The vector control system requires the dynamic model equations of the induction motor and returns to the instantaneous currents and voltages in order to calculate and control the variables. Figure4 presents the phasor diagram of the motor reference frames illustrating the relationship between circuit parameters.
The electromagnetic torque of an AC induction motor can be described by the interaction between the rotor currents and the flux wave resulting from the stator currents .

The FOC consists in controlling the components of the motor stator currents, represented by a vector, in a rotating reference frame d,q aligned with the rotor flux. The vector control system requires the dynamic model equations of the induction motor and returns to the instantaneous currents and voltages in order to calculate and control the variables.

$$T_{em} = \frac{2}{3} L_o . \Im m \left[(i_s . i_{mr} e^{j\varphi})^* \right] \qquad (1)$$

Where Tem is the obtained electromagnetic torque, Lo is the mutual inductance per phase. , is is the stator space current , imr is the rotor magnetic current, and φ is the phase angle of three phase network.
Since the rotor currents cannot be measured with cage motors, this current is replaced by an equivalent quantity described in a rotating system coordinates called d,q and following the rotor flux. The instantaneous flux angle ρ is calculated by the motor flux model. is_d and is_q are the stator current components in the d,q frame, and obtained directly from i_a, i_b and i_c. These current can be obtained by applying Park transformation :

$$\begin{bmatrix} i_{ds} \\ i_{qs} \end{bmatrix} = \begin{bmatrix} \cos\rho & \cos(\rho - 2\pi/3) & \cos(\rho + 2\pi/3) \\ -\sin\rho & -\sin(\rho - 2\pi/3) & -\sin(\rho + 2\pi/3) \end{bmatrix} \begin{bmatrix} i_{sa} \\ i_{sb} \\ i_{sc} \end{bmatrix} \qquad (2)$$

Then the electromagnetic torque can be expressed as follow:

$$T_{em} = k . i_{mr} . i_{sq} \Rightarrow \text{ with } \begin{cases} k = \frac{2}{3}(1-\sigma) L_S \\ i_{mr} = \frac{1}{Lm} \psi_R \end{cases} \qquad (3)$$

Where ψ_R is the rotor flux, L_S is the total stator inductance, σ is the leakage coefficient, and Lm is the magnetizing inductance.
In steady-state conditions the stator current is defined in the above mentioned rotating system is considered constant as well as the magnetizing current im_r representing the rotor flux and is_q being equivalent to the motor torque. δ is the load angle that equals to zero when no load, is_d is linked to im_r with the following equation:

$$i_{sd} = i_{mr} + \tau_R \frac{d}{dt} i_{mr} \qquad (4)$$

Where T_R is the rotor time constant.

This system together with the angle transformations change the induction motor
into a machine very similar to a DC motor where im_r corresponds to the DC motor main flux and is_q to the armature current.
The field orientated control method achieves the best dynamic behavior, whereby the lead and disturbance behavior can be improved with shorter control cycle times. The field orientated control method is a defacto standard to control an induction motor in adjustable speed drive applications with quickly changing load as well as reference speeds. Its advantage is that by transforming measurable stator variables into a system based on field coordinates the complexity of the system can be enormously reduced. As a result a relatively simple control method very similar to a separated exited DC motor can be applied [13,14].
The role of the DSP in such a system is to translate the stator variables (currents and angle) into a flux model as well as compare the values with the reference values and update the PI controllers. After the back transformation from field to stator coordinates the output voltage will be impressed to the machine with a symmetric, an asymmetric PWM whereby the pulse pattern is on-line computed by the DSP or a hardware generated space vector method. In some systems the position is measured by an encoder, this extra cost can

be avoid implementing an observer model or in particular cases, a Kalman filter. These algorithms are complex and therefore require a fast processor, a fixed-point DSP is able to perform the above controls with short cycle times.

Space Vector Modulation

Pulse Width Modulation technique is used to generate the required voltage or current to feed the motor or phase signals. This method is increasingly used for AC drives with the condition that the harmonics current is as small as possible. Generally, the PWM schemes generate the switching position patterns by comparing three-phase sinusoidal waveforms with a triangular carrier. In recent years, the space vector theory demonstrated some improvement for both the output crest voltage and the harmonic copper loss.

The maximum output voltage based on the space vector theory is 1.155 times as large as the conventional sinusoidal modulation. It enables to feed the motor with a higher voltage than the easier sub-oscillation modulation method. This modulator allows to have a higher torque at high speeds, and a higher efficiency.

For a better understanding of the space vector process and to represent the switching state of the inverter we define a switching function S_a for phase A as follows: S_a = 1 when the upper transistor of phase A is on (fig.2), and S_a = 0 when the lower transistor of phase A is on. Similar definitions can be made for phase B and C. The signals S_a^{--}, S_b^{--}, and S_c^{--} controlling the lower transistors, are the opposite of S_a, S_b, and S_c with an addition of dead-bands.

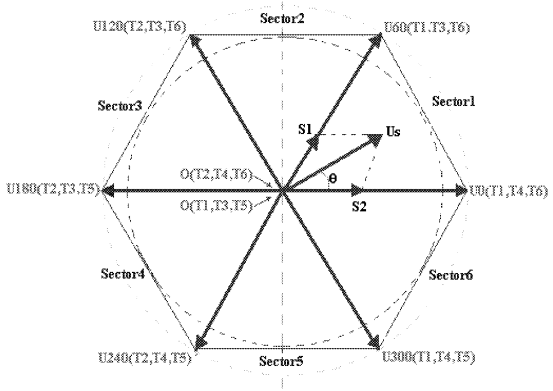

Figure 5: Space vector combinations of switching transistors.

In the space vector theory the motor voltage vector is approximated by a combination of 8 switching patterns of the 6 power transistors. Us is decomposed as follows:

Where $\vec{Ux}$ and $\vec{Uy}$ are two consecutive vectors. The third vector $\vec{O}(0,0,0)$ and $\vec{O}(1,1,1)$ is chosen in a way to minimize the number of switching commutations defined by eq.(4).
This can be expressed with the formula:

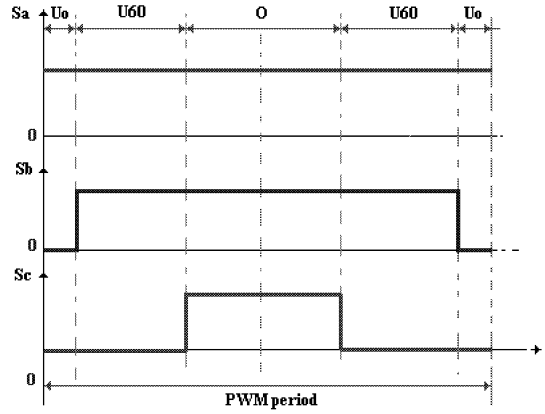

Figure 6: PWM S- states for $0 \le \theta \le 60^o$.

$$T.\vec{Us} = S_1\vec{Ux} + S_2\vec{Uy} + (T - S_1 - S_2)\vec{O} \qquad (6)$$

Taking into account the mathematical representation of commutation combinations the PWM scheme describe a vector Us with an angle θ as $0 \le \theta \le 60^o$ is shown on figure 6 for switching functions S_a, S_b, and S_c. Full operation period which is equivalent to full cycle control (360º) consists of eight combinations with results shown in table1.

Switching state	On Switches	Vsa	Vsb	Vsc
0	T2 T4 T6	0	0	0
1	T1 T4 T6	2/3Vdc	-1/3Vdc	-1/3Vdc
2	T1 T3 T6	1/3Vdc	1/3Vdc	-2/3Vdc
3	T2 T3 T6	-1/3Vdc	2/3Vdc	-1/3Vdc
4	T2 T3 T5	-2/3Vdc	1/3Vdc	1/3Vdc
5	T2 T4 T5	-1/3Vdc	-1/3Vdc	2/3Vdc
6	T1 T4 T5	1/3Vdc	-2/3Vdc	1/3Vdc
7	T1 T3 T5	0	0	0

Where V_{SA}, $V_{SB,}$ and V_{SC} respectively phase voltage of the motor phases a, b and c .
The obtained equivalent circuit for one phase is shown on figure 7.

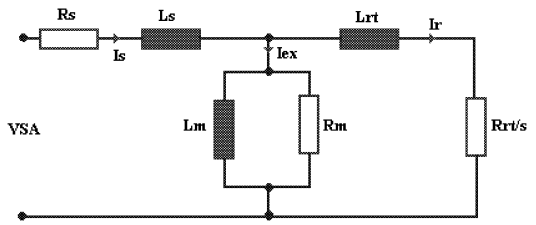

Figure 7 : Per- phase equivalent circuit

The set of space vectors corresponds to voltage, current and flux by assuming that there is a full electrical symmetry, no effect of motor non-linearity, and no saturation of the core :

$$\vec{Us} = \frac{2}{3}\left[V_{SA} + aV_{SB} + a^2 V_{SB}\right]$$
$$\vec{is} = \frac{2}{3}\left[i_{SA} + a\, i_{SB} + a^2 i_{SC}\right]$$
$$\vec{\psi}\, s = \frac{2}{3}\left[\psi_{SA} + a\,\psi_{SB} + a^2 \psi_{SC}\right]$$
$$a = e^{j\frac{2\pi}{3}} \qquad (7)$$

Where : V_{SA}, $V_{SB,}$ and V_{SC} are the three stator phase voltage, i_A, i_B, and i_C are the stator phase current, and ψ_{SA}, ψ_{SB}, and ψ_{SC} are the stator flux linkage. The vector **a** is the rotation operator.
Rs, Lls Stator resistance and leakage inductance; Rr, Llr Rotor resistance and leakage inductance;
Lm- Magnetizing inductance, Ls, Lr - Total stator and rotor inductances.

Vqs, iqs - q axis stator voltage and current; Vqr, iqr - q axis rotor voltage and current; Vds, ids- d axis stator voltage and current; Vdr, idr - d axis rotor voltage and current; ψqs, ψds - Stator q and d axis fluxes; ψqr, ψdr - Rotor q and d axis fluxes.
ωs, ωr -Angular velocity of the stator and the rotor;
θ - Rotor angular position; p - number of pole pairs; Tem- electromagnetic torque; Tm- Shaft mechanical torque;

J-combined rotor and load inertia coefficient;
H-combined rotor and load inertia constant; and F-combined rotor and load viscous friction coefficient.

In d-q rotation frame, the Park transform of three-phase voltage is express as follow:

$$V_{ds} = R_s.i_{ds} + \frac{d}{dt}\psi_{ds} - \omega_s.\psi_{qs}$$
$$V_{qs} = R_s.i_{qs} + \frac{d}{dt}\psi_{qs} + \omega_s.\psi_{ds}$$
$$V_{dr} = R_r.i_{dr} + \frac{d}{dt}\psi_{dr} - (\omega_s - \omega_r).\psi_{qr}$$
$$V_{qr} = R_r.i_{qr} + \frac{d}{dt}\psi_{qr} + (\omega_s - \omega_r)\psi_{ds}$$
$$T_{em} = \frac{3}{2}p(\psi_{ds}.i_{qs} - \psi_{qs}.i_{ds}).$$
$$\frac{d}{dt}\omega_m = \frac{1}{2H}(T_{em} - F\omega_m - T_m); \quad \omega_m = \frac{d}{dt}\theta_m$$

$$\psi_{ds} = L_s.i_{ds} + L_m.i_{dr}; \psi_{qs} = L_s.i_{qs} + L_m.i_{qr}$$
$$\psi_{dr} = L_r.i_{dr} + L_m.i_{ds}; \psi_{qr} = L_r.i_{qr} + L_m.i_{qs}$$
$$L_S = L_{ls} + L_m; L_r = L_{lr} + L_m$$

(9)

The inverse Park transform of the motor phase currents taking into account eq.(2) can be expressed in matrix form as follow:

$$\begin{bmatrix} i_A \\ i_B \end{bmatrix} = \begin{bmatrix} \cos\rho & \sin\rho \\ \frac{-\cos\rho + \sqrt{3}\sin\rho}{2} & \frac{-\sqrt{3}\cos\rho - \sin\rho}{2} \end{bmatrix} \begin{bmatrix} i_{qs} \\ i_{ds} \end{bmatrix}$$
$$i_C = -(i_A + i_B)$$

(10)

The rotor phase current referred to the primary side of the stator equivalent circuit can be expressed in matrix form as follow:

$$\begin{bmatrix} i_{Ar} \\ i_{Br} \end{bmatrix} = \begin{bmatrix} \cos\beta & \sin\beta \\ \frac{-\cos\beta + \sqrt{3}\sin\beta}{2} & \frac{-\sqrt{3}\cos\beta - \sin\beta}{2} \end{bmatrix} \begin{bmatrix} i_{qr} \\ i_{dr} \end{bmatrix}$$
$$i_{Cr} = -(i_{Ar} + i_{Br})$$

(11)

Where β is the difference between the position of the reference frame and the position of the rotor.

Modeling of Linear induction motor:

The magnetic flux of the motor leads to producing electromagnetic force that can be evaluated by considering the airgap power [15,16].

The relation between mechanical power, speed and force is reported underneath:

$$F_{el} = \frac{P_{mech}}{V_m} \quad (12)$$

Where: Vm is the linear velocity of the motor, Fel is the electromagnetic force, and Pmech is the mechanical power.

$$P_{mech} = P_{el}(1-s) \quad (13)$$

Where s is the motor slip, Pel is the electromagnetic power that can be expressed as follow:

$$P_{el} = P_{INP} - P_{CU} - P_{rot}$$

$$P_{INP} = 3.V_{SA}.I_{SA}.\cos\varphi \quad (14)$$

Where Pinp is the input consumed power, PCU is the copper losses, Prot is the rotational losses. In other hand, the mechanical speed of the motor can be expressed using the stator pulsation and the slip:

$$V_m = \frac{\tau_p.\omega_s}{\pi}(1-s) \quad (15)$$

The described few formulas are directly deductible from the formulas concerning a rotating motor by using the following transformation:

$$p \rightarrow \frac{\pi}{\tau_p} \quad (16)$$

Replacing (12) and (13) into (14) yields a new expression for the electromagnetic force:

$$F_{el} = \frac{\pi . P_{el}}{\tau_p . \omega_s} \quad (17)$$

MOTOR SIMULATION & PERFORMANCES

The motor performance are obtained by applying MATLAB/Simulink software and comparison analysis between performances are going to be discussed such as circuit current, velocity, torque, mechanical force.

Block diagram using MATLAB/ imulink

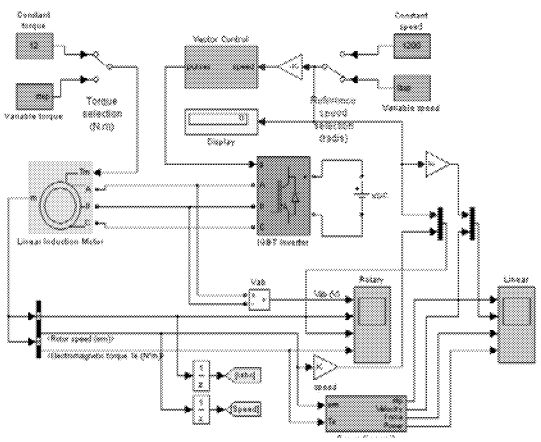

Figure 8 : Overall motor control circuit using MATLAB/ Simulink approach.

First diagram illustrated on figure8 presents the overall system of the motor simulation consists Vector control unit, three-phase induction motor, rotary to linear motion converting unit, power switching unit, torque-speed selector with purpose to regulate the torque and speed ratings.

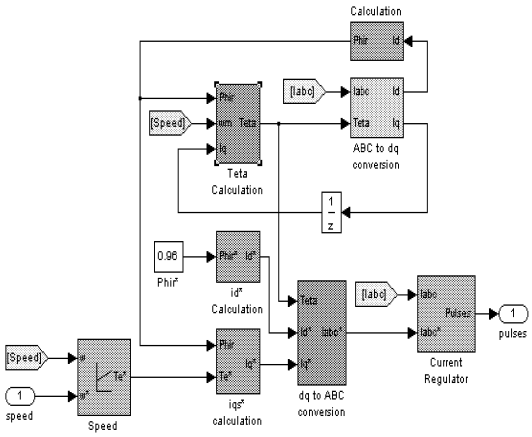

Figure 9 : Vector control unit using MATLAB/ simulink approach.

Second diagram illustrated on figure 9 presents the Vector control unit that consists d-q Park and Clark transforms, PI controller, Pulse generator, flux- current converter, i.e..

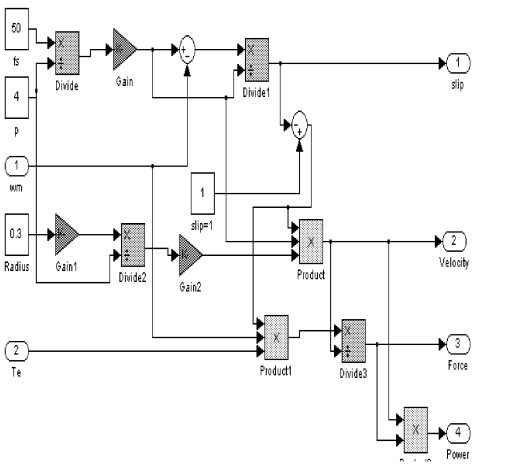

Figure 10 : Rotary to Linear motion converting unit using MATLAB/ simulink approach.

Third diagram illustrated on figure10 presents Linear motion converting unit, that consists of mathematical formulas (10)..(15) gives the relationship between rotary and linear motion.

Fourth diagram illustrated on figure11 presents speed change unit, where the motor speed is adjusted at three values : start at zero time, speed is adjusted at 900rpm, then, at t=0.15 second the speed falls to 600rpm, after that at t=0.4 second the speed rises to 700rpm.

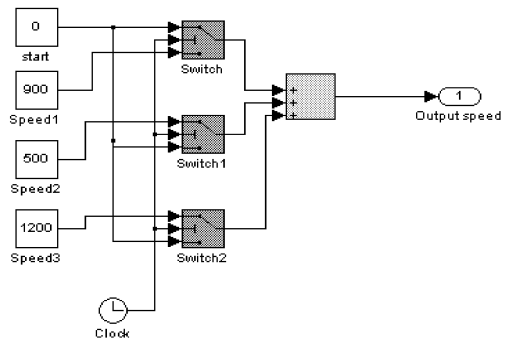

Figure 11 : Speed adjusting unit MATLAB/simulink

Simulation results

Taking into account the motor data parameters given in appendix (1) several simulation parameters could be described with purpose to discus and estimate these results. Hereinafter some of these results graphically illustrated as follow:

- The phase voltage : The applied phase voltage to the motor windings has a step form character with sinusoidal Pulse Width Modulation as well shown on the figure12.

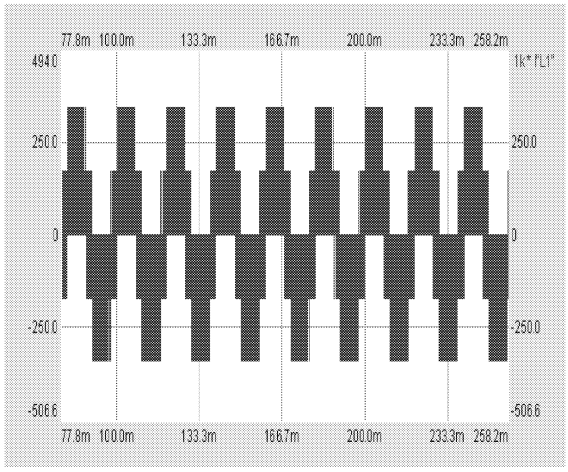

Figure 12 : Phase voltage applied to the motor windings.

- The motor slip at various speed values: as the motor start up, stabilized at speed 900rpm, falls to 600rpm, and then rises to 700rpm, therefore the slip varies consequently as well shown on figure13.

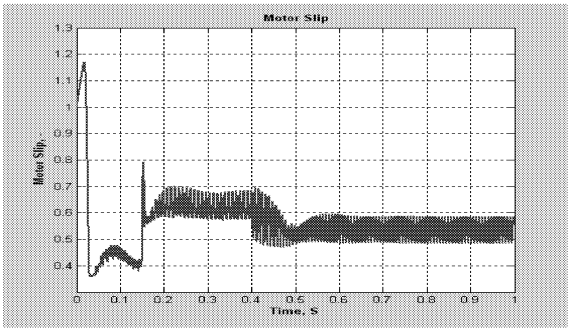

Figure 13 : Motor slip at various motor speed.

- The linear velocity: as motor angular frequency varies the obtained linear velocity varies in the same manner as well shown on figure 14, where the reference speed and actually obtained are illustrated. It's clearly shown that the actual speed slides the reference value.

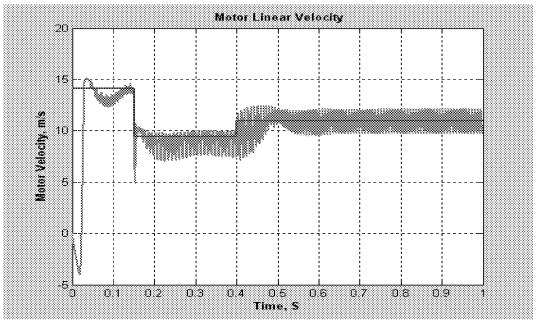

Figure 14 : Linear motor velocity at various speed values and constant loading.

- The phase current at various speed values: Figure15 illustrates the phase current at different speeds and constant loading, where it clearly shown that after the speed being stabilized the current returns back to it's rated value.

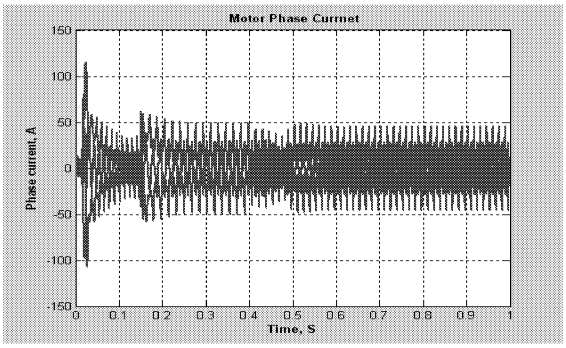

Figure 15 : Phase current at various speed values and constant loading.

- The motor linear force and output mechanical power at various speed values: as the motor start up, stabilized at speed of 900 rpm, and after that the

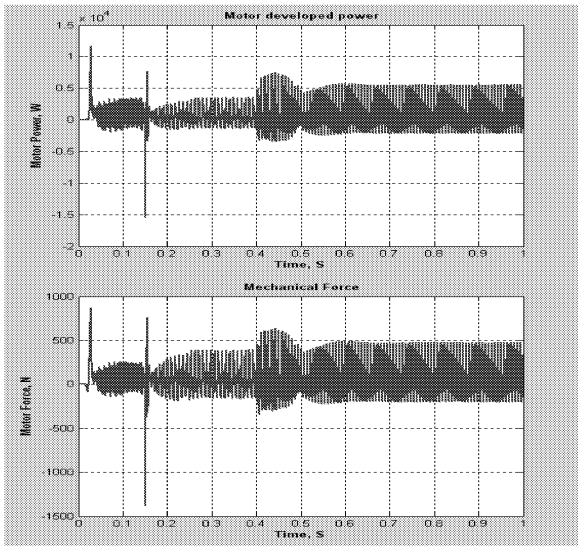

Figure 16 : Phase current at various speed values and constant loading.

speed falls to 600rpm, the obtained motor linear(thrust) force and output power varies consequently as well shown on figure16.

♦ Figure 17, presents slip, current and velocity at various speed values displayed in one coordinate system with purpose to link the processes occurs due to speed changes.

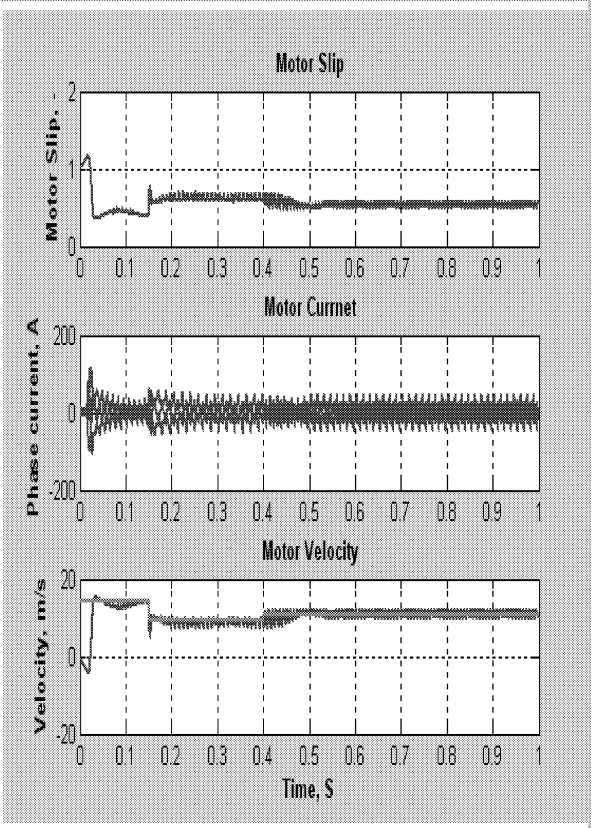

Figure 17 : Slip, current and velocity at various speed values and constant loading.

PROTOTYPE MODEL

Prototype model of linear three-phase induction motor has been designed as well shown on figure18, where the linear induction motor, electronic power switching circuit, PC interfacing circuit, and full montage of the system are illustrated with aluminum conducting plate fixed to the motor rails are illustrated. Experimental results should be taken after fully calibration of the motor subunits, and discussed in the next paper.

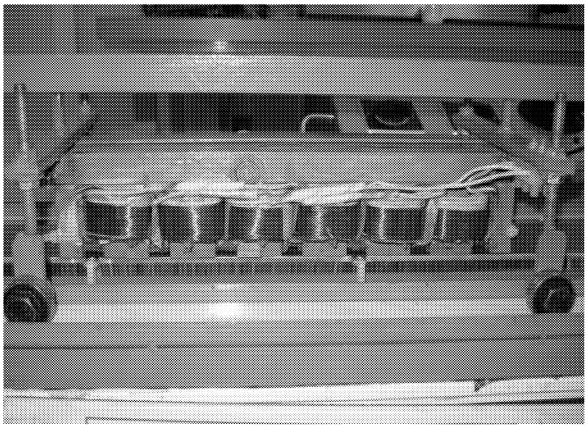

a- Stator windings

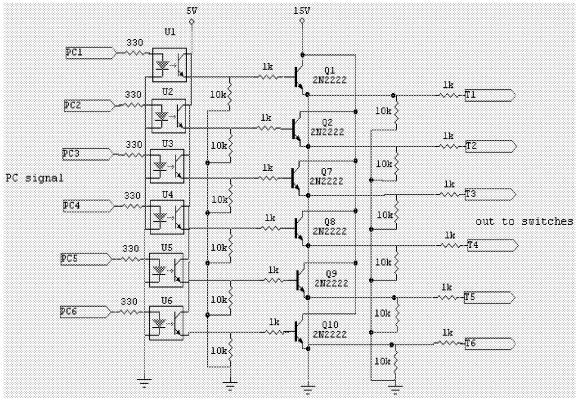

b- PC Interfacing circuit of the switching devices.

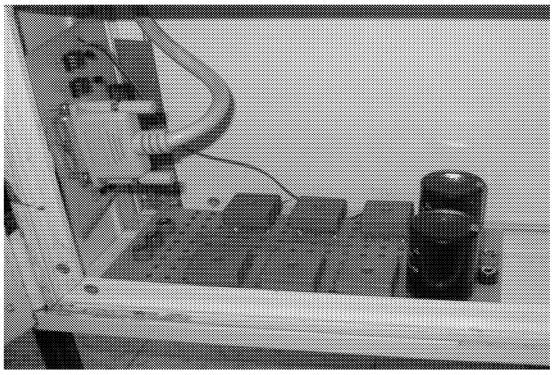

c- Switching transistor with DC link and PC interfacing.

Figure 18 : Some of designed machine's parts.

CONCLUSION

This paper has proposed the coupled method of VCM and MATLAB/Simulink. We have applied the proposed method to analyze behaviors of Linear induction motor parameters and their interaction with the control system, taking into consideration the loading approach, specific parameters of the motor, and the control approach.
It's shown that by applying MATLAB/ Simulink, the electromagnetic processes can be observed, estimated, and corrected in order to obtain optimized operation mode.
Furthermore applying MATLAB/simulink helps the designer to investigate, process the system parameters and apply the successful optimized motor design.
The obtained simulation results for control of Linear Induction Motor explained that the linear motor behaviors are similar to that of rotary type despite the stator and rotor construction.
Prototype model has been designed and implemented, where the experimental results should be obtained and discussed and compared with another approaches. Good results are expected to be obtained and published in future paper.

REFERENCES

[1] Takeo Ishikawa, David Mori, Seiji Hashimoto, and Michio Matsunami, "Analysis of a Brushless DC Motor by the Method Coupling MATLAB/Simulink and Finite Element Method", IEEJ Trans.IA, 124, pp.1283-1284 , 2003.

[2] D. Colombo, A Monti, and G. Secondo, "Mixed mode approach to system modeling in high performance drive design", IEE Conf. Publ, No. 468, pp317-320, 1999.

[3] Rakesh Parekh," VF Control of 3-Phase Induction Motor Using Space Vector Modulation", Microchip Technology Inc., 2005.

[4] MATLAB/Simulink Library, and Power System Blockset User's Guide, The MATH Works 2002.

[5] Boldea I., "Linear electric actuators and their control", 10th international conference on Power and Drives Association PEMC 2002, September 9-11,2002. pp 12-19.

[6] Budig P.K., " The application of Linear motor" , 3rd international conference on power Electronics and Motion Drives, 2000, Vol.3, pp 1336-1341.

[7] R. Krishnan," Switched reluctance motor drives: modeling, simulation, analysis design, and applications", CRC Press LLC, 2001.

[8] Rinkeviciene R., Petrovas, A.," New model of Linear Induction Motor", Electronika, ISSN 1392-1215, Vol. 2(51), 2004, pp 25-28.

[9] Do-Hyun Jang, Duck-Yong Yoon, IEEE transactions on Industry Applications, Vol.39, No. 2, March/April 2003.

[10] Linear Motors Installation and Operation Manual, Blador Electric Company, 2003, www.blador.com .

[11] Subhadra Devi Ganti, " Analaysis of Performance of Single- Phase Reluctance Linear Motor, Master Thesis, B.Techn., J.N.T.U, Hyderabad, India, 2005

[12] Jenkinas P.," Study the performances of Linear Motor with variable frequency", Master thesis, Vilnius TU, Vilnius, 2004.

[13] Mandrela E.A, " comparison of the performance of a linear reluctance oscillating motor operating under AC supply with one under DC supply", IEEE Trans. On energy Conversion, Vol.14, No.3, September, 1999.

[14] Murray A., Kettle P., Margio A., and Moynihan F.," Advances in DSP Based Motor Control Solutions, Proc. PCIM, pp.465-476, Nuerberg, 1997.

[15] Moynihan F., Kettle P., Murray A., Motion Control Group , Analog Devices, Intelligent Motion Proceedings 213, May, 1998.

[16] Strubin J.M., Venestra M., Rufer A., " Linear Induction Motor Demo-Track: a Tool for Renewed Motivation in Electrical Engineering", EPEL, Ecole Polytechnic Federal de Lausanne. CH. 10, 15 Lausanne, France .

Appendix (1): Main Motor Parameters

Parameter	Value
Line to Line Voltage V_{LL} , V	400
Nominal power Pout, kW	4
Source voltage frequency fs, Hz	50
Number of pole pairs, p	2
Rated rotor speed n, rpm	1430
Stator phase resistance R_S , Ω	1.405
Stator phase leakage inductance Lls, mH	5.839
Rotor phase resistance R_r , Ω	1.395
Rotor phase leakage inductance Llr, mH	5.839
Magnetizing inductance Lm, mH	17.22
Rotor inertia J, $Kg.m^2$	0.0131
Friction coefficient F, N.m.s	0.0131
Stator active length(flatted) ,mm	350
Reaction plate length, mm	1000
Active airgap, mm	2

ABOUT THE AUTHOR

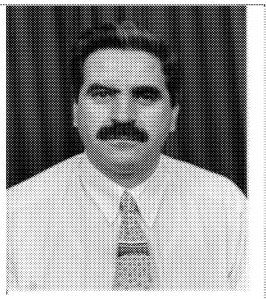

Sameer Hanna Khader was born in Jenien- Palestine 1962. He received a Master's degree in Electrical Engineering from the Institute of Electrical & Mechanical Engineering, Sofia-Bulgaria in 1988. And Ph.D. degree from TU- Sofia in 1993.

Since 1995 he worked in the college of Engineering and technology at Palestine Polytechnic University (PPU) as a Lecturer and researcher in the Field of Electrical Machines and Power Electronics .
Since 1999- till 2008, he occupied several admintrative psots (chairman, Dean, and Vice president for Academic Affairs) .
In 2008, he was awarded by the USAID-AMIDEAST for University Teaching Excellence in Palestine.
E-mail: sameer@ppu.edu

AN EVALUATION OF MPLS EFFICACY USING COLORED PETRI NET MODELS

Dmitry Zaitsev and Aleksey Sakun
Odessa National Academy of Telecommunications
Kovalska, 1, Odessa, 65029
Ukraine
E-mail: zsoftua@yahoo.com

KEYWORDS

IP-routing, MPLS, performance, colored Petri net, simulation

ABSTRACT

Colored Petri net models of Internet backbones' routers with classical IP-routing and label switching technology MPLS were constructed. On the example of the model for the fragment of European Internet backbone the comparative evaluation of IP-routing and MPLS performances was implemented. For construction and investigation of models CPN Tools was used. It was shown that the involving of MPLS technology allowed the increase of traffic in 1,7 times on average.

INTRODUCTION

The technology of label switching MPLS (RFC 3031; RFC 3032; RFC 3270) is aimed to the increase of the throughput either in global or corporative networks. In the networks with packets' switching the review of routing tables for each transmitting packet by each router requires considerable expenses of time and frequently bounds the general throughput of a network. The label assigned according to MPLS technology has smaller size than IP-address and constitutes in essence an identifier of a virtual channel which is processed with effective algorithms.

The construction of analytical models of MPLS networks is hampered due to the comparative sophistication of the technology with standard specifications counting approximately five hundreds pages. That is why simulation of MPLS networks becomes a prospective direction of research. Colored Petri nets of simulation system CPN Tools (Beaudouin-Lafon et al. 2001) constitutes a combination of Petri net graph (Jensen 1997) and programming language CPN ML used for the description of net elements' attributes. Recently CPN Tools was used for modeling of switched Ethernet (Zaitsev 2004a; Zaitsev 2004b; Zaitsev and Shmeleva 2006). The method of measuring fragments (Zaitsev 2004b) allows the evaluation of nontrivial characteristics of modeled object in the process of Petri net dynamics simulation. However, the construction of MPLS models requires a special study concerning its essential distinctions with classical switching technology.

The goal of the present work is the construction of typical models of IP and MPLS routers in the form of colored Petri nets as well as the comparative evaluation of IP-routing and MPLS performances on the example of European Internet backbone model.

AN OVERVIEW OF LABEL SWITCHING TECHNOLOGY MPLS

Recently about twenty IETF documents are devoted to the specification of MPLS standards. The basic documents are (RFC 3031; RFC 3032; RFC 3270), moreover, the peculiarities of the technology are defined more accurately in RFC with numbers 2547, 2702, 2917, 3035, 3063, 3346, 3353, 3429, 3443, 3468, 3469, 3471, 3472, 3473, 3474, 3496, 3564.

The standard terminology is introduced in (RFC 3031). It was claimed the necessity of networks' paths aggregation in FEC (Forwarding Equivalence Classes) and assigning a unique label to each class identifying its belonging to a definite FEC. The label is forwarded together with a packet and after its assignment is the only object that is analyzed by routers and used for delivery of the packet. Further, on next hops, the initial label may be replaced by new labels. Thus, the analysis of packet's header is executed only once by the first router in MPLS network. At the transmission of the packet the label constitutes an index in the label switching tables defining the next hop and new label. The standard stipulates also the stack of labels. For assigning of labels special Label Distribution Protocol (LDP) is specified; it describes the way neighboring Label Switching Routers (LSR) are exchanging by routing information and constructing their label switching tables.

The format of the label and the stack of labels as well as the procedures of labels' processing by LSR are described in (RFC 3032). The label has the length of 32 bits and possesses the format represented in Figure 1. The Label Value occupies 20 bits, Time to Live (TTL) takes 8 bits, bit 23 is intended for the creation of labels' stack (it is equal to unit at the bottom of stack), bits 20-22 are reserved for experimental usage.

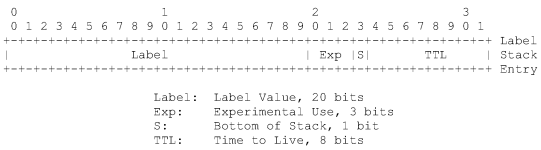

Figures 1: Standard Format of the Label

Notice that, routers situated at the border of MPLS networks are named Label Edge Router (LER); an additional classification divides them into ingress and egress also.

THE MODEL OF IP-ROUTER

Let's remind that colored Petri net (Jensen 1997) of simulation system CPN Tools (Beaudouin-Lafon et al. 2001) constitutes a combination of Petri net graph and programming language CPN ML used for description of net elements' attributes. A token of colored net constitutes an object of abstract data type named by color set.

In the present work the static routing is considered. The model of IP-router port is represented in Figure 2. The model of a concrete router is assembled by cloning of port's model in the required number of copies. As distinct from early studied models of Ethernet switches (Zaitsev 2004a; Zaitsev 2004b; Zaitsev and Shmeleva 2006), the presented model of router uses complete specifications of IP-addresses for hosts and networks. The processing of IP-addresses has required extra functions for determining the belonging of IP-address to a definite subnet listed in the routing table.

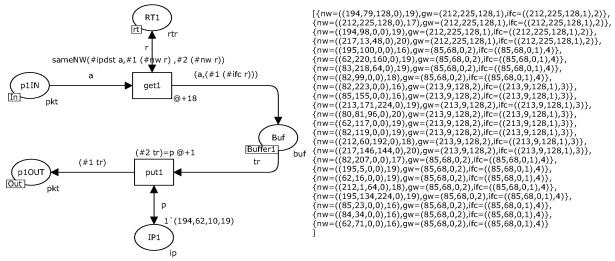

Figures 2: Model of IP-router Port

Four basic types of tokens are used in the model: type **pkt** describes packets transmitting in the network, type **rtr** – record of routing table, type **buf** – routed packets containing IP-address of the destination port, type **ip** – IP-addresses. The function **SameNW** determines the belonging of IP-address to IP-network. Descriptions of types, variables and functions are represented in Figure 3. Fusion places **rt** and **Buffer1** provides the usage of the same common routing table and output buffer by all the ports of the router.

Ports of the router work in full-duplex mode. A packet is extracted from input channel **p1IN** of a port by transition **get1** and is situated into internal buffer **Buf** of the router while the function **sameNW** determines IP-address of destination interface according to the routing table represented by place **RT1**. Transition **put1** extracts packet from the buffer according to IP-address of interface stored into place **IP1** and puts it into place **p1OUT** modeling the output channel of the port.

```
colset ip=product INT*INT*INT*INT timed; colset mask=INT;
colset nwt=product ip*mask timed;        colset b=INT timed;
colset pkt=record ipsrc:ip*ipdst:ip*data:b timed;
colset nif=int; colset interf=product ip*nif;
colset gw=ip; colset buf=product pkt*ip;
colset rtr=record nw:nwt *gw:ip*ifc:interf  timed ;
colset lpkt=record label:INT*ipsrc:ip*ipdst:ip*data:b timed;
colset rtrs=list rtr timed;
colset lt=record ininterf:INT*L1:INT*outinterf:INT*L2:INT;
colset aux=INT timed;
fun pow(x,0)=1 | pow(x,y)=pow(x,y-1)*x;
colset buffer=product lpkt*INT timed;
fun sameNW(a1:ip,a2:ip,m:INT)=if (32-m) < 8 then ( if ((#1 a1) =
(#1 a2)) andalso ((#2 a1) = (#2 a2)) andalso ((#3 a1) =(#3 a2))
andalso ((((#4 a1) div pow(2,(32-m)))*(pow(2,(32-m)))) = (#4 a2))
then true else false ) else if (32-m)<16 then ( if ((#1 a1) = (#1
a2)) andalso ((#2 a1) = (#2 a2)) andalso ((((#3 a1) div
pow(2,((32-m)-8))) * pow(2,((32-m)-8))) = (#3 a2)) then true else
false) else  if (32-m)<24 then  (if ((#1 a1)=(#1 a2)) andalso
((((#2 a1) div pow(2,((32-m)-16)))*pow(2,((32-m)-16)))=(#2 a2))
then true else false) else  if ((((#1 a1) div pow(2,((32-m)-
24)))*pow(2,((32-m)-24)))=(#1 a2)) then true else false;
var i,c,k:INT;      var q:nwt;                    var r:rtr;
var p,src,dst:ip;   var a:pkt;                    var tr:buf;
var v:aux;          var la:lpkt;
```

Figures 3: Descriptions of Types, Variables and Functions of the Model

THE MODEL OF MPLS-ROUTER

The standard of MPLS technology distinguishes two different types of routers: LSR-routers are situated inside MPLS network and realize labels' switching only; LER-routers are situated at the border of MPLS network and are used for docking with networks of other standards. The main difference consists in that LER-router calculates the initial label of a packet on the base of routing information, for instance, on the base of IP-routing tables for IP-networks. As a rule, border routers constitute the combination of LSR/LER types. For structuring of models the typical submodels of LSR and LER ports are constructed. Models of concrete routers are assembled by cloning of ports' models of required type: LSR at docking with MPLS network and LER at docking with IP-network. In the present work the algorithm LDP of FEC assigning isn't modeled; there were used FECs of labels obtained as the result of its application to the chosen network.

The typical model of LSR port of router is represented in Figure 4. The main difference from the model of IP-router port (Figure 2) consists in that the label switching table is used for forwarding of a packet. Moreover, the replacement of labels is modeled and for identification of interfaces their numbers are used. For an input packet on its label the corresponding record of labels' switching table **Ltable1** is determined. Output arc of transition **get1** replaces input label **L1** by new label **L2** and assigns the number of destination interface for forwarding of the packet. Data type **lpkt** describes packet supplied with the label, type **lt** – records of labels' switching table, type **buffer** – records of the internal buffer of packets. Notice that, in the present work the stack of labels stipulated by the standard (RFC 3031; RFC 3032) isn't modeled and only the replacement of labels is executed.

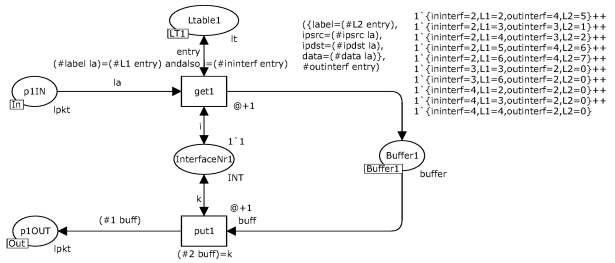

Figures 4: Model of LSR Port of MPLS Router

The typical model of LER port of router is represented in Figure 5. The port implements the initial assignment of labels according to aggregated paths of network. By the appearance the model looks like the combination of IP and LSR ports; both routing table **RT2** and labels' switching table **Ltable2** are used. The difference of routing table consists in that it contains the value of the initial label assigning to the packet obtained as the result of LDP algorithm execution. Place **Buffer2** constitutes the internal buffer of packets of router; place **Buf1** is intended as a temporary storage of packets after initial assignment of labels. Notice that, the packet is put into the output channel of port **p2OUT** without the label.

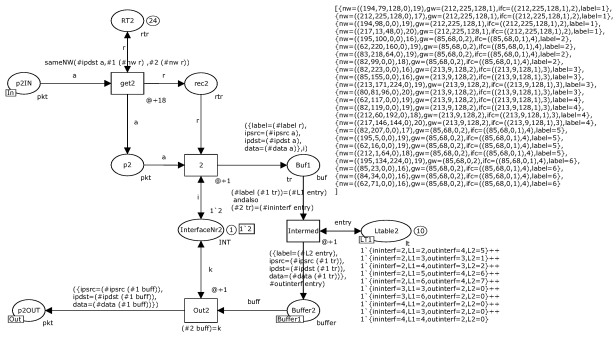

Figures 5: Model of LER Port of MPLS Router

THE MODEL OF THE EUROPEAN INTERNET BACKBONE

For evaluation of efficacy of MPLS technology the models of a fragment of European Internet backbone were constructed on the structural scheme of network represented in Figure 6. Notice that, in the scheme (Figure 6) terminal networks containing IP-addresses in the address space of corresponding countries are pointed out; totally 24 IP-networks are used. The backbone is constituted by 7 routers from which 6 routers (R1-R3, R5-R7) are of LER/LSR type and one router (R4) is of LSR type.

The main page of the model is represented in Figure 7. It is constructed on the structural scheme of the network (Figure 6). Two kinds of models were investigated: IP-routing obtained at substitution of **Router1-Router7** by submodels of IP-routers; MPLS-routing obtained at substitution of **Router1-Router7** by submodels of LER/LSR-routers described in the previous sections. For modeling of realistic traffic special models of terminal networks **Terminal1-Terminal6** were constructed; they are described in the next section. Transitions **Transmit*** model the transmitting of packets in the channels without loss of packets. Fusion place **Trafic** helps for evaluation of traffic; it is described in the next sections. Let's consider the peculiarities of IP and MPLS routing models construction.

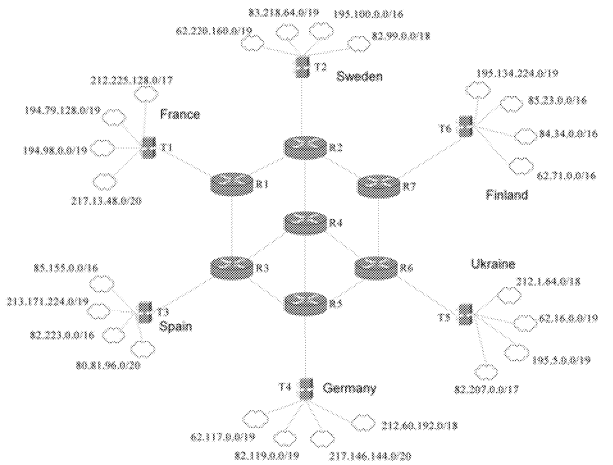

Figures 6: Scheme of Fragment of European Internet Backbone

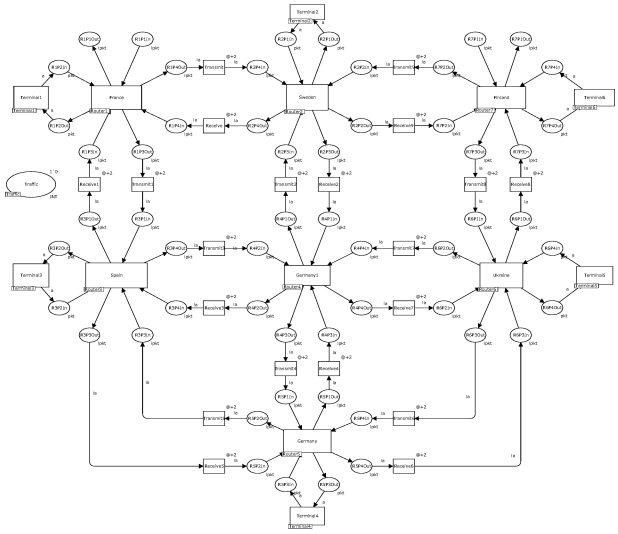

Figures 7: Model of Fragment of European Internet Backbone

For IP-routing static routing tables are used containing 24 records for each router; notice that, the tables of routers' are distinguished in the fields of gateways' addresses and interfaces' numbers. An example of routing table for **Router1** is shown in Figure 2.

For MPLS-routing aggregated network paths were constructed that may be obtained as the result of LDP algorithm execution. In Table 1 the basic paths of packets' delivery are listed for each pair of terminal networks; in the brackets the values of assigned labels are written.

For instance, the path of packets sent from network T1 to network T5 is defined by the sequence of labels 6-15-6. On

the Table 1 the initial marking of places **Tlebel*** and **RT*** of routers' submodels was constructed representing the labels' switching tables and labels' assignment tables correspondingly. In Figures 4, 5 the tables for router **Router1** were shown.

Table 1: Table of Labels' Assignment

	T1	T2	T3	T4	T5	T6
T1	0	R1(5) -R2	R1(1) -R3	R1(2) -R3(6) –R5	R1(6) -R2(15) –R4(6) -R6	R1(7) -R2(8) –R7
T2	R2(2) -R1	0	R2(2)-R4(4) -R3	R2(3) -R4(10) –R5	R2(1) -R4(9) –R6	R2(3) -R7
T3	R3(3) -R1	R3(1) -R4(9) –R2	0	R3(3) -R5	R3(2) -R4(10) –R6	R3(3) -R4(4) –R2(6) -R7
T4	R5(5) -R3(6) –R1	R5(11) -R4(13) –R2	R5(4) -R3	0	R5(16) -R6	R5(8) -R6(10) –R7
T5	R6(7) -R4(5) –R2(3) -R1	R6(12) -R4(10) –R2	R6(11) -R4(5) –R3	R6(10) -R5	0	R6(2) -R7
T6	R7(5) -R2(4) –R1	R7(4) -R2	R7(7) -R2(8) –R4(6) -R3	R7(8) -R6(5) –R5	R7(9) -R6	0

THE MODELS OF TERMINAL NETWORKS

The model of the realistic traffic is a significant part providing the total adequacy of constructed models to real-life processes. Colored Petri nets provide wide opportunities for description of streaming traffic with various types of random magnitudes distribution (uniform, Poisson, Erlanger) as well as protocols of interaction in client-server systems (Zaitsev 2004a; Zaitsev 2004b; Zaitsev and Shmeleva 2006). In the present work the streaming traffic was modeled. A terminal network generates periodically packets with a random address of sender and receiver. The address of sender is in the range of own IP-networks and the receiver address – in the range of addresses of the entire valid networks for modeled fragment of Internet.

Model of terminal network **Terminal1** is represented in Figure 8. The processing of input packets is modeled by the simple absorption of them using transition **Counter** in the upper-left part of the model while the calculation of the number of delivered packets is implemented with fusion place **Traffic** used for accumulation of statistical information. The generating of packets is based on the pair of places **ownNW** and **allNW** that contain IP-addresses and masks of own IP-networks and all the networks of modeled fragment of Internet correspondingly. Addresses are extracted into places **ipsrc** and **ipdst**; notice that, the usage of extracted addresses is blocked with the duration of time written on output arcs of transitions **IpGenerate1**, **IpGenerate2**. The most sophisticated action is the generating of a random IP-address on a given IP-network's address and mask. For this purpose the code segment of transitions **IpGenerate1**, **IpGenerate2** represented in the bottom of the picture is constructed. Circulation of the token in the sequence of places **1**, **2**, **3** provides the cyclic repetition of actions. Place **Clock** serves for the periodical launching of packets' generating; the time delay on the input arc of place **Clock** defines the period of the generating. Place **Data** models the content of packets. The creation of output packet is implemented by transition **Create** via uniting addresses of sender, receiver and data.

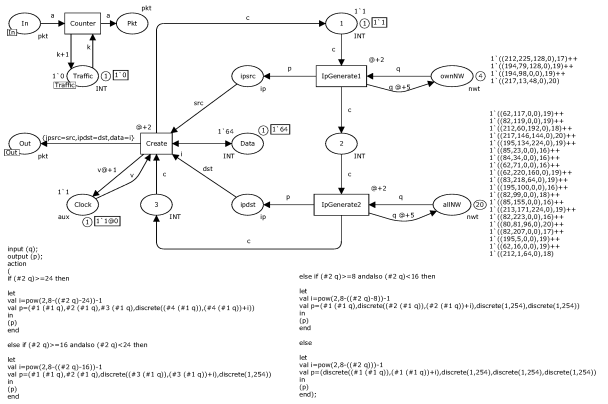

Figures 8: Model of Terminal Network

COMPARATIVE EVALUATION OF IP-ROUTING AND MPLS

For the debugging of the model the step-by-step mode of simulation of CPN Tools (Beaudouin-Lafon et al. 2001) was used; the tracing of separate packets transmitting through network for the chosen pairs of terminal networks was implemented. For analysis of MPLS efficacy the speed modeling on the protracted intervals of time was used. The traffic was measured under the condition of peak load provided by terminal networks. Fusion place **Traffic** for traffic measuring is represented in submodels of terminal networks (Figure 8) as well as in the main page of the model (Figure 7) for the convenience of the estimating.

The topics of times' scaling were studied in (Zaitsev 2004b; Zaitsev and Shmeleva 2006). In the present work the unit of model time equaling to 0,65 ns was chosen providing the modeling of highly productive routers; the time of labels' switching was chosen as 50% of router's time that corresponds to more than twice decrease of tables' length. Three basic types of backbone routers were studied; their characteristics are represented in Table 2.

Table 2: Characteristics of Routers

Router	Throughput (packets/s)	Time of packet's processing, ns	Model time of packet's processing
Cisco 12000	25 000 000	40	60
Juniper T320	385 000 000	2,6	4
Juniper T640	770 000 000	1,3	2

On the results of traffic measurement for protracted intervals of model time the graph of comparative efficacy of IP-routing and MPLS represented in Figure 9 was obtained. Moreover, at traffic's measurement on protracted intervals of model time the diagram of network's throughput for various backbone routers represented in Figure 10 was created.

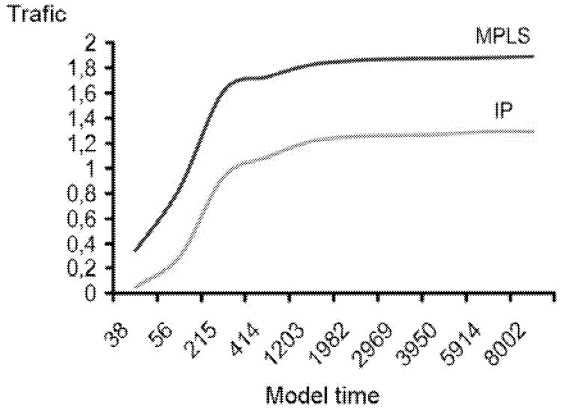

Figures 9: Comparative Evaluation of Efficacy for IP-Routing and MPLS

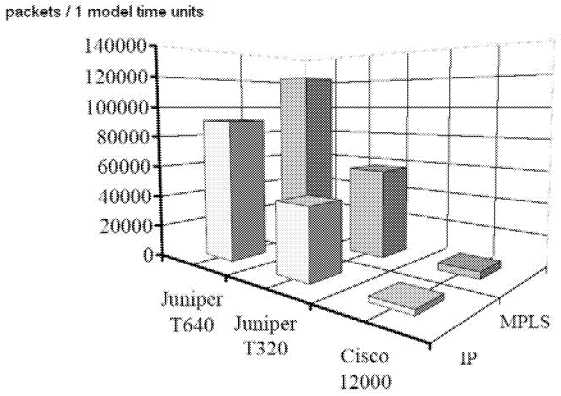

Figures 10: Diagram of Network's Throughput for Various Routers

The analysis of simulation results allows the conclusion that MPLS technology is in 1,7 times more effective on average than classical IP-routing. Notice that, the results were obtained for comparatively small fragment of Internet with the size of routing tables equaling to 24 records. For real-life backbones of Internet where routing tables count thousands of IP-networks the more considerable growth of throughput is foreseen.

CONCLUSIONS

Thus, in the present work the models of IP and MPLS routers were constructed in the form of colored Petri nets in the environment of simulation system CPN Tools. The evaluation of efficacy of label switching technology MPLS was implemented on the example of the model for a fragment of European Internet backbone. It was shown that even for comparatively small networks numbering dozens of nodes the increase of network's throughput in 1,7 times on average was obtained. Constructed typical models of routers may be applied for modeling of an arbitrary MPLS and IP network given by a structural scheme, hardware and software characteristics.

REFERENCES

Beaudouin-Lafon M. et al. 2001. "CPN Tools: A Tool for Editing and Simulating Coloured Petri Nets". *LNCS 2031: Tools and Algorithms for the Construction and Analysis of Systems*, 574-580.

FRC 3031. 2001. *Multiprotocol Label Switching Architecture.* IETF, Rosen, E. et al.

RFC 3032. 2001. *MPLS Label Stack Encoding.* IETF, Rosen, E., et al.

RFC 3270. 2002. *Multi-Protocol Label Switching (MPLS) Support of Differentiated Services.* IETF, Le Faucheur, F. et al.

Jensen, K. 1997. *Colored Petri Nets – Basic Concepts, Analysis Methods and Practical Use.* Springer-Verlag, Vol. 1-3.

Zaitsev, D.A. 2004a. "Switched LAN simulation by colored Petri nets". *Mathematics and Computers in Simulation* 65, No. 3, 245-249.

Zaitsev, D.A. 2004b. "An Evaluation of Network Response Time using a Coloured Petri Net Model of Switched LAN". In *Proceedings of Fifth Workshop and Tutorial on Practical Use of Coloured Petri Nets and the CPN Tools* (Aarhus, Denmark, Oct. 8-11), 157-167.

Zaitsev, D.A. and Shmeleva, T.R. 2006. "Switched Ethernet Response Time Evaluation via Colored Petri Net Model". In *Proceedings of International Middle Eastern Multiconference on Simulation and Modelling* (Alexandria, Egypt, Aug. 28-30), 68-77.

MODELLING OF THE BIODYNAMIC RESPONSES TO WHOLE-BODY VERTICAL EXCITATION

Naser Nawayseh
Mechanical Engineering Department,
College of Engineering, Dhofar University,
PO Box 2509, Postal Code 211
Salalah, Oman
Email: nnawayseh@yahoo.co.uk

KEYWORD
Model, biodynamics, vibration

ABSTRACT

Modelling of the dynamic responses of humans to vibration is widely reported in the literature with more focus on responses in the direction of vibration excitation than responses in other directions. The aim of this paper is to develop a model that can predict the biodynamic responses in both the direction of excitation and in other directions during whole-body vertical excitation. The apparent mass was used to represent biodynamic responses in the direction of excitation and the fore-and-aft cross-axis apparent mass was used to represent the biodynamic response in the fore-and-aft direction. A series of lumped parameter linear models with rotational capabilities were developed to predict the vertical apparent mass and the fore-and-aft cross-axis apparent mass measured on the seat with vertical excitation. The final model suggested that three degrees-of-freedom (rotational, vertical and fore-and-aft) were needed to predict the vertical apparent mass and the fore-and-aft cross-axis apparent mass. The final model also suggested a fore-and-aft sliding motion (or possibly deformation of tissue in contact with the seat) of the human body on the seat when exposed to vertical excitation.

INTRODUCTION

Experimental Biodynamic studies suggest that the seated human body moves in two dimensions when exposed to whole-body vertical excitation (Nawayseh and Griffin 2003) or to whole-body fore-and-aft excitation (Nawayseh and Griffin 2005). The fore-and-aft forces on the seat during vertical vibration and the vertical forces measured on the seat during fore-and-aft vibration were of considerable values and should be taken into account when modelling the responses of humans to vibration.

The two dimensional motion might suggest axial as well as shear forces applied to the spine when the body is exposed to vertical vibration and fore-and-aft vibration (Fritz 2000). Attenuating the cross-axis movement as well as attenuating the movement in the direction of vibration should help in reducing the discomfort, interference with activities and the effects on health associated with exposure to vibration.

Previous, single degree-of-freedom and multi degree-of-freedom models have focused on modelling the force response in the direction of excitation (Suggs et al. 1969; Fairley and Griffin 1989; Boileau and Rakheja 1998; Matsumoto and Griffin 2003). A few models have taken into account, using transmissibility measurements, the cross-axis movements of the upper body associated with vertical vibration (Kitazaki and Griffin 1997; Matsumoto and Griffin 2001). However, no known work has attempted to include in a model the cross-axis forces on the seat induced by vertical or fore-and-aft excitation.

In this paper, mathematical models taking into account the cross-axis forces measured on the seat are developed. A series of models have been investigated to obtain prediction for the responses measured experimentally during vertical vibration. It was hypothesised that three degrees of freedom will be necessary to predict both the vertical forces on the seat (represented as vertical apparent mass) and the fore-and-aft forces on the seat (represented as fore-and-aft cross-axis apparent mass).

DEVELOPMENT OF THE MODELS

Five alternative linear lumped parameter models have been investigated in an attempt to obtain good predictions for the magnitudes and phases of the vertical apparent mass (complex ratio between vertical force and vertical acceleration on the seat) and the fore-and-aft cross-axis apparent mass (complex ratio between fore-and-aft force and vertical acceleration on the seat). Two postures have been investigated, a feet hanging posture (feet unsupported) and an average thigh contact posture (feet supported on an adjustable footrest with the upper legs horizontal and lower legs vertical).

The five investigated models are shown in Figure 1.

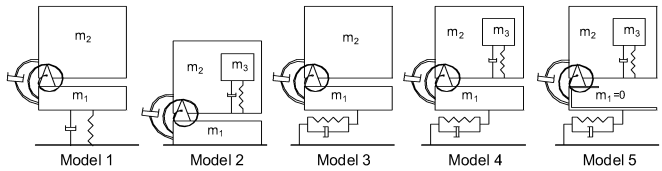

Figure 1 Alternative lumped parameter models.

Model 1: Model 1 is two degree-of-freedom model with vertical and pitch degrees of freedom.
Model 2: Two degree-of-freedom model. Initially, the input to the vertical degree of freedom is the pitching motion of mass 2. The centres of gravity of mass 2 and mass 3 lie on the same vertical line and mass 3 is restricted to vertical motion.
Model 3: Two degree-of-freedom model. The pitching motion of mass 2 is expected to induce fore-and-aft motion in mass 1 and mass 2 and, hence, a horizontal spring and a horizontal damper were installed beneath mass 1 to represent the fore-and-aft motion. The horizontal degree-of-freedom could be considered to represent any shear deformation in the tissue beneath the pelvis.
Model 4: Three degree-of-freedom model. This model is a combination of Model 2 and Model 3.
Model 5: The same as Model 4 but with mass 1 set to zero.

The models parameters are described as follows:
m_1, m_2 and m_3 are the masses of mass 1, mass 2 and mass 3, respectively.
J_2 is the moment of inertia of mass 2 about the connection point.
k_{1z} and c_{1z} are the vertical stiffness and damping beneath mass 1 in Model 1.
k_{1x} and c_{1x} are the fore-and-aft stiffness and damping beneath mass 1 in Model 3, Model 4 and Model 5.
k_2 and c_2 are the rotational stiffness and damping of mass 2.
k_{3z} and c_{3z} are the vertical stiffness and damping beneath mass 3 in Model 2, Model 4 and Model 5.
e is the distance between the centre of gravity of mass 2 and the connection point.
α is the angle that e has with the horizontal when the model is in equilibrium.

MATHEMATICAL EQUATIONS OF THE MODELS

The equations of motion of each model were derived using Lagrange's Equations. As an example, the equations of motion of Model 5 are (the notations are as above and as in Figure 1. θ is the angular displacement of mass 2):

$$m_3\frac{d^2z_3}{dt^2}+c_{3z}(\frac{dz_3}{dt}-\frac{dz_b}{dt}+e\cos\alpha\frac{d\theta}{dt})+k_{3z}(z_3-z_b+e\theta\cos\alpha)=0$$

$$m_1\frac{d^2x_1}{dt^2}+m_2(\frac{d^2x_1}{dt^2}+e\sin\alpha\frac{d^2\theta}{dt^2})+m_3\frac{d^2x_1}{dt^2}+c_{1x}\frac{dx_1}{dt}+k_{1x}x_1=0$$

$$m_2e\cos\alpha\frac{d^2z_b}{dt^2}+m_2e\sin\alpha\frac{d^2x_1}{dt^2}+J_2\frac{d^2\theta}{dt^2}+c_{3z}e\cos\alpha(\frac{dz_3}{dt}-\frac{dz_b}{dt}+e\cos\alpha\frac{d\theta}{dt})+$$
$$k_{3z}e\cos\alpha(z_3-z_b+e\theta\cos\alpha)+c_2\frac{d\theta}{dt}+k_2\theta=0$$

The vertical and fore-and-aft forces can be written as:

$$f_z(t)=m_1\frac{d^2z_b}{dt^2}+m_2(\frac{d^2z_b}{dt^2}+e\cos\alpha\frac{d^2\theta}{dt^2})+m_3\frac{d^2z_3}{dt^2}$$

$$f_x(t)=(m_1+m_2+m_3)\frac{d^2x_1}{dt^2}+m_2e\sin\alpha\frac{d^2\theta}{dt^2}$$

The prediction and all models parameters (inertia properties, stiffness, damping coefficients, and location of the centre of gravity of mass 2) were optimised using the Nelder Meade simplex search method provided in MATLAB. The parameters of the models were obtained by comparing moduli and phases of both the vertical apparent mass and the fore-and-aft cross-axis apparent mass obtained experimentally (Nawayseh and Griffin 2003) at 1.25 ms^{-2} r.m.s. in the frequency range 1 to 10 Hz with those obtained from the models as shown in the error function below.

$$\text{err}=\sum_{i=1}^{N}(M_p-M_m)_i^2+F_1*\sum_{i=1}^{N}(CM_p-CM_m)_i^2$$
$$+F_2*\sum_{i=1}^{N}(Ph_p-Ph_m)_i^2+F_3*\sum_{i=1}^{N}(CPh_p-CPh_m)_i^2$$

where,

M_p and CM_p are the predicted vertical apparent mass and fore-and-aft cross-axis apparent mass, respectively.
M_m and CM_m are the measured vertical apparent mass and fore-and-aft cross-axis apparent mass, respectively.
Ph_p and CPh_p are the predicted phases of the apparent mass and cross-axis apparent mass, respectively.
Ph_m and CPh_m are the measured phases of the apparent mass and cross-axis apparent mass, respectively.
F_1, F_2 and F_3 are arbitrary factors used to improve the prediction

RESULTS

MODELLING OF MEDIAN DATA

Starting from Model 1, the models were developed in stages until reasonable agreements between the experimental and theoretical results in the magnitudes and phases of the vertical apparent mass and the fore-and-aft cross-axis apparent mass were achieved. The prediction of the median data of 12 subjects will be shown for all models but the parameters of the final model only were analysed.

In the first stage, Model 1 was used with optimisation of all the model parameters. Although this model gave good prediction of the magnitudes of the median apparent mass and the median cross-axis apparent mass for both postures, the model did not give good prediction for the phases of either the apparent mass or the cross-axis apparent mass in either the feet hanging posture (Figure 2) or the average thigh contact posture (Figure 3).

In the second stage, the vertical degree of freedom beneath mass 1 was removed while a vertical degree of freedom and mass 3 were added as shown in Model 2 (Figure 1). The vertical degree of freedom beneath mass 1 in Model 1 was removed in Model 2 since a previous study (Wei and Griffin 1998) showed that a model with two degrees of freedom was sufficient to provide reasonable prediction for the vertical apparent mass. The response of Model 2 showed good agreement with the vertical apparent mass magnitude and phase but not with the cross-axis apparent mass (Figures 2 and Figure 3). In models with rotational degrees-of-freedom, Matsumoto and Griffin (2001) found that adding a vertical degree of freedom (representing the viscera) above a pitching mass (representing the pelvis) in an arrangement similar to that of Model 2 was necessary to improve the quality of the model prediction.

In the third stage, the vertical degree of freedom beneath mass 3 was replaced by a fore-and-aft degree of freedom beneath mass 1 in an attempt to improve the prediction in the fore-and-aft direction. The prediction showed good agreement with the vertical apparent mass but not with the fore-and-aft cross-axis apparent mass (Figures 2 and Figure 3). Although this model is not a mechanistic model, there is evidence in previous mechanistic models that some mechanisms involving fore-and-aft motion of the pelvis and shear deformation of the buttocks tissue, together with bending modes in the upper body, contribute to the principal mode in the vertical apparent mass (4.9 Hz) and to a mode at a higher frequency (5.6 Hz; Kitazaki and Griffin 1997). The interactions between these two modes in Model 3 might have helped in improving the prediction in the vertical apparent mass magnitude and phase.

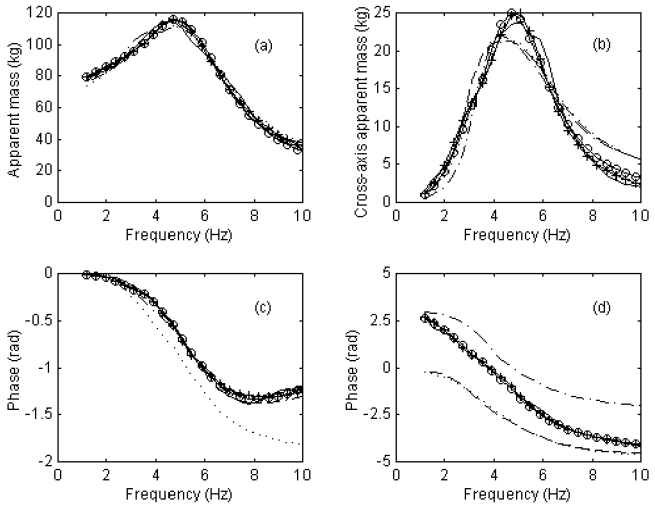

Figure 2 Median responses obtained experimentally and calculated using 5 models in the feet hanging posture. (a) and (c), vertical apparent mass; (b) and (d) fore-and-aft cross-axis apparent mass. ——, experimentally;····· , Model 1; –·–·–, Model 2; – – – –, Model 3; —+—, Model 4; —o—, Model 5.

In the fourth stage, it was clear that a third degree of freedom was necessary to improve the prediction of the fore-and-aft cross-axis apparent mass, as a two degree of freedom model will be sufficient only to give a good prediction for the vertical apparent mass. It was then decided to re-insert the degree of freedom beneath mass 3 (see Model 4, Figure 1). At this stage, good agreement between the experimental and theoretical responses was achieved in both the vertical apparent mass and the cross-axis apparent mass. However, the value of m_1 was always zero in Model 4.

In the final stage, m_1 in Model 4 was set to zero producing Model 5. It seems that m_1 had no effect on the response of the final model, as shown in Figures 2 and Figure 3. The final model (i.e. Model 5) is shown in Figure 4 with all the parameters.

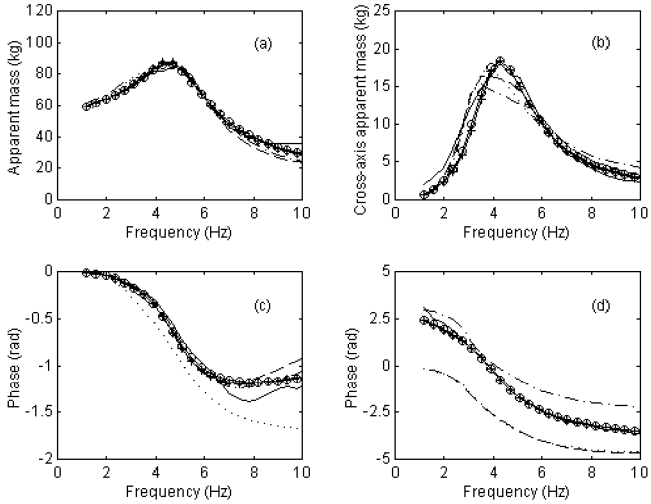

Figure 3 Median responses obtained experimentally and calculated using 5 models in the average thigh contact posture. (a) and (c), vertical apparent mass; (b) and (d) fore-and-aft cross-axis apparent mass. ——, experimentally;····· , Model 1; –·–·–, Model 2; – – – –, Model 3; —+—, Model 4; —o—, Model 5.

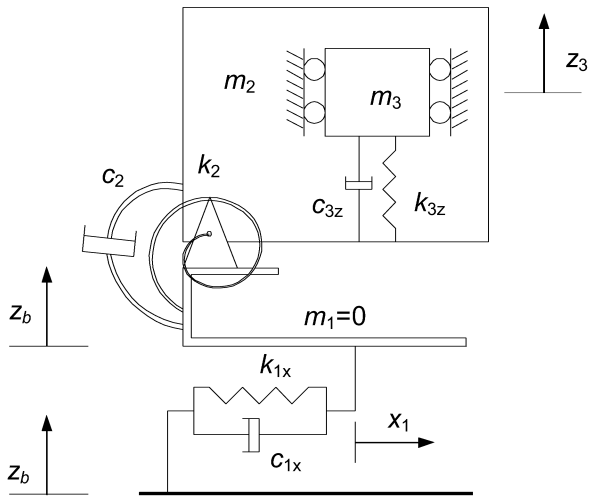

Figure 4 Model 5.

MODELLING OF INDIVIDUAL DATA

Model 5 was used to predict the magnitudes and phases of both the vertical apparent masses and fore-and-aft cross-axis apparent masses of 12 subjects sitting in the feet hanging posture and the average thigh contact posture. The calculated and the measured responses were in good agreement as shown in Figure 5 to Figure 8 in the feet hanging posture and in Figure 9 to Figure 12 in the average thigh contact posture. The optimised parameters obtained for each individual from Model 5 are shown in Table 1 for the feet hanging posture and in Table 2 for the average thigh contact posture.

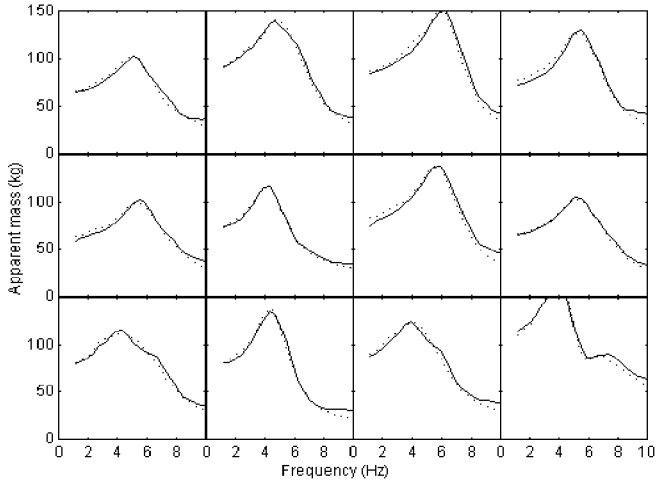

Figure 5 Vertical apparent masses of 12 subjects in the feet hanging posture: ———, experiment;·····, model.

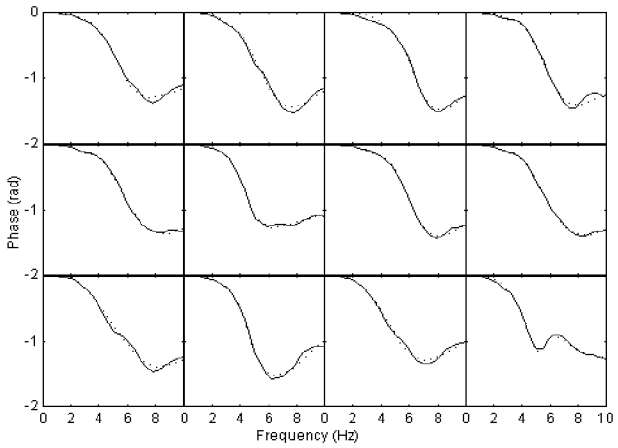

Figure 6 Vertical apparent masses phase of 12 subjects in the feet hanging posture: ———, experiment;·····, model.

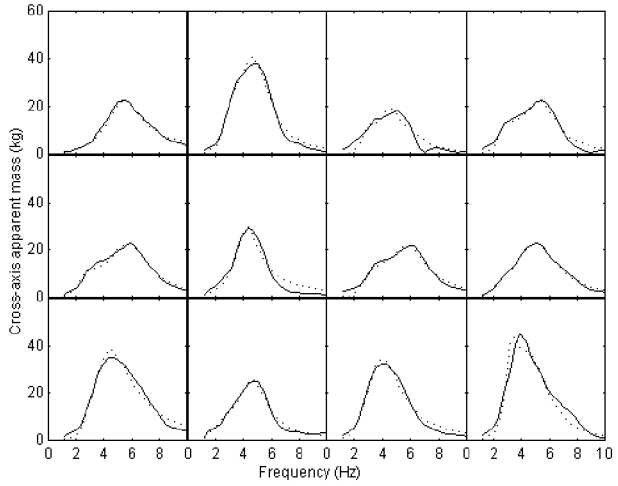

Figure 7 Fore-and-aft cross-axis apparent masses of 12 subjects in the feet hanging posture: ———, experiment; ·····, model.

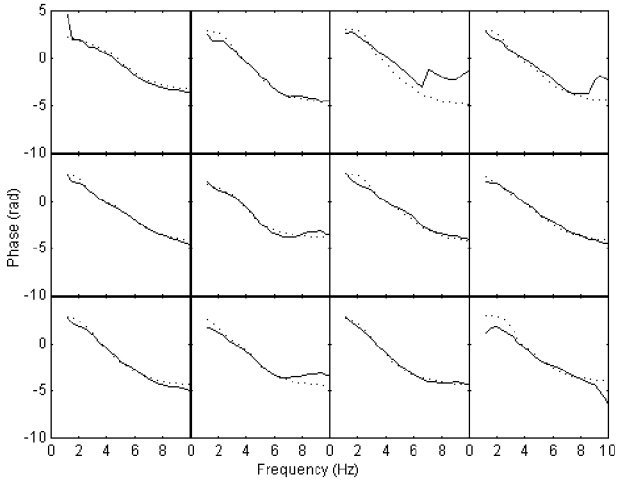

Figure 8 Fore-and-aft cross-axis apparent masses phase of 12 subjects in the feet hanging posture: ———, experiment;·····, model.

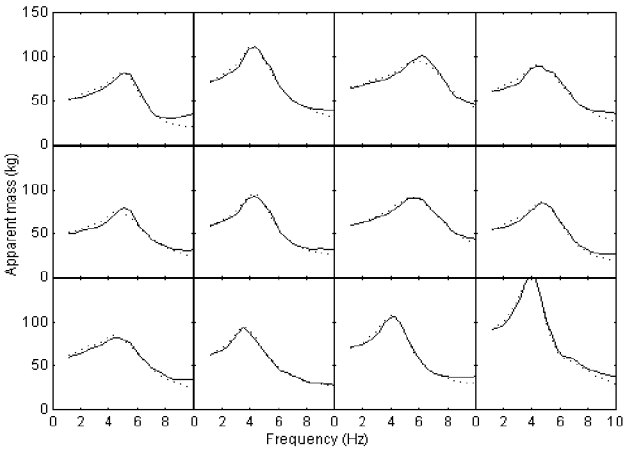

Figure 9 Vertical apparent masses of 12 subjects in the average thigh contact posture: ———, experiment; ·····, model.

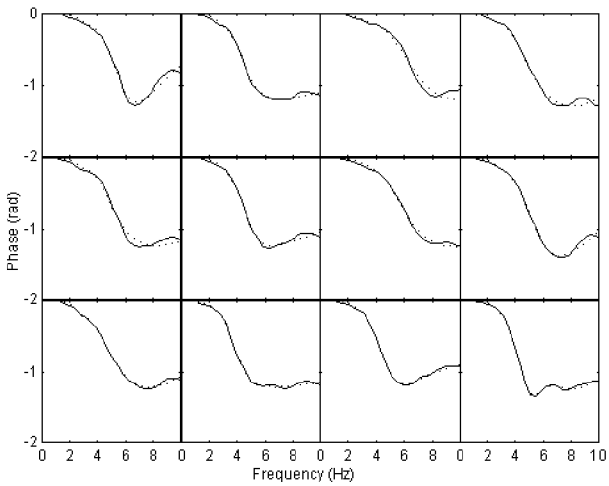

Figure 10 Vertical apparent masses phase of 12 subjects in the average thigh contact posture: ———, experiment; ·····, model.

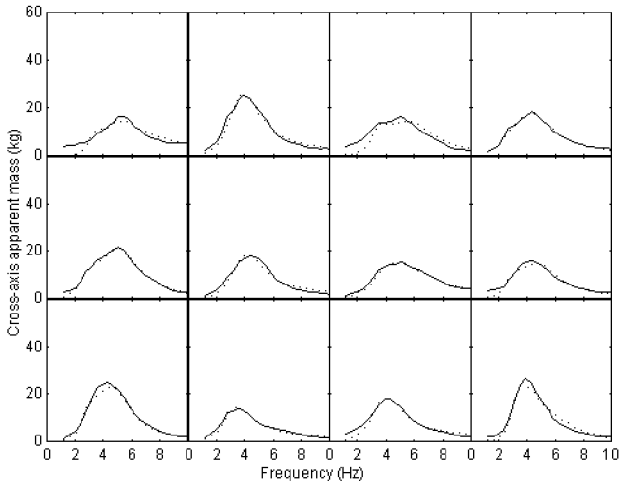

Figure 11 Fore-and-aft cross-axis apparent masses of 12 subjects in the average thigh contact posture: ———, experiment;·····, model.

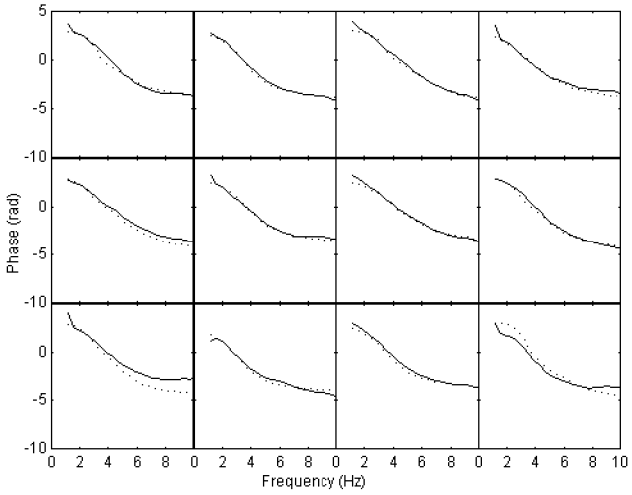

Figure 12 Fore-and-aft cross-axis apparent masses phase of 12 subjects in the average thigh contact posture: ——— , experiment;····· , model.

Table 1 Parameters obtained from Model 5 in the feet hanging posture, (m_1=0).

Sub	m_2	m_3	J_2	k_{1x}	k_2	k_{3z}	c_{1x}	c_2	c_{3z}	e	α
	kg	kg	kgm^2	N/m	Nm	N/m	Ns/m	Nsm	Ns/m	m	rad
1	19	45	6.85	75239	5011	59103	1106	687	633	0.60	1.03
2	28	61	14.75	69586	6423	65037	956	145	891	0.43	1.18
3	32	52	18.06	32433	10838	78783	432	94	816	0.50	1.36
4	25	50	0.72	68572	228	64860	1048	4	866	0.11	1.34
5	18	44	0.24	76590	71	59661	1002	2	857	0.09	1.35
6	25	46	0.18	46203	49	38514	730	15	283	0.09	0.73
7	30	51	0.30	95174	125	70681	1807	2	833	0.05	1.17
8	20	44	0.10	50647	27	57593	811	2	738	0.06	1.28
9	34	44	9.77	56065	6273	36967	1081	194	318	0.41	0.75
10	23	53	7.15	65973	1424	45023	1165	75	666	0.34	1.29
11	31	55	3.75	49170	1555	43722	988	64	620	0.23	0.98
12	15	91	3.07	46350	3246	91985	553	23	2295	0.45	1.42

Table 2 Parameters obtained from Model 5 in the average thigh contact posture, (m_1=0).

Sub	m_2	m_3	J_2	k_{1x}	k_2	k_{3z}	c_{1x}	c_2	c_{3z}	e	α
	kg	kg	kgm^2	N/m	Nm	N/m	Ns/m	Nsm	Ns/m	m	rad
1	26	26	0.29	26024	142	25631	2879	2	344	0.07	1.00
2	24	45	0.12	32887	76	44264	551	7	406	0.07	0.99
3	21	43	0.18	69002	90	74587	1132	1	1135	0.06	1.35
4	16	44	0.14	33170	41	48193	694	4	787	0.09	1.33
5	14	35	1.14	41203	414	40549	558	14	679	0.28	1.39
6	20	37	0.17	29561	145	36458	636	11	296	0.09	0.93
7	20	39	0.08	37212	67	64479	660	5	409	0.06	0.96
8	17	36	0.51	44320	186	35845	1167	4	545	0.10	1.25
9	17	42	0.13	49202	49	40155	758	1	786	0.06	1.27
10	24	35	0.13	19457	36	21967	514	8	149	0.07	0.61
11	24	43	0.21	32545	162	37923	744	14	445	0.09	0.98
12	23	64	9.41	38990	12409	52602	469	127	936	0.49	1.32

DISCUSSION

Previous studies have shown that the vertical apparent mass could be reasonably modelled by two degree-of-freedom lumped parameter models with the masses of the model moving only in the vertical direction (e.g. Wei and Griffin 1998). Other studies used models with more than two degrees-of-freedom with the masses of the model moving only in the vertical direction (e.g. Payne and Band 1971). The models investigated in this paper showed that the vertical apparent mass obtained experimentally could also be obtained theoretically by using lumped parameter two degrees-of-freedom models with vertical and rotational motions as opposed to motion only in the vertical direction. However, the position of each degree-of-freedom in the model is important to obtain an agreement between the experimental and theoretical results, as has been shown by Model 1 and Model 2 (see Figure 2 and Figure 3). This paper also showed that a two degree-of-freedom model consisting of a rotational degree-of-freedom and a fore-and-aft degree-of-freedom would be sufficient to reproduce the vertical apparent mass obtained experimentally with vertical excitation, as has been shown by the response of Model 3 (Figure2 and Figure 3).

Despite the agreement between the apparent mass obtained from Model 2 and Model 3 and the apparent mass obtained experimentally, neither the cross-axis apparent mass obtained from Model 2 nor the cross-axis apparent mass obtained from Model 3 were in agreement with the cross-axis apparent mass measured experimentally, especially with the phase response. The combination of the degrees-of-freedom of Model 2 and Model 3 (to produce Model 4) was needed to obtain good agreement between the measured apparent mass and cross-axis apparent mass and the calculated apparent mass and cross-axis apparent mass. Model 4 and Model 5 suggest that the human body undergoes a fore-and-aft movement on the seat when exposed to vertical excitation, which may indicate shear deformation of the tissue of the ischial tuberosities. This conclusion is consistent with the conclusion of Broman et al. (1996) who modelled the transmissibility to the third

lumbar vertebra L3 using vertical, horizontal and rotational sub-systems and concluded that all vertical, rotational and horizontal sub-systems ('that allows the subject to slide on the seat') were needed to produce the experimentally measured transmissibility to L3. Using a finite element model of the human body, Kitazaki and Griffin (1997) also referred to shear deformation of the tissues of the buttocks at the principal resonance frequency. They reported that 'a principal resonance of the human body at about 5 Hz consisted of an entire body mode, in which the skeleton moved vertically due to axial and shear deformations of buttocks tissue, in phase with a vertical visceral mode, and a bending mode of the upper thoracic and cervical spine'.

The optimised model parameters differed between subjects and showed high variability, especially with the feet hanging posture (see Table 1 and Table 2). In the average thigh contact posture, the optimised parameters showed less variability between subjects than in the feet hanging posture and so, the optimised parameters in the average thigh contact posture are of a similar order between subjects (except for subject 12). This could be expected as the experimental data showed less inter-subject variability in the average thigh contact posture than in the feet hanging posture (Nawayseh and Griffin 2003). It is possible that in the feet hanging posture, swinging in the lower legs contributed to the force measured on the seat in the fore-and-aft direction. Since, the effect of the swinging of the feet is not accounted for when deriving the equations of the model, it will be reflected in the optimised parameters. This might have contributed to the high variability in the parameters between subjects in the feet hanging posture.

Although the models investigated in this paper were not intended to be mechanistic models, the predicted masses m_2 and m_3 with the average thigh contact posture seem broadly similar to the masses of the pelvis (and the part of the legs supported on the seat) and the upper body without the pelvis, respectively, bearing in mind the simplicity of the model. The values of the moment of inertia (except for subject 12), and the geometrical parameters of mass 2 with respect to a reference located at the ischial tuberosities seem also to be similar to those of the pelvis, given the simplicity and the assumptions made when deriving the equations of the model. For example, in the models, the springs and dampers used were assumed to be linear and the parameters were assumed to be independent of time and frequency while this might not be true. Moreover, when deriving the equations of motion, the effect of gravity was not taken into account. This means that, since the models are linear models, the effect of gravity will be included in the value given by the rotational stiffness, as both the stiffness term and the gravity term in the equations of motion are proportional to the rotational displacement, θ, for linear models. It was also assumed that the centre of gravity of mass 2 and the centre of gravity of mass 3 have the same fore-and-aft distance from the connection point, while this might not necessarily be the case, if mass 2 and mass 3 were the pelvis and the upper body, respectively.

CONCLUSIONS

Five lumped parameter models have been investigated to simultaneously predict the vertical apparent mass and the fore-and-aft cross-axis apparent mass of seated subjects exposed to vertical vibration. The investigation showed that three degrees-of-freedom model with rotational, vertical and fore-and-aft capabilities was needed to predict the vertical apparent mass and the fore-and-aft cross-axis apparent mass. The model suggested a fore-and-aft sliding motion (or possibly deformation of tissue in contact with the seat) of the human body on the seat when exposed to vertical excitation.

REFERENCES

Boileau, P.E. and S. Rakheja. 1998. "Whole-body vertical biodynamic response characteristics of the seated vehicle driver-Measurement and model development." *International Journal of Industrial Ergonomics* 22, 449-472.

Broman, H., M. Pope. and T. Hansson. 1996. "A mathematical model of the impact response of the seated subject." *Medical Engineering and Physics*. 18, 410-419.

Fairley, T. and M.J. Griffin. 1989 "The apparent mass of the seated human body: vertical vibration." *Journal of Biomechanics* 22 (2), 81-94.

Fritz, M. 2000. "Description of the relation between the forces acting in the lumbar spine and whole-body vibrations by means of transfer functions." *Clinical Biomechanics* 15, 234-240.

Kitazaki, S. and M.J. Griffin. 1997. "A modal analysis of whole-body vertical vibration using a finite element model of the human body." *Journal of Sound and Vibration* 200 (1), 83-103.

Matsumoto, Y. and M.J. Griffin. 2001. "Modelling the dynamic mechanisms associated with the principal resonance of the seated human body." *Clinical Biomechanics* 16 (1), 31-44.

Matsumoto, Y. and M.J. Griffin. 2003. "Mathematical models for the apparent masses of standing subjects exposed to vertical whole-body vibration." *Journal of Sound and Vibration* 260, 431-451.

Nawayseh, N. and M.J. Griffin. 2003. "Non-linear dual axis biodynamic response to vertical whole-body vibration." *Journal of Sound and Vibration*, 268, 503-523.

Nawayseh, N and M.J. Griffin. 2005. "Non-linear dual axis biodynamic response to fore-and-aft whole-body vibration." *Journal of Sound and Vibration*, 282, 831-862.

Payne, P.R. and E.G.U. Band. 1971. "A four-degree-of-freedom lumped parameter model of the seated human body." Report AMRL-TR-70-35. Aerospace Medical Research Laboratory, Wright-Patterson Air Force Base.

Suggs, C.W., C.F. Abrams. and L.F. Stikeleather. 1969 "Application of a damped spring-mass human vibration simulator in vibration testing of vehicle seats." *Ergonomics* 12 (1), 79-90.

Wei, L. and M.J. Griffin. 1998 "Mathematical models for the apparent mass of the seated human body exposed to vertical vibration." *Journal of sound and vibration* 212 (5), 855-874.

AUTHOR BIOGRAPHY

NASER NAWAYSEH was born in Jordan and studied Mechanical Engineering at the University of Jordan and graduated in 1993. He got his MSc by research in Solar Water Desalination in 1996 and published several journal and conference papers in this field. He worked as a site engineer, as a design engineer and as a lecturer between 1993 and 2000. In 2000, he started his PhD on biodynamic

responses to vibration at the Institute of Sound and Vibration Research (ISVR) of the University of Southampton in The United kingdom and graduated in 2004. He was, immediately appointed as a Research Fellow at the Institute of Sound and Vibration Research where he worked for 3 years on different small and big European and International projects investigating biodynamic responses, seating dynamics, postural stability, motion sickness and performance of anti-vibration gloves. He published several journal papers, conference papers, and technical reports in those areas. In September 2007, he joined Dhofar University in Oman as an Assistant Professor and is still working there.

SIMULATION AND AI

PARAMETER IDENTIFICATION IN HEAT TRANSFER PROBLEMS: COMPARISON OF A GENETIC ALGORITHM AND PARTICLE SWARM OPTIMIZATION

Yoann Cavallin
Jean-Daniel Lan Sun Luk
Richard Lorion
Miloud Bessafi
Jean-Pierre Chabriat
LE2P, University of La Réunion
15 avenue René Cassin, BP 7151,
97715 Saint Denis Messag Cedex 9
France
E-mail: yoann.cavallin@univ-reunion.fr

KEYWORDS
Thermal metrology, heat transfer, stochastic optimization, inverse problems.

ABSTRACT

This communication deals with a parameter identification inverse problem in thermal metrology. Source identification as well as quantification of the losses of the system are studied. The model method is considered, in order to estimate simultaneously two parameters connected to the experimental conditions: the input excitation and the convective heat exchange. Experimental data are obtained with the "Flash"' method applied to three different layered composite materials, whereas the model results from the quadrupoles method. A comparison of two optimization methods applied to this problem is studied: a Matlab implementation of the Genetic Algorithm and the PSO method that we have implemented. Lastly their performances are evaluated.

1. INTRODUCTION

In thermal metrology, several methods are used, depending on the parameter to be studied: the thermal conductivity, the heat capacity or the thermal diffusivity. The "flash method" (Parker 1961) is the most common method to measure the thermal diffusivity. In addition to the simple implementation of the method, the thermal conductivity can be estimated if the heat capacity and the density are known. Thermal diffusivity estimated by the flash method has been successfully applied to different media like semi-transparent media (Lazard et al. 2004), polymers (Santos et al. 2005), and to layered materials (Vozar and Hohenauer 2001). Experimental constraints have also been studied like the effect of a thin layer on the measurement (Maillet et al. 2000).
In parallel, in order to evaluate the experimental constraints such as noise effects, the heterogeneous materials or the heat pulse duration, models of the measurement with the flash method have been developed. The method used to resolve the heat transfer inside the material allows us to define three main classes of models: an analytical resolution of the system which leads to a time series (Ozisik 1993); a solution based on the Laplace transform of the system (Carslaw and Jaeger 1959; Lu et al. 2005), such as the quadrupoles method (Carslaw and Jaeger 1959); a numerical solution of the problem using the finite difference or the finite element method (Ozisik 1993). In what follows, only the quadrupoles method will be considered.
In this communication, we are interested in the estimation of two parameters connected to the experimental conditions: the input excitation and the convective heat exchange. The parameter identification uses the model method. The minimization of the distance between theoretical and experimental data is carried out according to a specific fitness function based on the Tikhonov regularization (Tikhonov and Arsenin 1977).
In the heat conduction analysis the inverse problem is ill-posed, hence the uniqueness of the solution cannot be ensured (Jarny et al. 1991). Moreover, the parameter estimation considers simultaneously two correlated parameters. So the minimization will be performed using stochastic optimization. Since the early 1950s, the area of evolutionary computation has experienced an increased interest. In an optimization problem, this seems to be an efficient method to compute the global solution. This is especially the case when the equations describing a problem are complex and nonlinear, or when a mathematical model of the process is not sufficiently precise.
Genetic Algorithms (GA), (Holland 1975), and Particle Swarm Optimization (PSO), (Kennedy and Eberhart 2001), are the two mostly commonly adopted evolutional methods. They have been applied with success to problems in many fields such as biomedical analysis (Lu et al. 2004), transmission systems (El Dib et al. 2007), communications in wireless sensor networks (Mao et al. 2007), data analysis (Paterlini and Krink 2006), but also in thermal property estimation (Garcia and Scott 1998). To improve optimization performance, many proposed solutions consider a PSO-GA hybrid algorithm in order to take advantages of each algorithm (Mao et al. 2007; Shi et al. 2005).
The concept of GA is inspired by the Darwinian theory of evolution applied to genetics, whereas PSO is inspired by the social behavior of a population of animals such as birds or fish. Both are stochastic search tools and population based

algorithms. They create a population of potential solutions, and select the best solution (or set of solutions) according to the fitness function. The population is iteratively refined taking account of the solution of the last iteration.
The originality of this work consists in the use of experimental data obtained with the flash method as well as the simultaneous estimation of parameters. The choice to use the model method associated to an evolutional method allows us to include experimental parameters in the identification process.
This paper is organized as follows: Section 2 describes the formalization of the heat conduction problem and the context of the experimentation. Section 3 introduces the optimization framework and the fitness function. Section 4 gives the results of parameter identification in terms of speed of convergence, reliability and so on, in order to evaluate and compare the performance of GA and PSO. Finally, Section 5 concludes our study.

2. PROBLEM STATEMENT

In a nonstationary heat transfer process, the thermal diffusivity is the capacity of a material to diffuse the heat. Due to its rapidity and simplicity of use, the flash method is the main technique for measuring the thermal diffusivity.

The flash method
In the flash experiment the front face of an *L*-thickness disk-shaped and homogeneous sample is subjected to a short duration heat pulse (compared to the transient time) through the sample (see figure 1). The measurement of the temperature response at the rear face allows us to estimate the thermal diffusivity of the sample.

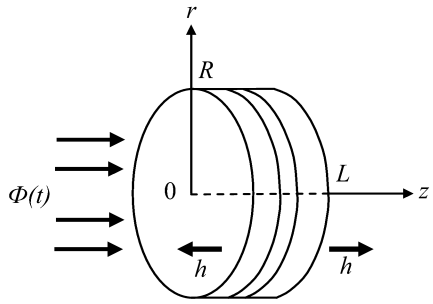

Figure 1: Principle of the flash method

In the ideal experimentation the heat flux density $\Phi(t)$ is a Dirac pulse uniformly distributed on the front face of the sample, and heat losses are not considered. The formulation of the problem directly results on heat conduction law. First we assume that the heat supply is perfectly known (pulse of heat). Then we consider a mathematical formulation based on one-dimensional transient heat conduction. Furthermore, contacts between each layer are considered as perfect. Under these assumptions, the heat conduction law defines a non-linear system, as follows:

$$\frac{\partial}{\partial z}\left[\lambda(z)\frac{\partial T(z,t)}{\partial z}\right] = \rho(z)c(z)\frac{\partial T(z,t)}{\partial t}; \qquad (1)$$

for $0 < z < L$ and $t > 0$.

where $\lambda(z)$ is the thermal conductivity, $\rho(z)$ the density and $c(z)$ the heat capacity. The thermogram $T(z,t)$ characterizes the evolution of the temperature through the sample at position z and time t. Global heat exchanges on lateral faces of the sample are not considered, so we deduce these boundary conditions:

$$\begin{aligned} &\frac{\partial T(z,t)}{\partial z} = 0; \quad z = 0, t > \delta t, \\ &\frac{\partial T(z,t)}{\partial z} = 0; \quad z = L, t > 0, \\ &\frac{\partial T(z,t)}{\partial z} = -\frac{Q}{\lambda(z)\delta t}; \quad z = 0, t < \delta t, \end{aligned} \qquad (2)$$

where Q is the energy density and δt the duration of the pulse. $T(z,t)$ can be obtained with the quadrupoles method (Carslaw and Jaeger 1959) by considering the Laplace space. Moreover, many experimental constraints can be introduced: the influence of heat losses, the influence of spatial and temporal pulse distribution, and the heterogeneous materials. Here, we will only consider the radial heat losses with the assumption that the convective heat exchange coefficient, h, is uniform in the front and rear faces. In this case, in the Laplace space the solution of system (1) is of the form:

$$\begin{bmatrix} \tilde{T}(0,p) \\ \tilde{\Phi}(0,p) - h\tilde{T}(0,p) \end{bmatrix} = K_1 \dots K_N \begin{bmatrix} \tilde{T}(L,p) \\ h\tilde{T}(L,p) \end{bmatrix}, \qquad (3)$$

$$K_i = \begin{bmatrix} A_i & B_i \\ C_i & D_i \end{bmatrix},$$

where $\tilde{T}(z,p)$ and $\tilde{\Phi}(z,p)$ be the Laplace transforms of $T(z,t)$ and $\Phi(t)$, and the K_i matrices represent the quadrupoles related to the i^{th} layer.
Applying a numerical inverse Laplace transform, the thermogram $T(z,t)$ is then obtained. In what follows, the model used for the rear and front thermograms results from the inverse Laplace transform of the matrix system (3).

Data sets
The flash method has been applied to three different samples of 80mm disk-shaped, in order to evaluate the estimation performance as a function of the number of layers:

- a 1-layer 5mm thickness PVC material;
- a 2-layer 10mm thickness PVC/steel material;
- a 3-layer 11.5mm thickness steel/PVC/copper material.

Front face temperature (z=0) and rear face temperature (z=L) have been used as data sets. Figures 2, 3 and 4 show the thermograms for the three samples. These thermograms are compared to the best realization obtained with the quadrupoles model.
To respect condition (2), the thermograms have been translated in such a way that $T(z,t)$=0 for t=0. Flash duration (see table 2) has been chosen in order to provide a change of temperature equal to at least 1.5°C. For each sample, several measurements (see table 2) have been carried out in the same conditions. Hence, to reduce the noise level, parameter identification uses the mean thermogram.
Table 1 gives the thermal properties used in the computation of the quadrupoles model for each material. The thermal excitation is obtained with a halogen lamp (tungsten filament) providing a maximal power of 2000W. Two thermal sensors (thin-film thermocouple) are connected to

the front and rear faces of the sample. Acquisition data is carried out with the classical LabView routine and the sample period is 100ms. Using a thick material and recording the mean evolution of temperature allows us to consider a uniform heat pulse (Lorion 2000).

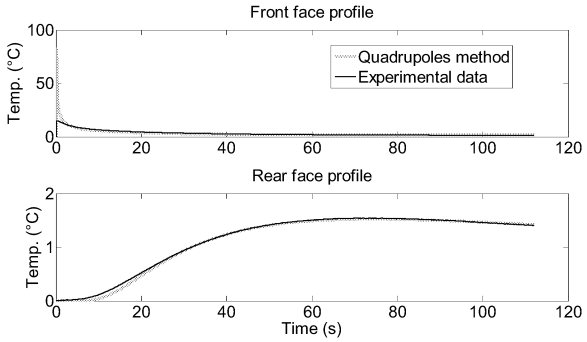

Figure 2: PVC material

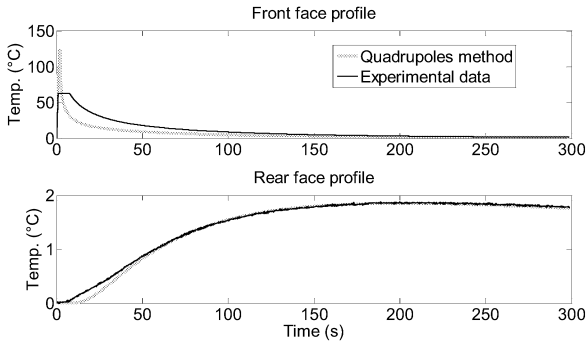

Figure 3: PVC/steel 2-layer material

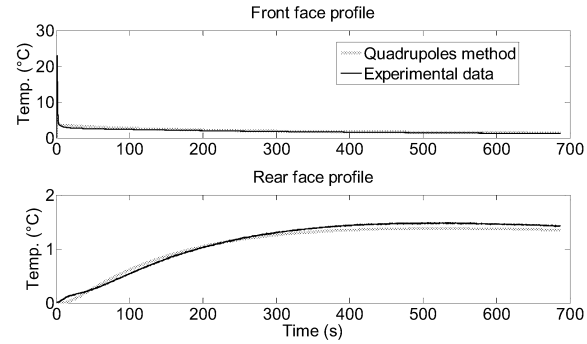

Figure 4: steel/PVC/copper 3-layer material

Table 1: Thermal properties of materials

	ρ (Kg.m^{-3})	λ (W.m^{-1}.K^{-1})	c (J.Kg^{-1}.K^{-1})
Copper	8950	390	380
Steel	7850	46	490
PVC	900	0.16	1600

Identification parameters

The input excitation, Q, and the convective heat exchange, h, define the vector parameters $\boldsymbol{\theta}$=[Q h] to estimate. It is important to note that this choice can be extended to other parameters like the thermal conductivity or the flash duration. The theoretical and experimental thermograms are respectively denoted $T(z,t;\boldsymbol{\theta})$ and $D(z,t)$ below. Optimization is based on the minimization of a criterion $J(\boldsymbol{\theta})$ related to a distance between $T(z,t;\boldsymbol{\theta})$ and $D(z,t)$:

$$\widehat{\boldsymbol{\theta}} = \arg\min_{\theta} \mathrm{J}[\mathrm{T}(\mathrm{z},\mathrm{t};\boldsymbol{\theta}),\mathrm{D}(\mathrm{z},\mathrm{t})].$$

In order to improve the performance, estimation is carried out using all the information, *i.e.* the front and rear face thermograms simultaneously. Nevertheless, the thermograms are weighted by the standard deviation resulting from the set of realizations. In parallel all the thermograms are centered and reduced.

Table 2 gives the estimated values of Q and h for the three studied samples. Coherent results are obtained. In particular, Q depends on the thermal conductivity and the heat capacity of the first layer material. The PVC, of small conductivity, produces a higher energy density than the steel taking into account the flash duration.

Table 2: Thickness, number of series of experimental thermograms, flash duration and estimated values of Q and h for the three studied samples

	Thick (mm)	Nb exp.	flash (s)	Q (J.m^{-2})	h (W.m^{2}.K^{-1})
PVC	5	12	0.2	207430	12.27
PVC/steel	10	2	2	520240	14.02
Steel/PVC/ Copper	11.5	10	1	51010	5.95

3. STOCHASTIC OPTIMIZATION

Simulations are conducted on an Intel Core Duo processor, 2GHz computer, in the Matlab 7 environment. The GA part is performed using the standard Matlab toolbox with the following parameters: Crossover rate, p_C=0.7; Mutation rate, p_M =0.08. Lorion has proved the effectiveness of GA for this application with these parameters with regard to maximizing the convergence (Lorion 2000). The PSO method has been implemented by the team of the LE2P laboratory. The parameters of the PSO part are: Inertial weight, w=1.5; Learning parameters, c_1=c_2=1.5. For both GA and PSO parts, the population is based on 20 individuals, and 80 generations are considered.

Of course, the same fitness function is applied to the algorithms. Denote $T_n(z;\boldsymbol{\theta})$ and $D_n(z)$ the discrete expressions of $T(z,t;\boldsymbol{\theta})$ and $D(z,t)$ composed of N time samples. Let us consider two vectors $F_n(\boldsymbol{\theta})$ and $R_n(\boldsymbol{\theta})$ related to the front and rear face thermograms, so that:

$$F_n(\boldsymbol{\theta}) = \frac{T_n(0;\boldsymbol{\theta}) - D_n(0)}{D_n(0)}, \quad R_n(\boldsymbol{\theta}) = \frac{T_n(L;\boldsymbol{\theta}) - D_n(L)}{D_n(L)},$$

Then the fitness function is defined as:

$$J(\boldsymbol{\theta}) = 0.5[\textstyle\sum_{n=1}^{N} F_n(\boldsymbol{\theta})^2]^{-1/2} + 0.5[\sum_{n=1}^{N} R_n(\boldsymbol{\theta})^2]^{-1/2}$$
$$+0.1[\textstyle\sum_{n=1}^{N} F_n(\boldsymbol{\theta})^2 \sum_{m=1}^{N} R_m(\boldsymbol{\theta})^2]^{-1/2} + 0.1(\sqrt{1-\gamma^2} - 1)$$

where $\gamma = 0.001L - 2$, is a regularization parameter. Based on the Tikhonov regularization, this fitness function allows us to smooth $\widehat{\boldsymbol{\theta}}$ in order to stabilize the solution.

4. ESTIMATION RESULTS AND DISCUSSION

To compare the performance of GA and PSO we have considered 3 situations depending on the lower and upper bounds of the variables to estimate:

- *strong constraint*: bounds close to the true value (1%),
- *moderate constraint*: bounds more distant (30%),
- *weak constraint*: unconstrained optimization.

Note that, with GA, total unconstrained optimization does not allow us to reach a suitable solution. Thus the unconstrained optimization corresponds to a very broad constraint. This is not the case with PSO where we can reach the global solution using the real unconstrained optimization.

Table 3: Results of simulations for 1-layer material

		Fitness		$\hat{Q}$		$\hat{h}$	
		Mean	STD	Bias (%)	MSQE ($\times 10^6$)	Bias (%)	MSQE ($\times 10^6$)
PSO	strong	0.286	0.047	3.33	20.16	18.11	12.82
	moderate	0.338	0.083	6.49	70.15	36.12	45.20
	weak	0.541	0.640	6.95	415.25	28.69	163.12
GA	strong	0.253	0.003	0.06	0.33	0.3	0.2
	moderate	0.389	0.070	8.55	133.45	48.54	81.4
	weak	0.651	0.358	17.98	738.34	18.8	308.51

Table 4: Results of simulations for 2-layer material

		Fitness		$\hat{Q}$		$\hat{h}$	
		Mean	STD	Bias (%)	MSQE ($\times 10^6$)	Bias (%)	MSQE ($\times 10^6$)
PSO	Strong	0.906	0.068	34.67	6.58	23.37	21.24
	moderate	0.973	0.120	7.17	17.69	36.44	57.22
	Weak	1.095	0.404	14.14	389.94	53.38	67.09
GA	Strong	0.852	0.002	0.25	0.12	1.06	0.36
	moderate	0.954	0.100	4.27	17.78	22.05	53.62
	Weak	1.776	1.109	30.20	1939.6	49.70	491.03

Table 5: Results of simulations for 3-layer material

		Fitness		$\hat{Q}$		$\hat{h}$	
		Mean	STD	Bias (%)	MSQE ($\times 10^6$)	Bias (%)	MSQE ($\times 10^6$)
PSO	strong	1.652	0.059	1.66	12.85	22.70	17.73
	moderate	1.679	0.108	2.13	24.13	30.17	30.48
	weak	1.914	0.566	18.20	451.97	172.62	362.05
GA	strong	1.620	0.018	1.01	2.59	12.06	3.78
	moderate	1.810	0.455	6.74	271.5	52.91	216.58
	weak	2.148	0.533	17.99	526.64	120.83	334.64

Tables 3, 4 and 5 show the results of simulation for the three samples under the three cases of constraint: mean and standard deviation of the best fitness value, bias and mean square error (MSQE) for $\hat{Q}$and $\hat{h}$. Statistics are based on a series of 50 estimated values. The best fitness value is obtained after 80 generations. The bias is expressed in percentage of the best solution of $\hat{\boldsymbol{\theta}}$.

First, tables 3, 4 and 5 illustrate that estimation performance does not depend on the number of layers of the material. Of course, the mean fitness value increases with the number of layers due to the increasing difficulty to fit the data. Nevertheless, the standard deviation around this mean value only depends on the constraint of optimization.

In the constraint optimization (strong case) the results obtained with GA are more stable, variances of the estimated parameters being much weaker. This is explained by the introduction in the PSO routine of a coefficient which increases the radius of convergence of the population in order to avoid premature convergence. It is no longer the case in the unconstrained optimization where the reliability of PSO is clear. This shows that the PSO approach is superior to the GA approach for this application, what is confirmed for other problems (El Dib et al. 2007, Shi et al. 2005).

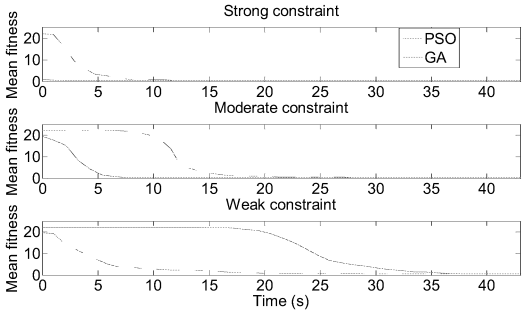

Figure 5: Mean fitness function for the 1-layer material as a function of the optimization algorithm

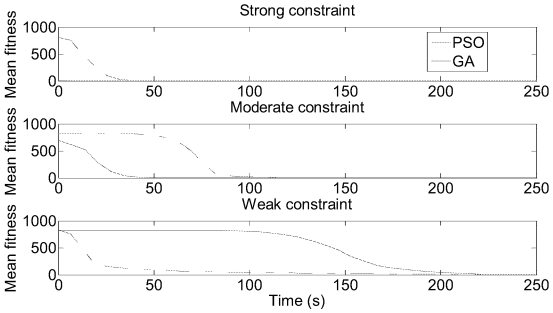

Figure 6: Mean fitness function for the 3-layer material as a function of the optimization algorithm

Moreover in figures 5 and 6, it appears that the PSO algorithm reduces the speed of convergence. A comparison of the mean fitness functions between GA and PSO as a function of the optimization constraints shows that the convergence is achieved more quickly with PSO, except for the unconstrained optimization. In this case, the convergence of GA is faster but less precise than PSO, as shown in figures 7, 8 and 9.

Finally, we can remark that estimation results are not related to the data noise: the 2-layer material has been obtained from two realizations whereas 1-layer and 3-layer have been obtained from about 10 realizations.

5. CONCLUSION

In this paper, the performance of GA and PSO for a parameter identification inverse problem in thermal metrology has been compared. We have used a Matlab

implementation of the GA whereas the PSO method has been entirely implemented. The comparison with GA shows that PSO is capable of dealing with weaker constraints. In particular, the speed of convergence is reduced and the reliability is improved. So this work shows the robust convergence of PSO compared to GA for the problem considered.

The proposed method of parameters identification, based on experimental data and the quadrupoles model, allows us to estimate simultaneously the input excitation and the convective heat exchange. The estimated values correspond to typical values. So this work leads to the source identification and allows us to quantify the losses of the system.

We have only considered two parameters, but the thermal conductivity, the thermal diffusivity or the duration of heat pulse could be integrated. More generally, this study could be applied to the source identification of an unspecified input excitation.

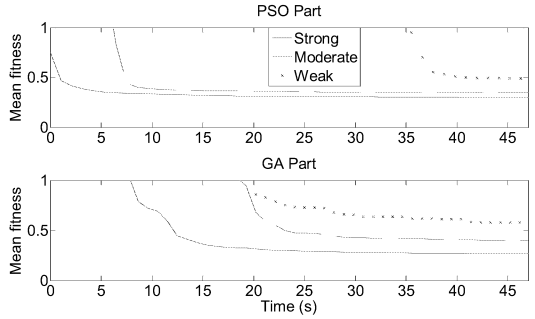

Figure 7: Mean fitness function for the 1-layer material as a function of the optimization constraints

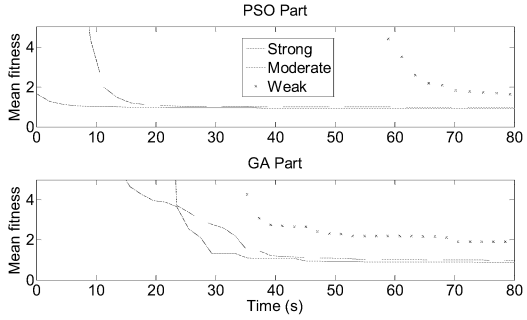

Figure 8: Mean fitness function for the 2-layer material as a function of the optimization constraints

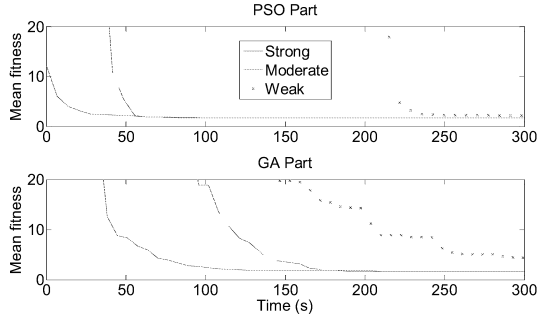

Figure 9: Mean fitness function for the 3-layer material as a function of the optimization constraints

REFERENCES

Carslaw H. S. and Jaeger J. C. 1959. *Conduction of heat in solids, 2nd ed.* Oxford at the Clarendron Press, London.

Dos Santos W. N., Mummery P. and Wallwork A. 2005. "Thermal diffusivity of polymers by the laser flash technique". *Polymer Testing*, No.24, 628-634.

EL-Dib A. A., Youssef H. K. M., EL-Metwally M. M. and Osman Z. 2007. "Optimum VAR sizing and allocation using particle swarm optimization". *Electric Power Systems Research*, No.77 (8), 965-972.

Garcia S. and Scott E. P. 1998. "Use of genetic algorithms in thermal property estimation. I. experimental design optimization". *Numerical Heat Transfer, Part A: Applications*, No.33, 135-147.

Holland J. H. 1975. *Adaptation in Natural and Artificial Systems*, University of Michigan Press, Ann Arbor.

Jarny Y., Ozisik M. N. and Bardon J. P. 1991. "A general optimization method using adjoint equation for solving multidimensional inverse heat conduction". *International Journal of Heat and Mass Transfer*, No.34 (11), 2911-2919.

Kennedy J. and Eberhart R. C. 2001. *Swarm intelligence*, Morgan Kaufman Publishers, San Francisco.

Lazard M., André S. and Maillet D. 2004. "Diffusivity measurement of semi-transparent media: model of the coupled transient heat transfer and experiments on glass, silica glass and zinc selenide". *International Journal of Heat and Mass Transfer*, No.47, 477-487.

Lorion R. 2000. "Application des algorithmes génétiques à la caractérisation thermique des matériaux" Ph.D. thesis, Université de la Réunion (INIST-CNRS, Cote INIST : T 132242).

Lü J. X., Shen Q., Jiang J. H., Shen G. L. and Yu R. Q. 2004. "QSAR analysis of cyclooxygenase inhibitor using particle swarm optimization and multiple linear regression". *Journal of Pharmaceutical and Biomedical Analysis,* No.35 (4), 679-687.

Lu X., Tervola P. and Viljanen M. 2005. "An efficient analytical solution to transient heat conduction in a one-dimensional hollow composite cylinder" *Journal of Physics A: Mathematical and General*, No.38, 8337-8351.

Maillet D., Moyne C. and Rémy B. 2000. "Effect of a thin layer on the measurement of the thermal diffusivity of a material by a flash method". *International Journal of Heat and Mass Transfer*, No.43, 4057-4060

Mao J., Wu Z. and Wu X. 2007. "A TDMA scheduling scheme for many-to-one communications in wireless sensor networks". *Computer . Communications*, No.30 (4), 863-872.

Ozisik M. N. 1993. *Heat conduction*, John Wiley and Sons Inc., New-York.

Paterlini S. and Krink T. 2006. "Differential evolution and particle swarm optimisation in partitional clustering". *Computational Statistics & Data Analysis,* No.50 (5), 1220-1247.

Parker W. J., Jenkins R. J., Butler C. P. and Abbott G. L. 1961. "Flash method of determining thermal diffusivity, heat capacity and thermal conductivity". *Journal of applied physics,* No. 32 (9), 1679-1684.

Shi X. H., Liang Y. C., Lee H. P., Lu C. and Wang L. M. 2005. "An improved GA and a novel PSO-GA-based hybrid algorithm". *Information Processing. Letters* , No.93 (5), 255-261.

Tikhonov A. N. and Arsenin V. A. 1977. *Solution of ill-posed problems*, Winston & Sons, Washington DC.

Vozar L. and Hohenauer W. 2001. "Accuracy of the thermal diffusivity estimation of layered materials". *Analytical Sciences*, No.17, 181-184.

TOWARD OPTIMAL ARABIC KEYBOARD LAYOUT USING GENETIC ALGORITHM

Tareq M. Malas, Sinan S. Taifour, and Gheith A. Abandah
Faculty of Engineering and Technology
The University of Jordan, Amman 11942, Jordan
E-mail: tarik.malas@gmail.com, staiii@gmail.com, abandah@ju.edu.jo

KEYWORDS
Genetic Algorithm, Optimization, Arabic Keyboard Layout.

ABSTRACT

The common Arabic keyboard layout is derived from the Arabic typewriter keyboard's layout. This layout is not optimized for typing speed and has several problems. We use a genetic algorithm to optimize the design of the Arabic keyboard layout for typing speed. In the genetic algorithm, we use a fitness function that includes into consideration key distance, finger used, and hand alternation. We also use this fitness function to evaluate the optimized layout against other layouts including the common layout. The optimized layout is relatively 35% faster than the common layout and has additional advantages.

INTRODUCTION

As the keyboard is the main device for text entry in computers, it is very important to have a comfortable keyboard layout which also promotes fast text entry. In a look at the history of the English keyboard layout, we see that the standard layout (QWERTY) is not optimized for efficient typing, but is actually quite arbitrary (Noyes 1998). A more optimized keyboard layout known as the Dvorak Simplified Keyboard (DSK) has been developed(Campbell-Kelly 2005). But the QWERTY layout remains most widely used because many people were already trained on using the QWERTY, and were reluctant to change.

Arabic Keyboard History

The layout of the Arabic keyboard is derived from the Arabic typewriter keyboard's layout. In the 1970s and 1980s, many computer companies developed more than 20 variants for this layout (JISM 1994). These various variants had consistent allocation for some letters (namely ا ب ت ث ج ح خ س ش ص ض ع غ ف ق ك ل م ن ه ي). However, they have differences in allocating the other letters particularly the letters in the lower row (such as أ د آ ئ ر ط ء ؤ ة ز ظ و ى إ ذ). Some of the famous keyboard layouts in the late 1980s are the layouts of Microsoft Arabic Word, Apple MAC, Sakher, AMEER, ALIS, and Nafitha.

To solve this chaos created by the existence of many Arabic keyboard layouts, the Arab Standardization and Metrology Organization (ASMO) developed a standard for the Arabic keyboard layout shown in Figure 1 (ASMO 1987). This keyboard standard supports the ASMO standard for the 7-bit Arabic characters code (ASMO 1985). However, this keyboard standard was not used by the computer industry and the market adopted instead the currently used Arabic keyboard layout shown in Figure 2. This keyboard layout gained wide acceptance in PCs and servers over other layouts when Microsoft adopted it for its Arabized products. Another Arabic keyboard layout currently in use is the layout shown in Figure 3. This layout is used in Apple MAC computers.

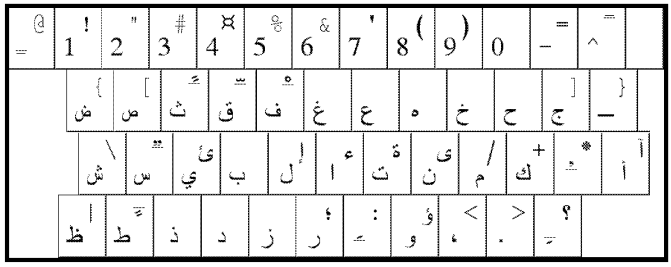

Figures 1: ASMO 663 Arabic Keyboard Layout

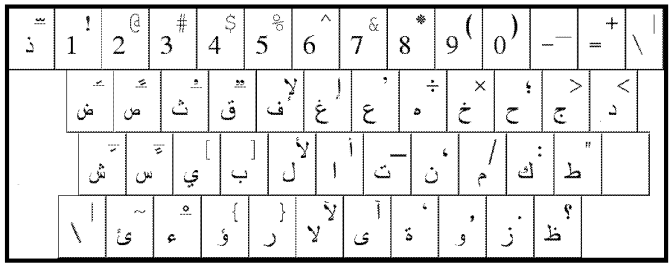

Figures 2: Common Arabic Keyboard Layout

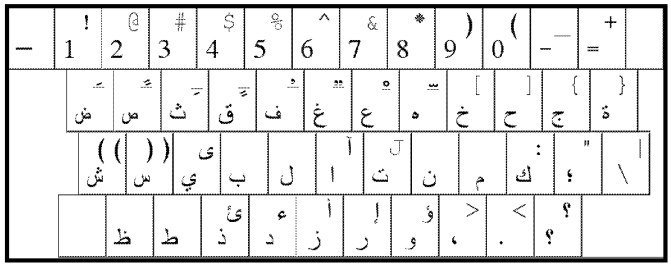

Figures 3: Apple MAC Arabic Keyboard Layout

The common Arabic keyboard layout is not optimized for performance and also has many obvious drawbacks. For example, Letter Thal "ذ" is placed in an awkward place in the top-left corner of the keyboard despite its frequent use. This letter is more frequently used than other well-positioned letters such as Letter Ghain "غ". Moreover, the two-letter

combination Lam-Alef "ﻻ" has one key dedicated for it despite the fact that it is not as frequent as other letter combinations.

Related Work

Many researchers used various algorithms to design better keyboard layouts for other languages. A simulated annealing algorithm was used by (Light and Anderson 1993) to optimize the English keyboard. They used the travel time and the frequency of letter pairs to optimize for typing speed. An evolutionary algorithm was used by (Walker 2003) for the English keyboard to evolve it for a layout faster than the QWERTY layout by 30%. Also a genetic algorithm was used by (Goettl et al. 2005) to rearrange the English letters and some punctuation marks.

Ant Colony algorithm was used by (Wagner et al. 2003) to optimize keyboard layouts for English, French, and German text. They used ergonomic criterion to develop the desired keyboard layouts.

A new design for Hindi keyboard layout was done by (Deshwal and Deb 2003) using a genetic algorithm. They used an ergonomic criterion to optimize the layout for typing convenience. We are unaware of similar optimization work done for the Arabic keyboard layout.

Approach Used

A keyboard layout can be optimized for several characteristics such as typing speed, comfort, low error rate, and trainability. In this paper, we use a genetic algorithm to design a layout optimized for typing speed. We also evaluate the typing speed of important Arabic keyboard layouts. Although our focus is on optimizing the typing speed, the designed layout is also more comfortable than the common keyboard layout.

The rest of this paper is organized as follows. The next section describes the procedure used in this research. Section 3 presents the results obtained and analyzes these results. Finally, Section 4 presents the paper conclusions and future work.

PROCEDURE

Our procedure consists of two stages. First we collect data and find the letters' frequencies, and then we use these frequencies in a genetic algorithm to optimize the design of the keyboard layout for speed. The keyboard layout is divided into two sets: the *main set* and the *shift set*. The main set contains all keys that can be accessed without using the shift key, while the shift set contains the same keys when the shift key is pressed.

Finding Frequencies of the Arabic Characters

The used optimization requires information about the Arabic characters and character pairs' frequencies. The data we used to find these frequencies was taken from the Arabic Wikipedia (http://ar.wikipedia.org), which contains articles from almost all fields. So the related character frequencies are not biased to any particular field. This site contains more than 10,000 articles, mostly well-written. These articles can be conveniently and freely downloaded in a single XML file (http://en.wikipedia.org/wiki/Wikipedia:Database_download). The Arabic Wikipedia was downloaded, parsed, and analyzed to find frequency information.

The single XML file, around 200 MB in size, contains all the articles structured with some meta information. The first step was to extract the articles and save them in separate files for analysis. The meta information was kept in an accessible format for latter usage. Due to the large size of this XML file, it is not possible to use a parsing tool that loads the entire file into the memory, such as the Document Object Model (DOM). Instead, a serial event-driven method must be used. We use the Simple API for XML (SAX), which is available in the Python programming language.

The next step was to remove all wikitext. Wikipedia articles are formatted using a special syntax called wikitext (http://en.wikipedia.org/wiki/Wikitext). For removing the wikitext, we used the Regular Expressions (RegExp) tool, which is also available in Python. The regular expressions describe patterns of text that can be matched against longer strings of text or used for substitution. Most of the wikitext can be fully described using rather simple RegExp patterns.

The last step was to count occurrences of characters and character pairs and generate result files. In this step, the user is prompted every time a new unknown character is encountered. The user is given three options: taking the character into consideration (for Arabic characters), considering it as a special character (for special characters and white space), and ignoring it (for non-Arabic characters). The special characters are given special status to enable finding word boundaries. This allows finding the probabilities of words starting or ending with particular Arabic characters.

Genetic Algorithm for Design Optimization

A genetic Algorithm is a guided random search technique inspired by evolutionary Biology (Goldberg 1989). It involves a population of candidate solutions to a problem, called individuals, which live, reproduce, and die based on their fitness relative to the rest of the population. The genetic algorithm consists of five phases: initialization, evaluation, selection, reproduction, and competition. A typical genetic algorithm requires two definitions:

1. Genetic representation of the solution domain
2. Fitness function to evaluate the solution domain

The optimization performed by a genetic algorithm has the ability to search a large space for a solution which is close to the optimum with relatively short time. The space of possible keyboard layouts is the factorial of 33 keys (8.68×10^{36}). Evaluating all these layouts is infeasible as it takes very long time.

The genetic algorithm is applied on the main set of the keyboard, where we allocated the most frequent Arabic

letters and symbols. The representation of the individuals is done using a 33-element vector, which corresponds to the characters allocated on the 33 keys of the main set.

The used fitness function is the typing time using the keyboard layout. This fitness function takes into consideration attributes that give short typing time such as hand alternation and using the home row. It also take into consideration attributes that give long typing time such as typing two consecutive letters with the same finger. Smaller fitness values are better. The used fitness is the aggregate of the products of all letter pair frequencies f_i and the corresponding letter pair typing times t_i, formally

$$Fitness = \sum_i f_i * t_i \,. \qquad (1)$$

The pair typing times are found using a linear regression model (Hiraga et al. 1980). This model was built after measuring the time intervals between key presses. We used the following model to find the key pair typing time.

$$t_i = 185.8 - 40.0h + 18.3r - 11.0f + 0.514R + 1.07F \quad (2)$$

Table 1 describes the attributes used in this model and the possible values of these attributes. Letters mapped in the shift set are given the maximum pair typing time of the main set pair typing times.

Table 1: Attributes Affective Key Pair Typing Times

Attribute	Symbol	Values
Hand Transition	*h*	0: same hand, 1: alternate hand
Row Transition	*r*	Number of rows moved across in the same hand transition
Finger Transition	*f*	The distance of finger columns in the same hand
Row Weight	*R*	Linear sum of weights for each row position, where the weights given are 1, 2, and 3 for home, upper, and bottom rows, respectively.
Finger Weight	*F*	Linear sum of weights on each of the finger positions of the key pair, where the weights given are 4.5, 4.5, 1, 2, and 3 from the outer column inwards.

The following paragraphs describe our implementation of the used genetic algorithm.

Initialization
Initially 2000 individuals (layouts) were randomly generated to form an initial population. The population was generated randomly so that the algorithm is not biased. This helps to avoid convergence to a local minimum. The randomness gives disperse layouts that cover wide regions of the space.

Selection
During each successive generation, a proportion of the current population is selected to breed a new generation. The selected individuals "parents" comprise the best individuals and randomly selected individuals. The randomly selected individuals ensure maintaining high diversity of the population. Thus preventing the algorithm from getting stuck in a local minimum.

Reproduction
The reproduction is usually made by crossover and/or mutation from the parents. The produced individuals "children" share many of the characteristics of their "parents". We only use mutation, because there is no direct method to apply crossover. The mutation is applied by swapping the locations of a number of the parent's keys. We breed more children than we need so that we can select the best children to compete with the original population. The children who have better fitness replace some of the original population. This process gives the next generation population, which is different from the initial generation. Generally the average fitness increases by this process.

Termination
The termination is performed manually. The program saves logs of the population every 200 generations. We monitor these logs seeking satisfactory results and convergence. The program was stopped after 160,000 generations. This took 32 hours of execution time on a 2.2 GHz Core 2 Duo notebook.

RESULTS AND ANALYSIS

Figure 4 shows the frequencies for Arabic letters. The most frequent three letters (Alef "ا", Lam "ل", and Yeh "ي") have aggregate frequency of 34%. The most frequent 32 letters in addition to the period were selected for allocation on the main set. The three least frequent letters and the special characters are allocated in the shift set.

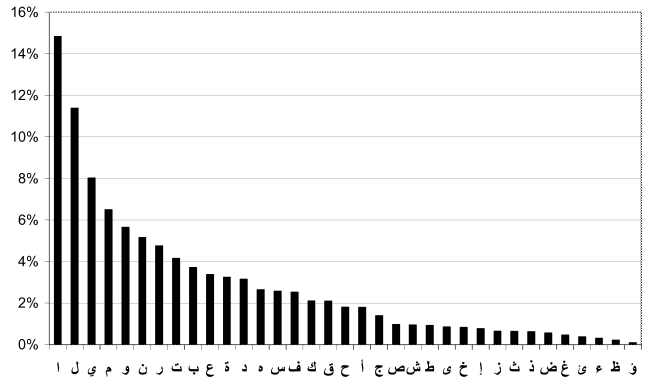

Figures 4: Frequency of the Arabic Letters

Table 2 shows the frequencies of letter pairs. Columns are for the first letter and rows are for the second letter. This table shows that the frequency of the frequent pair Alef followed by Lam "ال" is 8.3%, Lam-Meem "لم" is 1.6%, Yeh-Teh Marbuta "ية" is 1.3%, and Lam-Alef "لا" is 1.3%.

Table 2: Frequency of Arabic Letter Pairs (First letter on the column, second letter on the row)

	ا	ل	ي	م	و	ن	ر	ت	ب	ع	ة	د	ه	س	ف	ك	ق	ح	أ	ج	ص	ش	.	ط	ى	خ	إ	ز	ث	ذ	ض	غ	ئ
ا	0.0	1.2	0.7	1.0	1.1	0.6	0.8	0.3	0.7	0.6	0.0	0.4	0.7	0.4	0.2	0.5	0.4	0.3	0.0	0.3	0.2	0.2	0.0	0.2	0.0	0.1	0.0	0.1	0.1	0.2	0.1	0.1	0.0
ل	8.3	0.5	0.4	0.3	0.7	0.0	0.0	0.2	0.2	0.7	0.0	0.1	0.1	0.2	0.1	0.2	0.1	0.1	0.1	0.1	0.1	0.0	0.0	0.1	0.0	0.2	0.3	0.0	0.1	0.1	0.0	0.0	0.1
ي	0.3	0.9	0.1	0.5	0.4	0.6	0.8	0.3	0.6	0.2	0.0	0.6	0.2	0.4	1.3	0.2	0.2	0.3	0.1	0.2	0.1	0.1	0.0	0.1	0.0	0.1	0.0	0.2	0.1	0.1	0.1	0.1	0.2
م	0.8	1.6	0.3	0.1	0.4	0.1	0.1	0.3	0.1	0.2	0.0	0.2	0.3	0.2	0.0	0.2	0.0	0.2	0.2	0.2	0.0	0.1	0.0	0.0	0.0	0.0	0.0	0.0	0.1	0.0	0.0	0.0	0.0
و	0.2	0.4	0.3	0.4	0.0	0.2	0.3	0.3	0.2	0.1	0.0	0.3	0.2	0.2	0.1	0.2	0.2	0.1	0.3	0.1	0.1	0.0	0.0	0.1	0.0	0.0	0.0	0.1	0.0	0.0	0.0	0.0	0.0
ن	1.2	0.3	0.9	1.1	0.5	0.0	0.1	0.1	0.3	0.3	0.0	0.1	0.1	0.1	0.0	0.2	0.0	0.0	0.3	0.1	0.1	0.0	0.0	0.0	0.0	0.0	0.0	0.2	0.0	0.0	0.0	0.0	0.0
ر	0.8	0.2	0.6	0.3	0.5	0.0	0.0	0.3	0.4	0.3	0.0	0.2	0.1	0.1	0.2	0.2	0.2	0.2	0.1	0.1	0.1	0.2	0.0	0.1	0.0	0.1	0.0	0.0	0.1	0.0	0.0	0.1	0.0
ت	0.9	0.7	0.3	0.2	0.2	0.3	0.1	0.1	0.1	0.1	0.0	0.0	0.0	0.4	0.1	0.2	0.1	0.2	0.0	0.0	0.0	0.0	0.0	0.0	0.0	0.1	0.0	0.0	0.0	0.0	0.0	0.0	0.0
ب	0.4	0.4	0.2	0.1	0.2	0.1	0.3	0.2	0.0	0.2	0.0	0.0	0.0	0.2	0.0	0.1	0.1	0.0	0.1	0.1	0.1	0.0	0.0	0.1	0.0	0.0	0.0	0.0	0.0	0.0	0.0	0.0	0.0
ع	0.3	0.6	0.2	0.4	0.2	0.0	0.1	0.2	0.3	0.0	0.0	0.0	0.0	0.1	0.1	0.0	0.1	0.0	0.1	0.0	0.0	0.1	0.0	0.0	0.0	0.0	0.0	0.0	0.0	0.0	0.0	0.0	0.0
ة	0.1	0.3	1.3	0.2	0.0	0.2	0.4	0.0	0.1	0.2	0.0	0.3	0.0	0.1	0.1	0.1	0.1	0.1	0.0	0.1	0.0	0.0	0.0	0.1	0.0	0.0	0.0	0.0	0.0	0.0	0.0	0.0	0.0
د	0.5	0.3	0.4	0.3	0.2	0.2	0.1	0.1	0.2	0.3	0.0	0.1	0.1	0.0	0.0	0.0	0.3	0.3	0.0	0.1	0.1	0.0	0.0	0.0	0.0	0.1	0.0	0.0	0.0	0.0	0.0	0.0	0.0
ه	0.2	0.4	0.3	0.1	0.1	0.3	0.1	0.3	0.2	0.1	0.0	0.1	0.0	0.1	0.1	0.0	0.0	0.0	0.1	0.1	0.0	0.1	0.0	0.0	0.0	0.0	0.0	0.0	0.0	0.1	0.0	0.0	0.0
س	0.4	0.4	0.3	0.3	0.2	0.2	0.2	0.1	0.1	0.0	0.0	0.0	0.0	0.0	0.1	0.1	0.0	0.1	0.2	0.0	0.0	0.0	0.0	0.0	0.0	0.0	0.0	0.1	0.0	0.0	0.0	0.0	0.0
ف	0.2	0.3	0.1	0.0	0.2	0.1	0.1	0.1	0.0	0.0	0.0	0.0	0.0	0.0	0.0	0.0	0.0	0.0	0.0	0.0	0.1	0.0	0.0	0.0	0.0	0.0	0.0	0.0	0.0	0.0	0.0	0.0	0.0
ك	0.2	0.5	0.2	0.1	0.1	0.0	0.2	0.1	0.1	0.0	0.0	0.0	0.0	0.1	0.0	0.0	0.0	0.1	0.1	0.0	0.0	0.1	0.0	0.0	0.0	0.0	0.0	0.0	0.0	0.0	0.0	0.0	0.0
ق	0.2	0.4	0.2	0.1	0.2	0.1	0.1	0.2	0.1	0.1	0.0	0.0	0.0	0.0	0.1	0.0	0.0	0.1	0.0	0.0	0.0	0.0	0.0	0.1	0.0	0.0	0.0	0.0	0.0	0.0	0.0	0.0	0.0
ح	0.2	0.4	0.1	0.2	0.1	0.0	0.1	0.2	0.1	0.0	0.0	0.0	0.0	0.0	0.0	0.0	0.0	0.0	0.1	0.0	0.1	0.0	0.0	0.0	0.0	0.0	0.0	0.0	0.0	0.0	0.0	0.0	0.0
أ	0.0	0.6	0.0	0.0	0.1	0.0	0.0	0.1	0.0	0.0	0.0	0.0	0.0	0.0	0.0	0.0	0.0	0.0	0.0	0.0	0.0	0.0	0.0	0.0	0.0	0.0	0.0	0.0	0.0	0.0	0.0	0.0	0.0
ج	0.2	0.3	0.1	0.2	0.2	0.1	0.2	0.1	0.0	0.0	0.0	0.0	0.0	0.0	0.0	0.0	0.0	0.0	0.0	0.0	0.0	0.0	0.0	0.0	0.0	0.0	0.0	0.0	0.0	0.0	0.0	0.0	0.0
ص	0.1	0.2	0.0	0.1	0.1	0.1	0.0	0.1	0.0	0.0	0.0	0.0	0.0	0.0	0.0	0.0	0.1	0.0	0.1	0.0	0.0	0.0	0.0	0.0	0.0	0.1	0.0	0.0	0.0	0.0	0.0	0.0	0.0
ش	0.1	0.3	0.1	0.1	0.0	0.1	0.0	0.1	0.0	0.0	0.0	0.0	0.0	0.0	0.0	0.0	0.0	0.0	0.0	0.0	0.0	0.0	0.0	0.0	0.0	0.0	0.0	0.0	0.0	0.0	0.0	0.0	0.0
.	0.1	0.0	0.1	0.1	0.0	0.1	0.0	0.0	0.0	0.0	0.2	0.0	0.0	0.0	0.0	0.0	0.0	0.0	0.0	0.0	0.0	0.0	0.0	0.1	0.0	0.0	0.0	0.0	0.0	0.0	0.0	0.0	0.0
ط	0.1	0.1	0.1	0.0	0.1	0.1	0.0	0.1	0.1	0.0	0.0	0.0	0.0	0.1	0.0	0.0	0.1	0.0	0.0	0.0	0.0	0.0	0.0	0.0	0.0	0.1	0.0	0.0	0.0	0.0	0.0	0.0	0.0
ى	0.0	0.7	0.0	0.0	0.0	0.0	0.1	0.1	0.0	0.0	0.0	0.0	0.0	0.0	0.0	0.0	0.0	0.0	0.0	0.0	0.0	0.0	0.0	0.0	0.0	0.0	0.0	0.0	0.0	0.0	0.0	0.0	0.0
خ	0.1	0.2	0.1	0.1	0.0	0.0	0.0	0.1	0.0	0.0	0.0	0.0	0.0	0.0	0.0	0.0	0.0	0.0	0.1	0.0	0.0	0.0	0.0	0.0	0.0	0.0	0.0	0.0	0.0	0.0	0.0	0.0	0.0
إ	0.0	0.3	0.0	0.0	0.0	0.0	0.0	0.0	0.0	0.0	0.0	0.0	0.0	0.0	0.0	0.0	0.0	0.0	0.0	0.0	0.0	0.0	0.0	0.0	0.0	0.0	0.0	0.0	0.0	0.0	0.0	0.0	0.0
ز	0.1	0.1	0.1	0.0	0.1	0.0	0.0	0.0	0.0	0.0	0.0	0.0	0.0	0.0	0.0	0.0	0.0	0.0	0.0	0.1	0.0	0.0	0.0	0.0	0.0	0.0	0.0	0.0	0.0	0.0	0.0	0.0	0.0
ث	0.1	0.1	0.1	0.1	0.0	0.0	0.0	0.0	0.0	0.0	0.0	0.0	0.0	0.0	0.0	0.1	0.0	0.0	0.0	0.0	0.0	0.0	0.0	0.0	0.0	0.0	0.0	0.0	0.0	0.0	0.0	0.0	0.0
ذ	0.0	0.2	0.0	0.0	0.0	0.0	0.0	0.0	0.0	0.0	0.0	0.0	0.2	0.0	0.0	0.0	0.0	0.0	0.0	0.0	0.0	0.0	0.0	0.0	0.0	0.0	0.0	0.0	0.0	0.0	0.0	0.0	0.0
ض	0.1	0.0	0.1	0.0	0.1	0.0	0.1	0.0	0.0	0.1	0.0	0.0	0.0	0.0	0.0	0.0	0.0	0.0	0.0	0.0	0.0	0.0	0.0	0.0	0.0	0.0	0.0	0.0	0.0	0.0	0.0	0.0	0.0
غ	0.0	0.1	0.0	0.0	0.0	0.0	0.0	0.0	0.0	0.0	0.0	0.0	0.0	0.0	0.0	0.0	0.0	0.0	0.0	0.0	0.0	0.0	0.0	0.0	0.0	0.0	0.0	0.0	0.0	0.0	0.0	0.0	0.0
ئ	0.3	0.0	0.0	0.0	0.0	0.0	0.1	0.0	0.0	0.0	0.0	0.0	0.0	0.0	0.0	0.0	0.0	0.0	0.0	0.0	0.0	0.0	0.0	0.0	0.0	0.0	0.0	0.0	0.0	0.0	0.0	0.0	0.0

Figure 5 shows the convergence curve of the genetic algorithm. This curve shows the best fitness value in a generation. Note the log scale of the generation number. This curve shows that the algorithm stabilizes fast after around 1000 generations (10 minutes of execution).

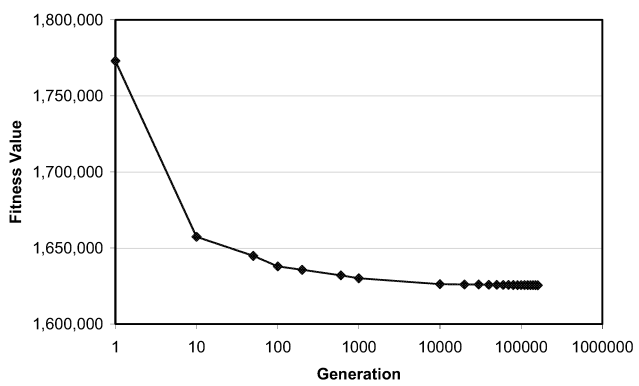

Figures 5: Convergence of the Genetic Algorithm

Figure 6 shows the optimized keyboard layout as found by the genetic algorithm. This layout has the common letters located in the comfortable home row and gives good hand alternation. The following can be noticed from the main set layout:

1. The most frequent key-pair Alef-Lam "ال" are under different hands, on the middle row, and under the strongest fingers (the index and the middle fingers).
2. Most of the frequent letters are placed in the middle row and/or using the strongest fingers, as in the case of Yeh "ي", Waw "و", and Teh "ت".
3. The least frequent letters are placed in the bottom and top rows and most of them are under the pinky finger (the weakest finger), as in the case of Thal "ذ", Dad "ض", and Ghain "غ".

No algorithm was used to optimize the shift set because the letters in this set are infrequently used in Arabic typing. The shown arrangement was done manually to keep the layout

similar to the common layout. However, some modifications were necessary to accommodate for the additional letters not included in the main set. The letters which were moved to the shift set are put on keys of similar letters in the main set; where users expect to find them. For example the pair Tah "ط" and Zah "ظ", and the pair Alef with Hamza Above "أ" and Hamza "ء" are put on same keys.

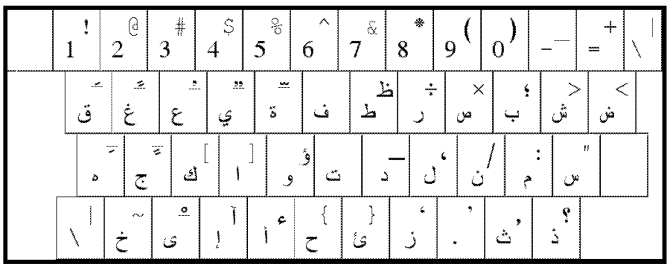

Figures 6: Arabic Keyboard Layout Optimized for Speed

A comparison is made between the optimized keyboard layout and some other layouts by applying the fitness function. Table 3 presents the results of this comparison. The worst layout was found by running the genetic algorithm with the fitness function complemented. The random layout was built by generating a random layout. We note that the common layout is better than the ASMO standard layout. The main reason for this difference is mapping the moderately used letter Teh Marbuta "ة" to the shift set in the ASMO layout. Taking the interval between the worst and optimized layouts as a reference base, the common layout is 6% better than the ASMO standard and the optimized layout is 35% better than the common layout.

Table 3: Comparison for Arabic Keyboard Layouts

Layout	Fitness Value	Relative Performance
Worst	1,942,000	0%
Random	1,773,000	53%
ASMO 663	1,756,100	59%
Apple MAC	1,740,600	64%
Common	1,735,000	65%
Optimized	1,637,000	100%

CONCLUSIONS

In this paper we have used a genetic algorithm to optimize the layout of the Arabic keyboard. The optimized layout gives 35% relative increase in the typing speed. Moreover, the optimized layout solves some of the problems found in the common Arabic keyboard layout. This layout gives better allocation for the frequently used letters such as Thal "ذ", and does not dedicate precious key locations for two-letter key combinations such as Lam-Alef "لا". We have also found that the common layout by is 6% better than the ASMO 663 layout.

For future work, we intend to train volunteers on using the optimized layout to obtain experimental data about the optimized layout's performance, comfort, and trainability. We can collect timing data from these volunteers and use the letter pair times to adjust the model used in Equation (2). Moreover, we intend to try to take more factors in the optimization such as typist comfort and error rate.

REFERENCES

Arab Standardization and Metrology Organization (ASMO). 1985. *Standard 449: 7-Bit Arabic Code*. Arab League, Cairo, Egypt.

Arab Standardization and Metrology Organization (ASMO). 1987. *Standard 663: Arabic Keyboard Layout*. Arab League, Cairo, Egypt.

Campbell-Kelly M. 2005. The User-friendly Typewriter. *The Rutherford Journal*. Retrieved Jul 20, 2008 from http://www.rutherfordjournal.org/article010105.html

Deshwal P.; and Deb K. 2003. "Design of an Optimal Hindi Keyboard for Convenient and Efficient Use." Technical report KanGAL 2003005, Indian Institute of Technology, Kanpur.

Goettl J.; Brugh A.; and Julstrom B. 2005. "Call Me E-Mail: Arranging the Keyboard with a Permutation-Coded Genetic Algorithm." In *Proceedings of the ACM Symposium on Applied Computing* (Santa Fe, New Mexico, USA, Mar), 947-951.

Goldberg E. 1989. *Genetic Algorithms in Search, Optimization and Machine Learning*. Addison-Wesley Longman, Boston, MA.

Hiraga Y.; Ono Y.; and Yamada-Hisao. 1980. "An Analysis of the Standard English Keyboard." In *Proc. 8th Conf. on Computational Linguistics* (Tokyo, Japan). 242-248.

Jordan Institution for Standards and Metrology (JISM). 1994. *Minutes of Meeting of the Arabic Letter Committee*. Mar 10, 1994, Amman, Jordan.

Light L.; and Anderson P. 1993. "Typewriter Keyboards via Simulated Annealing." *AI Expert*, (Sep).

Noyes, J. 1998. "QWERTY-The Immortal Keyboard." *Computing & Control Engineering Journal* 9, No.3 (Jun), 117-122.

Wagner M.; Yannou B.; Kehl S.; Feillet D.; and Eggers J. 2003. "Ergonomic Modeling and Optimization of the Keyboard Arrangement with an Ant Colony Algorithm." *European Journal of Operations Research* 148, No.3 (Aug), 672–686

Walker C. 2003. "Evolving a More Optimal Keyboard." Technical Report (Dec).

AUTHOR BIOGRAPHY

Tareq Malas is a bachelor student in the Computer Engineering Department at the University of Jordan. He is expected to graduate in Sep 2008. He has won a full scholarship for pursuing postgraduate studies in King Abdullah University of Science and Technology (KAUST).

Sinan Taifour is a bachelor student in the Electrical Engineering Department at the University of Jordan. He is expected to graduate in Feb 2009.

Gheith Abandah holds BS degree in Electrical Engineering from the University of Jordan (1985) and MS and PhD degrees in Computer Engineering from the University of Michigan (1995 and 1998). He is an Assistant Professor of Computer Engineering in the University of Jordan since 1998, and department chair since 2006. His areas of research are Computer Arabization, Arabic Optical Character Recognition, Computer Architecture, Parallel Processing, and Software Development.

COMPUTER-GENERATED MUSIC USING GRAMMATICAL EVOLUTION

Abdel Latif Abu Dalhoum (1), Manuel Alfonseca (2), Manuel Cebrián (2), Rafael Sánchez-Alfonso (3) and Alfonso Ortega (2)
(1) University of Jordan, Computer Science Department, a.latif@ju.edu.jo
(2) Escuela Politécnica Superior, Universidad Autónoma de Madrid SPAIN, {Manuel.Alfonseca, Manuel.Cebrian, Alfonso.Ortega}@uam.es
(3)
Universidad Autónoma de Madrid & Neoris, Rafael.Sanchez@neoris.com

KEYWORDS

Evolutionary Computation, Grammatical Evolution, Genetic Algorithms, Computer Generated Music, Coding and Information Theory, Clustering

ABSTRACT[1]

This paper proposes a new musical notation with Lindenmayer grammars, and describes the use of grammar evolution for the automatic generation of music expressed in this notation, with the normalized compression distance as the fitness function. The computer music generated tries to reproduce the style of a selected pre-existent piece of music. In spite of the simplicity of the algorithm, the procedure obtains interesting results.

INTRODUCTION

The automatic generation of musical compositions is a long standing, multi disciplinary area of interest and research in computer science, with over thirty years history at its back [1-7]. Our group is interested in the simulation of complex systems by means of formal models, their equivalence and their design, not only by hand, but also by means of automatic processes, such as evolutionary computation, genetic programming and grammar evolution [8-9].

This paper extends Grammatical Evolution to the generation of music similar to a given target or guide piece, in such a way as to capture some of its stylistic properties. Two different generating procedures and fitness functions have been tested and compared.

This paper is organized thus: the second section provides a short introduction to musical concepts, with an enumeration of different ways of representing music, one of which is first presented here. The third section provides an introduction to grammatical evolution, and explains how it has been implemented to generate music. The fourth explains the normalized compression distance, which has been used to compute the distance of the results of the genetic algorithm from the target musical pieces. In the fifth section we describe our experiments. Finally, the last section presents our conclusions and possibilities for future work.

MUSICAL REPRESENTATION

The three fundamental elements in music are melody, rhythm and harmony. In the experiments performed in this paper, we shall restrict ourselves to melody, leaving the management of rhythm and harmony as future objectives. In this way, we can forget about different instruments (parts and voices) and focus on monophonic music: a single performer executing, at most, a single note on a piano at a given point in time. Melody consists of a series of musical sounds (notes) or silences (rests) with different lengths and stresses, arranged in succession in a particular rhythmic pattern, to form a recognizable unit.

In the English notation for Western music, the names of the notes belong to the set {A, B, C, D, E, F, G}. These letters represent musical pitches and correspond to the white keys on the piano. The black keys on the piano (the sharp or flat notes) are modifications of the white key notes. From left to right, the key that follows a white key is its sharp key, while the previous key is its flat key. A black key is indicated by adding a symbol to the white key name (as in A# or A+ to represent A sharp, or in B♭ or B- to represent B flat).

[1] ***Acknowledgement***: This work has been partially sponsored by the Spanish Ministry of Science and Technology (MCYT), project number TIC2002-01948.

The distance from a note to its flat or sharp notes is called a "half step" and is the smallest unit of pitch used in the piano, where any two adjacent keys are separated by a half step, no matter their color. Two consecutive half steps are called a whole step. Instruments different from the piano may generate additional notes; in fact, flat and sharp notes may not coincide; also, in different musical traditions (such as Arab or Hindu music) additional notes exist. In this paper we shall restrict to the Western piano lay-up, thus simplifying the problem to just 88 different notes separated by half steps. By counting the number of half steps between two notes, we can obtain the interval, or difference in pitch between the two notes. Intervals between two successive notes are called melodic intervals, whereas those between two simultaneously sounding notes are harmonic intervals. Since this work focuses on monophonic music, only melodic intervals will be considered.

Notes and rests have a length or time duration. There are nine different standard lengths, each double than the next. We will consider only the first seven: whole, half, quarter, quaver, semi-quaver, quarter-quaver and half quarter-quaver. Intermediate durations are obtained by means of dots or periods. The complete specification of notes and silences includes their lengths.

A piece of music can be represented in several different, but equivalent ways:

- With the traditional Western bi-dimensional graphic notation on a pentagram.

- By means of certain coding systems which are used to keep and reproduce music in a computer or a recording system, with or without compression, such as wave sampling, MIDI, MP3, etc.

- Through a set of character strings: notes are represented by letters (A-G), silence by a P, sharp and flat alterations by + and – signs, and the lengths of notes by a number (0 representing a whole note, 1 a half note, and so on). Adding a period provides intermediate lengths. Additional codes define the tempo, the octave and the performance style (normal, legato or staccato). Polyphonic music is represented with sets of parallel strings.

- By means of sets of integer pairs. The first number in the pair represents the pitch of the note in the piano keyboard (1 to 88), with 0 representing a silence. The second corresponds to the length of the note, as a multiple of the minimum unit of time. Polyphonic music may be represented by means of parallel sets of integer pairs.

- In this paper we are offering a new way to represent music by means of a character string, similar to those used with turtle graphics [10]. the alphabet used consists of four symbols: Σ = { F, f, +, - }. A given note with a given length is represented by a string of successive letters 'F' (as many as the length of the note is a multiple of the minimum length). The pitch of the note is represented by the state of the turtle, which is defined as the number of '+' signs minus the number of '-' signs previous to the first F in the current note. If this number is positive, the current note is located as many half steps above the initial state note; if it is negative, the same number of half steps below the initial note. The initial note (which corresponds to the initial state of the turtle) is assumed to be note C in octave 3 in the piano. Strings with the letter 'f' represent silences with the appropriate length (in this case the pitch information is ignored). For example: the set of two notes O3C3D3 would be translated as FF++FF if we consider semiquavers to be the minimum note length.

In our experiments, we represent melodies by the last three notation systems. We have built functions which translate music represented in one of those three formats into any of the others and into the MIDI format, for reproduction.

GRAMMATICAL EVOLUTION

Grammatical Evolution (GE) [11-12] is a grammar based, linear genome system, which has been applied in the area of automatic programming to automatically generate programs or expressions in a given language that solve a particular problem. Chomsky serial derivation grammars have been applied in most GE applications. We have also used Lindenmayer parallel derivation grammars [13]. The genotype is usually a string of 8 bit binary numbers, treated as integer values from 0 to 255. The phenotype is a running computer program generated by a genotype-phenotype mapping process. The mapping benefits from genetic code degeneracy, i.e. different integers in the genotype generate the same phenotype. The genotype-phenotype mapping in Grammatical Evolution is deterministic: each individual is always mapped to the same phenotype.

In Grammatical Evolution, standard genetic algorithms are applied to the different genotypes in a population, using crossover and mutation operators. For each domain, the proper fitness function must be designed to be used by the genetic algorithm to perform selection. This technique has been successfully applied to the automatic programming of problems in many different domains. We have used it to generate fractal curves with a given dimension [13].

Our genetic algorithm generates music from an initial population of 64 vectors of integers in the [0-255] interval. The genotypes of individuals in the population are translated into music by means of the following Lindenmayer grammar:

```
F ::= F                    (0)
    | FF                   (1)
    | F+                   (2)
    | F-                   (3)
    | +F                   (4)
    | -F                   (5)
    | F+F                  (6)
    | F-F                  (7)
    | +                    (8)
    | -                    (9)
    | FFFF                 (10)
    | FFFf                 (11)
f ::= f
+ ::= +
- ::= -
```

The translation is performed according to the following algorithm:

1. The axiom (first word) of the Lindenmayer grammar is the string 'F'. Rules in the previous grammar are numbered 0 to 11.
2. As many elements from the remainder of the genotype are taken (and removed) from the left of the genotype as the number of F in the current word. If there remain too few elements in the genotype, the required number is completed circularly.
3. The current word derives a new one in the following way: each F in the word is replaced by the right hand side of the rule whose number is equal to the remainder of the corresponding genotype integer obtained in the previous step modulo 12.
4. If the genotype is now empty, the algorithm stops and the last derived word is the output, a piece of music represented by the notation we are proposing, which has been described in the previous section.
5. If the derived word contains no 'F', the whole word is replaced by the axiom.
6. Go to step 2.

Example: Let the genotype be the string of integers `112 125 203 14 87 136 224`. The initial string 'F' contains one 'F'. The first element in the genotype is 112. Its remainder module 12 is 4. Rule 4 is applied, generating the string '+F'. This is the end of the first loop.

In the second loop, we start with genotype `125 203 14 87 136 224`. The current string '+F' contains one 'F'. The first element in the genotype is 125, whose remainder module 12 is 1. Rule 1 is applied, generating the string '+FF'. Here ends the second loop.

In the third loop, we start with genotype `203 14 87 136 224`. The current string '+FF' contains two 'F'. The first two elements in the genotype are 203 14, whose remainders module 12 are 11 and 2. Rules 11 and 2 are applied (one to each 'F'), generating the string '+FFFfF+'.

In the fourth loop, we start with genotype `87 136 224`. The current string '+FFFfF+' contains four 'F'. The genotype has only three elements, therefore the first one is added to the end circularly, giving 87 136 224 87, whose remainders module 12 are 3, 4, 8 and 3. Rules 3, 4, 8 and 3 (one to each 'F'), generating the string '+F-+F+fF-+'. Since the genotype is now empty, this string is the phenotype, which corresponds to notes 'C+C+PD', all with the same basic length.

We have used the following genetic algorithm to generate music:

1. One musical piece is selected as the target or guide for music generation.
2. The program generates a random population of 64 vectors of N integers, where N is the length of the guide piece. Each vector represents a genotype.
3. The fitness of the genotypes is computed as the distance to the guide set, measured by means of the normalized compression distance (see below).
4. The genotypes are ordered by their increasing distance to the guide set.
5. If the goal distance has been reached, the program stops.
6. 30 pairs of parent genotypes are built. Genotypes with better fitness have a higher probability of being used. Each pair of parents gives rise to two pairs of children, made of copies of the parents and modified by four genetic operations. The 60 genotypes with least fitness are removed. (The 4 genotypes with the best fitness remain in the next population). The 60 children are added to the population to make again 64, and their fitness is computed as in step 3.
7. Go to step 4.

The four genetic operations mentioned in the algorithm are:

- Recombination (applied to 100% generated genotypes). The genotypes of both parents are combined using different procedures to generate the genotypes of the progeny. Different recombination procedures have been tested in this set of experiments to find the best combination.

- Mutation (one mutation was applied to every generated genotype, although this rate may be modified in different experiments). It consists of replacing a random element of the vector by a random integer in the same interval.

- Fusion (applied to a certain percentage of the generated genotypes, which in our experiments was varied between 5 and 10). The genotype is replaced by a catenation of itself with a piece randomly broken from either itself or its brother's genotype.

- Elision (applied to a certain percentage of the generated genotypes, in our experiments between 2 and 5). One integer in the vector (in a random position) is eliminated.

The last two operations, together with some recombination procedures, allow longer or shorter genotypes to be obtained from the original N element vectors.

THE NORMALIZED COMPRESSION DISTANCE

The fitness function we have used for the genetic algorithm computes the distance between two pieces of music by expressing both as note-length pair sequences (the third notation in the previous discussion), converting the sequence of notes to a sequence of intervals (this is done by subtracting each note from the next) and computing the distance between both sequences of intervals by means of the normalized compression distance [14-16], an approximation of the universal distance between any two objects defined as a function of the Kolmogorov complexities of the objects, which can be computed by means of standard compressors. The expression we have used to compute the normalized compression distance is the following:

$$\tilde{d}(x,y) = \frac{C(xy) - min\{C(x), C(y)\}}{max\{C(x), C(y)\}}$$

Where `C(x)` is the length obtained by compressing object `x` with compressor `C`, and `xy` is the concatenation of `x` and `y`. This metric has been reported to outperform some of the finest algorithms for clustering music by genre [17]. This suggests that the normalized compression distance works well to extract features shared between two musical pieces. The compressor used to compute the distance between the musical objects (the two sequences of intervals) was the LZ77 algorithm [18-19].

We decided to apply the fitness function only to the relative pitches of the notes in the melody (this is done by working on intervals rather than absolute notes), ignoring the absolute pitches and the note lengths, because our own studies and other's [17] suggest that a given piece of music remains recognizable when the lengths of its notes are replaced by random lengths, while the opposite doesn't happen (the piece becomes completely unrecognizable if its notes are replaced by a random set, while maintaining their lengths).

EXPERIMENTS

In our experiments, we first used as the guide *Yankee Doodle*, represented by the following string:

M2T2O3L2C+4C+4D+4F4C+4F4D+4O2G+4O3C+4
C+4D+4F4C+3C4P4C+4C+4D+4F4F+4F4D+4C+4C4
O2G+4A+4O3C4C+3C+4P4O2A+4.O3C5.O2A+4G+
4A+4O3C4C+4P4O2G+4.A+5.G+4F+4F3G+4P4A+4.
O3C5.O2A+4G+4A+4O3C4C+4O2A+4G+4O3C+4C4
D+4C+3C+3

After applying the genetic algorithm, the succession of notes obtained was completed by adding length information in the following way: each note was assigned the length of the note in the same position in the guide piece (the guide piece was shortened or circularly extended, if needed, to make it the same length as the generated piece, which could be shorter or longer). The number of generations needed to reach a given distance to the guide depends on the guide length and the random seed used in each experiment, and follows an approximate Poisson curve [20]. In successive executions of the algorithm with different random seeds, we obtained different melodies at different distances from the guide. For instance, the distance to the guide of the following generated piece is 0.58 (figure 1 shows the beginning in typical musical notation):

T1O3M2C+4O3D4O3D3O3D4O3C+4P4O3E3.O3F+4P4O3E4P4O3D4O3C+4O3C3O3C+3O2M1B3.P4O2M2B4O3C+2O2A3O2G+3O2M1A2P4O2M2A4O2A+2O2A3.O2G4O2F+4O2G3P3O2F4O2F+4O2F+4P3.O2D+4O2F1P4O2F4O2F3O2E4P4O2F4P4O2E4P4O2F4O2D4O2C4O2M1C+3.P4O2M2C2O2C+4O2D4O2D+4O2D+3.O2M1E3.P4O2M2F4O2F3O2G2O2A4O2A+3O2A4O2A+4O2B4P4P4O2B4O3C4

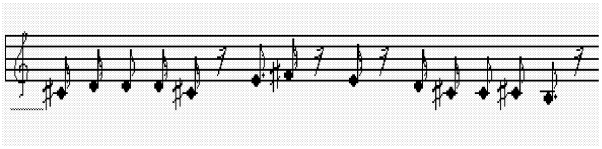

Figure 1: Beginning of music generated from *Yankee Doodle*.

In another experiment, we used the seventh prelude by Chopin as the guide piece, getting the following result at a distance of 0.67 from the guide (see also the beginning in figure 2):

T0O3M2C4O2M1A+3.P4O2M2A+4O2B4P4O2A+4O2M1B3.P4O2M2A+4O2B4O3E4O3E4O3M1E2P4O3M2E4O3F4P4O3F4O3F4O3F4O3M0D1P3O3M2D+4O3E4O3C+4O3M1C+3.P4O3M2C+4O3D4P4O3C+4O3M1D3.P4O2M2B3O3C4O3D+4P4O3D+4O3M0C+3.P3O3M2C4O3C+4O3C4O3C4O3C+4P3O2A4O2A+2O2A2O2A3O2A4O2M1A+3.P4O3M2D4O3F4O3D+4O3M1D+3.P4O3M2D+3O3E4P4O3D+4

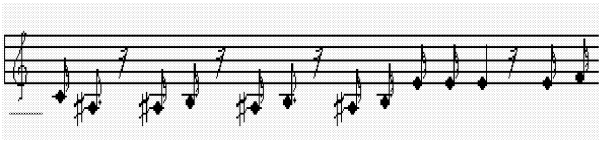

Figure 2: Beginning of music generated from Chopin's seventh prelude.

It can be noticed that our first generated music has a lighter sound to the ear than the second, which may be a consequence of the different guide pieces used in both cases.

In our third experiment we changed the fitness function to work directly at the level of the music represented by the turtle strings. The normalized compression distance was also used to compute the distance of the two character strings (the guide piece and each member of the population). In this case, both the pitches and the lengths of the notes were evolved at the same time. The following shows one result we obtained using Chopin's seventh prelude as the guide piece (see also the beginning in figure 3):

T1O2M2D+4O2F2.O2F+4O2G+3O2G+3P4O2G+4P4O2A2O2A+4O2A4O2A+4O2A4O2A+4P4O3F4O3D+3O3E4O3F3O3A+4O3A3O3G+4O3A3O3B3O3A+4O3B4O3B4O3A+4O3G+4O3G+4O3F+3O3G4O3M1G3.P4O3M2G2O3F+4P4O3G2.O3F+4O3G4O3F+4O3F4O3F+4O3F+2O3G+4O3G4P4O3G+4O3A3O3G+4O3A3O3A+4O3A4O3A+3O3A+4O3M1B3.P4O3M2B3P4O3B4O3A+4O3A2O3G+4P4O3B4O3B4O3A+4O3G+4O3G+4O3A3O3G+4P4O3A4O3A2O4C2P4O3M1B3.P4P3O3M2B4O4C4O3B4O4C4P4P4O4C+4O4D4O4E4O4M1D+2P4O4M2D+4P4P4O4F+2O4G4O4F4O4E4O4D+3P4P4O4G+4O4G4O4E4O4F4O4F+4O4G4O4G4O4F+4P4O4G4O4F+4O4G3.O4A3O4A4O4G+4O4A3O4G+4O4A4P4O4M1F+3.P4P3O4M2G1.O4G+3O4E3O4C+4O3A3O3M1G+3.P4O3M2F4O3F3O3E3O3E3O3G4O3G4O3F+4O3M1G2.P4O3G1O3M2G+4O3A3O3G+4P4O3A4O3G+4O3A4O3A3.O3G4P4O3F4O3F+4O3M1F2P4O3M2F+1O3F+3O3F4P4O3F2O3D4

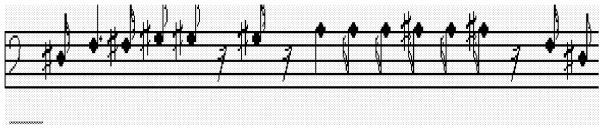

Figure 3: Beginning of another piece of music generated from Chopin's seventh prelude.

CONCLUSIONS AND FUTURE WORK

We have defined a new musical notation which can be used to automatically generate music by means of grammatical evolution and a genetic algorithm, minimizing its distance from a given guide piece. In the first set of experiments, just the pitches of the notes were evolved, in another set of experiments both pitches and lengths evolved at the same time. Some of the pieces thus generated seem to capture some of the characteristics of the guide piece (such as sounding lighter or classical-like).

In the future we intend to combine our results with those of other authors [18-19] to use as the target for the genetic algorithm more than one piece of music by the same author, thus trying to capture the style in a more general way. We also intend to test different fitness functions and the effect of different recombination procedures.

REFERENCES

[1] J. McCormack (1996). Grammar-based music composition. *Complex International,* Vol 3.

[2] J. Biles (1994). GenJam: A Genetic Algorithm for Generating Jazz Solos, *Proceedings of the 1994 International Computer Music Conference*, ICMA, pp. 131-137, San Francisco, 1994.

[3] E. Bilotta, P. Pantano, V. Talarico (2000). Synthetic Harmonies: an approach to musical semiosis by means of cellular automata, *Leonardo*, MIT Press, vol. 35:2, pp. 153-159, April 2002.

[4] D. Lidov, J. Gabura (1973). A melody writing algorithm using a formal language model, *Computer Studies in the Humanities* Vol. 4:3-4, pp. 138-148, 1973.

[5] P. Laine, M. Kuuskankare (1994). Genetic Algorithms in Musical Style oriented Generation, *Proceedings of the First IEEE Conference on Evolutionary Computation*, pp 858-862, Orlando, Florida, vol. 2, 1994.

[6] D. Horowitz (1994). Generating Rhythms with Genetic Algorithms, *Proceedings of the ICMC 1994*, pp. 142-143, International Computer Music Association, Århus, 1994.

[7] B. Jacob (1995). Composing with Genetic Algorithms, *Proceedings of the 1995 International Computer Music Conference*, pp. 452-455, ICMC, Banff Canada, 1995.

[8] Alfonseca, M., Ortega, A., Suárez, A. (2003). Cellular automata and probabilistic L systems: An example in Ecology, in *Grammars and Automata for String Processing: from Mathematics and Computer Science to Biology, and Back*, ed. C. Martin-Vide & V. Mitrana, Taylor & Francis, pp. 111-120. ISBN: 0415298857.

[9] Ortega, A., Abu Dalhoum, A., Alfonseca, M. (2003). Grammatical evolution to design fractal curves with a given dimension, *IBM Journal of Research and Development*, Vol. 47:4, p. 483-493, Jul. 2003.

[10] Papert, S.: "Mindstorms: Children, Computers, and Powerful Ideas", Basic Books, New York, 1980.

[11] M. O'Neill and C. Ryan: *Grammatical Evolution*, IEEE Transactions on Evolutionary Computation, 5, Np.4, 349-358 (2001).

[12] M. O'Neill and C. Ryan: *Grammatical Evolution: Evolutionary Automatic Programming in an Arbitrary Language*, Kluwer Academic Publishers, 2003, Book Series: Genetic Programming: Volume 4, ISBN 1-4020-7444-1.

[13] A.Ortega, A.Abu Dalhoum, M.Alfonseca: *Grammatical evolution to design fractal curves with a given dimension*, IBM Journal of Res. and Dev., Vol. 47:4, p. 483-493, Jul. 2003.

[14] M. Li, X. Chen, X. Li, B. Ma and P. Vitányi (2003). The similarity metric, *Proc. 14th ACM-SIAM Symposium on Discrete Algorithms*, pp. 863-872.

[15] P. and M. Li (1993). An Introduction to Kolmogorov Complexity and its Applications, *Springer-Verlag*.

[16] R. Cilibrasi and P. Vitanyi (2005). Clustering by Compression, *IEEE Trans. Information Theory*, Vol.51 No.4, pp. 1523-1545.

[17] M. Li and R. Sleep (2004). Melody Classification using a Similarity Metric based on Kolmogorov Complexity, *Sound and Music Computing*.

[18] J. Ziv and A. Lempel (1997). A universal algorithm for sequential data compression, *IEEE Transactions on Information Theory*, Vol.23:3, pp. 337-343.

[19] S. R. Kosaraju and G. Manzini (1997). Some entropic bounds for Lempel-Ziv algorithms, *Data Compression Conference*, pp. 446.

[20] M. Alfonseca, M. Cebrián, A. Ortega. *A simple genetic algorithm for music generation by means of algorithmic information theory*. IEEE Congress on Evolutionary Computation (CEC'2007), Singapore, Sep.25-28, 2007. Published in the Proceedings, pp. 3025-3042, ISBN 1-4244-1340-0, IEEE Press.

SUMMARY OF AUTHOR BIOGRAPHICAL DATA

Abdel Latif Abu Dalhoum is a doctor in computer science and teaches at the university of Jordan, Manuel Alfonseca is a doctor in electronics engineering and computer scientist, and full professor at the Universidad Autónoma of Madrid, Manuel Cebrián is a doctor in computer science, Rafael Sánchez-Alfonso is a Ph. D. student and Alfonso Ortega is a professor at the Universidad Autónoma of Madrid.

Perceptual Modelling of Wavelet Coefficients for Grey Scale Images

G. Al-Hudhud
Software Engineering Department.
Al-Ahliya Amman University
email: ghudhoud@ammanu.edu.jo

KEYWORDS
Uniform Quantisation, Human Visual System, Automatic Quantisation Matrix

ABSTRACT

Wavelet domain statistical models have been shown to be useful for certain applications, e.g. image compression, watermarking and Gaussian noise reduction. One of the main problems for wavelet-based compression is to overcome quantization error efficiently. Inspired by Weber-Fechners Law, we introduce a logarithmic model that approximates the non-linearity of human perception and partially precompensates for the effect of the display device. A logarithmic transfer function is proposed in order to spread the coefficients distribution in the wavelet domain in compliance with the human perceptual attributes. The standard deviation σ of the logarithmically scaled coefficients in a subband represents the average difference from the mean of the coefficients in that subband. The standard deviation is chosen as a measure of the visibility threshold within this subband. Computing the values of σ's for all subbands results in a quantisation matrix for a chosen image. A major advantage of this model is to allow for observing the visibility threshold and automatically produce the quantisation matrix that is content dependant and scalable without further interaction from the user.

INTRODUCTION

Wavelet algorithms have been widely studied for certain image processing applications. Image compression and watermarking are the most common among these applications (Watson et al. 1997) and (Lam 2004). Wavelets can also decorrelate the coherent portions of the image for the purpose of reducing the number of significant coefficients required to represent this portion locally (Beylkin and Vassiliou 2001).

Wavelet coefficients should exhibit a certain structure or behavior that can be well modelled to extract the relevant information. The feature extraction depends on the requirements of that certain application. However, modelling wavelet coefficients is a complex task because it must involve different factors, e.g. the nature of the image, the human visual perception and a response of the visualisation device.

Feature extraction that satisfy the human perception and display factors requires choosing an appropriate domain to process the image information. A non-linear representation of images is required to bring the human visual perception and /or the characteristics of the display device into consideration. In addition, when a non-linear domain is choosen, choosing the type of transform function is essential. The γ-correction function and the logarithmic scaling function are the most popular transform functions in the image processing field. Nonlinear representation of the images is also widely used within the computer graphics community to code the brightness and colour (Schlick 1994). The model presented in this paper is motivated by Weber-Fechner's Law. Weber-Fechner's Law describes the differential sensitivity of the human perception using a logarithmic transfer function to represent the perceived intensity of a certain source.

The work presented in this paper describes a wavelet-based statistical model that provides an automatic production of a quantisation matrix that serves image compression application. The derived quantisation matrix produces errors bellow the visibility threshold of the human eye. Nevertheless, none of the existing proposed techniques provide an automatic way to calculate a wavelet-dependent and image-content adapting quantisation matrix as we are proposing.

The organization of the paper is as it follows. In section 2, an overview on modelling wavelet coefficients as well as the theoretical justifications of processing the wavelet coefficients in the nonlinear domain are given. The proposed model and feature extraction on subband basis, is detailed in section 3. Results on tests of the effectiveness of the subband-based features are reported in Section 4. Conclusions and future research directions can be found in Section 5.

Theoretical Background

Due to the multi-channel nature of the human visual system (HVS), researchers in the field have paid attention to the wavelet multi-channel features. This is because it supports representing the image into spatial-frequency and orientation components. Hence, this representation facilitates integration of HVS properties into the quantisation stage. The invisibility of quantisation errors in the reconstructed image necessitates a good representation of the image contents and appropriately chosen quantisation steps for each subband. Many wavelet-based quantization strategies are not spatially dependent, i.e. a specific step-size is used to quantize each wavelet band (Chandler and Hemami 2002, Watson et al.

1997). Ideally, a model that supports both automating the process of producing image-contents-adaptable quantisation matrix and produces quantisation errors below the visibility thresholds should lead to efficient compression algorithms. Depending on the application, current methods for modelling wavelet coefficients are either statistical models or Human Visual System HVS based systems.

Statistical Modelling of Wavelet Coefficients

Statistical models are widely used as they describe the distribution of wavelet coefficients as Gaussian or Generalised Gaussian. For example, the Gaussian Mixture model, described in (Chipman et al. 1997), and the Generalized Gaussian distribution presented in (Moulin and Liu 1999) are commonly used to model the wavelet coefficients distribution. A typical statistical model falls into one of two categories: Marginal Probabilistic Model or Joint Probabilistic model. A good review of statistical modelling and statistical properties of wavelet coefficients can be found in (Romberg et al. 1997, Buccigrossi and Simoncelli 1999).
The Marginal distributions of wavelet coefficients, described in (Strela et al. 2000) usually have a prominent peak at zero and heavy tails. An example of Marginal Probabilistic model is presented in (Portilla et al. 2002) as a Gaussian Scale Mixture model in which each neighborhood of wavelet coefficients is a product of a Gaussian random vector, and an independent random scalar multiplier. Joint Probabilistic models, as the one presented by Strela *et. al.* in (Strela et al. 2000), are efficient in detecting inter-scale dependencies, e.g. Hidden Markov Models (Romberg et al. 1997), or intrascale correlations, e.g. Random Markov Field models (Malfait and Roose 1997). Gaussian-based models are considered efficient in image denoising algorithms especially for noise removal.
Recently published work, (Li and Gray 2000, Vetterli and Kovacevic 2000), assumes that wavelet coefficients in high frequency subbands, i.e. the LH, HL, and HH subbands , tend to follow Laplacian distributions. Simoncelli and Adelson (Simoncelli and Adelson 1996), modelled the wavelet coefficients of the image using a two parameter Laplacian distribution. This approximation is seen to work quite well as a means of distinguishing continuous-tone images from graphics and text by means of the goodness of fit. Another example is presented by Mallat in (Mallat 1989) and assumes that the wavelet coefficients follow the Laplacian distribution. Strella *et al.* designed a uniform quantiser (Strela et al. 1999) based on Mallat's assumption.
Based on observations of many distributions, the coefficients have been shown to demonstrate a Laplacian-like but not an accurate Laplacian behaviour. To visualize the behaviour of the wavelet coefficients in the high frequency subbands (HH and LH), the histograms of the $BI9/7$ wavelet transformed image are displayed in Figure 1a and 1c.
The above mentioned models exploit the statistical features of the wavelet coefficients in order to provide an appropriate modelling of image contents. Yet, an appropriate modelling of the coefficients is in high demand for providing subband statistical parameters that can be used for further processing/preprocessing operations. In addition, the above mentioned statistical models do not consider the HVS properties.

Proposed Logarithmic Model of Wavelet Coefficients

Based on the fact that the non-linear response of human visual perception to intensity is effectively the inverse of display non-linearity. Motivated by the nonlinearity of the human visual perception, non-linearity of display devices γ, and non- Laplacian behaviour of the wavelet coefficients, the transform function is proposed in order to transform the image coefficients in the wavelet domain. This function is proposed because it: a) approximates the human visual perception, and b) provides better fits for Laplacian distribution of the wavelet coefficients than the original coefficients.
Since the logarithm is not defined for 0, a typical implementation of this operator is to add 1 to the original values before taking the logarithm. Let $C(i,j)$ denote a wavelet coefficient in a subband, the logarithmic mapped value of this coefficient, denoted by $E(i,j)$, is given by

$$E(i,j) = log_{\gamma^*}(1+|C(i,j)|) \quad (1)$$

The goodness of fit of an observed distribution within a subband and ideal Laplacian distribution was obtained by running a few trials to choose a value for the base γ^*. Experimental results for different images and different wavelet families have shown that a value of γ^* less than 2.5 gives the best fit.
Figure 1 displays both the histograms of $BI9/7$ wavelet coefficients for subband HL and the logarithmically scaled coefficients of the same image with a Laplacian distribution superimposed on both distributions. The histogram of the original coefficients, presented in Figure 1c, demonstrates a high peak at zero and long fat tails with the superimposed Laplacian distribution mismatching the coefficients distribution. In Figure 1d, the distribution of the logarithmically scaled coefficients for the same subband is not as steep as the original coefficients and the histogram shows a better fit to the Laplacian distribution.
The distribution of the coefficients in the nonlinear domain using $BI9/7$ wavelets have been tested and the results are similar to those reported in figures 1a and 1c.

Scalable Image Dependent Quantisation Matrices

From this model, a quantisation matrix can be automatically computed based on defining a visibility threshold which produces quantisation errors just below the visibility threshold of the human eye. The procedure to compute this matrix is independent of the wavelet basis functions but it produces image-dependent quantisation matrices (Q_{log}) for a specific wavelet. In one sense, one can also say that this leads to a basis-dependent quantisation matrices. The idea is to achieve better perceptual results by maintaining an approximately

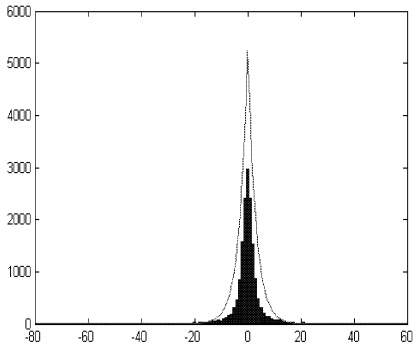

(a) ***Lena: Original coefficients.***

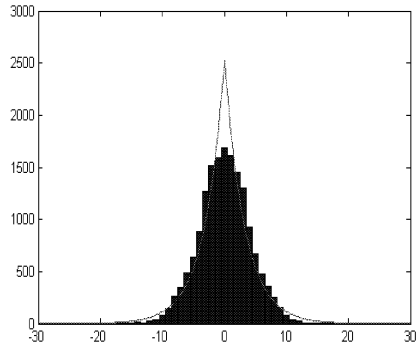

(b) ***Lena: logarithmic scaled coefficients.***

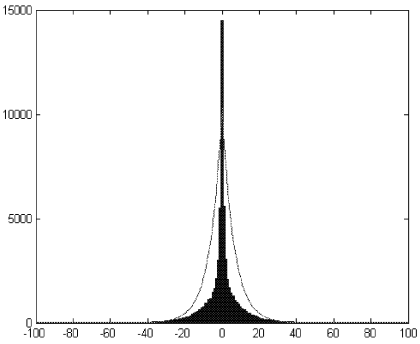

(c) ***Mallorca: Original coefficients.***

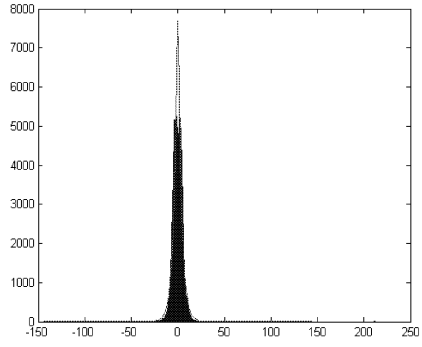

(d) ***Mallorca: logarithmically scaled coefficients.***

Figure 1: The histograms of the Lena HH and the Mallorca HL subbands for the $BI9/7$ coefficients.

constant ratio between adjacent intensity levels, placing the quantisation levels apart by a just below noticeable change according to the linear domain. Similar approach is currently being used to design quantisation matrices based on the visibility of quantisation errors resulted from the Discrete Cosine Transform (Jr. and Peterson 1992) and (Peterson et al. 1993). The quantisation matrix Q_{log} is produced by computing the standard deviation (σ) for the logarithmically scaled coefficients in each subband. The standard deviation (σ) as the average difference from the mean value in each subband represents the quantisation factor assigned to that subband. The coefficients in a subband are then quantised using this quantisation factor into a number of levels. Since the logarithmic scale uniformly spreads coefficients distribution over a wider range according to the human perception, using this σ as the quantisations factor allows for the most effective perceptual use to be made of the number of levels available. This implies that for a given subband, any difference less than the average difference σ produces an invisible quantisation error. Let $M_{L,S}$ denote the mean value of the subband S in the Lth level of decomposition, computed as follows:

$$M_{L,S} = \frac{1}{N \times M}\{\Sigma C(i,j)\} \quad i = 1:N\ ,\ j = 1:M \qquad (2)$$

The standard deviation $\sigma_{L,S}$ for the same subband, is given by:

$$\sigma_{L,S} = \frac{1}{N \times M}\sqrt{\Sigma(C(i,j) - M_{L,S})}\ \ L = 1:4,\ \ S = 1:4 \quad (3)$$

For $four$ levels of decomposition, the quantisation matrix Q_{log} holds 4×4 quantisation factors., as there are four subbands for each level of decomposition.

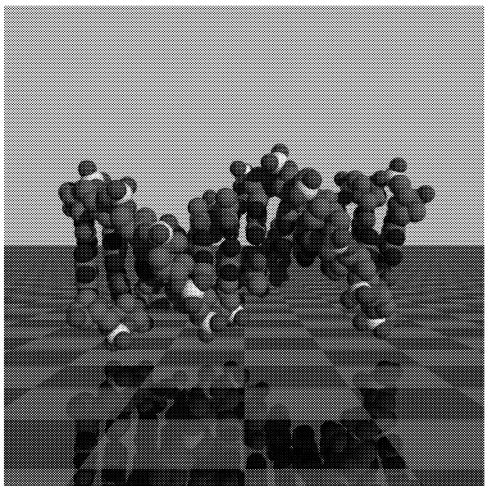

Figure 2: DNA image: Synthetic Images.

Experimentation Results

The above procedure was first experimented for the Antonini $BI9/7$ wavelet as this allows a direct comparison between

our model and Watson's model (Watson et al. 1997), which was derived for this wavelet basis. We compare the results of quantising different natural and synthetic images using quantisation matrices provided by both methods. We refer to the quantisation matrix calculated by Watson's model as Q_W and the quantisation matrix produced by our model as Q_{log}.
An example synthetic image, shown in Figure 2, is used to test the proposed technique using the Antonini $BI9/7$ wavelet to perform four levels of decomposition. The computed quantisation matrix Q_{log} for the image shown in Figure 2 is presented in Table 1. Table 2 presents the results of using the same procedure and the same wavelet, $BI9/7$, for natural images. The mean square error (MSE) and peak signal to noise ratio ($PSNR$) are computed in order to objectively compare the visual quality offered by the two methods.

Table 1: The quantisation matrices, produced by Watson's model Q_W and by the proposed model Q_{log} for the DNA image, Figure 2.

Model	Level	Orientation			
		1	2	3	4
Q_W	1	14.05	23.03	58.76	23.03
	2	11.11	14.68	28.41	14.69
	3	11.36	12.71	19.54	12.71
	4	14.5	14.16	17.86	14.16
Q_{log}	1	23.524	18.222	36.527	22.84
	2	15.611	17.794	51.246	26.682
	3	11.36	11.937	30.885	17.848
	4	8.3862	12.654	13.287	11.756

Table 2: The results of quantising standard images and synthetic images using both Thresholds quantisation and log-based quantisation, for 4 levels ($BI9/7$).

Image	*NZRS*	*MSE*	*PSNR*
Synthetic Images			
DNA			
Q_{log}	227480	1.6630	43.7128
Q_W	227975	1.6180	43.9515
Natural Images			
Lena			
Q_{log}	46926	2.777	39.2592
Q_W	48347	2.8984	38.8876
Mallorca			
Q_{log}	166050	2.1440	41.5065
Q_W	180587	2.6164	39.7769

Table 2 shows the results of applying the quantisation matrix produced by both methods, proposed method and the threshold method, to a set of images. Table 2 compares the peak signal to noise ration of the output images. For Lena image, applying the generated quantisation matrix Q_{log} to $BI9/7$ coefficients results in 0.95% improvement in the visual quality. Table 3 shows the results of applying the generated quantisation matrix produced by the proposed method to a set of natural images with different wavelet families. The experi-

(a) Q_W.

(b) Q_{log}

Figure 3: Quantised Lena image, ($BI9/7$).

ment involved comparing the results of applying the threshold model using $BI9/7$ to each of the natural images included in table 2 with the results of applying log-based method using different families. For Lena image, the generated quantisation matrix for Daubechies $D4$ wavelet coefficients results in 0.09% improvement in the visual quality. For the same image, applying the generated quantisation matrix Q_{log} to $LA8$ coefficients results in 0.5% improvement in the visual quality. Using the *HAAR* wavelet, the results in Figure **??** show 0.08% loss in visual quality.

(a) Q_W

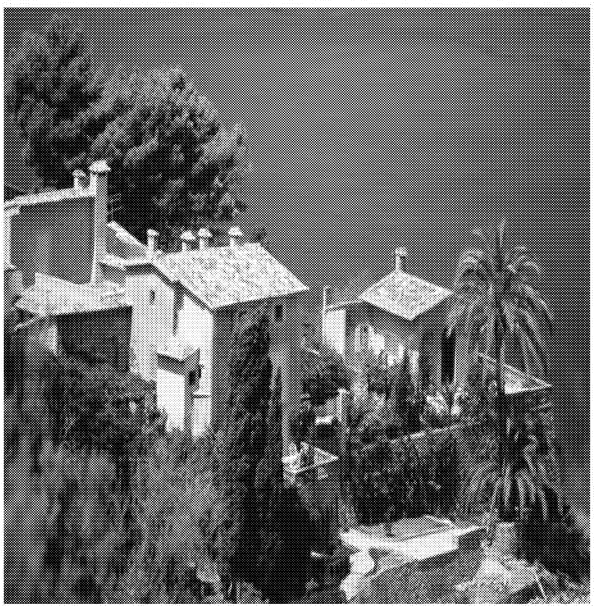

(b) Q_{log}

Figure 4: Quantised Mallorca image, ($BI9/7$).

Table 3: The results of applying the Q_{log} to different images for different wavelet families.

Image	Filter	*NZRS*	*MSE*	*PSNR*
Lena	HAAR	43685	3.0361	38.5844
	D4	45694	2.8537	38.9226
	LA8	46417	2.7584	39.0777
	BI5/3	51647	4.1345	35.4023
	Bi9/7	46926	2.7770	39.2592
Mallorca	HAAR	153426	2.5343	40.0538
	D4	159791	2.3201	40.8207
	LA8	162489	2.1612	41.4369
	BI5/3	205524	4.6264	34.5260
	BI9/7	166050	2.1440	41.5065

Conclusions

In this paper we presented a statistical model of the wavelet coefficients that provides an automatic way to generate a scalable and image-dependent quantisation matrices for wavelet-based compression. The proposed log-based model generates quantisation matrices that will produce quantization errors bellow the visibility threshold. In addition, the proposed logarithmic-based wavelet model maintains the non-linear response of the human visual perception.

Compared to our model, the model presented by Watson *et.al.*, in (Watson et al. 1997), allows for calculating a quantisation matrix that maintains the quantisation errors just below the visibility threshold. However, there are some drawbacks of this model. First, it is designed for a specific wavelet family (i.e. Antonini $BI7/9$). Second, it uses different fits individually that seems to work only partially when combined together because there is no uniform distribution considered for the coefficients. The model we present here, works for any wavelet family, and is based on the Laplacian distribution of the coefficients as a uniform distribution .

The major benefits of the method proposed in this paper for generating the quantisation matrices over other established human visual model are: a) the automation of the process, and b) the scalability feature which allows to opt for the desired trade-off between the compression rate and visual quality, and c) generating image-dependent quantisation matrix.

REFERENCES

Beylkin G. and Vassiliou A., 2001. *Wavelet Transforms and Compression of Seismic Data. Mathematical Geographics Summer School.*

Buccigrossi R.W. and Simoncelli E.P., 1999. *Image compression via joint statistical characterization in the wavelet domain. IEEE Image Process*, 8, no. 12.

Chandler D.M. and Hemami S.S., 2002. *Contrast-based quantization and rate control for wavelet-coded images.* In *in Proceedings on the International Conference on Image Processing, 2002.*

Chipman H.A.; Kolaczyk E.D.; and McCulloch R.E., 1997. *Adaptive Bayesian wavelet shrinkage. J Amer Stat Assoc,*, 92, no. 440.

Jr. A.J.A. and Peterson H.A., 1992. *Luminance-Model-Based DCT Quantization for Color Image Compression.* In *Human Vision, Visual Processing, and Digital Display III, Proceedings of the SPIE,*. B. E. Rogowitz, ed.

Lam E., 2004. *Statistical Modelling of the Wavelets Coefficients with Different Bases and Decomposition Levels. IEE Proc-Vis Image Signal Process*, 151, no. 3.

Li J. and Gray R.M., 2000. *Context-Based Multiscale Classification of Document Images Using Wavelet Coefficient Distributions. IEEE Transactions on Image Processing*, 9, no. 9.

Malfait M. and Roose D., 1997. *Wavelet based image denoising using a Markov Random Field a priori model. IEEE Transactions on Image Processing*, 6, no. 4.

Mallat S.G., 1989. *A Theory for Multiresolution Signal Decomposition: The Wavelet Representation. IEEE Transactions on Pattern Analysis and Machine Intelligence*, II, no. 7.

Moulin P. and Liu J., 1999. *Analysis of multiresolution image denoising schemes using generalized Gaussian and complexity priors. IEEE Infor Theory*, 45, no. 3.

Peterson H.A.; Jr. A.J.A.; and Watson A.B., 1993. *The Visibility of DCT Quantization Noise.* In *SID Digest of Technical Papers.*

Portilla J.; Strela V.; Wainwright M.; and Simoncelli E., 2002. *Image Denoising using Gaussian Scale Mixtures in the Wavelet Domain.*

Romberg J.K.; Choi H.; and Baraniuk R.G., 1997. *Bayesian tree-structured image modeling using wavelet-domain hidden Markov models. IEEE ImaProcess*, 10, no. 7.

Schlick C., 1994. *Quantisation Techniques for Visualisation of High Dynamic Range Pictures.* In *Fifth Eurographics Workshop on Rendering*. Darmstadt, Germany.

Simoncelli E.P. and Adelson E., 1996. *Noise removal via Bayesian wavelet coring.* In *Proc. IEEE International Conference on Image Processing, Lausanne, Switzerland.*

Strela V.; Heller P.; Strang G.; Topiwala P.; and Heil C., 1999. *The Application of Multiwavelet Filterbanks to Image Processing. IEEE Transactions on Image Processing*, 8, no. 4.

Strela V.; Portilla J.; and Simoncelli E.P., 2000. *Image denoising via a local Gaussian scale mixture model in the wavelet domain.* In *n Proc. SPIEMeeting, San Diego, CA.*

Vetterli M. and Kovacevic J., 2000. *Wavelets and Subband Coding*. Englewood Cliffs, NJ: Prentice-Hall, ch 7.

Watson A.B.; Yang G.Y.; Solomon A.; and Villasenor J., 1997. *Visibility of Wavelet Quantisation Noise. IEEE Transactions on Image Processing*, 6, no. 8.

DECISION MAKING

Modeling Prices in Computational Resource Markets

R. Arfa and J. Broeckhove
Department of Mathematics and Computer Sciences,
University of Antwerp, Middelheimlaan 1, 2020, Antwerp, Belgium
email: {Arfa.Ramadan, Jan.Broechove}@ua.ac.be
Tel: +32 3 2653214 , Fax: +32 3 2653204

KEYWORDS
grid, resource management, grid economies, commodity market, price prediction, temporal neural network

ABSTRACT

In the context of grids, economic principles can be introduced in resource management systems to shift from away a system-centric towards a user-centered focus. Individual valuations of resource usage can be expressed on a per job basis through resource prices. In a commodity market model for CPU resources determination of an equilibrium price balances supply and demand.
Because of the possible disruptive effects on operational grids, such approachest need to be investigated with simulators. We use a grid economics simulator that supports the commodity market model to find out whether a temporal neural networks can be used to predict price evolution. Our investigation suggests that they can do so adequately.

INTRODUCTION

One of the key components of any grid is the resource management system that allows resources of a grid to be accessed and utilized efficiently in a coordinated fashion (Krauter et al. 2002). Traditionnally, resource management systems favor system-centric metrics such as e.g. throughput to gauge their effectiveness. Large-scale infrastructures, covering multiple administrative domains have an inherently diverse user base. In such a situation the focus should shift to allocation algorithms that are driven by the user's valuation of the task to be executed. Such user-centric approach will maximize the utility of the grid to the users if when their requirements are extremely diverse.
In this context the introduction of economics based resource management systems has been considered by a number of authors. Indeed, an economic framework where resources are acquired on the basis of supply and demand, allows the user to express the value that a task represents. It provides a means to have the resource management system take this into account in allocation and scheduling algorithms (Buyya et al. 2002). In this work we will focus exclusively on CPU resources.

Such an economics based approach involves the definition of a computational market where grid resources are traded. Prices signal the abundance of resources provided by suppliers with respect to the resource demand formulated by the consumers. Willingness to meet a certain price to acquire a resource for completing a task reflects the value attached to the task. The market organisation can be of different types such as e.g. posted price where each resource provider posts a fixed price for resource usage, auctions, or commodity markets (Buyya et al. 2002).

We will consider the commodity market with equilibrium pricing (Wolski et al. 2001). It corresponds to a situation where each resource is consider equivalent i.e. prices are not tied to specific machines. Evidently such an approach has a scope that is limited to compute-intensive tasks without considerations of data locality for input and output. Market participant communicate their valuation of resource as a willingness to supply (for providers) or acquire (for consumers) a certain amount of resources as a function of the price. The market the sets the price by computing the price level at which the supply equals demand.

Conducting research into resource management systems on operational grids is not feasible because of adverse effects on productivity and the possibility of disruption of operations. Also new resource management systems need to be tested against a variety of workloads and infrastructural arrangements, which are all but impossible to realize with a real grid system. The only viable option is to resort to simulation. The equilibrium pricing has been investigated in (Wolski et al. 2001), (Stuer et al. 2007), (Abdelkader and Broeckhove 2008) on the basis simulation. It was found to work well in a wide variety of circumstances. We will also use the Grid Economics Simulator developed in (Stuer et al. 2007) and extended in (Vanmechelen et al. 2008) in this work.

We intend elaborate on the above studies and investigate the possibility of predicting price evolutions in such computational economies. If this turns out to be possible, it would provide a basis for endowing consumers and providers, or more precisely agents acting on their behalf, with intelligence. This would then allow them to optimize their actions in the market, increasing individual utility and value realized in the system.

COMMODITY MARKET MODEL

In this section we present the key abstractions of the computational commodity market. Given the space constraints of this contribution it is merely an outline. More details can be found in (Stuer et al. 2007).

Resource and job model

We include a single type of resources, namely CPU's in our model. In order to represent the diversification in CPU performance, we introduce two categories: $fastCPU$ and $slowCPU$. The $fastCPUs$ execute jobs twice as fast as the $slowCPUs$. These categories constitute substitutable commodities. This means that jobs can execute on both types of CPU's but consumers will value them differently in view of their different turnaround times for identical jobs.
As a consequence of limiting our resource model to CPU's, we also model jobs as a CPU-bound computational tasks. Every job has a nominal running time, i.e. the time it takes to finish on a reference CPU. Jobs are taken to be atomic , in the sense that they are always allocated to a single CPU and are non-pre-emptable.
Resource prices are expressed as rates i.e. a certain amount per time of resource usage. However, the market price at the time the resource is sold holds for that resource until the job has completed, irrespective of the intervening price evolution. In other words, the price is guaranteed for the duration of the job allocated to the resource.

Consumer model

The consumers are the grid users. Each consumer has a queue of computational jobs that need to be executed and for which resources must be acquired from providers through participation in the market. The price a consumer is willing to pay is a function of the job valuation and the remaining budget.
Consumers are provided with a budget that gets replenished periodically. The budget cannot be transferred to a future replenishment period i.e. it must be exhausted during the period it has been allocated. Also, the spending rate has an upper limit related to the time remaining in the current budget period to avoid extreme prices if every consumer were to try and acquire all necessary resources at the beginning of he budget period. In every simulation step, consumers are billed for all resources that are currently allocated to their jobs.

Provider model

Every provider hosts a number of CPUs in the $fastCPU$ and $slowCPU$ categories. These can be made available to the computational market. For a given price vector, providers have to determine how many CPUs they are willing to sell for each CPU category. Once the market determines a price that brings about equilibrium of global demand and supply, resources are allocated to jobs without further delay. When a resource is allocated to a job, it remains allocated until the job completes.
Providers determine whether or not to supply resource at a certain price on the basis of historical price information. Prices are compared to the average for which CPU slots were sold previously. For prices above this average, all resource are put on the market. For prices below this average only a fraction proportional to the price ratio is put on the market.

Pricing algorithm

The market mechanism that we adopt is a spot market, with a dynamic price for resources, adjusted to bring about market to equilibrium viz. a matching of supply and demand. The supply or demand information for a range of prices for each CPU category is used (after preprocessing and smoothing related to the fact that we are dealing with discrete resource units), to define an excess demand surface. The market equilibrium point is the zero of this surface and fixes the price at which the market will trade at that moment in time. The algorithm for computing this equilibrium is based on Smale's method (Smale 2001, Hirsch and Smale 1979), with a number of modifications and extensions (Vanmechelen et al. 2008, Stuer et al. 2007), and an augmented Lagrangian pattern search (Lewis and Torczon 2002).

Simulator

The Grid Economics Simulator of (Stuer et al. 2007), (Vanmechelen et al. 2008) is a Java-based discrete event simulator. For details we refer to these papers. A schematic representation of the core functions in the simulator is given in figure 1.

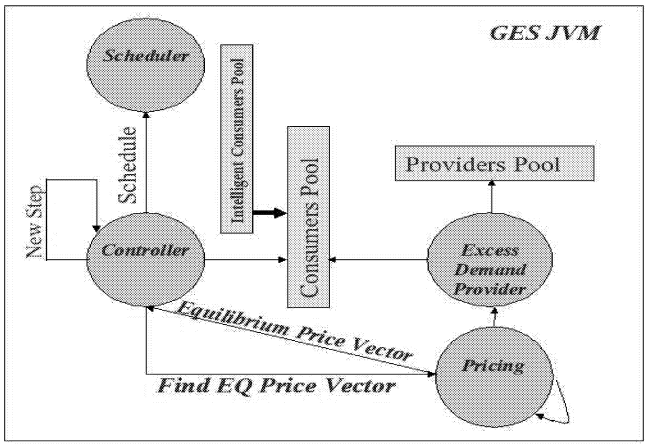

Figure 1: Representation of key GES functions.

NEURAL NETWORK

There are different approaches possible to address the price prediction problem. One of them is the use neural networks. A neural network is composed of interconnected, simple processing elements operating in parallel. The interaction of these nodes or neurons can be used to model complex relations between input and output data. The ability to detect patterns and non-linear connections in data is one of the strengths of neural networks (Skapura 1995). We aim to feed in a series of consecutive price data as input pattern to the neural network and expect to obtain the next price point as output. The use of such prediction-based temporal networks is discussed in (Kung 1993).

Background

We use a straightforward type of neural network namely a feedforward neural network with error backpropagation. They are characterized by the fact that data flows only in one direction through the network (i.e. no loops) and hence the nodes can be organized in layers. Each node in a layer has connections to nodes in the subsequent layer. The parameters of the network such as the connection weights are determined by minimizing the prediction error, the mean square deviation between actual and predicted values. Backpropagation of the error through the network leads to expressions for the adjustment of the network parameters. This process is effected over randomly sampled data in a training set until the error is sufficiently small. Once the network has been trained, it is checked against a validated data set to provide an indication of how well it performs.

Implementation

As indicated in the previous section, we have used a fairly common architecture for a small neural network. It is a feedforward network with input layer, a hidden layer and an output layer, with full connection topology between the layers.
The neuron activation is based on the use of a linear basis or net function and a sigmoid activation function

$$a_i = F(\sum_j o_j * w_{ij}) \tag{1}$$

where w_{ij} are the weights of the connection from neuron j to i and where o_j is the output of neuron j and F is the familiar sigmoid.
We have used supervised training through error backpropagation as a learning paradigm for the network. That is, we select a training set of input and corresponding output patterns. Subsets of the training set are presented to the network and the difference between anticipated output and actual output is viewed as a cost or error function. The objective is to minimize this error by adjusting the connection weight parameters of the network.
A straightforward approach is to use the mean square difference as an error function. The connection weights are initially assigned random values. The difference between actual and anticipated values at the output layers determines errors. These are backpropagated through the network. This leads to the so-called Delta rule (Mitchell 1997) for updating the weights of the connections:

$$\Delta w_{ij} = \mu \delta_i * x_{ij}. \tag{2}$$

where μ represents the learning rate, δ_i the error term and x_{ij} the input from node j to node i. We also include a momentum term in the above formula (Mitchell 1997) that helps deal with local minima in the error function. The process of presenting input data and adjusting weights, called a training cycle, is iterated until the total error is sufficiently small. In our application we typically use between a few hundred to thousend training cycles to gauge the relation between number of cycles and quality of the predictions.
The above applies to a network topology with fixed number of layers and fixed number of neurons per layer. Our network has four input nodes and one output node. We have experimented with different numbers of neurons for the hidden layer and found that three neurons are adequate for our purpose. The learning rate we have used is $\mu = 0.8$ and the momentum is $\eta = 0.3$.

RESULTS

In this section we look at numerical results. Using the Grid Economics Simulator (GES) we run simulations that implement the commodity market model with equilibrium pricing. The neural network is trained and validated with initial price data sets. The network is then used to predict price evolution and compare that to the price evolution generated with the simulator at later time intervals.

Parameter	Value
# Consumers	1000
# Providers	500
# number of fastCPU's per provider	$\{1, \cdots, 8\}$
# number of slowCPU's per provider	$\{2, \cdots, 15\}$
Performance ratio of fast vs slow	2.0
Job duration	$\{2, \cdots, 10\}$
Base allowance	500,00
Induction period for a job	100
Jobs submitted at induction step	$\{1, \cdots, 200\}$

Table 1: GES Simulation parameters

The parameters for the GES simulator runs are given in table 1. Values indicated by brackets indicate a random drawing in that range. In effect, we consider two scenario's which we will refer to as oversupply and overde-

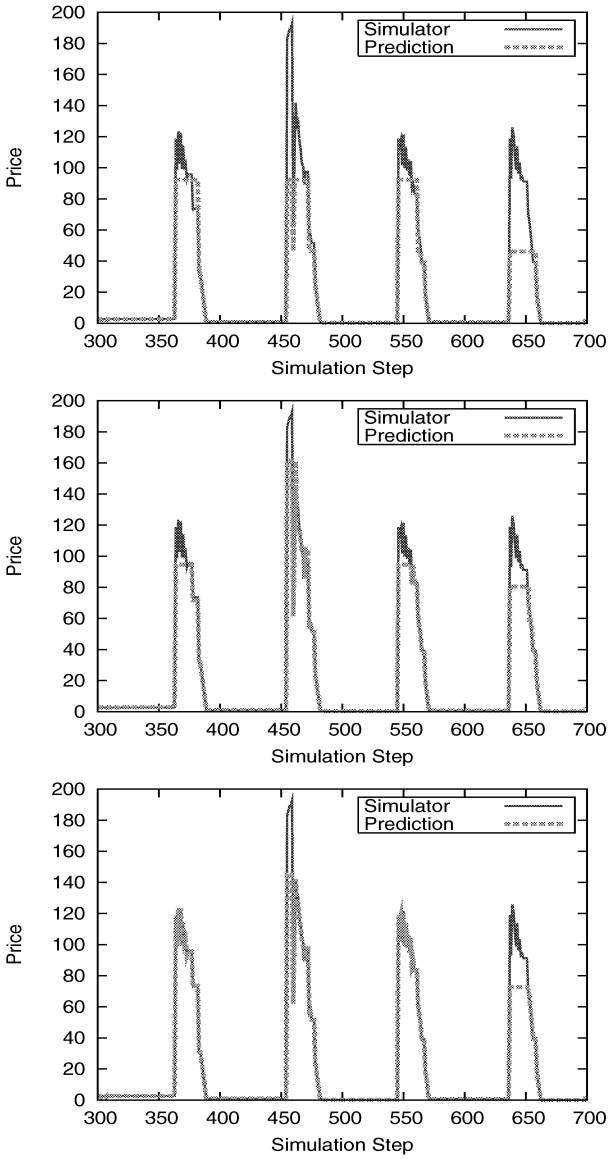

Figure 2: Price prediction for the oversupply scenario with 100, 500 and 1000 training cycles respectively.

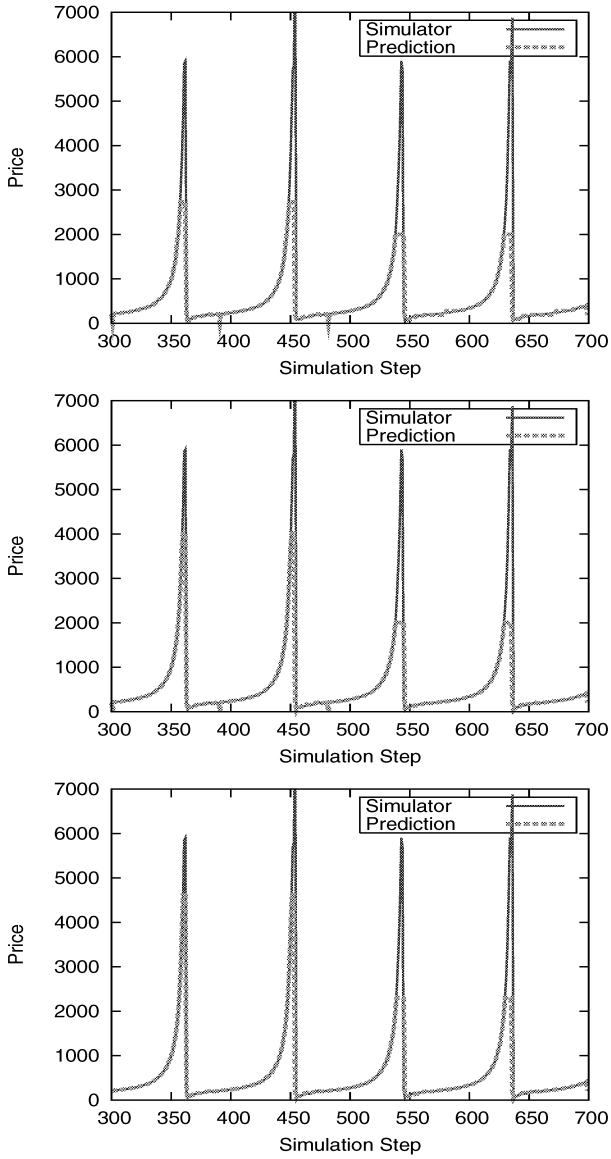

Figure 3: Price prediction for the overdemand scenario with 100, 500 and 1000 training cycles respectively.

mand respectively. Of course, each of these basic scenario's was run with several variations of the simulation parameters such as number of consumers or providers, job duration, background workload and so on. The results discussed here a representative with respect to these variations.

The simulations are started by putting an initial number of jobs in the consumer's queue. At non-periodic intervals jobs are injected into the consumers queue. In oversupply scenario there is also a small background load. It is generated by inserting, with small probability (10%), jobs into consumer queues at each time step. In overdemand scenario a continuous workload is generated by re-inserting the completed jobs into consumer's job queue.

Consumers start out with an initial budget that is replenished at certain intervals. In the oversupply scenario these coincide with the job injection.

Price evolution

The price evolution for the $fastCPU$ in the oversupply scenario is shown in figure 2. The $slowCPU$ price (not shown) has a similar profile at about half the price level, reflecting their relative performance. The instants of job injection and budget replenishment are clearly identifiable. Prices rise significantly due to the increase in demand and then tapers off to zero as the jobs get processed and demand falls. This is referred as an oversupply scenario, since clearly the total workload associ-

ated with supply of jobs is significantly smaller than the aggregate processing power of the resources.

The $fastCPU$ price evolution in the overdemand scenario is shown in figure 3. Here one notices an increase of the prices as the end of the budget allowance period draws near. At this time the spending rates increase to allow the consumer to exhaust his budget. This creates the possibility of rising prices because their is still a demand for resources in the market.

Price prediction

Figures 2 and 3 show the time evolution from simulation time 300 onwards. The first 300 time steps have been used to train and validate the neural network.

In figure 2 $fastCPU$ effective and predicted prices are compared for the oversupply scenario. The three panels show the simulator and predicted price evolution for different numbers (100, 500 and 1000) of training cycles of the network. Clearly the presence of the spikes in the price evolutions is reflected in the predictions at the appropriate times but the height and shape the peaks requires a well-trained network.

In figure 3 one finds the results for the overdemand scenario. A similar observation can be made with respect to the quality of the price prediction as in the oversupply scenario.

CONCLUSION

We have investigated the possibility of using a temporal neural network to effect price predictions in the setting of a grid economics simulator. The network proves adequate in predicting short term price evolutions, though it fails to track extreme price movement. Nevertheless this could provide a basis for enabling consumer and provider agents with intelligence.

FUTURE WORK

In a near future we plan to use these neural network results to improve a consumer and provider agents decision performance in grid economies, using the predicted price to provide a guidance to intelligent agents.

REFERENCES

Abdelkader K. and Broeckhove J., 2008. *Pricing computational resources in dynamic grid.* In *Proceedings of the 2nd International Workshop on P2P, Parallel , Grid and Internet Computing (3PGIC-2008).* IEEE Press, Barcelona, Spain, ISBN 978-0-7695-3109-0, 303–308.

Buyya R.; Abramson D.; and Giddy J., 2002. *Economic models for resource management and scheduling in Grid computing. Concurrency and Computation: Practice and Experience*, 14, 1507–1542. doi: 10.1002/cpe.690.

Hirsch M. and Smale S., 1979. *Algorithms for solving f(x)=0. Communications on Pure and Applied Mathematics*, 32, 281–312.

Krauter K.; Buyya R.; and Maheswaran M., 2002. *A taxonomy and survey of grid resource management systems for distributed computing. Softw Pract Exper*, 32, 135 – 164.

Kung S.Y., 1993. *Digital Neural Networks.* Prentice Hall, Inglewood Cliffs, New Jersey.

Lewis R.M. and Torczon V., 2002. *A Globally Convergent Augmented Lagrangian Pattern Search Algorithm for Optimization with General Constraints and Simple Bounds. SIAM J on Optimization*, 12, 1075 – 1089. ISSN 1052-6234. doi:10.1137/S1052623498339727.

Mitchell T.M., 1997. *Machine Learning.* McGraw-Hill International Editions, Computer Science Series.

Skapura D.M., 1995. *Building Neural Networks.* Addison-Wesley Publishing Company.

Smale S., 2001. *Dynamics in General Equilibrium Theory. Topology and Global Analysis*, 66, no. 2, 288–294.

Stuer G.; Vanmechelen K.; and Broeckhove J., 2007. *A commodity market algorithm for pricing substitutable Grid resources. Future Generation Computer Systems*, 23, no. 5, 688–701. doi:10.1016/j.future.2006.11.004.

Vanmechelen K.; Depoorter W.; and Broeckhove J., 2008. *A Simulation Framework for Studying Economic Resource Management in Grids.* In *Proceedings of the International Conference on Computational Science (ICCS 2008).* Springer-Verlag, Berlin Heidelberg, vol. 5101, 226–235.

Wolski R.; Plank J.; Brevik J.; and Bryan T., 2001. *Analysing Market-based Resource Allocation Strategies for the Computational Grid. Int J of High-Performance Computing Applications*, 1, 15(3).

AUTHOR BIOGRAPHIES

Ramadan Arfa is a PhD researcher and a member of the Computational Modeling and Programming (CoMP) University of Antwerp , Belgium. He completed his Master degree in 1999 from University of Krakow (AGH),Poland. His research interests include distributed computing, Monitoring and Scheduling System, Grid Computing and Grid Economics.

Dr. Jan Broeckhove is a professor in the Department of Mathematics and Computer Science at the University of Antwerp (UA), Belgium, and member of its Computational Modeling and Programming research group. He received his PhD. in Physics in 1982 from the Free University of Brussels (VUB), Belgium. His current research interests include a.o. distributed computing, in particular cluster and grid computing.

A NEW VERSION OF A DECISION SUPPORT SYSTEM FOR EVALUATING TAKEOVER BIDS IN THE PRIVATIZATION OF PUBLIC ENTERPRISES AND SERVICES

Silvija Vlah
Kristina Soric
Visnja Vojvodic Rosenzweig
Department of Mathematics
Faculty of Economics and Business Zagreb
Trg J. F. Kennedya 6
10000 Zagreb
Croatia
{svlah, ksoric, vvojvodic}@efzg.hr

KEYWORDS
Decision making, multiple criteria, decision support system, compromise programming, grouping, Monte Carlo simulations, privatization.

ABSTRACT

In Croatia, the Croatian Privatization Fund (CPF) takes control of the privatization of the public enterprises and services in the state portfolio. In order to provide potential investors with a fair and transparent transaction process CPF established tender procedures. The success of a privatization is highly dependent on the selection of a good investor which is done according to multiple criteria such as the price, further investments, the time of keeping current employees and others. In order to help CPF in this selection process we developed a decision support system (DSS) based on compromise programming, grouping of privatization bids according to their similarities and Monte Carlo simulations. This DSS is the improved version of the DSS developed in (Vlah et al. 2007).

1. INTRODUCTION

As we have mentioned above, in Croatia, the Croatian Privatization Fund (CPF) takes control of the privatization of the public enterprises and services in the state portfolio. The success of a privatization is highly dependent on the selection of a good investor. Simply looking for an investor offering the highest price is not "efficient sourcing" even when the price is considered to be almost the most important criterion. Multiple criteria need to be followed and taken into account when selecting the investor. Usually, besides the price, potential investors are asked to propose further investments, the time of retaining the current employees, the intention of paying the creditors and to satisfy other requests. CPF has to choose the best bid according to the criteria defined in the tender. These criteria depend on the special case of privatization. The problem is if all the criteria are equally important or we have to assign them some weights? How to assign the weights? In the literature there are mathematical models based on multiple criteria optimization, data envelopment analysis, analytic hierarchical process (AHP) and other multi-attribute rating techniques.

In order to help CPF we modeled this problem as a multi criteria optimization problem and created the decision support system (DSS). Our main goal was not to ask the decision maker (DM) for too many information. Namely, usually the DM wants to participate in the decision process, but she /he does not want to be involved too much. For this reason we improved the DSS from (Vlah et al. 2007) by grouping the criteria in three groups, very important criteria, less important and the least important criteria. And this is the only task that a DM has to do.

In the following pages, two heuristic methods for evaluating takeover bids in privatization will be described. Besides the grouping of the criteria in three groups by DM, we have grouped the bids according to these groups of criteria. The grouping algorithm that is used for grouping the bids according to their similarities will be described in the next section. The similarities will be considered regarding the criteria in the same group, for all three groups. Afterwards, two heuristics for evaluating takeover bids will be proposed. The first one will consider the same weights of the criteria inside the considered group of criteria. The second one will assign the weights to the criteria inside a group based on Monte Carlo simulations. This will be followed by an example and computational results of the proposed heuristics and DSS based on them. The conclusions and future research will be given in the last section.

2. GROUPING ALGORITHM

The motivation for introducing similarity groups comes from an idea to consider the privatization bids that are similar to each other. Namely, if two investors offered approximately the same price and the same level of further investments and approximately have the same values for all the other criteria by which the bids are being evaluated, one

could consider them approximately the same in satisfying the criteria used in the particular tender.

For our purpose, the problem of grouping can be well motivated by considering the set of points shown in Figure 1.

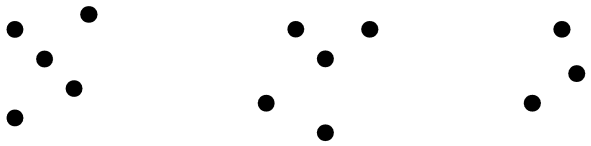

Figure 1: How many groups?

Typically, a human observer will easily perceive three groups of objects in the image. On the other hand, there has been a tremendous amount of effort devoted to achieving the same level of performance in computer vision. Prior literature on the related problems of clustering, grouping and image segmentation is huge. In this paper we are using the results obtained in (Shi and Malik, 2000). They treat image segmentation as a graph partitioning problem and propose a criterion of normalized cut for segmenting the graph.

A graph $G = (V, E)$, where the nodes are the points of an image and an edge is formed between every pair of nodes with the weight $w(i, j)$ representing the similarity between them, can be partitioned into two disjoint sets, $A, B, A \cup B = V, A \cap B = \varnothing$ by simply removing edges connecting the two parts. However, Shi and Malik propose a new measure of disassociation between two groups. Instead of looking at the value of the total weight connecting the two partitions, their measure computes the cut cost as a fraction of the total edge connections to all the nodes in the graph. They call this disassociation measure the normalized cut (Ncut):

$$Ncut(A,B) = \frac{cut(A,B)}{asso(A,V)} + \frac{cut(A,B)}{asso(B,V)},$$

where $asso(A,V) = \sum_{u \in A, t \in V} w(u,t)$ is the total connection from nodes A to all nodes in the graph and $asso(B,V) = \sum_{u \in B, t \in V} w(u,t)$ is defined in the same way.

Given a partition of the nodes of a graph, V, in two sets A and B, let x be an $N = |V|$ dimensional indicating vector where the i th component is 1 if node i is in A, and –1 otherwise. Let $d(i) = \sum_j w(i, j)$ be the total connection from node i to all other nodes, D an $N \times N$ diagonal matrix with d on its diagonal, W be an $N \times N$ symmetrical matrix with $w_{ij} = w(i, j)$ as elements.

From the paper on image segmentation (Shi and Malik, 2000) we have the following grouping algorithm:

(1) Given a set of points, set up a weighted undirected graph $G = (V, E)$, compute the weight on each edge and summarize the information into W and D
(2) Solve $(D - W)y = \lambda Dy$ for generalized eigenvectors with the smallest eigenvalues
(3) Use the eigenvector with second smallest eigenvalue to bipartition the graph
(4) Decide if the current partition should be subdivided and recursively repartition the segmented parts.

3. HEURISTICS

This section introduces the two heuristics that will be used by the DSS for evaluating takeover bids that will be created.

Prior to use of any of the heuristics that will be described here the data on privatization bids are being filtered according to the criteria that have eliminating nature. Namely, criteria may have upper or lower bounds on their values and the bids that do not satisfy them will be eliminated from further consideration.

As the next step, the elimination of takeover bids that are dominated by all other bids is made. Dominated bids are the bids where the values of all the criteria are lower than the values of the criteria from at least one of the other bids and will not be taken into account for sure. In case of the existence of a takeover bid that dominates all the other bids, there is no need for further investigations because the choice should be obvious. If there are bids left for evaluation, the decision making process comes to the third stage where it will require a heuristics for solving the problem.

The data about the bids will be normalized in order to avoid the problem of comparing the values of the criteria which have different scales of measure. The normalization will be done using linear transformation of the data by which the criterion values of all the bids are divided by the maximum offered value of that criterion. Without a loss of generality, it is assumed that the highest values are preferred for all of the criteria.

Furthermore, it is important to mention that the heuristics that are proposed here will allow changing the criteria which are taken into account. This means that the DSS will be created generally and can be adapted to any specific privatization case because it will allow the DM to import any criteria that are considered to be important for a privatization of a certain public enterprise.

It is assumed that the DM can provide the information on the criteria importance by simply ordering the criteria by their importance. Since some of the criteria may be of the same importance, it can be thought of as grouping the

criteria according to their importance. Thus, the decision maker should say which of the criteria taken into consideration are of the highest importance, which are of the lowest importance and which are somewhere in between. In this way the DM will not be burdened by defining the exact weight of each criterion or pairwise comparisons of the bids criteria values.

3.1 Heuristic Procedure 1

The first heuristic proposed is based on successive grouping of the privatization bids where the grouping is performed using the algorithm described in the previous section. The measure of similarity between the bids will be the difference in the distance from the ideal solution i.e. the ideal bid. The ideal solution corresponds to the best value that can be achieved for each criterion, ignoring all the others. In this particular problem of the evaluation of takeover bids, it is easy to obtain the ideal point since the number of bids is never very large. Thus, we obtain the ideal solution by taking the best value for a given criterion among the given takeover bids. For example, if the criterion was the price, we would like to achieve the maximum price possible. Thus the best value would be the highest price offered by the bidders.

In the first iteration the heuristic groups the bids according to the most important criteria group where we take the sum of all the criteria with the same weights. Afterwards, the best of the groups made in such a way is chosen for the next iteration. The group of bids that is considered to be the best will be the group that contains the bid that is closest to the ideal solution. The process of finding the solution that is closest to the ideal solution is known as compromise programming (Alves and Climaco 2004), (Ehrgott 2005). Compromise programming can be thought of as an effort to find a solution that comes as "close as possible" to the ideal values, i.e. the best approximation of ideal bid. To be more precise, we consider a situation where the DM evaluates I takeover bids based on J criteria. The values for each criterion for every bid are given as $a_{ij}, i = 1,\ldots,I,\ j = 1,\ldots,J$. For example, if the first criterion is price, the value a_{11} is the price offered by the first bid. The bid that is closest to the ideal point will be the bid with minimum value of

$$\left[\sum_{j=1}^{J}\left(a_j^{*} - a_{ij}\right)^2\right]^{1/2},$$

where $a_j^{*} = \max_i\left(a_{ij}\right), i = 1,\ldots,I,$ are the best values of criteria. To be more precise, the sum over the index *j* in the first iteration is the sum over indices of the most important criteria. In the second iteration, the index *j* is the index of the less important criteria and in the third iteration the index of the least important criteria. The heuristics continues by grouping the bids obtained by the first iteration according to the group of the criteria which is the next one by the importance. Again, the best of the groups obtained in such way is chosen for the next iteration.
The process continues until there is only one bid left in the group of the best bids or if the criteria are exhausted.

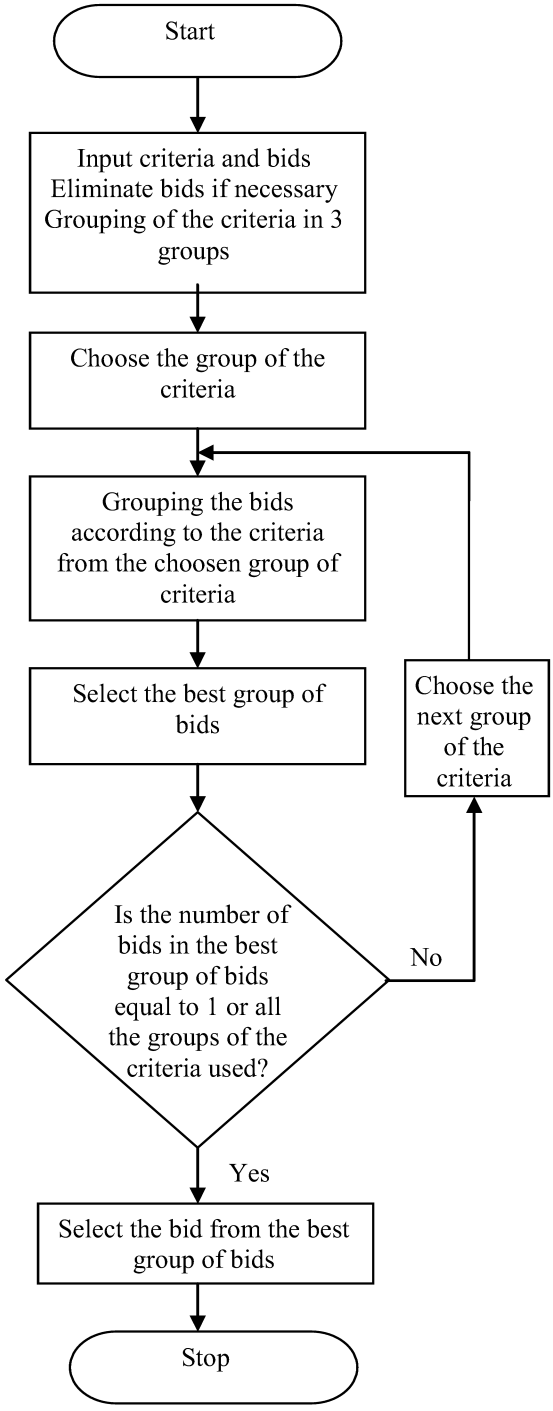

3.2 Heuristic Procedure 2

The second heuristics that is proposed here is again based on grouping of the privatization bids where the grouping is performed using the algorithm described in previous section. However, the grouping here is done with all the criteria taken into account at the same time. Thus, the measure of similarity will be the weighted distance to the

ideal solution:

$$\sqrt{\sum_{j=1}^{J} w_j \left(a_j^* - a_{ij}\right)^2},$$

where $a_j^* = \max_i \left(a_{ij}\right), i = 1,\ldots,I,$ are the best values of the criteria and $w_j, j = 1,\ldots,J$ are the criteria weights. To be more precise, the sum over the index *j* in the first iteration is the sum over indices of the most important criteria. In the second iteration, the index *j* is the index of the less important criteria and in the third iteration the index of the least important criteria.
Since the exact weights are not given by the DM, the heuristic uses Monte Carlo simulations (Gamerman 1997) with different values of the weights following the criteria ordering (that is, following the importance groups of criteria) given by the DM following an idea for solving classification problems as in (Tervonen and Lahdelma 2007).
The heuristic basically performs a large number of the groupings of the bids. In each grouping it selects the best group of bids. The result is the percentage of being selected for the best group for each bid. Thus, the heuristics ends with numbers that can be thought of as the probability of belonging to the best group of bids. Finally, it is up to the DM to select the bid according to the calculated probabilities.
The block diagram for both heuristics is the same. The difference is in defining the objective function according to which the grouping of bids is performed. In the first heuristic, the objective is to minimize the sum of the distances to the ideal point according to the criteria from a chosen group of criteria (with the same weights). The grouping is performed once. The best bid(s) is(are) the bid(s) from the best group. In the second heuristic, the objective is to minimize the weighted sum of the distances to the ideal point according to the criteria from a chosen group of criteria. The weights are chosen using Monte Carlo simulations following the importance of the criteria and the grouping is repeated many times. The best bid is the bid with the highest percentage of being chosen in the best group of bids.

4. COMPUTATIONAL RESULTS ON AN EXAMPLE

These two heuristics are implemented in the form of DSS created using Microsoft Excel Visual Basic. The graphical surface is friendly and easy to use. First the DM has to input the criteria and bids. After that, she/he has to choose the heuristic, 1 or 2. Then the criteria with lower and upper bound are typed and grouped by the DM. The final step for the DM is to press the button "Group the criteria" and the solution of the first iteration is obtained. The process continues with the group of the less important criteria and ends with the group of the least important ones. To illustrate the process of evaluating privatization bids, an example of the set of bids for evaluation is given as follows:

Criteria / Bids	Price	Keeping current employees	Number of new employees
A	5000000	3	400
B	4000000	4	500
C	6000000	4	400
D	10000000	3	350
E	11000000	3	300
F	13000000	2	200
G	13100000	2	190
H	13200000	1	0

The criteria in this fictive tender are the price, the number of years the actual employees will be kept and the number of new employees. Also, there is a lower bound on the price and the minimum price level is 5000000. It is presumed that the DM set the price to be the most important criterion and the other two criteria are less important than the price but equally important when compared one to the other.
In that case, the decision support system would firstly eliminate bid B because it does not satisfy the lower bound on price criterion. Afterwards, bid A would be eliminated because it is dominated by all other bids.

If the DM used the first heuristic that is proposed, the decision support system would first group the bids according to the price which would result with the following bids as the bids in the best group:

Criteria / Bids	Price	Keeping current employees	Number of new employees
F	13000000	2	200
G	13100000	2	190
H	13200000	1	0

In the next iteration, the decision support system would group the remaining bids according to the next two criteria which would result with the following bids as the bids in the best group:

Criteria / Bids	Price	Keeping current employees	Number of new employees
F	13000000	2	200
G	13100000	2	190

The process of heuristic 1 ends because the set of criteria is exhausted which leaves the DM with the final step of choosing the bid among bids F and G.

If the DM was to use the second heuristics that is proposed, the decision support system would make a large number of simulations, in each of the simulations performing grouping of the bids using different weights while following the order of the criteria importance which would result in the following information:

Criteria / Bids	Probability of belonging to the best bid group
C	0%
D	82%
E	92%
F	70%
G	70%
H	2%

Since bids E and D have the highest probabilities of belonging to the best group of bids, the DM should consider making the final decision of selecting the final bid among those two bids. However, bids F and G also have high probabilities which suggest they should not be completely eliminated from consideration either.

In the end, the final decision is always made by the DM and it is advised that he/she combines the two heuristics that were proposed here, especially taking into account their differences. Namely, the first heuristics is more rigorous in terms of following the criteria importance more rigidly. On the other hand, the second heuristics is more prone to compromises between the given criteria.

5. CONCLUSIONS AND FUTURE WORK

In this paper we presented the decision support system (DSS) developed in order to help the Croatian Privatization Fund (CPF) to make a decision of choosing an investor in a process of privatization. When CPF announces the tender for privatizing a public enterprise it should give the criteria which will be evaluated during the process. The potential investors should apply giving their bids. The investor is chosen according to all the criteria and not only one of them.

For evaluating takeover bids in order to make the decision according to the given criteria, we developed (DSS) based on compromise programming, grouping of privatization bids according to their similarities and Monte Carlo simulations. This DSS is the improved version of the DSS developed in (Vlah et al. 2007). We presented an example. In order to make a decision, for the DM (in this case CPF) it is not necessary to know any optimization technique. The only thing she/he has to do is to specify the criteria, rank them in three groups and input the data about the bids. Sometimes, at the end the DM has to choose among a few bids, but we believe that this is not a problem. Indeed, it is sometimes good marketing to include the DM in the decision process but in a reasonable way so as not to ask her/him to put too much effort. Also, the advantage of this solution method regarding the others known in the literature is the fact that the DM does not have to specify the weights for the criteria.

The DSS developed here could be used in a more general case where a decision according to more criteria should be made. It is not limited only to the case of privatization. The only requirement is to have numerical data, that is, the qualitative data should be measured in a certain way. Also, this DSS could be part of a more global system and incorporated in it without many problems.

6. REFERENCES

Alves, M.J. and J. Climaco. 2004. "A note on a decision support system for multiobjective integer and mixed-integer programming problems", E*uropean Journal of Operational Research*, 127(1), 258-265

Brauers, W.K. 1995. "PRIVATA: A model for privatization with multiple non-transitive objectives", *Public Choice*, 85, 353-370

Ehrgott, M. 2005. "Multicriteria Optimization", 2nd ed., Berlin, Springer

Gamerman, D. 1997. "Markov Chain Monte Carlo: Stochastic Simulation for Bayesian Inference" Boca Raton, FL: CRC Press

Ng W.L. 2008. "An efficient and simple model for multiple criteria supplier selection problem", *European Journal of Operational Research*, 127(3), 1059-1067

Shi J. and J. Malik. 2000. "Normalized Cuts and Image Segmentation", *IEEE Transactions on Pattern Analysis and Machine Intelligence*, 22(8), 888-905.

Tervonen T. and R. Lahdelma. 2007. "Implementing stochastic multicriteria acceptability analysis", *European Journal of Operational Research*, 127(2), 500-513

Vlah S., K. Soric, V. Vojvodic Rosenzweig and D. Tipuric. 2007. "Decision Support System for Evaluating Takeover Bids in Privatization", Contemporary Challenges of Theory and Practice in Economics, Belgrade, Serbia, A. Prascevic(ed.) 401-407

SILVIJA VLAH was born in Sombor, Serbia. She went to the University of Zagreb, Croatia, where she studied numerical mathematics and computer science. She is presently the assistant at Faculty of Economics Zagreb, Croatia. svlah@efzg.hr, www.efzg.hr/svlah

KRISTINA SORIC was born in Pula, Croatia. She went to the University of Zagreb, where she studied numerical mathematics and computer science. She obtained her PhD degree in operational research at Department of applied and pure mathematics, University of Padova, Italy. ksoric@efzg.hr, www.efzg.hr/ksoric

VISNJA VOJVODIC ROSENZWEIG was born in Zagreb, Croatia. She studied in Zagreb mathematics and obtained her PhD degree in operational research. vvojvodic@efzg.hr, www.efzg.hr/vvojvodic

A Simulation of Market-based Resource Management in Dynamic Grids

K. Abdelkader, and J. Broeckhove
Department of Mathematics and Computer Sciences,
University of Antwerp,
Middelheimlaan 1, 2020, Antwerp, Belgium
Email: Khalid.Abdelkader, Jan.Broechove@ua.ac.be

KEYWORDS
Computational market, Grids, Grid Computing, Grid Economics, Market-based Resource Management

ABSTRACT

In Grid economies the allocation of tasks to available resources is a key feature of resource management. This is particularly the case in large scale infrastructures spanning many administrative domains such as grids or public resource computing networks. While most of the widely solutions on resource controlling and a task scheduling in Grid computing has been driven by system-centric service provisioning, we develop a commodity market model of CPU bounded resources to become open system for user-centric approach. The key element is to encourage grid participants to deliver the maximum utility in the market. In this paper we present a commodity market resource management in dynamic computational grids, that are modeled using the Grid Economics Simulator (GES). The key design goals of the simulator are enabling a wide variety of economic and non-economic forms of resource management in a dynamic Grid fashion and exhibiting good scalability properties.

INTRODUCTION

Resource management systems play an essential role for efficiently handling resource allocation, especially in Grid environments, where the grid fabric and user population span many administrative domains and users have strongly varying requirements and preferences w.r.t to resource allocations. Usually, resource control and scheduling are driven by system-centric objectives such as optimizing system throughput. It is important that there be a shift towards a user-centric approach that provides the individual user with a means to express the value that a task represents and have the resource management take that valuation into account in its allocation and scheduling decisions (Buyya et al. 2005).
The introduction of market-based approaches into resource management addresses that issue. It involves the definition of a computational market in which grid users and providers interact. Prices are used to signal supply and demand of resources. They reflect the users' valuations of the resource usage and signal the abundance or scarcity of various types of resources. Providers sell resource usage to consumers in a market that can be organized in different ways, e.g. posted-price markets, different types of auctions or commodity markets (Buyya et al. 2002).

In this contribution we consider the commodity market model with equilibrium prices (Wolski et al. 2001). It corresponds to a vision of the grid where applications can treat computational resources as interchangeable and not as specific machines and systems. Market participants express their valuation of the resources as a function of its price. That means that for each price level the consumers, i.e. users wanting to obtain resources to have their jobs executed, indicate how many resources they will acquire. Similarly, for each price level the providers, organizations or individuals bringing their resources into the Grid, indicate how many of their resources they will make available. The market sets the actual price by computing the price at which supply equals demand.

This pricing scheme has been investigated in (Abdelkader and Broeckhove 2008, Abdelkader et al. 2008) using the java-based (GES) (Vanmechelen et al. 2006). It has been found to work well for static grids. Under those circumstances the determination of equilibrium price under variations of e.g. job load or disposable budget is fast and stable. In this contribution we investigate the scheme in a dynamic grid perspective. We find out whether the price determination algorithm whether it can handle the abrupt changes in supply and demand due to the dynamic nature of the market participation.

Analyzing resource management systems (RMS) based different market designs in operational grid systems is impractical. Firstly, one is confronted with the cost and technical difficulties of introducing an experimental RMS in an operational environment. Secondly, one needs to test with a wide variety of system loads which would probably not be observed unless the test period were very long. This leaves analysis through simulation as the viable option.

THE GES SIMULATOR

Our study is based on the Grid Economics Simulator (GES). It is a Java-based discrete event simulator developed to investigate resource management, including market-based approaches, on large-scale infrastructures. It is important to remark, however, that GES also supports non-economic resource management approaches.
Figure 1 gives a general overview of the simulator's architecture in terms of layers and components. In the GES Core, the domain layer contains base classes for all domain entities such as Consumer, Provider, Grid REsources, and GridEnvironment. Support for traditional forms of resource management is provided through the Non-Economic layer and for market-based resource management in the Economic layer. On top of each of those one finds specific resource management systems. Outside the Core one finds layers dealing with configuration of simulations and with distributed processing of simulations based on technologies such as Jini, Sun Grid engine (SGE) or directly through system-to-system secure shell connections (SSH). This can of course be extended to other distribution platforms. A more detailed technical overview, and a comparison with similar simulators can be found in (Vanmechelen et al. 2008). We describe, very briefly, the key abstractions used in the GES. More details can be found in (Vanmechelen et al. 2006).

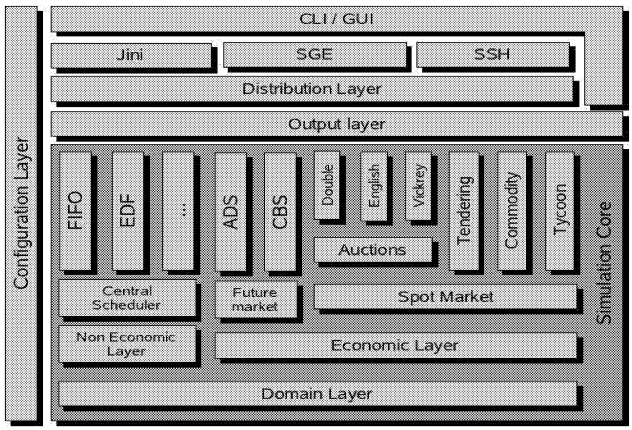

Figure 1: GES architecture.

Resource and job model

A single type of resources, namely CPU's has been used in our investigations to date. In order to represent the diversification in CPU performance, we introduce two categories: $fastCPU$ and $slowCPU$. The $fastCPUs$ execute jobs twice as fast as the $slowCPUs$. These categories constitute substitutable commodities (jobs can execute on both) but consumers will value them differently.
As a consequence of limiting our resource model to CPU's, we also model a job as a CPU-bound computational task. Every job has a nominal running time, i.e. the time it takes to finish on a reference CPU. Jobs are taken to be atomic , in the sense that they are always allocated to a single CPU and are non-pre-emptable.

Consumer model

The consumers are the grid users: each one has a queue of computational jobs that need to be executed and for which resources must be acquired from providers through participation in the market. The price a consumer is willing to pay depends on the valuation of the job. It is a price that, if and when a resource is acquired for job execution, remains fixed for the duration of the job.
A consumer is provided with an budgetary endowment that gets replenished periodically. The budget cannot be transferred to a future replenishment period i.e. it must be exhausted during the period it has been allocated. In every simulation step, consumers are billed for all grid resources that are currently allocated to their jobs.

Provider model

Every provider hosts a number of CPUs in either category that can be supplied to the computational market. For a given price vector, providers have to determine how many CPUs they are willing to sell for each CPU category. When the agreement between consumers and providers is reached, i.e. a price has been determined that brings about equilibrium of global demand and supply, resource are immediately allocated to jobs. Once a resource is allocated to a job, it remains allocated until the job completes. Also, the market price at the time the resource is sold will be charged as a fixed rate to the consumer for the duration of the job.

Resource pricing

The market mechanism that we adopt is a spot market, with a dynamic price for resources, adjusted to bring about market to equilibrium viz. a matching of supply and demand. Prices play the role of a communicator of complex provider and consumer valuations of the resources (Wolski et al. 2001). The market brings together all parties to quote their supply or demand for a range of prices for each CPU category. This information is used (after pre-processing and smoothing related to the fact that we are dealing with discrete resource units), to define an excess demand surface i.e. the difference between current demand and supply as a function of the price vector. The market equilibrium point is the zero of this surface and fixes the price at which the market will trade at that point in time. The algorithm that we use for computing this equilibrium is based on Smale's method (Smale 2001, Hirsch and Smale 1979),

with a number of modifications and extensions (Vanmechelen et al. 2006), and an augmented Lagrangian pattern search (Lewis and Torczon 2002).

Dynamics of providers and consumers

In this contribution we use the term grid in a broad sense as a large network of independent provider and consumer nodes cooperating to achieve computational tasks. We interpret this as an inherently dynamic setup, with nodes leaving and joining or rejoining the grid, for whatever reason.

We use a simple, straightforward model for the dynamics of peer participation or churn in the network. There is a pool of potential providers and a pool of active providers. A given rate governs the departure of providers from the former to join the latter. Similarly active providers depart at a given rate. In that event, we let the provider's CPU's finish processing the jobs currently executing on it. Only then does the provider enter the pool of potential providers. This state is referred to as the de-activated state for the provider. The size of the pools and the balance of the departure rates determines the evolution in time of the number of active providers. The simplicity of our model means that in the current implementation we have not looked at the problem of resubmitting jobs that are lost due to a provider exiting suddenly.

A similar mechanism is in place for consumers. Active consumers have jobs and are participating in the market. There is a pool of potential consumers that can enter the market. State changes are determined by departure rates. When a consumer departs and joins the pool of potential consumers, the jobs in its queue are kept there.

RESULTS

Using the GES simulator we will verify that the market operates correctly, i.e. the equilibrium price can be determined at each time step. We consider two scenario's, with parameters given in table 1. Values indicated by brackets indicate a random drawing in that range. The scenario's differ in the maximum job length, ten versus twenty time units, which is used to increase the global workload that needs to be processed.

Each simulation is started by putting an initial number of jobs in the consumer's queue. At each time step, a small background load is generated by having every consumer, with a probability of 15%, add a new job to its queue. In addition, peak loads are generated at every 50 time steps by injecting a large number of jobs in the consumer's queue. The latter is done in order to probe the stability and gauge the market's response in term of price levels. Consumers have an initial budget and there is a periodic replenishment of that budget. The results for the first scenario are presented in figure 2. The price evolution (panel 1) clearly signals the moments of job injection: each time the price increases considerably, due to the rise in demand, and then tapers off to zero as the jobs get processed and demand falls. Indeed, the background load in itself represents a situation of oversupply i.e. the aggregate workload of all jobs falls below the total resource capacity of the market. Hence prices drop to nearly zero. The initial cycle show a slightly different behavior because of the initial workload in the consumers queue.

Table 1: Simulation parameters.

Parameter	Value
initial size, active consumer pool	2000
departure rate, active consumer pool	0.1
initial size, potential consumer pool	2000
departure rate, potential consumer pool	0.1
initial size, active provider pool	1000
departure rate, active provider pool	0.1
initial size, potential provider pool	1000
departure rate, potential provider pool	0.1
number of fastCPU's per provider	$\{1, \cdots, 20\}$
number of slowCPU's per provider	$\{1, \cdots, 20\}$
performance ratio of fast vs slow	2.0
job running time in time steps	$\{2, \cdots, 10\}$
initial number of jobs per consumer	$\{1, \cdots, 150\}$
initial budget	50 000
budget allowance period	50

Panels 2 and 3 of figure 2 show the number of consumers and providers in the active, de-activated and potential states respectively. Because all departure rates are equal the flow back and forth is equal on average. The cycles in the number of de-activated consumers reflect the the budget replenishment. At that time a lot of consumers actually have resources allocated to them moment of deactivation and hence they transfer to the deactivated state. Later on, when consumers are idle, the deactivation transfers them directly to the potential consumers pool. Hence the number of deactivated consumers drops again.

Panel 4 of figure 2 shows the utilization of the grid infrastructure as a whole, i.e. the number of processor actually working in proportion to the total number of processors provided. This utilization is high after each job injection and drops to a level determined by the background load on injected jobs are processed. Also, one notices again the effects of the initial workload.

Results for the second scenario, where the range for the job duration was doubled to ($\{2, \cdots, 20\}$, are given in figure 3. This situation represents a doubling of the total workload and shifts the prices (in panel 1) to a higher level. One also notices that now the prices rise as the budget allowance replenishment step approaches. Consumers have an upper limit to their spending rate. Because budgets cannot be transferred across replenishment periods, this upper limit increases as replenish-

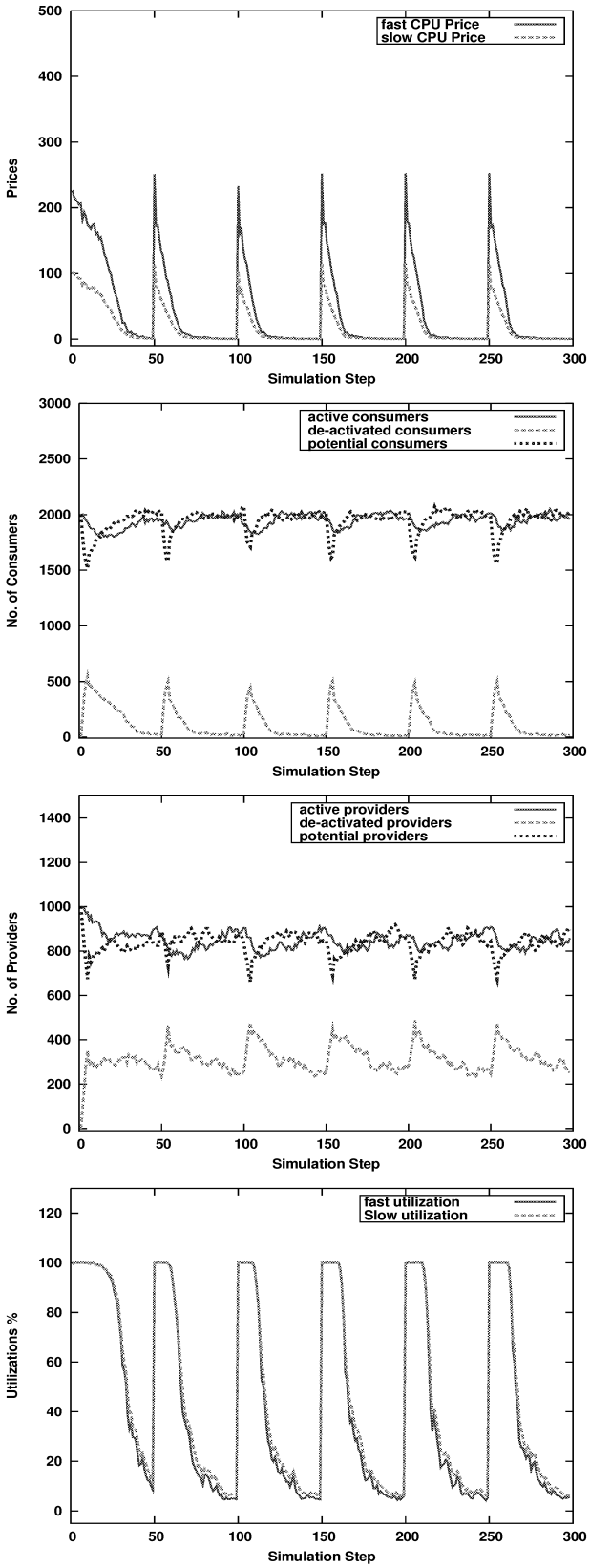

Figure 2: Scenario with maximum job length 10. Panels: (1) price evolution, (2,3) number of consumers and providers in each state, (4) utilization of both CPU categories

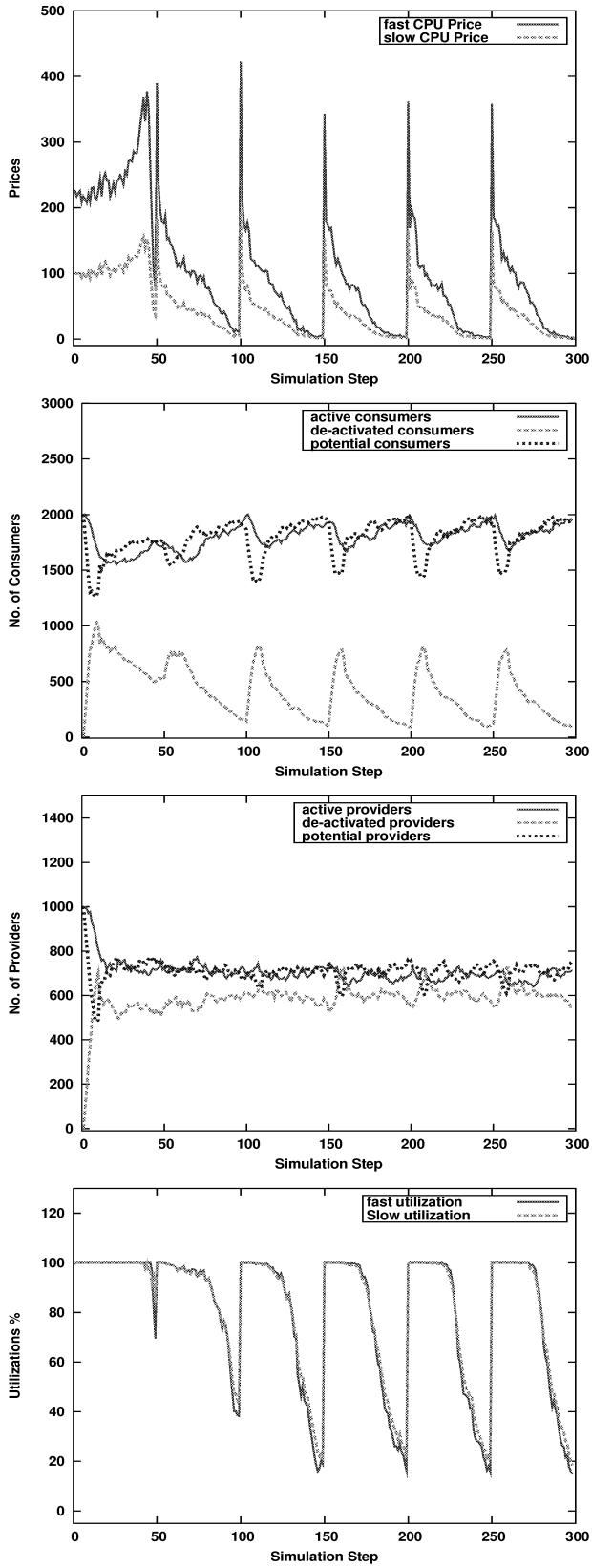

Figure 3: Scenario with maximum job length 20. Panels: (1) price evolution, (2,3): number of consumers and providers in each state, (4) utilization of both CPU categories

Table 2: Results for varying job duration.

Maximum Job Duration	5	10	20
Mean $price_{fast}$	25.9	41.2	100.8
Mean $price_{slow}$	11.4	18.2	44.5
Avg fast utilization%	26.4	43.9	80.2
Avg slow utilization%	28.6	46.4	81.4

ment draws near in order to allow users to exhaust their budget. Hence higher spending rates occur if the total workload is sufficiently large to sustain significant demand up to the end of the replenishment cycle.

The number of consumers and providers are shown in panels 2 and 3 of figure 3 respectively. The relative changes in the numbers are significant for both. That the pricing algorithm still succeeds in determining the supply-demand equilibrium indicates its robustness. The lengthening of job duration also increases the time spent in the deactivated state.

Panel (4) of figure 3 displays the utilization in this scenario. Clearly the workload is so extensive that the infrastructure is working at full utilization.

The table 2 gives an overview of quantitative results for the scenarios with different maximum job duration of five, ten and twenty time units respectively. They confirm the increase in price and utilization as the workload increases.

CONCLUSION AND FUTURE WORK

We have investigated the management of computational resources in dynamic grids using a commodity market model. We have presented results of different simulation scenario's showing price stability and resource utilization. The equilibrium pricing algorithm is shown to be robust against the disruptive effects of the dynamic grid fabric. The effects of increasing the workload in the grid system also demonstrate correct functioning of the algorithm.

Future research will focus first of all on extending the capability of the GES simulator to include the network. Indeed, w.r.t scalability the network overhead plays a crucial role. On a conceptual level we need to investigate the use of auction-based market mechanisms for dynamic grids and to improve our modeling of dynamic grids.

REFERENCES

Abdelkader K. and Broeckhove J., 2008. *Pricing computational resources in dynamic grid.* In *Proceedings of the 2nd International Workshop on P2P, Parallel , Grid and Internet Computing (3PGIC-2008).* IEEE Press, Barcelona, Spain, ISBN 978-0-7695-3109-0, 303–308.

Abdelkader K.; Broeckhove J.; and Vanmechelen K., 2008. *Commodity resource pricing in dynamic computational grids.* In *Proceedings of the 6th ACS/IEEE International Conference on Computer Systems and Applications (AICCSA-08).* IEEE Press, Doha, Qatar, no. CFP08283-CDR in ISBN: 978-1-4244-1968-5, 422–429.

Buyya R.; Abramson D.; and Giddy J., 2002. *Economic models for resource management and scheduling in Grid computing. Concurrency and Computation: Practice and Experience*, 14, 1507–1542. doi: 10.1002/cpe.690.

Buyya R.; Abramson D.; and Venugopal S., 2005. *The Grid Economy. Proceedings of the IEEE*, 93, no. 3, 698–714. doi:10.1109/JPROC.2004.842784.

Hirsch M. and Smale S., 1979. *Algorithms for solving f(x)=0. Communications on Pure and Applied Mathematics*, 32, 281–312.

Lewis R.M. and Torczon V., 2002. *A Globally Convergent Augmented Lagrangian Pattern Search Algorithm for Optimization with General Constraints and Simple Bounds. SIAM J on Optimization*, 12, 1075 – 1089. ISSN 1052-6234. doi:10.1137/S1052623498339727.

Smale S., 2001. *Dynamics in General Equilibrium Theory. Topology and Global Analysis*, 66, no. 2, 288–294.

Vanmechelen K.; Depoorter W.; and Broeckhove J., 2008. *A Simulation Framework for Studying Economic Resource Management in Grids.* In *Proceedings of the International Conference on Computational Science (ICCS 2008).* Springer-Verlag, Berlin Heidelberg, vol. 5101, 226–235.

Vanmechelen K.; Stuer G.; and Broeckhove J., 2006. *Pricing Substitutable Grid Resources using Commodity Market Models.* In H. Lee and S. Miller (Eds.), *Proceedings of the 3rd Int. Workshop on Grid Economics and Business Models (GECON 2006).* World Scientific, Singapore, 103–112.

Wolski R.; Plank J.; Brevik J.; and Bryan T., 2001. *Analysing Market-based Resource Allocation Strategies for the Computational Grid. Int J of High-Performance Computing Applications*, 1, 15(3).

AUTHOR BIOGRAPHIES

Khalid Abdelkader is a PhD researcher at the University of Antwerp. He completed his Master degree from University of Krakow (AGH), Poland in 1999. His research interests include distributed systems, Grid computing and Grid Economics.

Dr. Jan Broeckhove is a professor in the Department of Mathematics and Computer Science at the University of Antwerp (UA), Belgium. He received his PhD., in Physics, in 1982 at the Free University of Brussels (VUB), Belgium. His current research interests include a.o. distributed computing, in particular cluster and grid computing.

CACHE REPLACEMENT POLICY BASED ON FUZZY DECISION SYSTEM

Ali A. Al-Titinchi,
Department of Electrical and Computer Engineering
Applied Science University
Amman-Jordan
ali_1@asu.edu.jo

Munaf S. N. Al-Din,
Department of Electrical Engineering
Tafila Technical University
Tafila-Jordan
msnaldin2001@yahoo.com

KEYWORDS
Cache Memory, Page Replacement Policy, Fuzzy Decision System

ABSTRACT

Cache memory is integrated into the design of all computer systems. One of the cache memory management policies is the replacement technique. Conventional replacement procedures include least recently used (LRU) and least frequently used (LFU) algorithms. This paper presents a fuzzy replacement algorithm in cache page replacement. The fuzzy input variables used are the page's frequency of reference and the recency of reference. The fuzzy knowledge base is composed of 9 inference rules used to calculate an index value for each page in case there is a cache miss and no empty page in cache. The maximum value of this calculated index is used to select the victim page to replace. A simulation program was implemented to evaluate the proposed procedure, in addition to the existing replacement schemes. Comparisons between the different replacement procedures show an improvement in the cache page fault when using the fuzzy algorithm versus the traditional procedures.

INTRODUCTION

Caching is one of the oldest and most fundamental metaphor in modern computing. Several systems including Linux and Windows NT, 2000 and XP use page caching to cache both processes and file data (Silberschatz et al 2005). When the processor attempts to read a word of memory, a check is made to determine if the word is in the cache. If so, the word is delivered to the processor. If cache miss happens then a page is brought into the cache from the auxiliary memory (William 2003). The importance of the caching system is belonging to the fact that cache is significantly faster than the auxiliary memory, but is also significantly more expensive. Hence, the size of the cache memory is usually only a fraction of the size of the auxiliary memory. For this reason, it is not possible to bring all the process into the cache at a time. And hence, both memories are managed in units of uniformly sized items known as pages (Nimrod et al 2003). This difference in size and paging management will lead to a problem of page replacement. The page replacement problem happens when the cache becomes full and a demanding for a new page takes place. This causes the operating system to select one of the existing pages and paged it out. The victim page is selected using a cache replacement policy.

The aim of researches is to design an efficient replacement algorithm that maximizes the hit rate over a very long trace subject with over head that not exceed the anticipated time savings. Cache replacement algorithms play a central role in the design of any caching components. So the choice of replacement technique is one of the most critical cache issues (Jose et al 2004). Common replacement algorithms used with such caches are: First In First Out algorithm (FIFO), Least Recently Used algorithm (LRU) and the Least Frequently Used algorithm (LFU). These algorithms anticipate future references by looking at the past behavior of the programs. The later two algorithms are the most commonly used algorithms for replacement of cache objects. The LRU policy always replaces the least recently used page, where it exploits spatial locality in request sequence and the recency property, which states recently requested objects are more likely to be requested next than objects that have not been requested recently (Mgiddo et al 2004). One main disadvantage of the LRU algorithms; it does not capture and exploit the frequency features of the workloads. Therefore, the LFU is another policy that been developed to evict the pages in the cache that was requested the fewest number of times. LFU exploits the frequency property of request sequence which states that pages that have been requested more times are more likely to be requested again. As a disadvantage, it does not adopt well to variable access patterns (Aaho et al 1971).

Over last few years, interest has focused on combining recency and frequency. Several papers have attempted to bridge the gap between LRU and LFU by combining recency and frequency in various ways. The least recently frequently used (LRFU) policy is one of them (Lee et al 2001). The LRFU policy associates value with each block, this value is calculated according to a mathematical equation that mixes recency and frequency and comes to a single decision parameter. The problem with this policy is the difficulty to find exact mathematical formula to work with all kinds of workloads. Another recently developed page replacement policy is the Frequency-based replacement (FBR) policy, which is a heuristic algorithm that maintains a LRU list, but divides it into three sections: new, middle, and old. On a cache miss, the page in the oldest section with the smallest reference count is replaced. A limitation of the algorithm is that to prevent cache pollution due to stale pages with high reference count but no recent usage. The algorithm must periodically resize all the reference counts (Robinson et al 1990). Another method developed by (Gramacy et al 2002) is called a master-policy that simulates a number of caching policies (LRU, LFU, etc) and at any given time, dynamically chooses one of the competing policies. The limitation of the master-policy is that it must simulate all the competing policies, and, hence, requires high space and time overhead. As experiences shows,

it is not easy to correlate between the benefit of different replacement policies in one decision replacement model.

Fuzzy logic is a relatively young formal framework to process weak information that is affected by imprecision, vagueness, or uncertainty. Fuzzy logic is originally advocated by Zadeh (Zadeh 1965) and Mamdani and Assilian (Mamdani et al 1974). Fuzzy logic deals with the concept of partial truth which is often employed to capture the imprecise modes of reasoning that play an essential role in the human ability to make decisions in an environment of uncertainty and imprecision. Therefore, fuzzy logic seems very convenient to be used as a model for merging between the parameters of different formal replacement policies. Well designed fuzzy rules by an expert will improve the replacement policy for wide range of workloads as they execute in real worlds. In this paper we present a new cache replacement model using fuzzy logic technique. The rest of the paper is arranged as follow. Section 2 contains an overview of the fuzzy inference system. The designed model is described in section 3. Section 4 evaluates the proposed model with various types of simulated workloads. Finally, conclusion and future works are suggested in section 5.

FUZZY SYSTEMS

The basic concept underlying fuzzy logic may be viewed as a methodology for computing with words rather than numbers through the use of what is called fuzzy sets. A fuzzy set is described by a mathematical function called membership function. The membership function is a mathematical function used for carrying out approximate reasoning processes in the extent to which a value from a domain (also called universe) is included in a fuzzy concept. Input and output variables in the system are usually represented by a number of linguistic variables, where each linguistic variable is defined by a fuzzy set. Although, there is no restriction on the form of membership functions, we choose the piecewise linear description. The meaning of each linguistic value should be clear from its mnemonics; for example, VS stands for *very-short*, S for *short*, M for *medium*, L for *large*, and VL for *very-large*. A typical fuzzy system is shown in Figure 1 and it is conceptually very simple. They consist of an input, a processing, and an output stage. The main function of the system is to process the given inputs and produce an output by consulting an existing knowledgebase. Fuzzy systems consist of three main components, namely:

- Fuzzification.
- Inference mechanism.
- Defuzzification

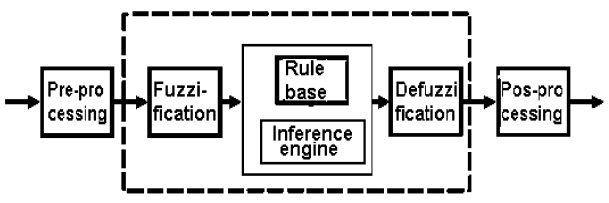

Figure (1): A typical fuzzy inference system

Bellow is a quick review of these steps:

- The Fuzzification which is the process that converts crisp inputs into fuzzy values and determines the degree to which they belong to each of the appropriate fuzzy sets via membership functions.

- The second component is the fuzzy inference mechanism. It consists of two parts, the knowledge base system and the inference engine. The knowledge base holds a set of rules about the system defined by using the human-like description. These rules are usually defined by experts to define the behavior of the fuzzy decision making system. The second part is the inference engine, which is the part of the fuzzy system that decides which rules should be used, and applies them. The inference engine performs a process by which the fuzzy sets that represent the outputs of each rule are combined into a single fuzzy set, and this process is call aggregation.

- The input for the defuzzification process is the aggregated output fuzzy set and the output is a single value. This can be summarized as follows: mapping input characteristics to input membership functions, input membership function to rules, rules to a set of output characteristics, output characteristics to output membership functions, and the output membership function to a single-valued output.

IMPLEMENTATION OF FUZZY REPLACEMENT CACHE SYSTEM

The fuzzy replacement cache system used is composed of a 2-input and 1-output. The inputs are the recency and frequency of references for each page in the cache. The output is a replacement weight that to be assigned to each page in the cache. The page with the highest replacement weight value will indicate the page to be replaced. Therefore, the replacement weight is a function of the instantaneous value of the two inputs.

With each page in the cache an integer number called number of hits, which indicates how many times the page has been referenced by the CPU, is associated. This page parameter is incremented every CPU cycle when there is a cache hit for the page in question. The frequency of reference that is input to the fuzzy replacement system is a normalized value, and it is computed by dividing the number of hits of a specific page to the number of hits of the page in the cache that has the maximum value of number of hits. Three membership functions are used to represent this parameter: LOW, MEDIUM, and HIGH as shown in figure (2).

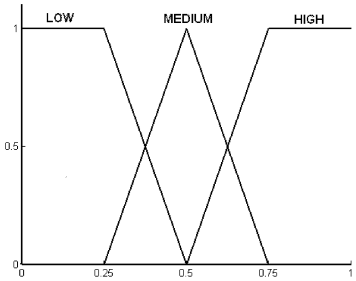

Figure (2): Membership functions for the normalized frequency of reference

Each page that is located the cache has a recency reference that is associated with it. This recency is an integer number that indicates the last CPU cycle in which the page has been referenced. This parameter is updated whenever a page in the cache is referenced or a new page is entered to the cache. Again this parameter is normalized with every CPU cycle. This input is represented by three membership functions: NEW, MEDIUM and OLD as shown in figure (3).

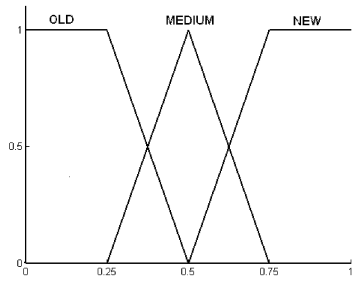

Figure (3): Membership functions for the normalized recency of reference

The page replacement weight is presented by five membership functions: VERY LOW. LOW, MEDIUM, HIGH and VERY HIGH as depicted in figure (4). The fuzzy replacement system is invoked only when the present CPU cycle has caused a cache miss and the cache is full. The cache is full when all the pages in it are flagged as being occupied by given page. Therefore, in each CPU cycle, when the fuzzy replacement system is activated the following steps are evaluated in order to find the page with the maximum page replacement weight.

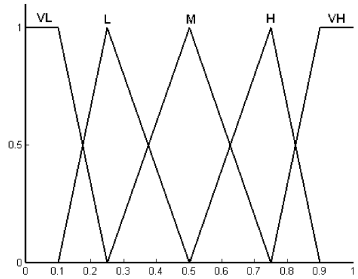

Figure (4): Membership functions for the page replacement weight

The first step is to take the inputs and determine the degree to which fuzzy sets they belong to. The input is a crisp numerical value limited to the universe of discourse which is in our case from [0, 1]. Since the recency and frequency of references are not limited to the range [0, 1], both are normalized against the maximum value of the recency and frequency of references respectively. Therefore, before fuzzifying the inputs, the maximum value of the recency and frequency of references are evaluated, and then are used for normalization. Fuzzification of a given input accounts for evaluation of the membership function output defined for those variables. The A set of rules have been defined for the fuzzy inference system as given in table (1):

Table (1): The rule-base matrix

Frequency	LOW	MEDIUM	HIGH
Recency			
OLD	VH	H	M
MEDIUM	H	M	L
NEW	M	L	VL

Once the inputs have been fuzzified, we know the degree to which each part of the antecedent has been satisfied for each rule. If the antecedent of a given rule has more than one part, the fuzzy operator is applied to obtain one number that represents the result of the antecedent for that rule. In the above examples, only the AND is used as a fuzzy operator. The input to the fuzzy operator is two or more membership values from fuzzified input variables. The AND operator can be evaluated using the minimum or product, and the OR using the maximum of its two inputs.

A consequent is a fuzzy set represented by a membership function, which weighs appropriately the linguistic characteristics that are attributed to it. The consequent is reshaped using a function associated with the antecedent. The input to the evaluation of an implication is a single number given by the antecedent, and the output is a fuzzy set. Implication is evaluated for each rule.

Aggregation is the process by which the fuzzy sets that represent the outputs of each rule are combined into a single fuzzy set. Aggregation only occurs once for each output variable, just before the final step, the defuzzification. The input of the aggregation process is the list of truncated output functions returned by the implication process for each rule. The output of the aggregation process is one fuzzy set for each output variable.

The input for the defuzzification process is a fuzzy set (the aggregated output fuzzy set) and the output is a single number. The final desired output for each variable is generally a single number. However, the aggregation of a fuzzy set includes a range of output values, and so must be defuzzified in order to resolve a single value from the set. The method used in this paper was the weighted average of the area under the aggregated output fuzzy set. It is worthwhile mentioning at this point that there are many defuzzification techniques that can be utilized (Saade et al 1999).

PERFORMANCE EVALUATION

We constructed a trace-driven simulator to evaluate and demonstrate the strength of our model comparing to LRU and LFU replacement algorithms. These traces are distinguished for different workloads, and can be classified into four cases according to their reference patterns.

Case1: Figure (5) shows the result of the evaluation when the reference pattern is of spatial clustered reference type, which means the referenced pages are close in the address space. The total size of the simulated program is roughly 4MB.

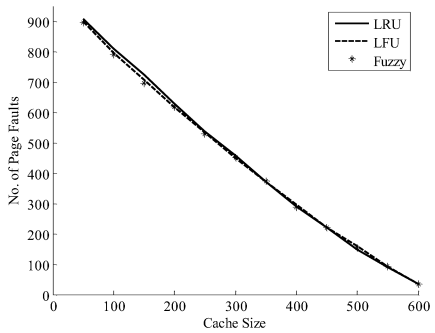

Figure (5): Spatial Clustered references Case

Case 2: Figure (6) shows the result of evaluation for the simulated trace when the pages are accessed at almost the same time in temporal clustered reference manner. In this case the program size is about 3MB.

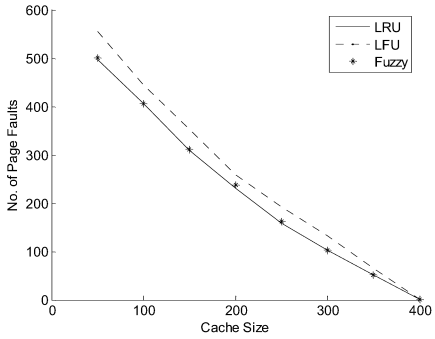

Figure (6): Temporal Clustered References Case

Case 3: Figure (7) is to state the evaluation result of looping pattern where the pages are referenced repeatedly during the cycle life of the simulated program. Here, the program under test is of size equal to about 28MB.

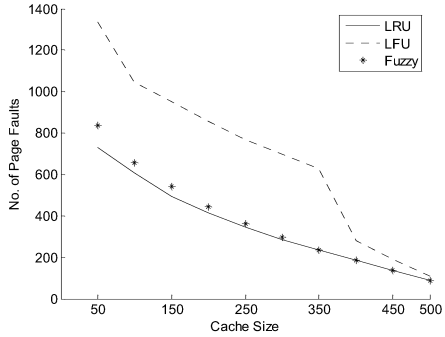

Figure (7): Loops References Case

Case 4: Figure (8) illustrates evaluation result, when all pages are accessed randomly using suitable probabilistic function in the simulated program. The size of the program that is used to test the model is roughly 1MB.

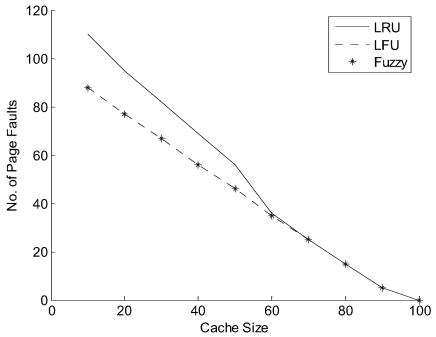

Figure (8): Probabilistic references case

CONCLUSION AND FUTURE WORKS

This paper has proposed a fuzzy logic model that merges the two traditional replacement algorithms, LRU and LFU. From the case studies that illustrated in the previous section, we found the fuzzy approach is very promising. The designed model performs well for all types of reference patterns, while LRU and LFU show disparate performance with the different tested workloads. However, the fuzzy logic model is somehow time consuming. Hence, as future work, we are looking to improve performance and the speed of the fuzzy approach by building a model based on neuro-fuzzy scheme for cache replacement.

REFERENCES

Silberschatz, Galvin, and Gagne. 2005. Operating System Concepts. Wiley, USA,.

William Stallings. 2003. Computer Organization & Architecture. Pearson Education International, New Jersey.

Nimrod Megiddo, and Dharmendra S. Modha. 2003. "ARC.A self-tuning low overhead replacement cache". Usenix File & Storage Technologies Conference FAST 2003, Usenix, pp. 115-130.

Jose Aguilar, and Ernst L. Leiss. 2004. "An adaptive coherence-replacement protocol for web proxy cache systems". Computation & systems, vol. 8, no. 1, pp. 1-14.

Mgiddo N., Modha DS. 2004. "Outperforming LRU with an adaptive replacement cache algorithm", Computer, April, pp. 4-11.

Aaho A. V., Denning P. J. and Ullman J. D. 1971. "Principles of optimal page replacement". J. ACM, Vol. 18, No. 1, pp. 80-93.

Lee D., Choi D., Kim J., Noh S. H., Min S. L., Cho Y., Kim C. S. 2001 "LRFU: A spectrum of policies that subsumes the least recently used and least frequently used policies" IEEE trans, Computers, Vol. 50, No. 12, pp. 1352-1360.

J. T. Robinson and M. V. Devarakonda 1990. “Data cache management using frequency-based replacement”. In Proc. ACM SIGMETRICS conf., pp. 134-142.

R. B. Gramacy, M. K. Warmuth, S. A. Brandt, and I. Ari. 2002. “Adaptive caching by refetching” in NIPS.

L.A. Zadeh. 1965. “Fuzzy sets”. Information and Control, No. 8, pp. 338–353.

E.H. Mamdani, S. Assilian. 1974. “Application of fuzzy algorithms for control of simple dynamic plant”. Proceedings of the Institute of Electrical Engineers 121, pp.1585–1588.

E Saade, J., and Diab, H. 1999. “Defuzzification techniques for fuzzy controllers”. IEEE Transactions on Systems, Man, and Cybernetics: Part B,.

.

Using Dynamic Data Mining in Association Rule Mining

Kifaya Qaddoum
Philadelphia University
Amman, Jordan
E-mail: sweetkq@hotmail.com

Keywords: Data Mining, Dynamic Approach, Knowledge Discovery, Association Mining, Frequent Itemsets.

Abstract. The main objective of data mining is to find interesting/useful knowledge for the user, as Rules are an important form of knowledge; some existing research has produced many algorithms for rule mining. These techniques, use the whole dataset to mine rules and then filter and/or rank the discovered rules in various ways to help the user identify useful ones.. Data mining should provide tactical insights to support the strategic directions. In this paper, we evaluate using a dynamic mining approach that uses knowledge discovered in previous episodes for classifying web documents. The proposed approach is shown to be effective for solving problems related to the efficiency of handling database updates, accuracy of data mining results, gaining more knowledge and interpretation of the results, and performance. Our results do not depend on the approach used to generate *itemsets*. In our analysis, we have used an *Apriori-like approach* as a local procedure to generate *large itemsets*.

1 Introduction

Data mining is the process of discovering potentially valuable patterns, associations, trends, sequences and dependencies in data [1-6,12,16,19,22,23]. There are many potential application areas for association rule technology which include catalog design, store layout, customer segmentation, telecommunication alarm diagnosis, and so on. Another trend example includes web site access analysis for improvements in e-commerce advertising, fraud detection, or product analysis, and customer segmentation. Data mining techniques can discover information that many traditional business analysis techniques fail to deliver.

Many knowledge discovery applications [8,10,11,14,15,17,18,20,21], such as on-line services and world wide web applications, require accurate mining information from data that regularly changes. For such cases an environment, frequent or occasional updates may change the status of some rules discovered earlier. During the data mining process data should be collected repeatedly to allow users to gain more complete knowledge of the significance or the importance of the generated data mining rules.

Discovering knowledge is an expensive operation [4,6,7,8,11,12,13]. It requires extensive access of secondary storage that can become a bottleneck for efficient processing. As data stored in databases is changed, data mining algorithm needs to start from scratch, which, is obviously, not an efficient strategy. Using previously discovered knowledge along with new data updates to maintain discovered knowledge could solve one of the most important problems, that have faced data mining techniques; that is, *database updates.*

This paper uses an approach that dynamically updates knowledge obtained from the previous data mining process to classify web documents which dynamically changes. According to Dynamic Mining, transactions over a long duration are divided into a set of successive episodes. Information gained during the current episode depends on the current set of transactions and the discovered information during the last episode. Our approach discovers current data mining rules by using updates that have occurred during the current episode along with the data mining rules that have been discovered in the previous episode.

In section 2, a formal definition of the problem is given. The dynamic data mining approach is introduced in section 3. In section 4, the paper is summarized and concluded.

2 Problem Definition

The association mining task simply can be stated as follows [1]: Let I be a set of items, and D a database of examples, where each example has a unique identifier (tid) and contains a set of items. A set of items is also called an ITEMSET. An ITEMSET with k items is called a k-ITEMSET. The support of an ITEMSET X, denoted $\sigma(X)$, is the number of examples in D where it occurs as a subset. An ITEMSET is frequent or large if its support

is more than a user-specified minimum support (min sup) value.

An association rule is an expression A ⇒ B, where A and B are ITEMSETs. The support of the rule is the joint probability of an example containing both A and B, and is given as σ (A ∪ B). The confidence of the rule is the conditional probability that an example contains B, given that it contains A, and is given as σ (A ∪ B) / σ (A). A rule is frequent if its support is greater than min sup, and it is strong if its confidence is more than a user-specified minimum confidence (min conf).

The problem of association mining, also referred to as the *market basket* problem, is formally defined as follows. Let $I = \{i_1, i_2, \ldots, i_n\}$ be a set of items and $S = \{s_1, s_2, \ldots, s_m\}$ be a set of transactions, where each transaction $s_i \hat{I} S$ is a set of items that is $s_i \acute{I} I$. An *association rule* denoted by $X \Rightarrow Y$, $X, Y \grave{I} I$, and $X \cap Y = F$, describes the existence of a relationship between the two itemsets X and Y.

Suppose we have divided the transaction set T into two subsets T_1 and T_2, corresponding to two consecutive time intervals, where F_1 is the number of transactions in T_1 and F_2 is the number of transactions in T_2, ($F=F_1+F_2$), and $F_1(S)$ is the number of transactions having S in T_1 and $F_2(S)$ is the number of transactions having S in T_2, ($F(S)=F_1(S)+F_2(S)$).

In order to find out if S is a large itemset or not, we consider four cases,

- S is a large itemset in T_1 and also a large itemset in T_2, i.e., $F(S) \geq F_1 * MINSUP_1$ and $F_2(S) \geq F_2 * MINSUP_2$.
- S is a large itemset in T_1 but a small itemset in T_2, i.e., $F(S) \geq F_1 * MINSUP_1$ and $F_2(S) < F_2 * MINSUP_2$.
- S is a small itemset in T_1 but a large itemset in T_2, i.e., $F(S) < F_1 * MINSUP_1$ and $F_2(S) \geq F_2 * min\ sup$.
- S is a small itemset in T_1 and also a small itemset in T_2, i.e., $F(S) < F_1 * MINSUP_1$ and $F_2(S) < F_2 * MINSUP_2$.

In the first and fourth cases, S is a large itemset and a small itemset in transaction set T, respectively, while in the second and third cases, it is not clear to determine if S is a small itemset or a large itemset.

3 The Dynamic Data Mining Approach

The value of accumulated knowledge determines how much history information would be carried. This history information can be used to determine the significance or the importance of the generated emerged-large itemsets, as well as to determine the significance or the importance of the generated declined-large itemsets, and to generate large itemsets with less SUPPORT values without having to rerun the mining procedure again.

The example in Figure 1 shows the steps how itemset is generated according to the specified steps withing our algorithm in Figure 2.

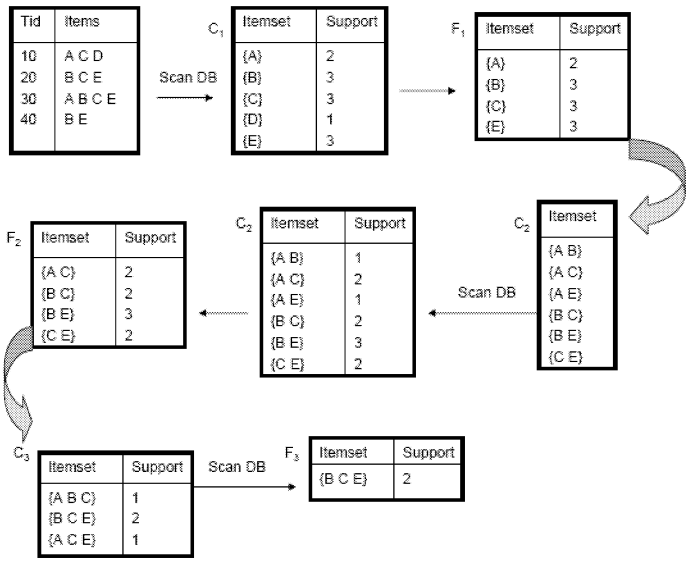

DB : Transactional database
F_n: Set of n-items that pass the *minsupp* threshold (frequent itemsets)
C_n : Set of n-candidate itemsets that are possibly frequent
F_1={frequent 1-itemsets};
for (n=2; $F_{n-1} \neq \emptyset$; n++) Do
C_n=generate_candidates(F_{n-1});
for each transaction T∈DB Do
P_t = subset(C_n, t)
Cl is the . accumulate d value of F where itemset x is l arg e $_{x\,i}$
begin
$D = D + F_i$
for $(k=2; f_{k-1}(T_n) \neq f; k++)$ ***do***
begin
C_k=***AprioriGen***($f_{k-1}(T_n)$ È $f_{k-1}*(T_n)$)
forall *transactions* $_n t \in T$ ***do***
forall *candidates* $c \hat{I} C_k$ ***do***
if $c \acute{I} t$ ***then*** *c.count++*
for each candidate c∈P_t
c.count++;
end //for
F_n={c∈C_n| c.count_ *minsupp*}
end// for
output = $_{n\,n} \cup F$

Fig. 2 Apriori Dynamic Algorithm

In the *DynamicMining* algorithm, we used an *Apriori approach* as a local procedure to generate large or *emerged-large itemsets*. We would like to emphasize the fact that our approach does not depend on the approach used to generate *itemsets*. The main contribution of our approach, is to dynamically generate *large itemsets* using only the transaction updates and the information collected in the previous data mining episode.

The experimental results, on the *Dynamic Mining* algorithm has shown a significant potential usage. Two main factors have been considered ,

- The performance of the *Dynamic Mining* algorithm in terms of *disk access*, and *CPU time*.
- The knowledge gained by using different values of *a*.

4 Conclusions and Future Work

This paper used a *Dynamic Data Mining* approach for finding associations withing database transactions for a group of given itemset. The proposed approach performs periodically the data mining process on data updates during a current episode and uses that knowledge captured in the previous episode to produce data mining rules. We have introduced the concept of *locality* along with the definitions of *emerged-large itemsets* and *declined-large itemsets*. The new approach solves some of the problems that current data mining techniques suffer from which is, *database updates,* the dynamically update knowledge obtained from the previous data mining process. Transactions grouop is treated as a set of successive episodes. In our approach, information gained during a current episode depends on the current set of transactions and that discovered information during the previous episode.

References

[1] S. Agarwal, R. Agrawal, P. Deshoande, A. Gupta, J. Naughton, R. Ramakrishnan, and S. Sarawagi, "On the Computation of Multidimensional Aggregates", In Proc. 1996 Int. Conf. Very Large Databases, Bomaby, India, Sept. 1996.

[2] R. Agrawal, T. Imilienski, and A. Swami, "Mining Association Rules between Sets of Items in Large Databases," Proc. of the ACM SIGMOD Int'l Conf. On Management of data, May 1993.

[3] R. Agrawal and R. Srikant, "Mining Sequential Patterns", In Proc. 11th Intl. Conf. On Data Engineering, Taipi, Taiwan, March 1995.

[4] R. Agrawal, and R. Srikant, "Fast Algorithms for Mining Association Rules," Proc. Of the 20 th VLDB Conference, Santiago, Chile, 1994.

[5] R. Agrawal, J. Shafer, "Parallel Mining of Association Rules," IEEE Transactions on Knowledge and Data Engineering, Vol. 8, No. 6, Dec. 1996.

[6] C. Agrawal, and P. Yu, "Mining Large Itemsets for Association Rules," Bulletin of the IEEE Computer Society Technical Committee on Data Engineering, 1997.

[7] S. Brin, R. Motwani, J. Ullman, and S. Tsur, "Dynamic Itemset Counting and Implication Rules for Market Basket Data," SIGMOD Record (SCM Special Interset Group on Management of Data), 26,2, 1997.

[8] S. Chaudhuri, "Data Mining and Database Systems: Where is the Intersection," Bulletin of the IEEE Computer Society Technical Committee on Data Engineering, 1997.

[9] M. Chen, J. Han, and P. Yu, "Data Mining: An Overview from a Database Prospective", IEEE Trans. Knowledge and Data Engineering, 8, 1996.

[10] M. Chen, J. Park, and P. YU, "Data Mining for Path Traversal Patterns in a Web Environment", Proc. 16th Untl. Conf. Distributed Computing Systems, May 1996.

[11] D. Cheung, J. Han, et al, " Maintenance of Discovered Association Rules in Large Databases: An Incremental Updating Technique", In Proc. 12th Intl. Conf. On Data Engineering, New Orleans, Louisiana, 1996.

[12] U. Fayyed, G. Shapiro, P. Smith, and R. Uthurusamy, "Advances in Knowledge Discovery and Data Mining", AAAI/MIT Press, 1996.

[13] A. Hafez, J. Deogun, and V. Raghavan ,"The Item-Set Tree: A Data Structure for Data Mining", DaWaK' 99 Conference, Firenze, Italy, Aug. 1999.

[14] C. Kurzke, M. Galle, and M. Bathelt, "WebAssist: a user profile specific information retrieval assistant," Seventh International World Wide Web Conference, Brisbone, Australia, April 1998.

[15] M. Langheinrichl, A. Nakamura, N. Abe, T. Kamba, and Y. Koseki ,"Un-intrusive Customization Techniques for Web Advertising," The Eighth International World Wide Web Conference, Toronto, Canada, May 1999.

[16] H. Mannila, H. Toivonen, and A. Verkamo, "Efficient Algorithms for Discovering Association

Rules," AAAI Workshop on Knowledge Discovery in databases (KDD-94) , July 1994.

[17] M. Perkowitz and O. Etzioni, "Adaptive Sites: Automatically Learning from User Access Patterns", In Proc. 6th Int. World Wide Web Conf., santa Clara, California, April 1997.

[18] P. Pitkow, "In Search of Reliable Usage Data on the WWW", In Proc. 6th Int. World Wide Web Conf., santa Clara, California, April 1997.

[19] G. Rossi, D. Schwabe, and F. Lyardet, "Improving Web Information Systems with Navigational Patterns," The Eighth International World Wide Web Conference, Toronto, Canada, May 1999.

[20] N. Serbedzija, "The Web Supercomputing Environment," Seventh International World Wide Web Conference, Brisbone, Australia, April 1998.

[21] T. Sullivan, "Reading Reader Reaction: A Proposal for Inferential Analysis of Web Server Log Files", In Proc. 3rd Conf. Human Factors & The Web, Denver, Colorado, June 1997.

[22] C. Wills, and M. Mikhailov, "Towards a Better Understanding of Web Resources and Server Responses for Improved Caching," The Eighth International World Wide Web Conference, Toronto, Canada, May 1999.

[23] M. Zaki, S. Parthasarathy, M. Ogihara, and W. Li, " New Algorithms for Fast Discovery of Association Rules," Proc. Of the 3 rd Int'l Conf. On Knowledge Discovery and data Mining (KDD-97), AAAI Press, 1997.

BIOGRAPHY

KIFAYA QADDOUM was born in Amman, Jordan and went to the University of Philadelphia, where she studied Computer Science and also obtained her Master degrees in 2003 and 2005. Since 2003 she works for one of the United Nations Units in Jordan which called UNRWA that serves the Palestinian refugees in Jordan and other countries, she works as Information Technology Instructor at one of UN colleges, in addition to her interest in research work.

SIMULATION IN ELECTRONICS

QoS Enhancement of Voice over Internet Protocol Based On Neural Network Model

Dr. Khaldoon Ghaidan

College of Engineering

University of Jerash

Jerash, Jordan

E-mail: Khldn45@yahoo.com

Abstract: Voice over Packet switching networks and more specifically Voice over Internet Protocol (VoIP) give us an alternative to the traditional circuit switching telephony networks existing today. VoIP is a strong competitor of the traditional circuit switching networks as it offers several advantages over the traditional circuit switching telephony networks. Among the advantages are: Lower equipment cost, Integration of voice and data services, Lower bandwidth requirements, and Lower operating and management expenses. Still several issues need to be resolved before announcing VoIP as the ultimate replacement of the traditional telephone network. This paper gives survey of the main advantage of VoIP network as well as presenting a new way of going around the problem of achieving high quality of service for VoIP.

Keywords: VoIP, QoS, circuit switching, packet switching, Neural Network

1. Introduction.

Traditional telephony companies use circuit switching networks for carrying voice traffic. Circuit switching build a dedicated path from the sender to the receiver and the resources across the path are allocated to the phone call from beginning to end of the call, so circuit switching is carrying voice very well from source to destination [1].

Today commercial telephone networks that based on circuit switching technology has number of attractive features: their availability is 99.999 percent; this corresponds to down time of no more about five minutes per year and is know as five nines reliability. Telephone networks also have the capability to support millions of subscribers and similar number of simultaneous calls. Also when one finishes dialling, the phone at the other end starts ringing within two or three seconds. And when someone answers and conversation takes place, the speech quality is very high, without any perceptible echo, noticeable delay, or annoying noise on the line [1].

Given that the current telephone networks are working in such a good way, why should any one consider an alternative carrier? The answer is circuit switching is dedicated to carry voice. This dedication is the major strength and at the same time the major weakness of the traditional telephony network because it cannot do anything else very well [1, 2]. Other reasons include: lower equipment cost, integration of voice and data and creation of new and advanced services, lower bandwidth requirement, and lower management effort as we need to manage one unified network in comparison with the effort needed to manage two separate voice and data networks.

Alternatively voice could be implemented over packet switching networks rather than over circuit switching network [3]. The most widely spread packet switching network is the Internet Protocol (IP) network [1, 4, 5, 6, 7, 8]. The new technology is known as Voice over Internet Protocol (VoIP). VoIP can be defined as transport of voice traffic using the Internet Protocol (IP).

This paper is organized as follows: In section 2, we survey major challenges that facing VoIP implementations and highlight some of the efforts developed to tackle these challenges. In section 3 we discuss briefly why we need to tackle these challenges and the importance of Quality of Service (QoS) in VoIP networks. In section 4 we present the proposed solution and discuss briefly some of our expectations the proposed solution is going to achieve. Finally in Section 5 we present some conclusions and future research directions.

2. Survey.

VoIP is an attractive alternative of the traditional telephony networks for carrying voice for several reasons [1, 2]:

a. **Lower equipment cost:** Circuit switching systems use proprietary hardware, proprietary operating systems, and applications running on proprietary software. This closed nature of the circuit switching systems makes an operator very

careful in choosing the vendors for their systems because when they choose their vendors, they have to choose that vendor for the whole system due to the lack of interoperability between products from different vendors and this result in monolithic architecture. On the other hand in the IP world, the operating system is less tightly coupled to the hardware and much of the hardware is standardized. This offer greater choice between vendors and this allows customers to pick those companies that are the best in the different areas to create a solution that is optimum in all respects. Furthermore, IP networks tends to use a distributed client-server model rather than the monolithic systems, which means that it is easy to start small and grow as demand dictates.

b. **Integration of voice and data:** IP was originally designed to carry data ranging from e-mail to web browsing to e-commerce, when we combine this capability with the transport of voice, many new and advanced services can be offered. One example is a web page with a menu to allow entering the user's location, when the user presses a button to talk to a customer representative. Based on the user's location, the user will be directed to the most appropriate customer representative.

c. **Lower bandwidth requirements:** G.711 is the standard voice coding for traditional telephony. While G.711 requires 64 kbps, more efficient and sophisticated voice coding algorithms exist, which enable speech to be transmitted at different ranges from 5.3 kbps to 32 kbps. These more advanced coding schemes could be applied to the current telephone system but this would require that these coding schemes be implemented in practically every telephone switch in the world.

d. **Lower operating and management expenses:** Today enterprises need to manage two separate networks: the telephone networks, and the data (IP) networks. Implementing VoIP simplify the life for the enterprises by merging these two networks into a unified network that can carry both voice and date. This unification results in a lower operational and technical effort and at the same time leads to a reduction in expenses.

Although VoIP enables us transport of voice traffic using the Internet Protocol (IP); however IP networks are originally designed to carry data rather than voice, therefore the most important issue in VoIP is ensuring high speech quality [1]. To ensure good voice quality, a number of issues should be addressed:

a. **Delay:** Real-time applications such as voice are extremely intolerable of delay. Mouth to Ear (M2E) delay is the delay measured from the moment a noticeable voice signal appears at the sending end (speaker's mouth) of a connection to the moment the same voice signal appears at the receiving end (listener's ear). International Telecommunication Union – Telecommunication Standardization Sector (ITU-T) Recommendation G.114 states that the M2E delay should be not more than 150 ms [1, 9]. In contrast delay requirement for data is much less restricted. It is hardly matter if sending data such as sending e-mail took 3 seconds or 3 minutes, provided it arrives correctly [1]. In order to maintain the liveliness of the speech, this rigid 150 ms delay requirement should be considered carefully.

Different components affect the transmission delay of the voice signal [1, 2, 9]:

i. Algorithmic delay: Speech coders need to collect data to be able to process. The size of the data frame to be collected depends on the speech coder. Careful selection of the speech coder to be used and a balance between the voice quality with the bandwidth consumption and algorithmic delay of that speech coder should be made [10, 11].

ii. Processing delay: Encoding and collecting samples for transmission purposes causes a processing delay. This delay affected by the processor execution speed and the type of the speech coding technique.

iii. Transmission (Network) delay: In contrast to data traffic where delay of few seconds, may be minute is rarely has an effect as soon as the data arrived correctly. Voice traffic is sensitive to network delay. Specialized techniques such as resource reservation have been developed to ensure minimum network delay between sender and receiver.

iv. Jitter compensation delay: jitter buffers as discussed next are used to compensate the effect of jitter on

the network, these buffers add to the overall delay [12].

b. **Jitter:** Packets in IP network may need difference times to reach their destination. The differences in the time needed may be result from two reasons. First, packets can take different routes from sender to receiver and consequently experience differ delays. Second, packets may experience different queuing times even they both travelled the same route. If the variation of delay-also known as jitter- is keep changing, then it is difficult to adjust the delay for smooth and natural play-out of the speech signal. To minimize the effect of jitter, buffers are used to buffer the speech packets so that they can be played-out to the receiver in a steady fashion [12, 13]. While jitter is a problem in packet switching networks, in circuit switching networks, open, dedicated path exists from the sender to the receiver for the duration of a conversation. Thus all speech follows the same path using dedicated resources, experiencing no or very small variation in delay.

c. **Packet Loss:** During transmission of packets in IP networks, queues might overflow in network nodes between sender and receiver, resulting in the loss of packets. Retransmission mechanisms can be applied in the case of lost data packets to compensate the lost packets. Those retransmission mechanisms cannot be applied to real-time communications (such as voice) because the time needed to detect the lost packets and retransmit them is long enough to the degree that lost packets become useless in such real-time communications (such as voice). Therefore, appropriate mechanisms are required to ensure packet loss is minimized and if present has a minor effect. For example some complex coding techniques deal with the problem of lost packets. Techniques such as resource reservation also eliminate or reduce the packet loss over the network [1, 2].

In addition to the above challenges, other requirements of the VoIP network should be presented. Among these requirements, the VoIP network should meet the five nines (99.999 percent) availability requirement described above if the VoIP is to be commercial challenge to the telephone network. To meet such condition, then redundancy of major system components should be applied and balance should be done between network cost and network quality. Other requirements such as scalability [3] and applying security techniques [14] are also desirable and easy to add to the VoIP network.

In VoIP we also need a specialized signalling protocol to control the start/end of the session, determination of the coding technique to be used, issues such as: authentication to make a call, etc. We have two competing protocols in the market: - the ITU-T H.323 recommendation and the Internet Engineering Task Force (IETF) SIP recommendation. These protocols and other supporting protocols such as MGCP, and MEGACO are existing in the market today [1, 4].

3. The need for QoS in VoIP.

Quality of Service (QoS) can be defined as a measurement of the level of service delivered to a customer. A customer that used to use the traditional telephony network is expecting something similar to what the traditional telephony is.

Several challenges could be tackled in a collaborative effort to improve the QoS of the VoIP network as described in the previous section. To achieve the high quality of the traditional telephony, we should reduce the packet loss, delay, and jitter. Also, bandwidth requirements should be met.

A question may arise wondering why we should concern about improving the QoS. The answer is high-quality service is essential if an operator want to attract customers to the new IP solution for carrying voice rather than using the traditional circuit switching telephony network. No matter how low the price, if the quality of voice over IP network is not capable of competing with the traditional telephony network, the customers are not expected to be attracted to the new solution.

4. The proposed solution.

Artificial Intelligent (AI) techniques are used to simulate the human intelligent in one-way or another and they have been employed successfully in many fields [15]. One of the most successful AI branches is Artificial Neural Networks (ANNs). ANNs are employed successfully in number of fields and are particularly good at pattern recognition in data.

As there are many challenges need to be tackled in VoIP such as minimizing delay, compensate packet loss, reducing the effect of jitter. These challenges will be looked into in a further detail, and will be tested under ANNs models. Human brain is capable to perform such tasks as compensation of loss in the middle of speech; therefore we strongly believe that such ANNs techniques used as a model of human brain could be employed successfully to improve the QoS of VoIP.

5. Conclusions and future research directions.

VoIP is a hot research area in the world of communication. The high revenue achieved by the telecommunication companies is an attraction to develop solution that transmit voice over other media rather than the traditional; circuit switching network. Several issues still need to be resolved before achieving a high quality voice over the IP networks that can compete with the traditional telephony network. These issues include such topics as: minimizing the delay, eliminate or reduce the packet loss, and reducing the effect of jitter.

6. References.

[1] Collins, D., *Carrier grade voice over IP*. 2nd ed. McGraw-Hill networking and telecommunications. Professional telecom. 2003, New York; London: McGraw-Hill. Xviii, 572 p.

[2] Nachiappan, N. and F. Sjoqvist, *Survey of Voice over IP (VoIP)*. 2004, available at http://www.stanford.edu/~nachi/VoIP_Survey.doc last visitied 16/07/2004.

[3] Chong, H.M. and H.S. Matthews. *Comparative analysis of traditional telephone and voice-over-Internet protocol (VoIP) systems*. In *IEEE International Symposium on Electronics and the Environment*. 2004.

[4] Jain, R., Voice over IP: Protocols and Standards. 1999, available at http://www.cse.ohio-state.edu/~jain/cis788-99/ftp/voip_protocols/index.html last visitied 16/07/2004.

[5] Jain, R., Voice over IP: Products, Services and Issues. 1999, available at http://www.cse.ohio-state.edu/~jain/cis788-99/voip_products/index.html last visitied 16/07/2004.

[6] Protocols.Com, Voice over IP Reference Page, available at http://www.protocols.com/pbook/VoIP.htm last visited 16/07/2004.

[7] Protocols.Com, Voice over IP, available at http://www.protocols.com/pbook/VoIPFamily.htm last visited 16/07/2004.

[8] Protocols.Com, H.323 Protocols Suite, available at http://www.protocols.com/pbook/h323.htm last visited 16/07/2004.

[9] Khasnabish, B., *Implementing voice over IP*. 2003, Hoboken, N.J.; Chichester: Wiley-Interscience. Xvi, 208 p.

[10] Al-Akaidi, M., P. Urwin, and J. Blackledge, *Speech Coders For Mobile Communications*.

[11] Xu, Y., M. Westhead, and F. Baker, *An Investigation of Multilevel Service Provision for Voice over IP Under Catastrophic Congestion.* IEEE Communications Magazine, 2004. **42**: p. 94-101.

[12] *T*seng, K.K., Y.C. Lai, and Y.D. Lin, *Perceptual Codec and Interaction Aware Playout Algorithms and Quality Measurement for VoIP Systems.* IEEE Transactions on Consumer Electronics, 2004. **50**(1): p. 297-305.

[13] Narbutt, M. and L. Murphy, *Improving Voice Over IP Subjective Call Quality.* IEEE Communications Letters, 2004. **8**: p. 308-310.

[14] Vuong, S. and Y. Bai. *A survey of VoIP intrusions and intrusion detection systems*. In *The 6th International Conference on Advanced Communication Technology*. 2004.

[15] Al-Akaidi, M., Simulating Speech Coders Using Neural Networks. Simulation, 1998. 71(1): p. 23-30.

Frequency Domain Iterative Compensation of High Power Amplifier Non-linearity

Saqib Ali
Dept. of Communication Systems
Lancaster University
a.saqib@lancaster.ac.uk

Garik Markarian
Dept. of Communication Systems
Lancaster University
g.markarian@lancaster.ac.uk

Marwan Al-Akaidi
School of Engg. & Tech.,
De Montfort University, Leicester
mma@dmu.ac.uk

Abstract: **This paper presents the results for the Predistorter based compensation of the HPA using an iterative methodology in an OFDM/OFDMA based system. Unlike the general trend, the iterations and compensation is performed on the frequency domain symbols. The output of a Saleh's baseband amplifier model is shown for various IBOs (Inputs Back Off). This system is then compensated at different IBO for a number of iterations. The resulting BER improvement is also shown. It is observed that for a 5 iteration case the total degradation of the system can be reduced from a figure of 13 dB (without pre-distortion) to a figure of 8dB (5-iteration, pre-distorter).**

Index terms: – HPA, OFDM, OFDMA, Orthogonal Frequency Division Multiplexing, High Power Amplifier, Saleh

I - INTRODUCTION

In the last few decades the usage of the OFDM has forecasted the further development of wireless standards on this very technology. Various well known standards, have already adopted OFDM at their physical layer. For example wired broad band technologies like xDSL[1] and Power line [2] has OFDM based PHY, wireless technologies which include broadcast technologies like DVB-T, DVB-H, DMB-T/H and DAB [3] and wireless broadband access technologies like 802.11a/g, 802.16d/e [4] [5] [6] and future coming technologies like UWB [7] and UTRAN-LTE [8], have in one or other way adopted the OFDM as the key technology at the PHY layer. This promising adoption for the recent and the future technology has made OFDM/OFDMA to be a strong contender.

In any OFDM based systems the output amplified signal needs to be transmitted on air as it is. Any non-linearity in the amplifier may result in artefacts. These artefacts are complex distortions which causes spectral leakage, warping and clustering of the constellation. Thus an overall penalty of the BER needs to be paid at the receiver. These artefacts have been studied in [9] and a mathematical model for the Travelling Wave Tube amplifiers has already been defined.

This work has been done as a part of the EU project "WiMAGIC". The authors would like to acknowledge the support provided by RINICOM Ltd.

It is highly desirable to overcome this issue so that the amplified signal that will be transmitted on air is the exact amplified replica of the baseband signal. This mitigation can be performed in either analogue or digital domain. Various solutions have been proposed in literature which range from "the use of linear amplifier", "power back off" to "pre-distortion of baseband signal".

Linear amplifiers are not feasible in the uplink, and cost prohibits the use. Backing off the transmitter, is actually using the amplifier in the linear region; thus resulting in reduction of SNR and the reduction in power efficiency.

In the recent years the base-band pre-distortion techniques have gained serious popularity. Reason is the ease of implementation at the baseband level due to the availability of much computation power.

This paper is organized as follows. Nonlinear behaviour of amplifier will be discussed in section II. In section III, IV&V digital pre-distortion is explained. Proposed algorithm along with the pseudo code will be presented in VI. Section VII will give insight into the simulation setup and results. Discussion on further research is presented in sec. VIII.

II – NON-LINEARITY IN AMPLIFIER

It is well understood that the non-linearity of the amplifier result in AM/AM and AM/PM distortions.

Considering input signal

$$x(t) = r(t)\cos(\omega_o t + \theta) \tag{1.1}$$

Where ω_o = angular frequency and θ = phase offset,

The output can be defined as

$$y(t) = A[r(t)]\cos[\omega_o t + \theta + \phi[r(t)]] \tag{1.2}$$

For the design consideration in this paper we will be considering Saleh's TWT model [1]. According to the Saleh's model AM/AM and AM/PM distortions can be modeled as

$$A(r) = \frac{\alpha r}{1 + \beta r^2} \tag{1.3}$$

$$\phi(r) = \frac{\rho r^2}{1+\lambda r^2} \quad (1.4)$$

Where

$A(.)$ = Magnitude non-linearity function.

$\phi(.)$ = Phase non-linearity function.

$r(t)$ = Input magnitude.

α, β ρ and λ are constants which govern the nonlinear behavior of the amplifier.

III - BASEBAND PRE-DISTORTION

Baseband predistortion can be classified in two types. These are (i) symbol pre-distortion (ii) waveform pre-distortion. The symbol pre-distortion tries to directly adjust the baseband symbols. In other words it plays with the constellation of the symbols to mitigate the non-linearity. But the waveform pre-distortion is the technique in which instead of symbols the waveform is distorted. For single carrier systems the waveform pre-distortion and the symbol pre-distortion are one and the same, but in an OFDM system a clear demarcation of the types can be seen.

IV - PRE-DISTORTION IN OFDM

In single carrier system we always have a discrete number of symbols at the input. This ease the situation in which we need to find the inverse function for these discrete number of symbols only. Once we have the function at hand we can apply it to any input symbol, which results in a compensation of the amplifier.

In contrary OFDM based multicarrier systems have a special Pre-distortion problem. The output symbols of OFDM do not have discrete values. Rather the amplitude and phase combination at the input of the OFDM may result from zero to any value within the input power limits. After application of the HPA TF the problem worsens.

V - GENERAL TECHNIQUE

Generally the pre-distortion is performed in time domain. That is quite a straight forward approach. In this method the time domain inverse of the system is found and it is placed in front of the amplifier. Block diagram of this system is as follows

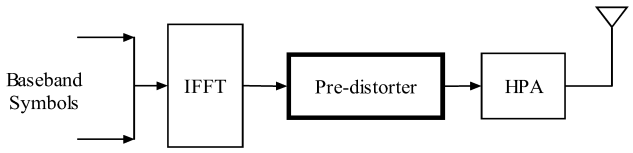

Fig: A time domain Compensation technique

VI - PROPOSED TECHNIQUE

As mentioned earlier the amplifiers are operated in the linear region to avoid the non-linearity, this is called as input backing off, and the extent to which the amplifier is backed off from its maximum input is called as the input back off.

It can be defined as

$$IBO = \frac{P_{i_{sat}}}{P_{i_{avg}}} \quad (1.5)$$

Where

$P_{i_{sat}}$ The input saturation power, and

$P_{i_{avg}}$ Is the average output power

The resultant back off that will be observed at the output is called as output back off and is defined as

$$OBO = \frac{P_{o_{sat}}}{P_{o_{avg}}} \quad (1.6)$$

Where

$P_{o_{sat}}$ is output saturation power

$P_{o_{avg}}$ is the average output power

If we can pre-distort the amplifier to compensate the non-linear behaviour; a much more dynamic range of the amplifier can be utilized. An obvious result will be benefit in terms of the efficiency of the HPA. A real good insight to this can be found in [9] [10] [11] .Various adaptive pre-distorter methodologies for both memory and memory less systems have been proposed [12] [13] [13]. All of these are focused in the estimation and compensation in time domain. Neural Network based approach has also been studied [14, 15]. But the approach is still remains to the estimation and compensation in time domain. A slight deviation from the above trend can be seen in which the estimation is done in the frequency domain and the compensation in time domain [16].

We here have taken this ideology one step further in trying to do the compensation in frequency domain. For this we have looked into an iterative approach in which pre-distortion is applied directly to the input baseband symbols. We will be iteratively pre distorting each input symbol, which can result in a cleaner amplified constellation at the amplifier output. Block diagram for the said technique is

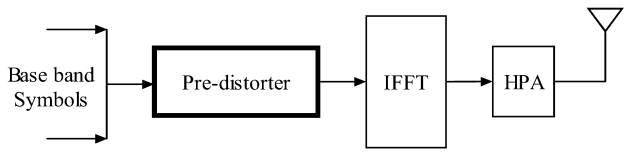

Fig 1: Proposed technique. Frequency domain compensation

By placing the distorter at the input of the IFFT we have managed to get a direct control of the input symbols. These symbols are iteratively distorted keeping in view the error from the reference symbols. This error is used to adjust the complex gains of each input symbol which contributes in making the time domain output of the OFDM.

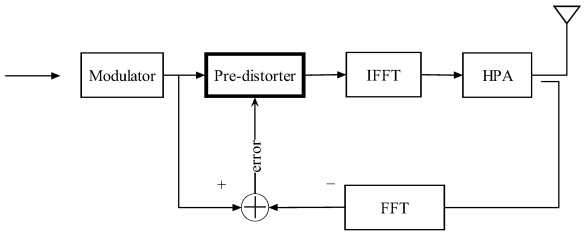

Fig 2: Iterative Pre-distorter block diagram

The pseudo code for the iterative frequency domain pre-distortion is

- Take OFDM symbol as reference
  - A_{ref}
- Multiply this with weights W_i (which are set to be all ones at initialization)
  - $A_{ref} \bullet W_i$
- Take IFFT of the result
  - $IFFT\left(A_{ref} \bullet W_i\right)$
- Pass this through the HPA baseband model
  - $HPA\left(IFFT\left(A_{ref} \bullet W_i\right)\right)$
- Take FFT of the output of HPA
  - $FFT\left(HPA\left(IFFT\left(A_{ref} \bullet W_i\right)\right)\right)$
- Subtract this from A_{ref} to compute the error
  - $E = A_{ref} - FFT\left(HPA\left(IFFT\left(A_{ref} \bullet W_i\right)\right)\right)$
- Generate new weights by using this error vector
  - $W_{i+1} = W_i - E \bullet \Delta$ (Δ = Convergence rate)

VII - SIMULATION

We have taken a 256 point OFDM under consideration. For the sake of simulation simplicity all the subcarriers are considered to be 16-QAM modulated. The input of the IFFT block is normalized to have power = 1. After passing through the IFFT block the time domain signal is given an input gain. This provides us with the input back off control. The three input back off levels considered in the simulation are 12dB, 14dB and 24dB. This amplified IFFT output is fed to the Saleh's TWT model whose parameters are

$$\alpha = 1, \quad \beta = \frac{1}{4} \quad \text{and} \qquad \rho = \frac{\pi}{12}, \lambda = \frac{1}{4}$$

Theoretical plot of the model on the above mentioned parameters is shown in Fig. 3.

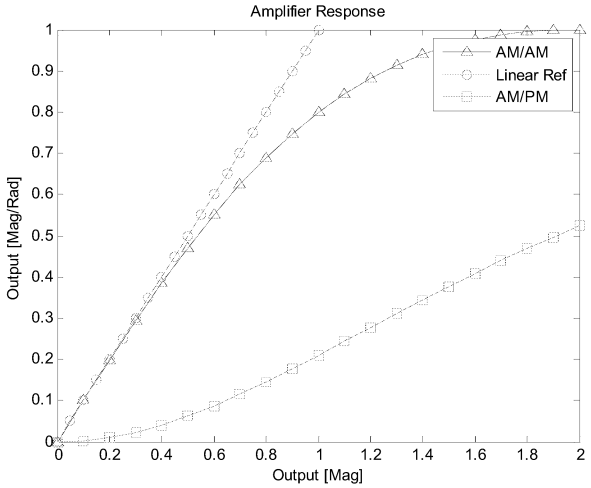

Fig 3: Saleh's amplifier model response for AM/AM & AM/PM conversion

The output of the HPA is then provided to the iterative compensator. The iterative compensator is nothing more than a rescaling of the HPA output followed by an FFT. The output of the FFT is compared with the reference input signal. The output of FFT is compared with the reference transmitted symbol sequence. And error vectors for each symbol are computed. These error vectors multiplied with a convergence factor are subtracted to adjust the input values of the symbols. This is done again in the next iteration. Based on the new error vector the input is pre-distorted to further extent. This process is repeated until the output of the HPA amplifier converges back to the original reference symbol or the maximum number of iterations is achieved.

It is observed that if the step size is kept within reasonable limits, the pre-distorter converges after a certain number of iterations. A pre-distortion which is achieved iteratively actually restores the desired constellation at the output of the HPA.

For the sake of simplicity we have only considered symbols whose amplitude remains within the maximum input bounds of the amplifier. In our case the maximum input that can be provided to the amplifier is 2.

We have shown the effect of nonlinear amplifier on the constellation in Fig. 4, 5 & 6. The extent of clustering and the rotation effect can clearly be seen at different IBOs.

We have generated the BER plots for the iterative compensation for different IBOs. It can be seen that at 24dB back off there is no effect of the non-linearity. This is because the amplifier is operating in the linear region. When we close the gap and move towards the 14dB IBO the effect become more pronounced. A clear degradation in the BER curve can be seen in Fig. 8. From the figure it is quite evident that the

iterative compensator compensates for the BER degradation and moves the curve real close to the theoretical one. For the 12dB IBO case the things worsen. In Fig. 7 the BER curve without any compensation moves far away from the ideal one. Even for the case of 30dB SNR, bit error rate is around 10^{-2} , which is not a good figure. The iterative Predistorter does compensate in this scenario and brings back the curve quite close to the ideal one. The benefit of more iteration can be clearly seen in this scenario.

In the Fig.10 the Total degradation vs. OBO is plotted. It is quite clear that the Total degradation can be reduced to 8dB with the help of Pre-distorter in comparison to 13 dB without any Pre-distorter.

VIII - DISCUSSION

The draw back in this type of pre-distortion is the computational cost. The cost of additional FFT /IFFT for every iteration, before transmitting the signal over the air is a real big figure. The computational cost will actually prohibit this kind of pre-distorter to actually being used.

But in this study it is shown that the pre-distortion which is generally employed in the time domain can also be implemented in the frequency domain. Irrespective of the cost, the pre-distortion of the input symbols at base band has actually resulted in the compensation of the HPA non-linearity

This work can be extended further in finding a non-iterative pre-distorter which can be implemented in the frequency domain.

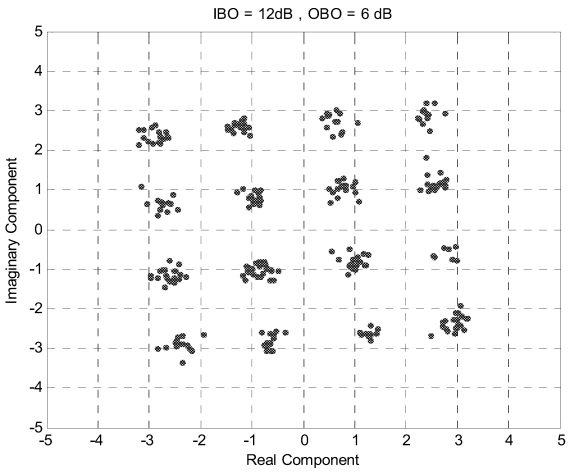

Fig. 4. Distortion in Constellation at IBO = 12dB

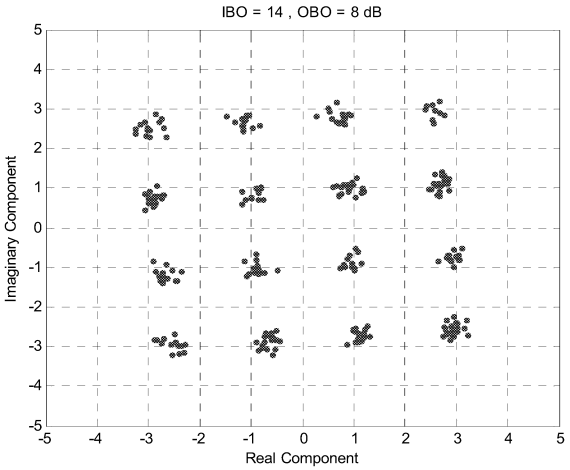

Fig. 5. Distortion in Constellation at IBO = 14dB.

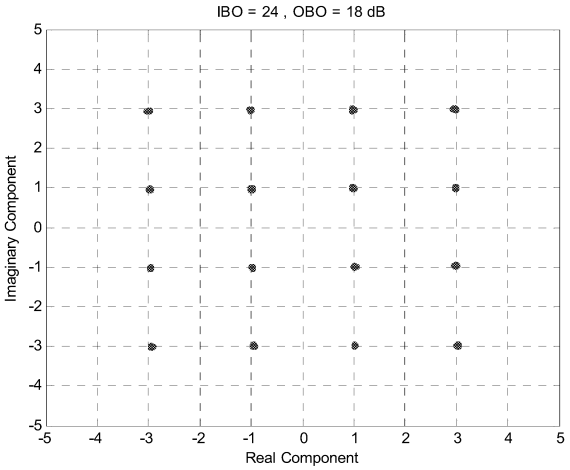

Fig. 6. Distortion in Constellation at IBO = 24dB.

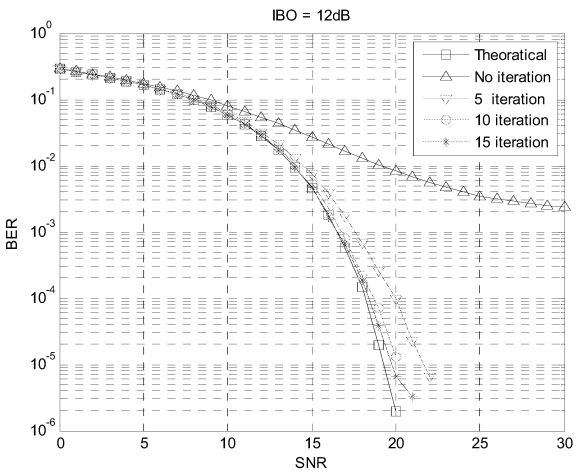

Fig. 7. BER at different number of iterations for IBO = 12dB.

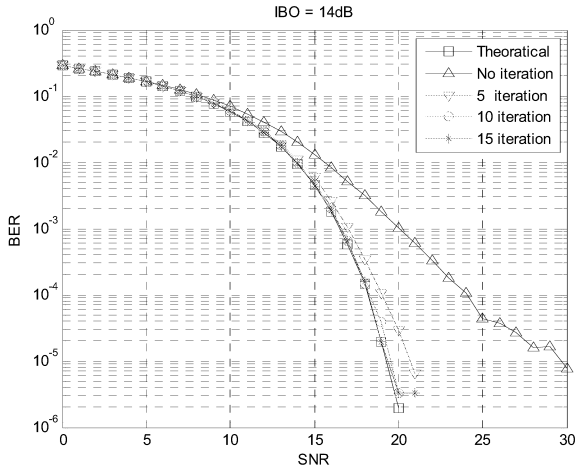

Fig. 8. Improvement in BER at different number of iterations for IBO = 14dB.

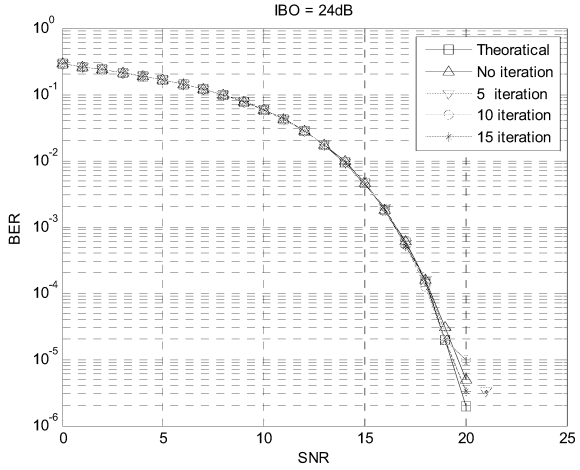

Fig. 9. Improvement in BER at different number of iterations for IBO = 24dB

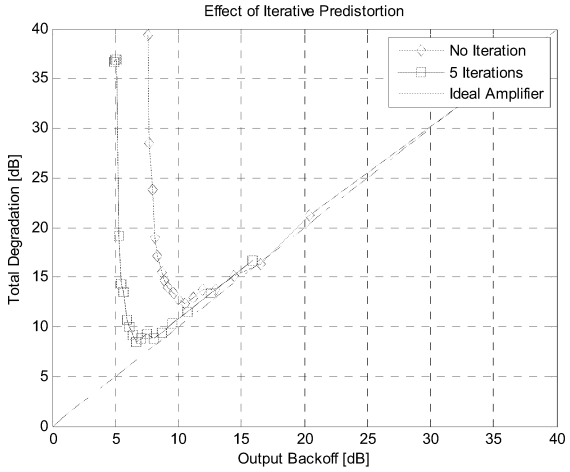

Fig. 10. Total Degradation vs. OBO for different number of iterations

REFERENCES

[1] W. Contributors, "Digital subscriber line." vol. 2008: Wikipedia, The Free Encyclopedia.

[2] W. Contributors, "IEEE P1901." vol. 2008: Wikipedia, The Free Encyclopedia, 2008.

[3] W. Contributors, "Oorthogonal frequency -division multiplexing." vol. 2008: Wikipedia, The Free Encyclopedia.

[4] W. Contributors, "IEEE 802.11." vol. 2008: Wikiepdia, The Free Encyclopedia, 2008.

[5] Contributors, "IEEE 802.16d-2004 Standard," IEEE 802.16 Task Group D, 2004.

[6] Contributors, "IEEE 802.16e-2005 Standard," IEEE Task Group e 2005.

[7] W. Contributors, "Ultra-wideband." vol. 2008: Wikipedia, The Free Encyclopedia.

[8] Contributors, "UTRA-UTRAN Long Term Evolution (LTE) and 3GPP System Architecture Evolution (SAE)." vol. 2008: 3rd Generation Partnership Project (3GPP).

[9] A. Saleh, "Frequency-Independent and Frequency-Dependent Nonlinear Models of TWT Amplifiers." vol. 29, 1981, pp. 1715-1720.

[10] G. Karam and H. Sari, "Generalized data predistortion using intersymbol interpolation." vol. 46, 1991, p. 21.

[11] E. Costa, M. Midrio, and S. Pupolin, "Impact of amplifier nonlinearities on OFDM transmission systemperformance." vol. 3, 1999, pp. 37-39.

[12] D. S. Han and T. Hwang, "An adaptive pre-distorter for the compensation of HPA nonlinearity." vol. 46, 2000, pp. 152-157.

[13] H. W. Kang, Y. S. Cho, and D. H. Youn, "On compensating nonlinear distortions of an OFDM system using anefficient adaptive predistorter." vol. 47, 1999, pp. 522-526.

[14] R. Zayani and R. Bouallegue, "A Neural Network Pre-Distorter for the Compensation of HPA Nonlinearity: Application to Satellite Communications," 2007, pp. 465-469.

[15] K. Kappler, H. A. Kuzma, and J. W. Rector, "A comparison of standard inversion, neural networks and support vector machines," SEG, 2005.

[16] M. C. Chiu, C. H. Zeng, and M. C. Liu, "Predistorter Based on Frequency Domain Estimation for Compensation of Nonlinear Distortion in OFDM Systems." vol. 57, 2008, pp. 882-892.

Unequal error protection using LT codes and block duplication

Shakeel Ahmad*, Raouf Hamzaoui†, Marwan Al-Akaidi†
* Department of Computer and Information Science, University of Konstanz, Germany.
Email:shakeel.ahmad@uni-konstanz.de
† School of Engineering and Technology, De Montfort University, Leicester, UK.
Email:{rhamzaoui,mma}@dmu.ac.uk

***Abstract*—Luby Transform (LT) codes are powerful packet erasure codes with low encoding and decoding complexity. We provide a simple method to improve the bit error rate performance of LT codes. Moreover, we exploit our method to design a new approach for unequal error protection with LT codes. We used simulations to compare our approach with a state of the art unequal error protection technique when the information symbols are partitioned into two protection levels (most important bits and least important bits). Our approach yielded lower bit error rates for the two protection levels and lower encoding complexity at the cost of moderately higher decoding complexity.**

Keywords: Communications, channel coding, performance analysis, fountain codes, unequal error protection.

I. Introduction

Fountain codes [1], [2], [3] are probabilistic forward error correction (FEC) erasure codes with many desirable features. Whereas traditional erasure codes like Reed-Solomon codes have a fixed code rate that must be chosen before the encoding begins, Fountain codes are rateless as the encoder can generate on the fly as many encoded symbols as needed. This is an advantage when the channel conditions are unknown or time-varying because the use of a fixed channel code rate would lead to either bandwidth waste if the erasure rate is overestimated or to poor performance if it is underestimated. Compared to Reed-Solomon codes, Fountain codes have lower encoding and decoding complexity, but require a few more encoded symbols at the receiver for successful decoding.

Luby [2] proposed the first class of practical Fountain codes and called them Luby Transform (LT) codes. Shokrollahi [3] introduced another class class of Fountain codes called Raptor codes by concatenating a fixed-rate channel code with an LT code. Raptor codes have been adopted as enhanced application layer FEC by Multimedia Broadcast/Multicast System (MBMS) of the 3rd Generation Partnership Project (3GPP), IP datacast (IPDC) of Digital Video Broadcasting - Handheld (DVB-H), as well as Digital Video Broadcasting Project's (DVB) global IPTV standard.

With the growing interest in Fountain codes, the question of how to achieve unequal error protection (UEP) with these codes has been addressed [4], [5], [6]. In contrast to equal error protection (EEP) where the same level of FEC is applied to all information symbols, UEP assigns different levels of protection to different information symbols. Typically, the information symbols are protected according to their importance. UEP has been successfully used [7] for the protection of scalable image and video coders such as JPEG2000 [8] and 3D SPIHT [9]. In these works, the importance of the information symbols is expressed in terms of their contribution to overall reconstruction quality.

This paper has two main contributions. The first one is a simple method to decrease the bit error rate (BER) of LT codes [2]. The idea, which is inspired by the sliding window technique of [10], consists of virtually increasing the number of information symbols. The second contribution of the paper is a new technique for UEP with LT codes.

The paper is organized as follows. Section II contains background material about LT codes. Section III discusses a state of the art UEP technique [4] for LT codes. Section IV introduces our idea for improving the BER performance of LT codes and explains how this idea can be exploited to provide UEP. Section V presents our simulation results and shows the gains achieved by our approach.

II. Background

In this section, we explain the encoding and decoding with LT codes. More details can be found in [2].

A. Encoding

The LT encoder takes a set of k information symbols (bits or bytes, for example) and generates a potentially infinite sequence of encoded symbols of the same alphabet. Each encoded symbol is computed independently of the other encoded symbols. More precisely, given k information symbols $i_1, \ldots, i_k$ and a suitable probability distribution $\Omega(x)$ on $\{1, \ldots, k\}$, a sequence of encoded symbols $e_n,\ n \geq 1, \ldots$, is generated as follows. For each $n \geq 1$

1) Select randomly a degree $d_n \in \{1, \ldots, k\}$ according to the distribution $\Omega(x)$.
2) Select uniformly at random d_n distinct information symbols and set e_n equal to their bitwise modulo 2 sum.

The relationship between the information symbols and encoded symbols can be described by a graph (Fig. 1).

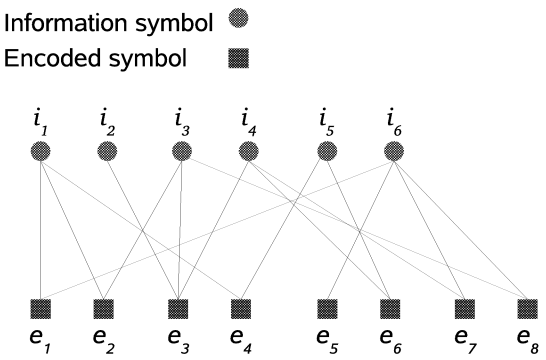

Fig. 1. Encoding graph of an LT code. Eight encoded symbols are generated from $k = 6$ information symbols. The degree of an encoded symbol is the number of information symbols that were used to generate it. For example, the degree of e_1 is equal to two.

B. Decoding

When an encoded symbol is transmitted over an erasure channel, it is either received correctly or lost. The LT decoder tries to recover the original information symbols from the received encoded symbols. We assume that for each received encoded symbol, the decoder knows the indices of the information symbols it is connected to. This is possible, for example, by using a pseudo-random generator with the same seed as the one used by the encoder.

The decoding process is as follows:

1) Find an encoded symbol e_m that is connected to only one information symbol i_j. If this is not possible, stop the decoding.
   a) Set $i_j = e_m$.
   b) Set $e_x = e_x \oplus i_j$ for all indices $x \neq m$ such that e_x is connected to i_j. Here $\oplus$ denotes the bitwise modulo 2 sum.
   c) Remove all edges connected to i_j.
2) Go to Step 1.

III. Previous work

Rahnavard, Vellambi, and Fekri [4] were the first to propose a method to provide UEP with LT codes. For simplicity, we describe their method when two levels of protection are used. Consider a source block having k information symbols. Partition these k information symbols into two sets S_1 and S_2 of size $|S_1| = \alpha k$ and $|S_2| = (1-\alpha)k$, respectively, where $0 < \alpha < 1$. The set S_1 is called the set of most important bits (MIB) while the set S_2 is called the set of least important bits (LIB). Define probabilities p_1 and p_2 ($p_1 + p_2 = 1$) to select S_1 and S_2, respectively. Given a suitable probability distribution $\Omega(x)$ on $\{1, \ldots, k\}$, a sequence of encoded symbols e_n, $n \geq 1$ is generated as follows. For each n

1) Select randomly a degree $d_n \in \{1, \ldots, k\}$ according to the distribution $\Omega(x)$.
2) Select d_n distinct information symbols successively. To select a symbol, first select one of the two sets S_1 or S_2 (S_1 with probability p_1 and S_2 with probability p_2). Then choose randomly a symbol from the selected set.
3) Set e_n equal to the bitwise modulo 2 sum of the d_n selected information symbols.

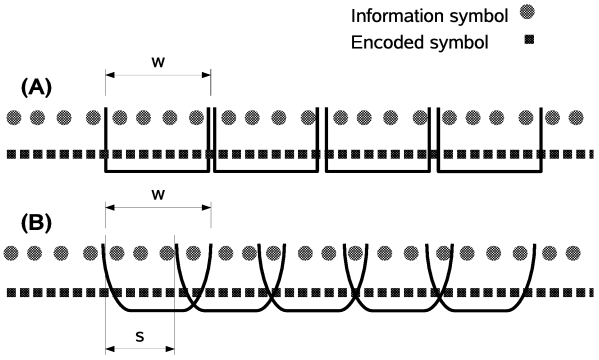

Fig. 2. Sliding window technique of [10]. (A): without window overlap. (B) with window overlap.

To ensure that the MIB symbols have lower BER than the LIB symbols, the probability of selecting an MIB symbol should be larger than that of selecting an LIB symbol [4], that is, $p_1 \frac{1}{|S_1|} > p_2 \frac{1}{|S_2|}$. To achieve this, one can set $p_1 = \frac{k_M |S_1|}{k}$ and $p_2 = \frac{k_L |S_2|}{k}$ for $0 < k_L < 1$ and $k_M = (1 - (1-\alpha)k_L)/\alpha$. Here the parameter k_M gives the relative importance of the MIB symbols.

IV. Proposed method

A. Virtual increase of source block size

We first explain our technique to improve the BER performance of an LT code. The idea is to virtually increase the size of the source block by duplicating the information symbols. This is motivated by the observation that the performance of a Fountain code improves with increasing size of the source block. Our idea is inspired by the sliding window technique proposed in [10] (see Fig. 2). This technique uses a sliding window and applies LT encoding to the information symbols within the window. The window has a size of w symbols and is shifted by s symbols until all information symbols are covered. Thus, the number of windows is $N_w = ((k-w)/s) + 1$. For example, when $s = w$, the windows do not overlap and $N_w = k/w$. When $s < w$, some information symbols are covered by more than one window. As the size of the overlap increases, the virtual size of the source block increases, resulting in higher decoding efficiency [10].

As in the method of [10], we propose to virtually increase the size of the source block. However, we do not use windows. Instead, we simply duplicate all information symbols. Simulations in Section V show that our approach gives in general better BER performance. In the following, we describe our approach in detail.

Consider a source block having k information symbols indexed from 1 to k. Let $\Omega(x)$ be the degree distribution of the LT code on $\{1, \ldots, k\}$. We expand the source block by appending the same k information symbols at

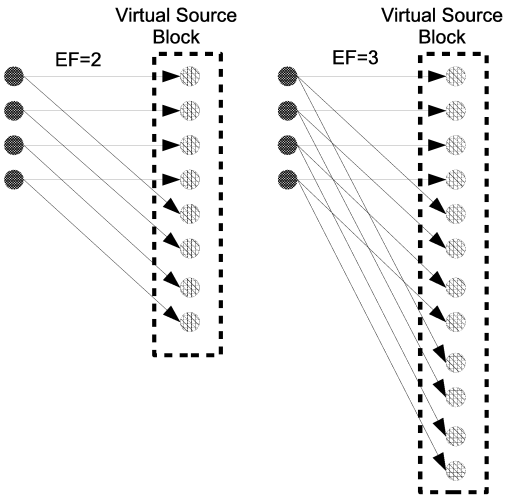

Fig. 3. Virtual increase of the source block size for $k = 4$, (left) $EF = 2$ and (right) $EF = 3$.

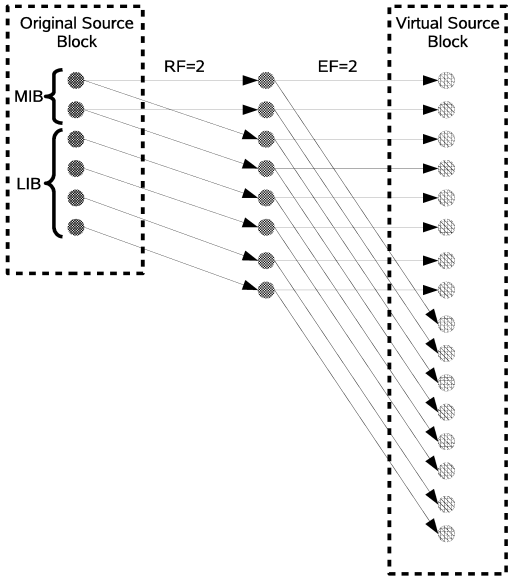

Fig. 4. UEP with $k = 6$, $EF = 2$, and $RF = 2$.

the end of the block. Let EF denote the number of times the source block is present in the new source block. Then the new source block has a length of $EF \times k$ and the information symbols have indices ranging from 1 to $EF \times k$ (Fig. 3). We call the parameter EF the expanding factor. Next, we extend the original degree distribution $\Omega(x)$ from $\{1, \ldots, k\}$ to $\{1, \ldots, EF \times k\}$. Using the standard LT encoder described in Section II with the new degree distribution, we generate the encoded symbols. If the index of an information symbol that is connected to an encoded symbol is between $k+1$ and $EF \times k$, we subtract $EF \times k$ from this index. In this way, the receiver can use the standard LT decoder for k information symbols.

B. Unequal error protection

The concept of virtually increasing the size of the source block by duplicating information symbols has a natural application to UEP. For simplicity and without loss of generality, we describe our UEP method for two levels of protection (MIB and LIB symbols). To realize UEP, we propose to duplicate the MIB symbols. We denote by RF the number of times a block of MIB symbols is present in the virtual source block. For example, suppose that we have six information symbols and the first two are MIB symbols. If we duplicate these two symbols as in the first step of Fig. 4, the virtual size of the source block becomes 8, corresponding to $RF = 2$. We next extend the degree distribution of the LT code from $k = 6$ to $k = 8$. To generate an encoded symbol, we find its degree d using the new degree distribution and then select d information symbols from the 8 virtual symbols. If the index of a selected information symbol is larger than 2, we map its virtual index to the actual index by subtracting 2. Finally, we note that our UEP technique can be used together with the method proposed in Section IV-A. For example, for $RF = 2$ and $EF = 2$, the source block consisting of 2 MIB symbols and 4 LIB symbols is transformed into a virtual block of size $EF(RF \times 2 + 4) = 16$ (Fig. 4).

V. Experimental results

We provide two sets of experiments. The first one shows the benefits of the method proposed in Section IV-A over the sliding window approach of [10]. The second one compares our UEP technique (see Section IV-B) to that of [4] (see Section III). In all simulations, a symbol consisted of eight bits and the robust soliton distribution [2] with parameters $c = 0.1$ and $\delta = 0.5$ was used as the underlying degree distribution. The simulations were done on a PC running an AMD Dual Core 4600, with 2GB RAM.

Fig. 5 shows a comparison between our method and the sliding window approach proposed in [10]. The simulations were run for $k = 20,000$ information symbols. The overhead is calculated as $(n-k)/k$ where n is the number of encoded symbols used in the decoding and k is the number of information symbols. The BER is calculated as the average value of $(k-d)/k$, where d is the number of (correctly) decoded symbols.

The performance of the two methods improved by increasing the virtual number of information symbols. However, there was a limit beyond which no improvement was observed (50 % overlap for the sliding window approach and $EF = 8$ for our approach). The BER performance of our approach was better than that of the sliding window approach when the overhead was larger than about 0.05. When the overhead was smaller than this value, the sliding window approach gave a lower BER. However, in this range, the BER is too high for the method to be useful.

Fig. 6 compares our UEP approach to that of [4]. The performance of equal error protection is also included as a reference. As in [4], the set of information symbols was partitioned into a class of MIB symbols and a class of LIB symbols. The parameter k_M in [4] and the repeat factor RF in our approach (see Sections III and IV-B,

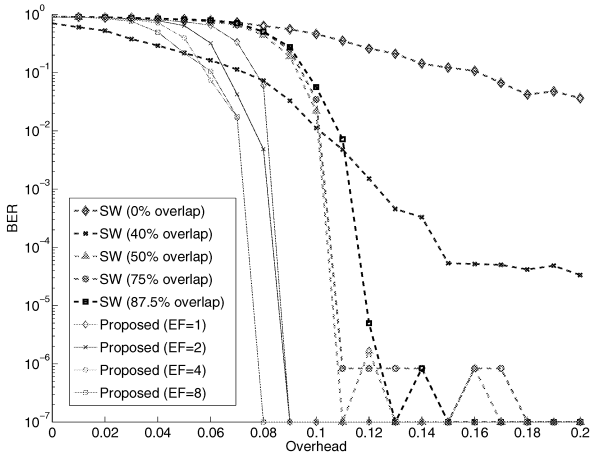

Fig. 5. Comparison between our approach and the sliding window method (SW) of [10] when the number of information symbols is $k = 20,000$. For the SW method, the window size is $w = 2,000$.

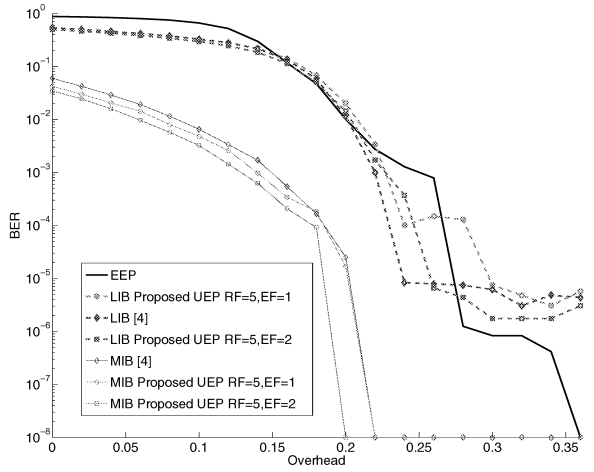

Fig. 6. BER vs. overhead for our UEP approach, that of [4], and equal error protection (EEP). There are $k = 2,000$ information symbols, 100 of which are in the MIB class.

respectively) were chosen to provide the same relative importance of the MIB with respect to the LIB. The source block consisted of $k = 2,000$ information symbols of which 100 were assigned to the MIB class.

The simulations show that with a proper choice of the parameter EF our technique can outperform that of [4] in terms of BER for both the MIB and the LIB. For example, when $EF = 2$ and $RF = 5$, our technique had a lower BER for the MIB and almost always a lower BER for the LIB. The encoding times of our technique were also lower (Fig. 7). The only penalty was in decoding times (Fig. 8).

VI. Conclusion

We presented a new method for decreasing the bit error rate of LT codes. We also exploited our approach to devise a new UEP technique for LT codes. Compared to the UEP

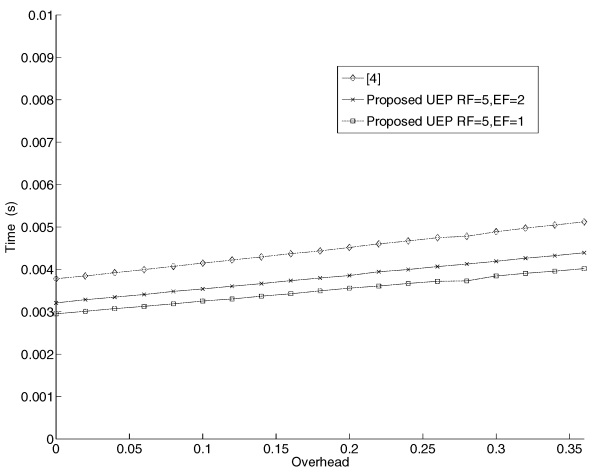

Fig. 7. Encoding times for Fig. 6.

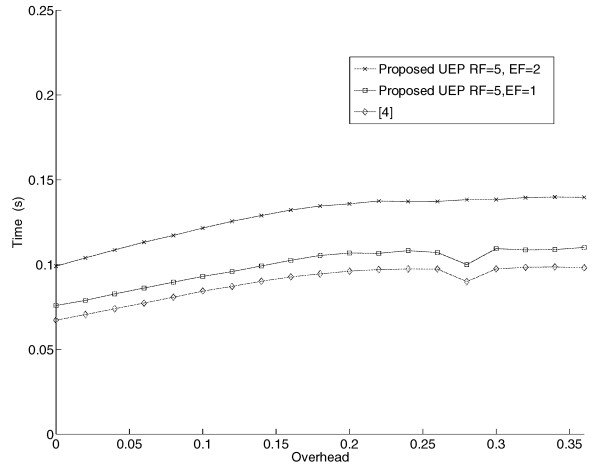

Fig. 8. Decoding times for Fig. 6.

method of [4], our technique provided lower BER for both the MIB symbols and the LIB symbols and lower encoding complexity. However, it had a slightly higher decoder complexity because of a larger average degree of the encoded symbols. It should be mentioned that the experimental work in [4] uses the optimized degree distribution of [3] rather than the robust soliton distribution used in our experiments. An interesting question is whether our UEP method also outperforms the method of [4] when the optimized degree distribution of [3] is used as the underlying degree distribution. Another topic for future research is to compare our UEP method to the UEP technique of [5]. We conclude by mentioning that by concatenating a traditional fixed-rate channel code with our UEP-LT code, we can build a UEP-Raptor code.

VII. Acknowledgement

This work was supported by the DFG Research Training Group GK-1042.

REFERENCES

[1] J.W. Byers, M. Luby, and M. Mitzenmacher, "A digital fountain approach to asynchronous reliable multicast", IEEE Journal on Selected Areas in Communications, vol. 20, pp. 1528–1540, Oct. 2002.

[2] M. Luby, "LT-Codes", Proc. 43rd Annual IEEE Symposium on Foundations of Computer Science, pp. 271–280, 2002.

[3] A. Shokrollahi, "Raptor Codes", IEEE Trans. Inf. Theory, Vol. 52, No. 6, June 2006, pp. 2551–2567.

[4] N. Rahnavard, B. N. Vellambi, and F. Fekri, "Rateless codes with unequal error protection property", IEEE Trans. Inf. Theory, Vol. 53, No. 53, pp. 1521–1532, April 2007.

[5] D. Sejdinovic, D. Vukobratovic, A. Doufexi, V. Senk, and R. Piechocki, "Expanding window fountain codes for unequal error protection", Proc. 41st Asilomar Conf., Pacific Grove, pp. 1020–1024, 2007.

[6] D. Vukobratovic, V. Stanković, D. Sejdinovic, L. Stanković, and Z. Xiong, "Scalable data multicast using expanding window fountain codes", Proc. 45th Allerton Conf., Monticello, Sept. 2007.

[7] R. Hamzaoui, V. Stanković, and Z. Xiong, "Optimized error protection of scalable image bitstreams, IEEE Signal Proc. Mag., vol. 22, pp. 91-107, Nov. 2005.

[8] D. S. Taubman and M. Marcellin, JPEG2000: Image Compression Fundamentals, Standards, and Practice, Norwell, MA: Kluwer, 2001.

[9] B.-J. Kim, Z. Xiong, and W. A. Pearlman, "Low bit-rate scalable video coding with 3-D set partitioning in hierarchical trees (3-D SPIHT)", IEEE Trans. Circuits Syst. Video Technol., vol. 10, pp. 1365-1374, Dec. 2000.

[10] M. Bogino, P. Cataldi, M. Grangetto, E. Magli, and G. Olmo,"Sliding-window digital fountain codes for streaming multimedia contents", IEEE International Symposium on Circuits and Systems (ISCAS), New Orleans, May, 2007.

BIOGRAPHIES

Shakeel Ahmad received the B.Sc. degree in Electrical Engineering from the University of Engineering and Technology, Lahore, Pakistan, in 2000, the M.Sc. degree in Information and Communication System from Hamburg University of Technology (TUHH), Germany, in 2005, and the Dr.-Ing degree from the University of Konstanz, Germany, in 2008. He is currently a Research Assistant at the Department of Computer and Information Science of the University of Konstanz, Germany. His research interests include multimedia communication, error-resilient video streaming and channel coding.

Raouf Hamzaoui received the Maîtrise de mathématiques from the Faculty of Sciences of Tunis, Tunis, Tunisia, in 1986, the M.Sc. degree in mathematics from the University of Montreal, Montreal, QC, Canada, in 1993, the Dr. Rer. Nat. degree from the Faculty of Applied Sciences, University of Freiburg, Freiburg, Germany, in 1997, and the Habilitation degree in computer science from the University of Konstanz, Konstanz, Germany, in 2004. He is currently a Professor of Media Technology in the School of Engineering and Technology at De Montfort University, Leicester, U.K. His research interests include image and video compression, multimedia communications, error control systems, and algorithms.

Marwan M. Al-Akaidi (M96-SM03) joined the Department of Electronic Engineering at De Montfort University in 1991. In November 2000 he became professor of Communication & Signal Processing. His main research interest is in the field of Digital Signal Processing & Digital Communications. This includes Speech Coding, Processing, Recognition, and Wireless and Mobile communication. In September 1999, Professor Marwan Al-Akaidi was appointed Chairman for the IEEE UKRI Signal Processing Society and in March 2000 as the IEEE UKRI Conferences chair. In December 2000 he was also appointed to join the board of IEEE Industrial Relations. He has won the award of the IEEE UKRI in recognition of outstanding leadership as a chapter chair for the years 2001 and 2002.

VIRTUAL ENVIRONMENTS

ACCELERATING LEAN PRACTICE TRAINING USING VIRTUAL REALITY

Riham Khalil
Nathan Wright
David Stockton
Centre for Manufacturing
De Montfort University
Leicester
United Kingdom

Cliff Gillis
Perkins Engines Company Limited
Peterborough
PE1 5NA
United Kingdom

KEYWORDS
Virtual reality, Discret Event Simualtion, Lean Maunfacturing, Manufactruing Simulation, Flow lines.

ABSTRACT

Over the last decade the competitive environment of manufacturing enterprises has changed considerably (Stalk and Hout, 1992). An initial emphasis on *quality* became the baseline from which to compete since high levels of quality quickly became taken for granted by customers. The focus of competitive attention then became those of reducing delivery lead time and improving delivery reliability (Bernard. 2004). In more recent years the provision of increasing levels of product choice and continuous reductions in costs have been added to the competitive mix. There is now increasing pressure on suppliers to provide higher levels of cost, quality and delivery performance in addition to ensuring the availability of a wider choice of products.

An essential methodology, increasingly being adopted by manufacturing organisations, that is capable of assisting manufacturing organisations in fulfilling these competitive demands is that of lean production which has been shown to provide (Monden 1983, Womack, Jones and Roos 1990, Smeds 1990, Yusuf 2002) significant advantages in the critical areas of shortening lead times, improving delivery reliability, reducing costs, improving quality, and widening product mixes.

Studies have shown that organisations making use of lean production techniques tend to have significant performance advantages over conventionally organised plants (Smeds 1990, Schonberger 1992, Chappell 2002). There is also research that has reported the limitations of the lean philosophy, most notably Burgelman, (1983), who argues that environmental and social conditions have not been taken fully into consideration in explaining the use of lean production in Japan's competitive advantage. However, it is generally accepted that lean manufacturing practices have the ability to provide improvements in the majority of those areas considered critical to the competitiveness of an organisation.

The paper will discuss a collaborative R&D project which will accelerate the adoption and use of lean practices within a wide range of industrial and service sectors. A Virtual Discrete Event Process Simulation (V-DEPS) tool will be developed capable of providing a learning, training and decision support environment for lean practitioners from complete novices to experienced lean champions. Novel virtual process modelling, discrete event simulation, advanced visualisation and adaptive optimisation tools will be developed that enable self-organisation of improvement teams, and provide assistance with identifying & prioritising problems, creative problem solving & autonomous decision-making and lean solution optimisation & implementation.

LEAN IMPLEMENTATION PROCESS

Manufacturing systems have been considered as a collection of sub-systems. These sub-systems form an integrated whole in which each sub-system possesses its own function and characteristics. This represents the 'systems approach' to the design of manufacturing systems where, according to Yeomans (1992), the complete system *"has more properties than the sum of the properties of its parts"*. Adopting this approach enables a complex manufacturing system to be designed by breaking it down into simpler sub-systems each of which are then individually designed.

Although this approach is said to enable individual system elements to be designed that satisfy a company's operational requirements (Hopp and Spearman 2000) individual system elements cannot be considered in isolation because of the inter-relationships that exist between them, i.e. a change in one element may have a significant effect on other elements and lead to reductions in overall system performance.

LEAN PRACTICE AND DISCRETE EVENT SIMULATION

The basic process steps involved in the implementation of lean production (Womack, Jones and Roos 1990, (Haque and Moore 2004) are:

(a) **listening to the voice of the customer** in order to ensure the precise definition of customer's needs and the successful conversion of these needs into operational activities,

(b) **mapping the value stream,** i.e. identifying the sequence of added-value activities that are required to convert raw materials to finished goods,

(c) i**mplementing flow processing** through the sequential layout of processing equipment according to the needs of the product and the balancing of work loads at workstations along the flow line,

(d) i**mplementing pull material control** which ensures that the production system is synchronised to customer demands, i.e. produces only what the customer wants when it is wanted. A major barrier to the implementation of pull systems is a lack of regularity in the flow of materials through the manufacturing system (Karmarkar, 1992),

(e) s**eeking perfection through continuous improvement** the main focus of which is to remove or reduce the sources of variability that prevent smooth material flow through the flow processing line (Imai 1986).

According to the literature review Discrete Event Simulation has played an important role in designing the flow processing systems. Methods involving discrete event simulation, using software packages such as Witness (1991), ProModel (1993), Simfactory (1990), GoldSim (1990), Arena (2002), Modsim (2001), EM-plant/Simple++ (2004), Taylor II (2002 -2003), Taylor ED (2001), and Modular Manufacturing Simulation (1996), (Shannon, 1998) overcome the limitations of queueing theory. Simulation is now often seen as the only effective means of evaluating the complex dynamic interactions that occur between manufacturing system elements. Although realistic models can be developed, the creation of a simulation model is often difficult and time-consuming. Successful use of simulation also depends on the user expertise to correctly interpreting the results of a simulation run to make system design improvements. Intelligent simulation systems have been proposed that overcome this need for user expertise, i.e.: Shannon et. al. (1985) linked expert systems with simulation for solving manufacturing problems, Wang and Bell (1991) developed a knowledge-based modelling system for designing flexible manufacturing systems, and Stockton and Finch (2000) developed automatic systems for designing flexible manpower lines by linking a commercial simulation system with genetic algorithm based optimisation routines.

CURRENT RESEARCH

As stated earlier the objective of this collaborative R&D project is to accelerate the adoption and use of lean practices within a wide range of industrial and service sectors i.e. lean practices aim to: (a) eliminate overproduction, thereby reducing waste and the use of energy and raw materials, (b) reduce excess inventory hence reducing energy use associated with transport, warehousing and reorganisation of unsold inventory, (c) less in-process and post-process inventory needed which avoids potential waste from damaged, spoiled, or deteriorated products, (d) reduce floor space needed for operations and storage hence potential decrease in energy use and less need to construct new facilities or purchase additional processing equipment, (e) reduce defects from processing and product changeovers hence reducing energy and resource needs and avoiding waste, (f) reduced contamination of products results in fewer product defects which reduces energy and resource needs, (g) lean eliminates waste at the product and process design stage and is, therefore, similar to "Design for Environment" methods, (h) a continuous improvement culture focuses on uncovering and eliminating hidden wastes and waste-generating activities , (i) less unneeded consumption of materials and chemicals when equipment, parts, and materials are organized and easy to find, (j) improving product durability and reliability.

At present traditional virtual process designs focus on modelling processing functionality whereas lean improvement characteristics within V-DEPS would need to include the ability to make changes for example to process set-up activities, a workplace's equipment and materials layout arrangements, and the layout of the processing facilities within a work system. In addition, performance metrics would need to be provided by which initial and changed states could be compared. Hence, discrete event simulation functionality needs to be provided to a greater range of modelling elements and at higher levels of operational detail. The development of the V-DEPS modelling capability will be achieved by identifying a comprehensive list of lean practices through literature search and industrial surveys, undertaking a gap analysis, ie comparing this list with current capabilities of V-DEPS systems, and developing V-DEPS modelling functionality to fill the gaps identified.

Figure 1 will illustrate the cycle of events occurring within the project methodology phases will include;

a) Development of an Advanced Visualization capability which is responsive to user needs and enables users to physically interact with V-DEPS models and understand the complexity of their behaviours. The research will seize the discrete event simulation ability to store large amounts of data with respect to the complex dynamic operational behaviours of work systems before and after improvement changes have been made. In addition, at the end of each simulation run data concerning the operational efficiency of the work system is stored. Methods will be developed for displaying this data in a manner that enables more experienced lean practitioners to determine the true benefits of their changes/decisions in a simulated real time environment. Also of importance will be to ensure the presentation and visualisation of high-level management information. Standard advanced visualization hardware, based on the Virtalis StereoWorks system, will be employed with the project work focusing on identifying the information needs for presentation to users and developing methods by which this can take place.

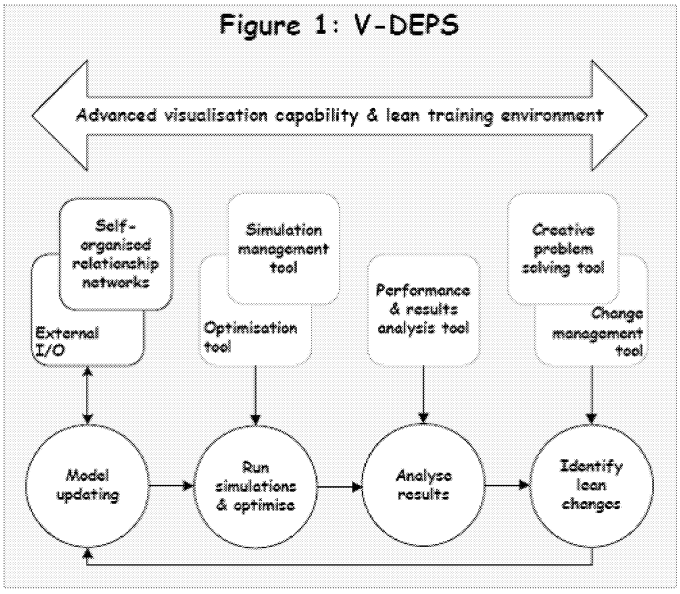

Figure 1: Advanced Visualisation & Lean Training Environment

b) Development of Self-Organising Relationship Matrices - in order to represent the complexity of relationships within a V-DEPS model it will be necessary to identify the various types of interactions that take place between the various types of modelling elements. These interactions will include those between physical modelling elements, (e.g. processing equipment and inventory queues), those between the rules used to control the sequence of activities that take place, (eg priority rules for selecting jobs to progress), and those associated with cultural/change management aspects.

c) Development of a Creative Problem Solving (CPS) tool capable of leading improvement teams through the CPS process from the initial selection of improvement team members based on ensuring that appropriate Continuous Improvement (CI) and Team Leadership skills are available within a team to the final selection of the best solution to adopt. Here it will be important to understand what modelling functionality is required to support the creative problem solving process particularly when multi-skilled teams are required. Principles from industrial psychology underpinning team working change management and motivation will play an important role. The basic processes involved in lean problem solving are well known. Hence, this task will involve automating these processes and making them available along with appropriate data and simulation results through the visualisation environment such that team-based autonomous decision making can be enabled.

d) Development of a Lean Training environment aimed at improving both the CI skills of lean practitioners and the process and operations skills of those required to implement and operate the lean improvements. Standard training scenarios will be developed for the main lean enabling methods. These scenarios will provide visual cues to lead new learners through individual lean change processes. Learners will be expected to undertake, using the V-DEPS environment, data collection tasks, data analysis tasks, generation of alternative solutions, selection of best solution and solution implementation tasks. Since the V-DEPS tools will be able to model an organisation's actual work environment then lean training environments can be specifically developed for these. Through use of the 'lean/change management skills and training requirements' relationship matrix the automatic identification of skills gaps will be possible and hence the self-organisation of training requirements.

SUMMARY

The project supplies competitive advantage to industrial & service sectors, including health care, aerospace & construction, where the 'institutionalised' implementation of lean is essential but highly problematic due to their organisational cultures and complexity of their high variety/low volume work environments. The work will involve the development and integration of virtual engineering & discrete event simulation (DES) software with existing advanced visualisation hardware. Using these tools, work systems can be modelled with a high level of process detail and with DES providing the ability to simulate the effects of model changes at process and system levels. Applying a 'complex systems' approach will enable the components of such systems to be organised into self-organising networks with DES identifying the interactions between networks. Accordingly , the project will introduce a novel Visual Lean Training application that will be able to overcome barriers that face industrial and serve sectors which include:

*a) **Market Barriers*** exist due to a lack of market familiarity with the use of V-DEPS based methods, i.e. there is no known 'lean support' application existing .

b) Technological Barriers exist due to a lack of expertise in applying V-DEPS within the 'lean support' domain, the variety of V-DEPS software components that will need to be employed and the complexity involved in integrating such components.

c) Prevailing Practice Barriers exist, i.e. current 'lean training and support' practices, although far limited in scope when compared with the use of V-DEPS, are straighter forward to understand and apply.

d) Investment Barriers exist, ie for the project to reach a critical mass a considerable fixed amount of cost & time resources are required to bring to fruition a prototype system.

Acknowledgements

The research reported here has been funded by the Technology Strategy Board Ref: K1532G

REFERENCES

ARDON-FINICH, J. (2000) "*Evolving Design & Control Strategies for Production Systems, PhD*. Thesis, De Montfort Universiyt, Leicester, UK.

HAGUE, B. AND MOORE, M.J. (2004), Measures of performance for lean production in the aerospace industry, *Proceedings of the Institution of Mechanical Engineers – Part B Engineering Manufacture*, Vol. 218 (10), pp. 1387-1398.

HOPP, J.W. AND SPEARMAN, M.L. (2000), *Factory Physics: Foundations of Manufacturing Management*, Irwin, Chicago.

IMAI, M., (1986) *Kaizen, the key to Japan's Competitive Success*", McGraw-Hill, New York and London.

KARMARKAR, U. AND NAMBIMADOM, R., (1992). Material allocation in MRP with tardiness penalties. In: *Working Paper QM 91-06*, William E. Simon School of Business, University of Rochester, Rochester, NY.

MONDEN, Y., (1983), *Toyota Production Systems*. , Industrial Engineering & Management Press, Norcross, GA.

SHANNON, R.E, (1988), "Knowledge based simulation technique for Manufacturing", *International Journal of Production Research*, Vol. 26, No 5 pp. 953-973.

STALK, H. JR, HOUT, T.M. (1990), *Competing Against Time, How Time-based Competition Is Reshaping Global Markets*, Free Press, New York, NY.

SMEDS, R. (1990), *Computerization and Strategy-structural Development in an Industrial Organization*, Licentiate's thesis, Helsinki University of Technology, Industrial Economics and Industrial Psychology.

WANG, W., BELL, R.(1991) "An intelligent user interface in a knowledge-based modelling system for the design of flexible manufacturing facilities", International Journal of computer Integrated Manufacturing, Vol.4, No6, pp. 364-374

WOMACK, J., JONES, D., ROOS, D. (1990), *The Machine that Changed the World*, Macmillan, Rawson Associates, New York, NY, .

YEOMANS, S., (1992), *Optimal level schedules for mixed-model just-in-time assembly systems*. , McMaster University, Hamilton, Ontario.

YUSUF , Y.Y, ADELEYE, E.O., (2002), "*Acompartive study of lean and agile manufacturing with a related survey of current practices in the UK*", International Journal of Production Research, Vol. 40 Issue 17, pp. 4545-4562.

Modelling Multi-Agent Communication Protocols in Virtual Environment to Direct Numerical Analysis

G. Al-Hudhud
Software Engineering Department.
Al-Ahliya Amman University
email: ghudhoud@ammanu.edu.jo

KEYWORDS
Modelling and Visualisation, Social Interaction, Virtual Robots, Flocking Robots

ABSTRACT

This paper presents an advanced implementation of a virtual environment base to develop and test communication protocols for multi-agent systems. The virtual environment provides as 3d simulation tools that allow for more realistic simulations. Embedding human capability into the control system software, the work considers the application of a multiple robots communication system. The currently used full-scale virtual environment is used to evaluate robotic applications; simulating and testing the hardware whilst producing single-robot applications but not to test the communication between multiple robots. The full scale virtual environment is shown to be efficient as it allows users to greater understand the robots' behaviours and increases the efficiency of the evaluation process. The visual assessment outputs using a semi-immersive full-scale environment also has been advantageous in directing numerical analysis.

INTRODUCTION

Visualisation and simulation tools within virtual environments have been used in many different areas including architectural design, urban planning (Tecchia et al. 2003), traffic control simulation (Wan and Tang 2004), and visualising construction processes as a teaching tool in civil engineering (Sampaio et al. 2004). Full-scale virtual environments have also been used in evaluating possible robotic feature applications; e.g. simulating and testing as yet unbuilt hardware. This paper defines a novel use of a 3D full scale semi-immersive environment for experimentation of different communication and co-operation algorithms between multiple robots has not yet been fully covered.
The major anticipation of using a full-scale virtual environment in simulating a multi-agents communication model is to speed up the development process cycle of testing and evaluating models before real world implementation. In addition, a second aim of using a virtual environment is that it improves the feeling of realistic spaces and gives a clearer insight into understanding the interactions within the real robotic systems. An interest of this work is the advantage that the visual assessments directs fruitfully quantitative analysis for system performance.
The rest of this paper is organised as follows. Section 2 discusses related work of the current implementations and its applications within virtual environments. Section 3 presents a description of the communication protocols that are being implemented and evaluated within the virtual environment. Section 4 discusses the simulation requirements, whilst section 5 displays the visual assessment outputs for the models and gives examples of these being used to direct numerical analysis.

VE Applications: Related Previous Work

Virtual environments have been useful in different research areas. For instance, real time semi-immersive simulations are useful in controlling the movements of mobile physical robots, and assessing the individual robotic behaviour (Navarro-Serment et al. 2002). Leevers *et al* in (Leevers et al. 1998) provided a working model of autonomous environmental sensors for telepresence allowing a robot to tour the inside of a building and automatically creating a 3-D map of the interior space. Rohrmeier (Rohrmeier 1997) presents virtual reality aiding handling the connection between the hardware and the software of the robots.
For the purposes of simulating a multi-agent communication model as a multiple-robots communication application, it is essential to consider all dimensions of the simulated world. To successfully simulate such systems require real time visualisation, a high level of geometrical realism in representing the world and the moving objects, and realistic support for the interaction aspects of the application. For example, in order for a set of agents, representing a set of autonomous mobile robots, to build their knowledge system they need to correctly perceive the environment. Therefore, specifying a sensing device and techniques is essential and can not be completely achieved by implementing 2D simulations
Major anticipations of using 3D-simulations are:

- 3D full-scale simulations can support realism in representing the simulated world in order to sense the depth, all dimensions, and other spaces, these are referred to as *geometrical realism.*
- 3D simulations can support the specifics of the simulations for example accurately simulating the *sensors.*

- 3D simulation allows the user and all the robots to interact with the simulated world at realistic rates, referred to as *behavioural presence*.
- 3D simulations must allow for real time visualisation of a large number of simultaneous agents.

A Multi-Agents Communication Model

The behaviour of a multiagent system can be defined by how its agents interact. In a multi-agent model, each agent does not only need to be able to do the tasks that arise locally, but also needs to interact effectively with other agents.
An important part of the interaction between agents takes the form of communication. A good interaction implies efficient communications among agents, and therefore often implies good performance. A protocol is the specification of these interactions/communications. This section discusses the theory of the communication protocol viewed as a two level structured model:

- The micro structure this relates to the specifications of the internal structure of an agent. The micro level part is designed to describe the specifications of an agent's knowledge.
- The macro structure relates to the design and construction of the agents' society that includes the specification of knowledge-based interaction techniques and rules.

The Micro Structure of the System

The capabilities of an intelligent agent is always limited by its knowledge, and available computing resources. In order for an agent to understand the outside world and to interact with it, an agent has a knowledge representational system (*KRS*) is required (Ferber 2002), (Tirassa 1997).
This knowledge can be described as the preconditions of actions. For example, an agent believes that an obstacle exists in the way and it decides to turn right in order to avoid this obstacle. This agent's belief, or knowledge, was *encountered an obstacle* and the agent's intention, is to avoid the obstacle. The next action, was *turn right* to avoid it. The agent's belief and intention are the preconditions of the action 'turn right'.
The set of beliefs and intentions for an agent constitutes its mental state. At point in time, a mental state comprises of a set of cognitive units. Intentions are referred to as provisional cognitive units whilst beliefs are referred to as factual cognitive units. Representing these cognitive units and interpreting them using a set of words or temporal strings defines the *KRS*, see figure 1.
When two opposite intentions are present at the same time which require an agent to act in a joint and opposed manner, the agent arbitrates as to which states it will respond. Thus, an agent ignores some of its *KRS* components such as beliefs-desires-intentions.
Unlike the current agents' cognitive models, in our model an agent's mental state results from the interaction between its

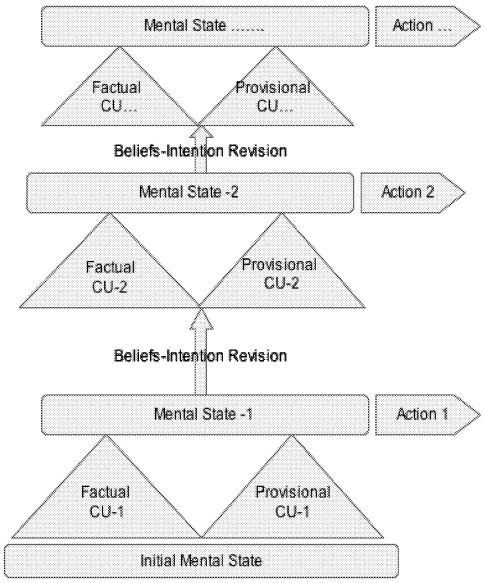

Figure 1: The agent's knowledge representational system

cognitive units , in other words each elementary cognitive unit is linked to others' cognitive units to form a dynamic mental configuration that changes with time. This implies that any provisional cognitive unit can be created or can disappear as a consequence of the creation or disappearance of other factual cognitive unit(s) in the *KRS*. For example, when an agent encounters an obstacle, a factual cognitive unit that represents part of the agent's overall mental state requires the agent to avoid this obstacle. But as soon as this agent avoids the obstacle, this belief is no longer true. As a consequence of changes in the environment (e.g. disappearance of this obstacle), an agent has to revise its beliefs on the basis of any new information it receives, together with the knowledge it already possesses. This belief revision leads to a dynamic mental configuration as a result of cognitive dynamics in the light of changes in the environment. Accordingly, an agent's cognitive dynamics must be tightly coupled to the changes in the environment, this implies that they depend on the adaptive interaction between its cognitive system and the surrounding (mental, physical, and social) environment.

The Macro Structure of the System

In order to develop a framework for a communication system, within a co-operative multi-agent system, the primary requirements of the model is to define the social relations between agents by identifying two levels of communication ; local and global.
In this work, the theory of communication is built on exploiting: a) an animal intelligence technique in order to co-ordinate movements of a group of objects as the local communication level, and b) a cognitive intelligence technique to co-ordinate actions in order to avoid goal conflicts as a global communication level.
The movement co-ordination exploits a flocking algorithm

to mimic the motion of a large group of animals (Al-Hudhud et al. 2004). This technique requires each agent to be both a member of a group and have a sensory inputs. Grouping the agents into teams reduces communication overheads whilst the sensors provide the agents with real information, about the local surroundings.
The action co-ordination concept exploits a blackboard negotiation technique that is communication is considered as a negotiation by passing messages from the user to agents for task allocation, and from agents to the user in order to report status and findings. All tasks are distributed within a hierarchal order via a user (Al-Hudhud et al. 2005).

Simulation Requirements

In order to implement the above model, it is essential that we choose visual simulation tools that supports the specifics of the application as well as creating the required realism in representing the simulated world. For instance, the above model requires a sensing device and sensing strategy for the purposes of building an agent's local knowledge (Al-Hudhud et al. 2005). A realistic representation of the agents and the environment is also required to implement the communication model. This is specifically useful to improve the feeling of depth, dimensions and sizes. Therefore, the proposed communication model has to be simulated within a 3D immersive environment. Accordingly, the agents' movements and interaction inside the virtual world are projected on a big screen using a full-scale environment in order to increase the level of realistic results enabling the user to test various scenarios.

Evaluating the System Performance in light of visual Assessment

This section displays how the visual assessment outputs of the model can direct the numerical analysis for evaluation purposes. Therefore, a series of experiments was designed to visually monitor and test the suitability of the model. These experiments resulted in addressing a set of problems in the system performance. In addition, these experiments helped in identifying other vital changes needed to boost the system performance. The visual outputs also highlighted interesting ideas to be investigated numerically. For example, on arrival, testing the ability to increase the covered area by a set of agents has visually revealed that this is subject to the condition that an agents opt to communicate locally. The problems and the highlighted issues by the visual assessments are described in the following subsystems.

Overcrowding

Overcrowding was first noticed through the visual assessment process during the design stage. It was extremely useful to spot this problem at a very early stage. According to this experiment, the user was able to specify the situations where overcrowding takes place and the impact of overcrowding on agents' progress by analysing the visual observations. Hence, the user was able to identify the reasons as overcrowding indicates the dominance of the cohesive force in the absence of any collision detections. This implies the necessity of controlling the Local Interaction between agents. Hence the next step was to modify and adjust the interaction weights to help accelerating the agents' progress.
The weights associated with the interaction rules are dynamically computed at each time interval τ depending on the rule's centroid and on the attitudes of each rule; these are the perception zone for this rule and are used to filter the inputs to each rule. According to most of the current implementations of the flocking rules, the collision avoidance weight is given precedence over other weights, as it is the most important interaction rule. Therefore, the visual tests involved the influence of the cohesion weight ($w_{A_i}^{R\beta}$) on the progress of the agents. The visual simulation has been useful at this stage in assessing and evaluating the extent to which varying the cohesion weight allows the agents in the same team to move as a unit but at the same time to make an acceptable progress with time limitations.
Visually, the experiment resulted in addressing a strong influence of the cohesion force, as a binding force, on the agents behaviour in the form of overcrowding in the surrounding area. Therefore, overcrowding is used as an indicator for examining the strength of this binding force. In addition, the visual assessment revealed another situation where an agent detects a large number of nearby agents, then each of these agents modifies its velocity to move towards the cohesion centroid. If one or more of these agents detects a wall and at the same time some of the other agents within the avoidance zone, it may become trapped. In this trap situation, a neighbour of this agent (who may not detect the same objects) will be influenced by the trapped agent. In the same manner, the remaining agents will be influenced by the trapped agents as a result of a high cohesion weight. This can become worse if this set of agents is assigned a task to reach a specified target. Considering this scenario, the trapped agent continuously checks its capabilities of performing this task using the mechanism described in (Al-Hudhud et al. 2005). According to this mechanism, the trapped agent may discard his commitment regarding completing the task. The other agents who detect the trapped agent will strongly be influenced by the trapped agent which can still significantly slow their progress. This leads to a longer expected completion time, or even prevents the influenced agents from completing the task.

Table 1: The values of set of interaction weights

Alignment $w_{A_i}^{R\alpha}$		Cohesion $w_{A_i}^{R\beta}$		Collision Avoidance $w_{A_i}^{R\gamma}$	
$C_{A_i}^{R\alpha} < S_d$	$C_{A_i}^{R\alpha} > S_d$	$C_{A_i}^{R\beta} < S_d$	$C_{A_i}^{R\beta} > S_d$	$C_{A_i}^{R\gamma} < S_d$	$C_{A_i}^{R\gamma} > S_d$
$1/C_{A_i}^{R\alpha}$	1	$1/C_{A_i}^{R\beta}$	1	1	1

In this respect, a main goal of analysing the interaction weights, numerically, then is to adjust the cohesion weight in

order to avoid these impacts of a high cohesion weights without loosing the benefits of the supportive role of this weight in the team performance. Therefore, the start point was to test the conventional implementation of the weights in flocking algorithms, and the values are shown in table 1, for the alignment $w_{A_i}^{R\alpha}$ and cohesion weight $w_{A_i}^{R\beta}$. For this implementation, the cohesion weight is computed as the inverse of the distance to the cohesion centroid ($C_{A_i}^{R\beta}$) if the $C_{A_i}^{R\beta}$ falls within the avoidance range, otherwise it set equal to one. This implies that the cohesion force is mostly inversely proportional to the distance to the centroid. The weight becomes bigger very quickly as the centroid position falls outside the avoidance range (S_d) whilst it does not become very small within the avoidance range.

In order to numerically assess the dominance of the cohesion weight in situations where the agents does not detect any avoidance cases, only the local communication level was used. Accordingly, these interaction weights are shown in figure 2. The bar graph shows the weights that control the strength of the interaction forces, according to the values shown in table 1, on an agent over the first 200 frames of the simulation. Points of high cohesion weight, in figure 2, implies that an agent will be highly influenced by the nearby agents, and via monitoring the trap problem can be observed.

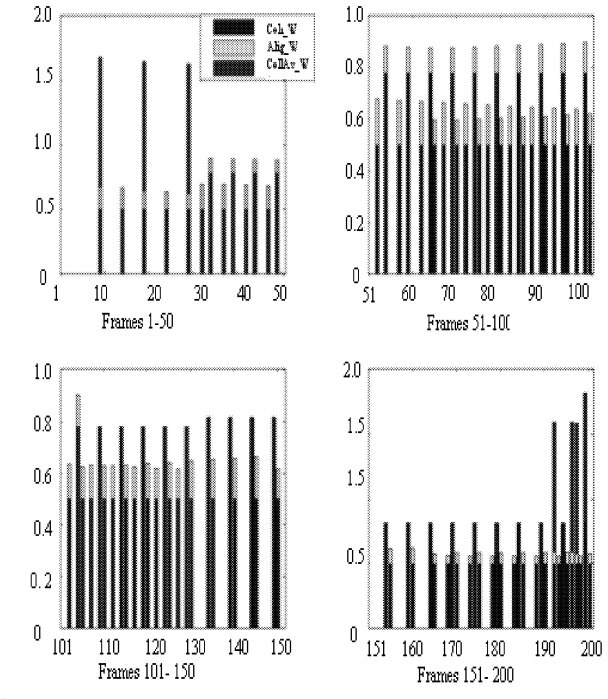

Figure 2: The interaction weights over the first 200 frames. The cohesion weight dominates the interaction weights whenever the avoidance weight is zero. The unmodified cohesion weight values are shown in table 1.

To overcome both the overcrowding and the trap problems,

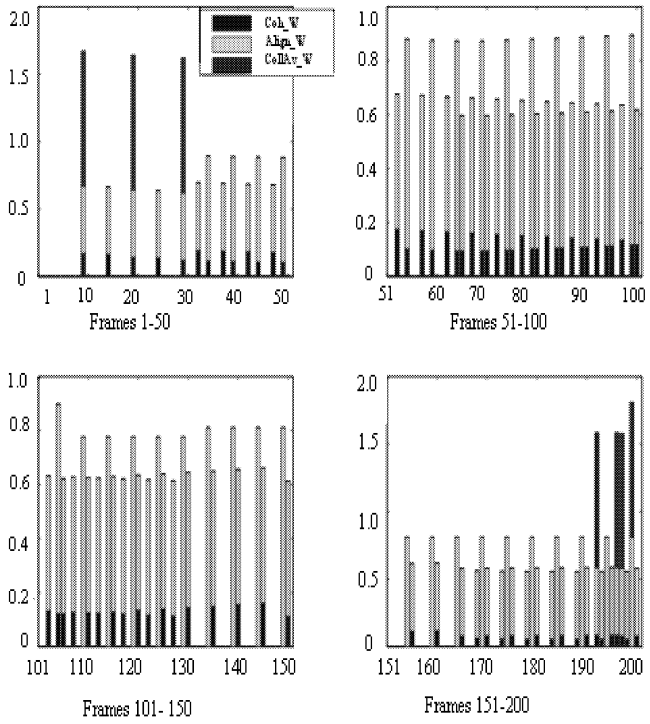

Figure 3: The interaction weights over the first 200 frames, with the cohesion weight modified according to the values shown in (table 2).

Table 2: The interaction weights, modified.

Alignment $w_{A_i}^{R\alpha}$		Cohesion $w_{A_i}^{R\beta}$		Collision Avoidance $w_{A_i}^{R\gamma}$	
$C_{A_i}^{R\alpha} < S_d$	$C_{A_i}^{R\alpha} > S_d$	$C_{A_i}^{R\beta} < S_d$	$C_{A_i}^{R\beta} > S_d$	$C_{A_i}^{R\gamma} < S_d$	$C_{A_i}^{R\gamma} > S_d$
$1/C_{A_i}^{R\alpha}$	1	$1/(C_{A_i}^{R\beta})^2$	$1/C_{A_i}^{R\beta}$	1	1

$w_{A_i}^{R\beta}$ is modified in the following manner. Within the cohesion range, $w_{A_i}^{R\beta}$ is inversely proportional to the square of the distance to $C_{A_i}^{R\beta}$ otherwise it is inversely proportional to the distance to $C_{A_i}^{R\beta}$ elsewhere as in table 2. Figure 3 shows the effect of modifying the way the cohesion weight is computed in reducing the influence of the cohesion force as well as in maintaining the essence of team performance. This can reduce the expected completion time when assigning a task to these agents.

In order to to examine the efficiency of the modified weight of the cohesion rule, we switched on the global communication channel in order to record the completion time of a specified task for both cases. The completion time (in frames) is used here as an indicator of the slowness or firmness of agents' progress.

In a comparison between the effect of the cohesion weight on the system performance using the values shown in tables 1 and 2, the results are shown in table **??** which shows the time

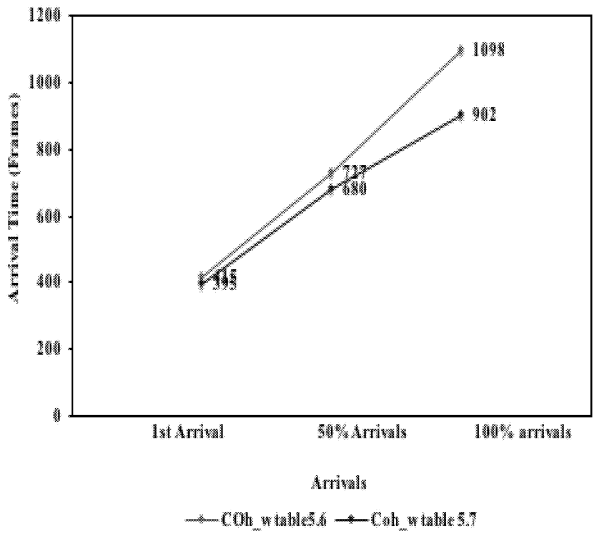

Figure 4: The completion time versus number of arrivals for a set of 20 agents, which shows the effect of reducing the cohesion weight, table **??**

elapsed until the first, 50%, and 100% arrivals, see figure 4. These values are the average values over five trials and all have a small standard deviation ($Dev <= 4$).

Although, reducing the impact of the cohesion weight leads to minimizing the completion time, it also demonstrates a non-uniformness in the arrival rate for the set of agents. Investigating the uniform rate of arrivals is dealt with in detail in section using the teaming technique.

Maximising the Coverage Area

In order to explore the influence of the flocking rules on the overall emergent behaviour, another experiment was carried out by viewing two aspects. These aspects are: the positions of the agents during movements and the area these agents cover after arriving at a specified target. These two issues can be especially useful when the agents are to perform a search or sweeping task, where there is an aim to visit many points whilst they are moving in a team. Therefore, this experiment is designed that considered both agents' local and global communications with a set of five agents forming one team. After launching the model, these agents are issued a team command that informs them of the target location. Unlike sending the set of agents towards a specifies location with the flocking system switched off, by monitoring the agents behaviour over time, it was found that the agents tend not to take the same route as they move towards a specified location.

In order to analyse this behaviour, the positions of these agents are recorded and by plotting the positions of the team members over time, it was found that agents within a team select different routes on their way to the target as illustrated

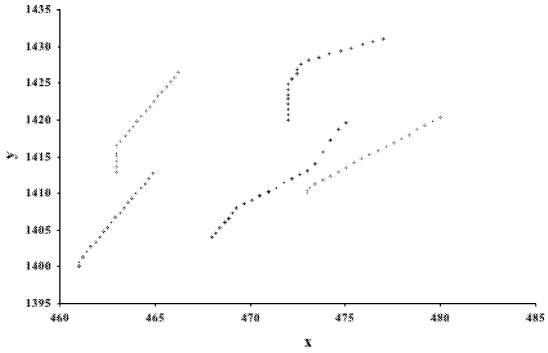

Figure 5: The agents select different route whilst they are moving in a team.

in figure 5. Another advantage of the flocking algorithm

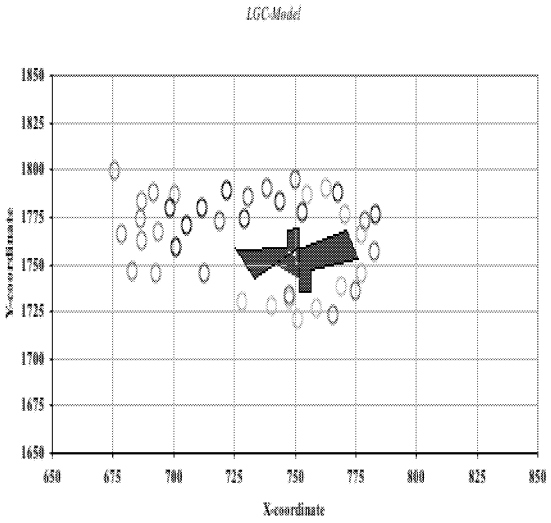

Figure 6: The flocking behaviour supports maximising the coverage area.

is that, on arrival, agents within a team will cover a wider area around the target position. This prevents the agents from overcrowding the target location and they are shown to appear to circle the target. This can be seen in figure 6, showing all the positions of the set of 5 agents over a period of time. These show how those agents swarmed about the location. The region of the covered area is computed as the number of occupied cells in the grid, each cell represents ($25\ cm \times 25\ cm$). This implies that as the number of occupied cells is 17, the agents cover 1.0625 m^2 during the last 6 frames. Comparing these results with those resulting from running the same number of agents by switching the flocking system off in figure 7, the number of occupied cells is 9 *cells* covering only 0.5625 m^2. This indicates that the coverage area by the flocking agents is about double that covered with individual agants.

The effect of the flocking system in the above results can be

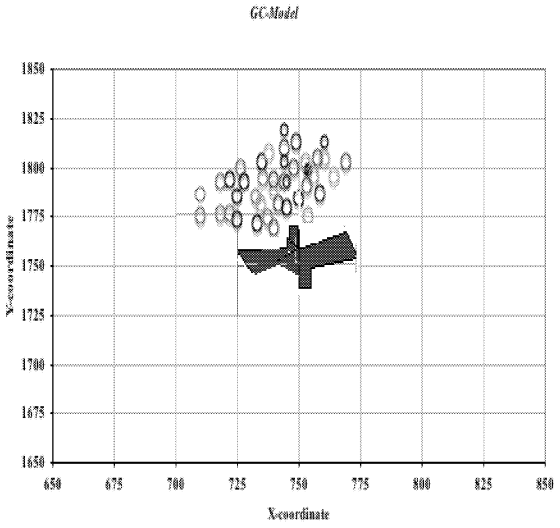

Figure 7: The covered area is less with the flocking system switched off.

explained as follows. By running the system with both communication channels are on, any agent is able to interact locally and globally. This means, all the agents are committed to move within a team to reach the target location, and correspondingly, the team centroid is moving towards the target. On arrival, as the first agent moves forward the team centroid, which affects the cohesive force, also moves forward. Accordingly, the other agents who detect this agent also consider this team centroid in each calculation which implies they are pulling each other forward and at the same time towards the target location. These local interactions lead to the progress of the team centroid which in turn leads to the movement of the detected team members as rolling around the target location.

On the other hand, by running the the system with the global communication channel only, the agents intend to reach the target and only check for collisions. Therefore, these agents, on arrival, are either trying to avoid each other or looking towards the target which leads to a reduced possibility of covering a larger area.

The question now is to what extent this flocking behaviour is required to gain system performance. This implies considering the inputs to the flocking system and the weights that controls the influence of each rule in the flocking system where the only source of inputs to the flocking system is via the sensor. So the sensor range and direction characterise the perception field within which these rules operate and contribute to the agents emergent behaviour. In addition, the weights corresponding to these rules control the strength of these rules and are also dependent on the sensory data. At this stage the main concern was to find the optimum sensor range that enables the agent to compromise between the local interaction and the global communication demands.

Sensor Range *SR*

As the sensor links an agent to the environment and controls its local interactions via the flocking rules, this section aims at testing the optimum sensor range that allows agents to: a) move and act as a team, and b) minimise the number of frames to complete a specified task. The number of frames indicates the number of steps, and consequently the distance an agent moves in order to reach this target. Completing the task means being within a distance equal to double the sensor range from the specified target. When an agent moves within a team towards a target, this implies that it activates both the local interaction rules together with the global communications. The local interaction rules require an agent to filter the sensory data according to the minimum separation distance allowed between those agents. Therefore, the separation distance S_d is also considered when adjusting the sensor range as it controls the influence of the local interactions.

By monitoring the and theoretically describing the emergent behaviour, the minimum number of frames required for an agent to reach a target is when it detects no objects during its path to the target. This can be done by setting the sensor range to zero which implies switching off the flocking system. Consequently, the number of frames times the step length an agent moves each frame exactly equals the direct distance to the target. However, the fastest route implies that agents move as a set of individuals rather than as team members. This also implies that agents do not interact locally with the surroundings in the environment; they do not align, cohere, or avoid colliding with other objects. On the other hand, using a large sensor range implies increasing the influence of the flocking system. This in turn increases the number of interactions as each agent moves towards the nearest agent to align with, as well as towards the team centroid to keep itself bound to the team. This implies that the number of frames or movements, towards the target increases and accordingly, an agent takes a slower route towards the target.

The effect of the minimum distance allowed between objects in the environment, that is the separation distances S_d, is also considered in the experiment. The visual tests have shown that with S_d less than $7 units$ [1] an agent is happy to slightly bump into things, as this distance is less than the agent's dimensions (radius, width). In reality, the separation distance must allow for an object to turn safely without hitting the detected object. In contrast, increasing the S_d increases the time for an agent to complete the task. This is partially because with a large separation distance an agent may not be able to go through the space between two closely detected objects or squeeze tightly round a corner.

For this, an experiment is designed to run the the system with both channels on with 20 agents. The user interactively chooses a start point to issue the team task command by giving the position of the specified target location. The agents are to move in a team to reach this target location. Within

[1] A unit is used with respect to the environment dimensions, in other words, if the dimensions of the environment is 1700 $units$ $\times$ 800 $units$ the separation distance is 7 $units$

the experiment, the number of frames to complete the task is recorded as well as the number of arrivals.
The experiment recorded the number of frames as a function of sensor range over four rounds. In each round, a single sensor range is tested with four values for the separation distance. For example, the first round tests four combinations using a sensor range of 70 *units*. These combinations are: $(SR = 70, S_d = 7)$, $(SR = 70, S_d = 10)$, $(SR = 70, S_d = 15)$, $(SR = 70, S_d = 20)$. For each combination, five trials were performed. Table 3 shows the averages of the outputs after running the system using a different S_d for each sensor range.
Figure 8 shows that the number of frames to complete the

Table 3: Completion time in terms of the sensor range using different S_d values for 20 agents.

Sensor Range	Completion Time (Frames)			
(Units)	$Sd = 7$	$Sd = 10$	$Sd = 15$	$Sd = 20$
70	11248	12259	13319	14450
60	9698	10782	11898	12950
50	7215	8421	9450	10512
40	5446	6581	7680	8760

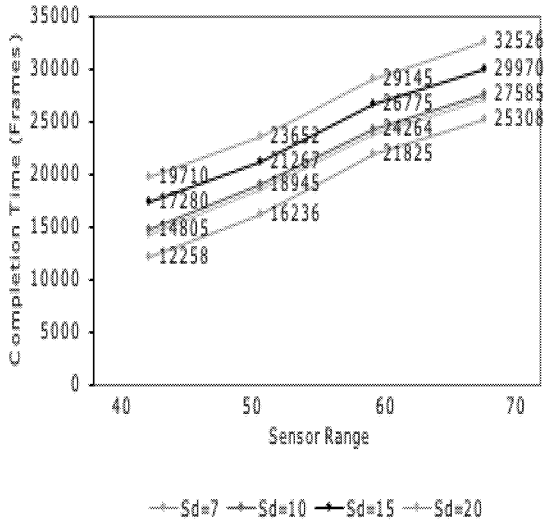

Figure 8: Number of frames as a function of sensor range.

specified task increases as the sensor range increases. The increase in the number of frames, is an indicator of the increase in the distance, and implies that an agent was highly influenced by the flocking rules which prevents the agent, to a certain degree from taking a direct route towards the target, see figure see figures 9. Increasing the sensor range results in an increase of the perception zones for the flocking system; i.e. an agent may see more agents, and therefore, the number of interactions increases, see figure 10. This implies more steps towards the target represented by more number of frames, see figure 11. To summarise, choosing a lower value for the sensor range leads to reducing the influence of

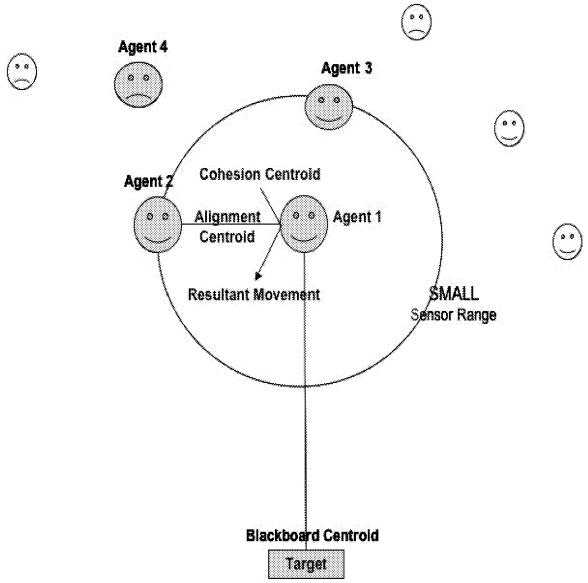

Figure 9: The smaller sensor range reduces the influence of the flocking system.

the flocking system. This in turn yields many individualists rather than team and group performance, each lives his own life for itself and does not try to co-operate with or follow others. Nevertheless, it is essential to maintain the influence of the flocking system by setting the sensor range that helps keep the essence of the group co-operation in the form of the team movements.

Grouping Technique

The nonuniform rate of arrival was one of the main visual outputs during the early design stages, which indicates the importance of adjusting and testing the population size; or follow a teaming technique. The efficiency of the grouping technique by specifying various sizes of the teams to support uniform rate of arrivals. A ratio (ρ) has been defined as the the ratio of team size to the number of teams.

$$\rho = \frac{Team\ Size}{No.\ of\ Teams} \tag{1}$$

The experiment is designed as follows:

- Specify the number of agents for the task.
- Compute the possible combinations of team size and number of teams for this population size.
- Run the model for each value of ρ, over multiple trials.
- For each trial, the completion time; i.e. for 100%, of arrivals is recorded.

From the graphs, figure 12 , one can see that the arrival time for the 50%, and 100% arrivals, as a number of frames, decreases as the number of teams increases. This is due to the fact that with a lower number of members in a team an agent

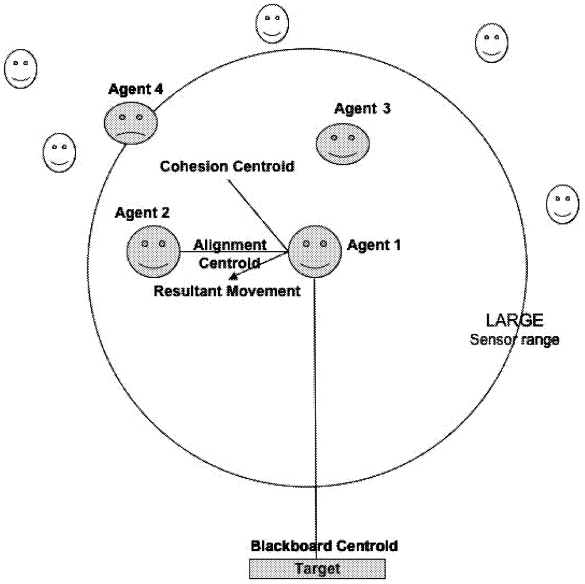

Figure 10: A larger sensor range increases the influence of the flocking system.

Table 4: The effect of varying ρ on the arrival rate.

Ratio	Completion Time in Frames (100%Arrivals)
0.0208	2040
0.0833	2150
0.1875	2260
0.3333	2400
0.75	2660
1.3333	2900
3	3080
5.3333	3170
12	3200
48	3200

needs to communicate and detect fewer social interactions. As the team size reaches one, the arrival time for the 100% agents is a minimum because the agents become individuals with no local interactions except avoidance. This can lead to the agents arriving almost at the same time which results in overcrowding with respect to time at the target position. In other words, the smaller team sizes result in a reduced arrival time for the 50% of agents. The plots show that the curve is negatively skewed as the ratio exceeds one which implies more clustering on arrival as they arrive almost in the same time. On the other hand, a long arrival time for 50% of agents, represents a big team size, and implies that the first arrival may remain for long time waiting for the rest of the team to arrive at the target position. The plot that satisfies a normally shaped distribution that is most likely zero skewed was at $\rho = 0.7500$. This implies 8 teams with 6 agents per team. Agents in this situation can be considered to be self-coordinated. This implies that teaming technique works with reasonable combination of team size and number of teams to

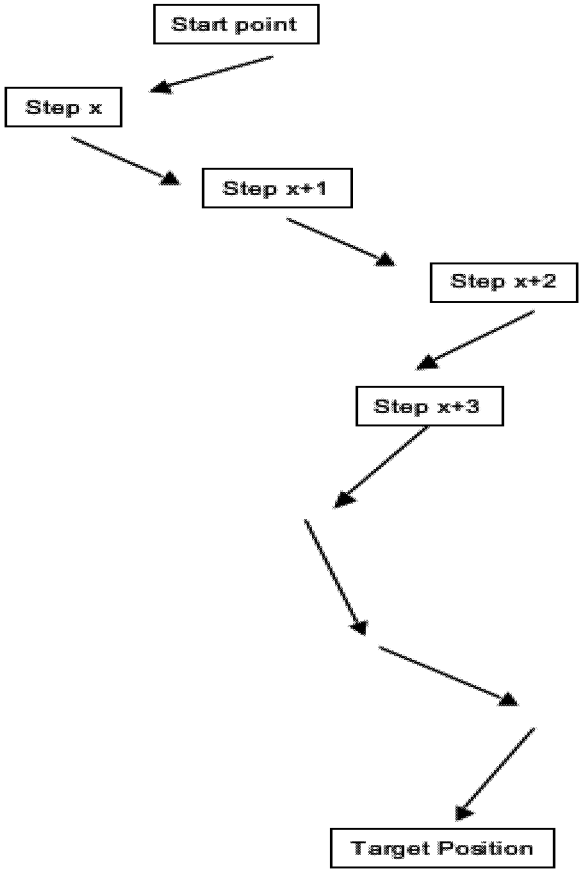

Figure 11: The number of movements towards the target increase as a result of a higher influence of the flocking system.

lead to either a fast arrival or a reasonable arrival time for the whole team, or a uniformity in that arrival rate.

Conclusion

This paper presented the advantages of implementing theoretical communication models within 3D visual simulation tools. First, it speeds up the evaluation of a model through all its design stages as it provides a platform to visualise and interact with agents in real time. Additionally, the improved level of realism helps in testing different emergent behaviours from the different communication level. The system performance ensures that the implemented algorithm within the simulation is feasibly transferable to real robots. This allows agents in a group to interact and produce believable behaviours both locally and globally. The use of the virtual environment allows the user to assess and evaluate the behaviour during any of the simulation stages and modify the algorithm. The visual assessment outputs has been fruitfully used to direct the numerical analysis. This numerical analysis has shown that the proposed system can be used as a toolkit to test different 'What If' situations. In addition, the results have shown that the real time simulation supports both the visual and numerical results minimising testing time for actual physical robots.

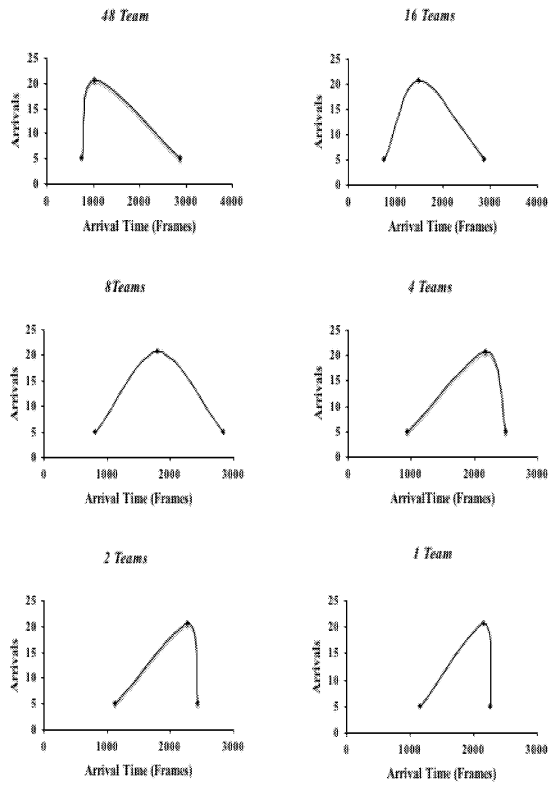

Figure 12: The uniformity of arrivals with respect to different ratios.

REFERENCES

Al-Hudhud G.; Ayesh A.; Istance H.; and Turner M., 2004. *Agents Negotiation & Communication within a Real Time Cooperative Multi-Agent System.* In *Proceedings of the 5th International Conference on Recent Advances in Soft Computing*. Nottingham Trent University, Nottingham, United Kingdom, 611–617. ISBN 1-84233-110-8.

Al-Hudhud G.; Ayesh A.; Turner M.; and Istance H., 2005. *Simulation and Visualisation of a Scalable Real Time Multiple Robot System.* In *Proceedings of the conference of Theory and Practice of Computer Graphics, TP.CG05*. Eurographics Association, University of Kent, Canterbury UK. ISBN 3-905673-56-8-70295-4.

Ferber J., 2002. *Multi-Agent System and Distributed Artificial Intelligence*. Addison-Wesley.

Leevers D.; Gil P.; Lopes F.; Pereira J.; Castro J.; Gomes-Mota J.; Ribeiro M.; Gonalves J.G.; Sequeira V.; Wolfart E.; Dupourque V.; Santos V.; Butterfield S.; and Hogg. D., 1998. *An Autonomous Sensor for 3D Reconstruction.* In *3rd European Conference on Multimedia Applications, Services and Techniques (ECMAST98)*. Berlin, Germany.

Navarro-Serment L.; Grabowski R.; Paredis C.; and Khosla P., 2002. *Millibots. IEEE Robotics & Automation Magazine*.

Rohrmeier M., 1997. *Telemanipulation of Robots via Internet Mittels VRML2.0 and Java*. Institute for Robotics and System Dynamic, Technical University of Munchen.

Sampaio A.Z.; Henriques P.; and Ferrieira P., 2004. *A Virtual Environment Tool Applied to Visualise Construction Processes*. In *Conference Proceedings of Theory and Practice of Computer Graphics*. IEEE.

Tecchia F.; Loscos C.; Conroy R.; and Chrysanthou Y., 2003. *Agent Behaviour Simulator (ABS): A Platform for Urban Behaviour Development.* In *Conference Proceedings of Theory and Practice of Computer Graphics*. IEEE.

Tirassa M., 1997. *Mental states in communication.* In *Proceedings of the 2nd European Conference on Cognitive Science*. Manchester, UK.

Wan T. and Tang W., 2004. *Agent-based Real time Traffice Control Simulation for Urban Environment. IEEE Transactions on Intelligent Transportation Systems*.

URBAN DYNAMICS MODELLING USING ANT NEST BUILDING

Rawan Ghnemat[(1)], Cyrille Bertelle[(1)], Gérard H.E. Duchamp[(2)]

[(1)]LITIS - University of Le Havre, 25 rue Philippe Lebon, BP 540, 76058 Le Havre Cedex, France
email: rawan.ghnemat@litislab.eu, cyrille.bertelle@litislab.eu

[(2)]LIPN - University of Paris XIII, 99 avenue Jean-Baptiste Clément, 93430 Villetaneuse, France
email: ghed@lipn.univ-paris13.fr

KEYWORDS
swarm intelligence, complex systems, self-organization, ant systems, spatial organization

ABSTRACT

Urban dynamics deal with spatial organizations where a great complexity of interactions appears. Social and economic aspects interact and environmental objectives are nowadays a major purpose for sustainable urban development. We propose some generic modelling processes able to face with this complexity, in order to simulate the evolution of the city centers. These organizational centers need a multi-criteria description for their evolution, including feed-back phenomena of them over their environment and components. We propose a swarm intelligence algorithm, using social-insect collective behavior. We combine a decentralized approach, based on emergent clustering mixed with spatial constraints or attractions, as an extension of the ant nest building algorithm with multi-center. Typically, this model is currently used by ourself, to model and analyze cultural equipment dynamics in urban area.

INTRODUCTION

Many natural and artificial systems have emergent properties based on spatial development. This spatial development is both the result of some mecanisms from the system behavior and the actor of the system formation by morphogenetic feedback. Natural ecosystems or social organizations in urban dynamics are typically such emergent spatial organizations. The goal of this paper is to study some computable mecanisms and algorithms able to model such spatial self-organization processes, taking into account the complexity of the phenomena.

In the next section, complex system concepts are defined and their applications to urban dynamics understanding are described, then swarm intelligence algorithms are described as methodologies to implement the complex systems concepts, using distributed computations. The following section proposes some specific swarm intelligence methods based on ant systems in order to model the spatial organizations emergence. Experiments are given, using RePast muti-agent platform mixed with a geographical information system.

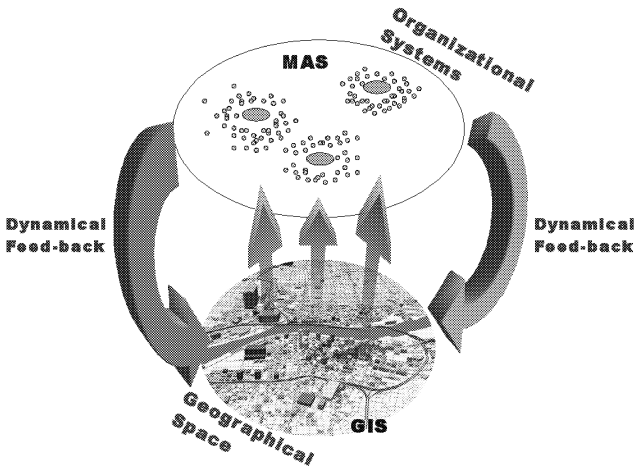

Figure 1: Spatial organizations Complexity Description and the Conceptual Generic Model Based on Swarm Intelligence

MODELLING SPATIAL COMPLEXITY

Complex System Concepts

Complex system theory (7) is based on the fact that for many applicative domains, we can find similar processes linking emergent global behavior and interaction network of constituents. The global behavior is generally not accessible using classical analytical methods.

In classical analytical methods, the global behavior of the system is the description of the equations. Simulations from these formulations, consist in obtaining the trajectories of the behavior predefined in the equation

formulation.

In complex systems modelling, we have to model the constituents of the system and the interaction network or system which link these constiuents, using a decentralized approach. So the global behavior of the system cannot be understood by the description of each constituent. In complex system modelling, the global behavior is an emergent property from the interaction network or systems between its constituents and lead to the creation of an dynamical organization of these constituents

This dynamical and emergent organization retro-acts on its own components. Two kinds of feedback allow to describe these phenomenon. The positive feedback means that the emergence increases the organization constitution. the negative feedback means that the emergence has regulator properties which finally stop the increasing organization constitution and allow the system stabilization.

Another major aspect of complex systems is that they can be considered as open systems. This means that they are crossed by energetical fluxes that make them evolve in a continuous way. From these energetical fluxes, complex systems can evolve through critical states, using bifurcation schema and attractors behaviors. One of the major vector or support of these energetical fluxes is the environment itself where the complex systems and their entities evolve. In many natural and artificial systems, the environement has some spatial effects which interact on the whole complexity of the phenomenon. This spatial environment can be modified by the system but he can also be the catalyst of its own evolution. Understanding and modelling the deep structural effect of the interaction between the systems and its spatial environment is the goal of the study presented in the sequel.

Application to urban dynamics

Social and human developments are typical complex systems. Urban development and dynamics are the perfect illustration of systems where spatial emergence, self-organization and structural interaction between the system and its components occur. In figure 1, we concentrate on the emergence of organizational systems from geographical systems. The continuous dynamic development of the organization feed-back on the geographical system which contains the organization components and their environment. The lower part of this figure explains our analysis methodology. It consists to describe many applicatives problems by dynamical graphs or environments in order to detect organizations over these dynamical environment. For the organization detection, we use swarm intelligence processes. We model the feed-back process of this emergent organization on the system constituents and its environment. To analyse or simulate urban dynamics, nowadays, we can use the great amount of geographical databases directly available for computational treatment within Geographical Information Systems. On the organizational level description, the new development of multiagent systems (MAS) allows nowadays to develop suitable models and efficient simulations.

The applications we focuss on in the models that we will propose in the following concerns specifically the multi-center (or multi-organizational) phenomona inside urban development. As an artificial ecosystems, the city development has to deal with many challenges, specifically for sustainable development, mixing economical, social and environmental aspects. The decentralized methodology proposed in the following allows to deal with multi-criteria problems, leading to propose a decision making assistance, based on simulation analysis.

Cultural dynamics processes in urban can be modelled using such methodology. It is typically a multi-criteria self-organization processes where appears emergent usage oo urban equipment. A modelling of these dynamics is presented latter in this paper.

Swarm Intelligence and Spatial Environment

Decentralized algorithms have been implemented for many years for various purposes. In this algorithm category, multi-agent systems can be considered as generic methods (11). We deal, in this paper, with agents based on reactive architecture and expected to be used inside numerous entity-based systems. The aim of programs using such architectures, is to deal with emergent organizations using specific algorithms called emergent computing algorithms. Swarm Intelligence is the terminology used to point out such reactive agent-based methods where each entity is built with the same basis of behavior, but reacts in autonoumous way.

Based on swarm intelligence concepts, Ant systems (3) propose some bio-inspired method from social insects mecanisms. For exemple, Ant Colony Optimization (ACO) methods is a such method family where the basic entities are virtual ants which cooperate to find the solution of graph-based problems, like network routing problems, for example. Using indirect communications, based on pheromon deposites over the environment (here a graph), the virtual ants react in elementary way by a probabilistic choice of path weighted with two coefficients, one comes from the problem heuristic and the other represent the pheromon rate deposit by all

the ants until now. The feed-back process of the whole system over the entities is modelled by the pheromon action on the ants themselves.

Particule Swarm Optimization (PSO) is a metaheuristic method initially proposed by J. Kennedy and R. Ebenhart (6) which is also based on swarm intelligence concepts. This method is initialized with a virtual particle set which can move over the space of solutions corresponding to a specific optimization problem. The method can be considered as an extension of a bird flocking model, like the BOIDS simulation from C.W. Reynolds (9). In PSO algorithm, each virtual particle moves according to its current velocity, its best previous position and the best position obtained from the particles of its neighborhood. The feed-back process of the whole system over the entities is modelled by the storage of this two best positions as the result of communications between the system entities.

Other swarm optimization methods have been developped like Artificial Immune Systems (4) which is based on the metaphor of immune system as a collective intelligence process. F. Schweitzer proposes also a generic method based on distributed agents, using approaches of statistical many-particle physics (10).

The method proposed in this paper is based on Ant systems, allowing to deal with self-organization processes emerging from spatial constraints and attractive areas.

MULTI-CENTER ANT NEST BUILDING TO MODEL EMERGENT SPATIAL ORGANIZATIONS

We will describe in this section, the general algorithm which is proposed to model emergent spatial organizations. This algorithm is based on the ant clustering. We introduce pheromon template to spatially control the clustering from local attraction. This method is a decentralized approach which allows to combinate multi-center and multi-criteria problem and we will show how we can apply it to model cultural dynamics in urban areas.

Ant clustering

Ant clustering algorithms are inspired by the corposes or larvea classification and aggregation that the ants colony are able to do in the real life. The ants are moving inside a closed area and are able to move some material which are randomly put on this area. After a while, and without any kind of centralized coordonation, the ants success to create some material clusters.

The algorithm is based on the following and very simple behavioral rules that each ant implements :

- When an ant is moving without carrying yet material and find some material, the ant will take the material respecting the probability number :

$$P_p = \left(\frac{k_1}{k_1 + f}\right)^2 \quad (1)$$

  where f is the material density that the ant perceives locally around itself and k_1 is the treshold. It is easy to check that if $f << k_1$ then P_p is near the value 1 and if $f >> k_1$ then P_p is near the value 0.

- When an ant is moving when carrying some material, the probability to deposite it is computed by :

$$P_d = \left(\frac{f}{k_2 + f}\right)^2 \quad (2)$$

  where f is still the material density that the ant perceives locally around itself and k_2 is another treshold. It is easy to check that if $f << k_2$ then P_d is near the value 0 and if $f >> k_2$ then P_d is near the value 1.

Spatial constraints using template

The ant clustering shows some spatial self-organizations but has the specificity to generate clusters at random places. According to the first random moves that the ants start to do in the beginning of the algorithm, some material will initiate aggregation and the clustering processus will complete this aggregation from these initial random first aggregations. To simulate some urban dynamics, we need to introduce specific location with respect to city center for example or cultural equipments. The clustering here will represent the people usage of these centers or equipments and we need to introduce an attractive effect by using a pheromon template. This method follow the algorithm known as Ant Nest Building (3). In ant colonies, the center corresponds to the position of the queen which needs to build the nest and the ant colony moves around it to protect the nest by various material taken on the ground. The queen emits a pheromon which allows to attract the ants during their building. The ant has to deposite the material carried only if the pheromon quantity perceived belongs to a specific range. We use an attractive fonction called P_t, corresponding to a pheromon template and represented by the part (a) of the figure 2.

Using this template function, we remplace in the clustering algorithm, the two provious probabilities defined in equation (1) and equation (2) by

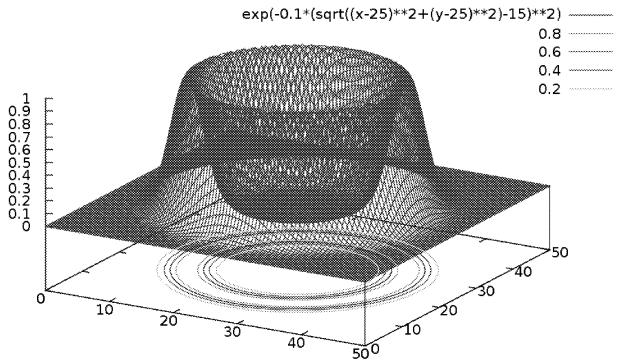

(a) Template function

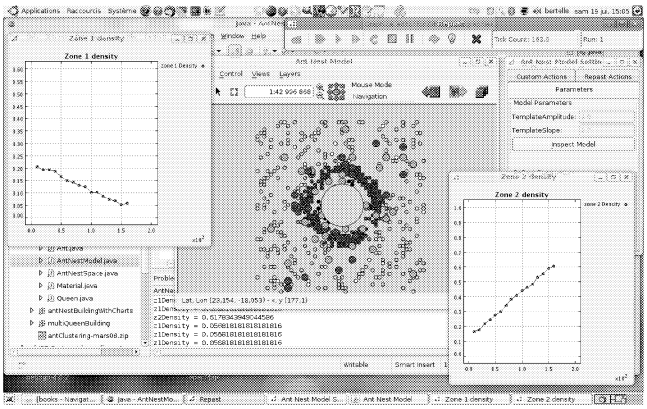

(b) Simulation on RePast

Figure 2: Ant nest building with one center using RePast MAS paltform over OpenMap GIS

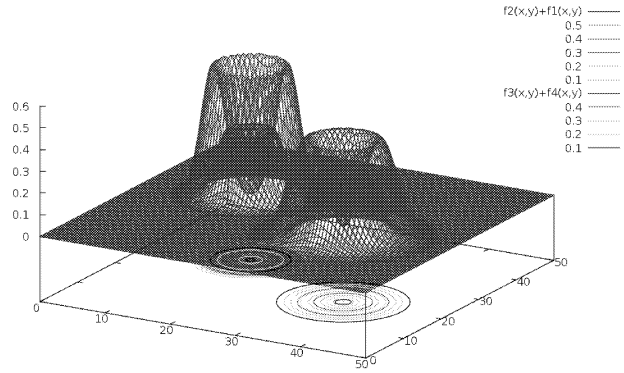

(a) Template functions

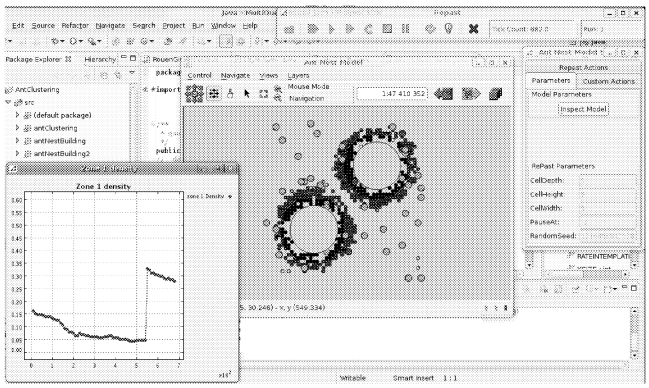

(b) Simulation on RePast

Figure 3: Multi-center ant nest buiding using RePast over OpenMap

$$P'_p = P_p(1 - P_t) \tag{3}$$

$$P'_d = P_d P_t \tag{4}$$

In figure 2, we show an implementation of this algorithm using the multi-agent platform called Repast (8). The java version of this platform includes some packages allowing to interface with geographical database and geographical information systems (GIS). The graphical output windows is made under OpenMap which is a GIS developped in Java. In figure, the materials moved by the ants are the small grey circles, the ant moving without material are the green circles, the ant carrying material are the red circles and the queen location is the yellow circle.

Multi-template modelling

The previous subsection describes one local attractive process characterized by the queen and its pheromon template emission. The advantage of this method is to be able to combine the solutions of multi-center and multi-criteria problems, using interactive processes, each one is represented by a queen and its pheromon template.

On the figure (3), we can see a simulation with two queens and two pheromon templates. It is possible also for each queen to emit many different kinds of pheromons : we called them colored pheromons. Each colored pheromon will attract only the ants associated to its color.

Application to cultural equipment dynamics

The multi-template modelling can be used to model cultural equipment dynamics as described in the figure (4). On this figure, we associate to each cultural center (cinema, theatre, ...) a queen. Each queen will emit many pheromon templates, each template is associated to a specific criterium (according to age, sex, ...). Initially, we put the material in the residential place. Each material has some characteristics, corresponding to the people living in this residential area. The simulation shows the self-organization processus as the result of the set

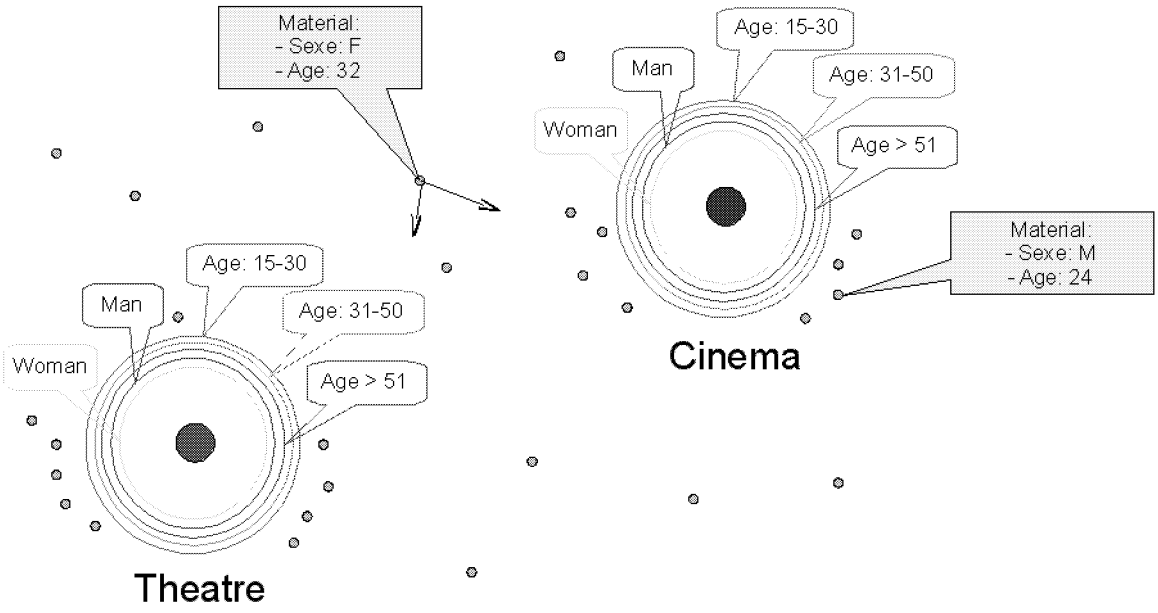

Figure 4: Cultural Equipment Dynamics Modelling

of the attractive effect of all the center and all the templates.

Conclusion and Perspectives

The paper develops some specific swarm intelligence algorithms based on ant colonies processes. Using such decentralized methods, we can model complex multi-center and multi-criteria self-organizations. Urban dynamics are one of the most relevent problems where these approaches can be efficient. These studies are supported by a french regional project (Haute-Normandie) dealing with the study of cultural dynamics over urban area.

REFERENCES

[1] Benenson, I., Torrens, P.M. (2004) *Geosimulation - Automata-based modeling of urban phenomena*, Wiley.

[2] C. Bertelle, G.H.E. Duchamp, H. Kadri-Dahmani (eds), *Complex Systems and Self-Organization Modelling*, "Understanding Complex Systems" series, Springer, 2008 (in press).

[3] Bonabeau, E., Dorigo, M., Theraulaz, G. (1999) *Swam Intelligence, from natural to artificial systems*, a volume in the Santa Fe Institute Studies in the Sciences of Complexity, Oxford University Press.

[4] De Castro, L.N., Timmis, J. (2002) *Artificial immune system: a new computational approach*, Springer-Verlag, London, U.K.

[5] Ghnemat, R., Bertelle, C., Duchamp, G.H.E. (2007) *Adaptive Automata Community Detection and Clustering, a generic methodology*, in *Proceedings of World Congress on Engineering 2007, International Conference of Computational Intelligence and Intelligent Systems*, pp 25-30, London, U.K., 2-4th July 2007.

[6] Kennedy, J., Eberhart, R.C. (1995) *Particle Swarm Optimization* In *Proceedings of IEEE International Conference on Neural Networks (Perth, Australia)*, IEEE Service Center, Piscataway, NJ, 5(3), pp 1942-1948.

[7] Le Moigne, J.-L. (1999) *La modélisation des systèmes complexes*, Dunod.

[8] Repast web site (2008) `http://repast.sourceforge.net`.

[9] Reynolds, C.W. (1987) *Flocks, Herds and Schools: a distributed behavioral model* In *Computer Graphics*, 21(4) (SIGGRAPH'87 Conference Proceedings), pp 25-34.

[10] Schweitzer, F. (2003) *Brownian Agents and Active Particles*, Springer.

[11] Weiss, G. (ed.) (1999) *Multiagent Systems*, MIT Press.

[12] Xiao, N. (2005) *Geographic optimization using evolutionary algorithms* In *8th International Conference on GeoComputation*, University of Michigan, USA.

LATE PAPER

Computing of the Volterra Kernels of a Nonlinear System Using Impulse Response Data

Vitaliy D. Pavlenko, Mohannad Massri, Vladimir Ilyin

Institute of Computer systems
Odessa National Polytechnical University
1 Shevchenko Avenue, Odessa 65044, Ukraine
pavlenko_vitalij@mail.ru, mohannad_massri@hotmail.com, vladimir_ilyin@mail.ru

Abstract

A method of identification of nonlinear dynamic systems, based on the models constructed as Volterra series with the use of pulse test signals, is proposed. To separate the response into partial components, the method based on differentiation of the target output signal with respect to the parameter – amplitude is applied. The errors of the identification method are analyzed. By the example of modeling a system with nonlinear feedback, the dependences of identification errors on the test signal amplitude are obtained. To increase the noise stability of the identification method, the smoothing of estimations of the Volterra kernels with the help of the wavelet transforms is used.

1. Introduction

In describing nonlinear dynamic systems and circuits the mathematical models in the form of Volterra integro-power series [1] find their increasing application. However, current applied algorithms of identification of nonlinear systems based on the Volterra series [2] do not yet allow using this mathematical tool to the full. It is caused by a series of reasons, most important of which is the essential influence of errors of measurements on the result of identification [3]. Another problem is that the identification of nonlinear systems as Volterra series includes the separation of the response of the system under study into partial components corresponding to separate terms of the Volterra series with subsequent determination of the multidimensional weight functions (Volterra kernels).

One of the ways of the separation consists in composing linear combinations of the responses to the test signals of various amplitudes [4]. In paper [5] the values of the amplitudes of the test influences and corresponding coefficients were obtained, allowing to minimize the methodical error of the model splitting into partial components, caused by the influence of the Volterra series terms which order is higher than the determined term. In paper [3] the ways of identification based on the methods of regularization of ill-posed problems have been proposed.

In the present work we propose a method of identification of nonlinear systems in the form of the Volterra series, based on the extraction of partial components of the system response with the help of differentiation of the target output signal with respect to the parameter – amplitude. The errors of the identification method are analyzed. By the example of modeling a system with nonlinear feedback, we obtain the dependences of the identification errors on the test signal amplitude. To increase the noise stability of the identification method we apply the smoothing of estimations of the Volterra kernels using of the wavelet transforms [6, 7].

2. On the Use of Volterra Series for Identification of Nonlinear Systems

In the general case the "input-output" relationship for a nonlinear dynamic object can be represented in terms of the Volterra series as

$$y[x(t)] = \sum_{n=1}^{\infty} y_n(t) = \sum_{n=1}^{\infty} \int_0^{\infty} \dots \int w_n(\tau_1, \tau_2, \dots, \tau_n) \prod_{i=1}^{n} x(t-\tau_i) d\tau_i, \quad (1)$$

where $x(t)$ and $y[x(t)]$ are the input and output signals, respectively, $w_n(\tau_1, \tau_2, \dots, \tau_n)$ is the Volterra kernel of the n-th order and $y_n(t)$ stands for the n-th partial component of the object response.

Commonly, the Volterra series are replaced by a polynomial, with only taking several first terms of series (1) into consideration. Then the identification procedure consists in extracting the partial components with subsequent determination of Volterra kernels $w_n(\tau_1, \tau_2, \dots, \tau_n)$.

Expanding function $f_k(x_1, x_2, \dots, x_k)$ into the Taylor series in the vicinity of point $x^0 = (x_1^0, x_2^0, \dots, x_k^0)$, one has:

$$f_k(x_1, x_2, \dots, x_k) = f_k(x_1^0, x_2^0, \dots, x_k^0) + \sum_{l=1}^{n} \left.\frac{\partial f_k}{\partial x_l}\right|_{x^0} \Delta x_l + \\ + \frac{1}{2!} \sum_{l_1=1}^{k} \sum_{l_2=1}^{k} \left.\frac{\partial^2 f_k}{\partial x_{l_1} \partial x_{l_2}}\right|_{x^0} \Delta x_{l_1} \Delta x_{l_2} + \dots \quad , \quad (2)$$

where $\Delta x_l = x_l - x^0$.

We henceforth consider the case $x^0 = 0$ and $f_k(x_1, x_2, \dots, x_k) = 0$, i.e. it is supposed that prior to signal injection the object is at rest (zero initial conditions). Function f_k depends also on parameter t, i.e. $f_k(t, x_1, x_2, \dots, x_k)$, so that expression (2) can be written as

$$F[x_k(\tau), 0 \le \tau \le t] = \sum_{l=1}^{k} w_1(t, \tau_l) \Delta x_l \Delta \tau_l + \\ + \sum_{l_1=1}^{k} \sum_{l_2=1}^{k} w_2(t, \tau_{l_1}, \tau_{l_2}) \Delta x_{l_1} \Delta x_{l_2} \Delta \tau_{l_1} \Delta \tau_{l_2} + \dots \quad , \quad (3)$$

where $\Delta \tau_l = \tau_l - \tau_{l-1} = \Delta \tau, \quad \Delta \tau = \frac{t}{k}$;

$$w_n(t,\tau_{l_1},...,\tau_{l_n}) = \frac{1}{n!(\Delta\tau)^n}\frac{\partial^n f_k}{\partial x_{l_1}...\partial x_{l_n}}\bigg|_{x=0}. \quad (4)$$

In the limit $\Delta\tau \to 0 (k \to \infty)$ Eq.(3) turns into series (1).

2. Estimation of Volterra kernels

We use the method of extracting the partial components with the help of *n*-fold differentiation of the response *y*(*a, t*) with respect to parameter - amplitude *a* and the use of the derivative value at *a*=0 [5].

Injecting an input signal *ax*(*t*) where *a* is the scaling factor (signal amplitude), one has the following response of the nonlinear system:

$$y[a\cdot x(t)] = a\int_0^t w(\tau)\cdot x(t-\tau)d\tau +$$

$$+a^2\int_0^t\int_0^t w_2(\tau_1,\tau_2)\cdot x(t-\tau_1)x(t-\tau_2)d\tau_1 d\tau_2 + \quad (5)$$

$$+a^n\int_0^t ...\int_{n\ time}^t w_n(\tau_1,...,\tau_n)\prod_{r=1}^n x(t-\tau_r)d\tau_r +...$$

To distinguish the partial component of the *n*-th order, differentiate the system response *n* times with respect to the amplitude:

$$\frac{\partial^n y[a\cdot x(t)]}{\partial a^k} = n!\int_0^t ...\int_{n\ time}^t w_n(\tau_1,...,\tau_n)\prod_{r=1}^n x(t-\tau_r)d\tau_r +$$

$$+(n+1)!\cdot a\int_0^t ...\int_{n+1\ time}^t w_{n+1}(\tau_1,...,\tau_{n+1})\prod_{r=1}^{n+1} x(t-\tau_r)d\tau_r +... \quad (6)$$

Taking the value of the derivative at *a*=0, we finally obtain the expression for the partial component:

$$y_n(t) = \int_0^t ...\int_{n\ time}^t w_n(\tau_1,...,\tau_n)\prod_{r=1}^n x(t-\tau_r)d\tau_r = \quad (7)$$

$$= \frac{1}{n!}\frac{\partial^n y[a\cdot x(t)]}{\partial a^n}\bigg|_{a=0}$$

Given the function in the discrete form, the differentiation is performed numerically. The corresponding formulae for the first and second derivatives in finite (equidistant) differences read [6]:

$$y_0' = \frac{1}{2a}(-y_{-1} + y_1),$$

$$y_0' = \frac{1}{12a}(y_{-2} - 8y_{-1} + 8y_1 + y_2),$$

$$y_0'' = \frac{1}{a^2}(y_{-1} - 2y_0 + y_1),$$

$$y_0'' = \frac{1}{12a^2}(-y_{-2} + 16y_{-1} - 30y_0 + 16y_1 - y_2),$$

$$y_0''' = \frac{1}{2a^3}(-y_{-2} + 2y_{-1} - 2y_1 + y_2). \quad (8)$$

where

$$y_0' = y'(0),\ y_0'' = y''(0),\ y_i = y(ia),\ i = -2,-1,0,1,2$$

To find the Volterra kernel of the 2nd order we use the third and fourth formulae in (8). They allow us to find the values of the second derivative in node y_0 using the values of the function in nodes y_{-2}, y_{-1}, y_0, y_1, y_2. Actually, since the zeroth node value (at *a*=0) of the function is equal to zero, for extracting the 2nd order partial component it is necessary to conduct two experiments minimum, injecting signals of the same form and amplitude but of different polarity.

After extracting partial component $y_n(t)$ and applying additional processing one can determine the section of the Volterra kernel of the *n*-th order.For the diagonal section we have [7]:

$$\hat{w}_n(t,t,...,t) = \frac{y_n(t)}{(\Delta\tau)^n}, \quad n = 1,2,..., \quad (9)$$

where $\hat{w}_n(t,t,...,t)$ is the estimation of the the diagonal section of the Volterra kernel of the *n* order and $\Delta\tau$ stands for the test pulse duration.

For the lateral sections of multidimensional Volterra kernels of a nonlinear object we have the following approximate expression:

$$\hat{w}_n(t-t_1,...,t-t_n) = \frac{(-1)^n}{n!(\Delta\tau)^n}\sum_{\delta_{t_1},...\delta_{t_n}=0}^{1}(-1)^{\sum_{i=1}^n \delta_{t_i}} y(t,\delta_{t_1},...,\delta_{t_n}). \quad (10)$$

where $\hat{w}_n(t-t_1,...,t-t_n)$ is the estimation of the lateral section of the Volterra kernel of the *n*-th order, obtained as a result of processing experimental data, $y(t,\delta_{t_1},...,\delta_{t_n})$ is the system reaction measured at instant *t* provided that the injected delta-like pulses are of amplitude *a* and duration $\Delta\tau$ and applied at instants $t_1,..,t_n$, respectively ($\delta_t = 1$ corresponds to an injected pulse at instant *t* while $\delta_t = 0$ means no injected pulse).

3. Simulations

To analyze the identification method, its accuracy and noise stability by computer modeling within the package of applied programs MATLAB we choose an object described by the following nonlinear differential equation:

$$\frac{dy(t)}{dt} + \alpha\cdot y(t) + \beta\cdot y^2(t) = x(t) \quad (11)$$

where α and β are constant coefficients (α=2.64 and β=1.45). For such an object the model in the form of three terms of the Volterra kernel under zero initial conditions reads:

$$y(t) = \int_0^t w_1(\tau_1)x(t-\tau_1)d\tau_1 + \int_0^t\int_0^t w_2(\tau_1,\tau_2)x(t-\tau_1)x(t-\tau_2)d\tau_1 d\tau_2 +$$

$$+\int_0^t\int_0^t\int_0^t w_3(\tau_1,\tau_2,\tau_3)x(t-\tau_1)x(t-\tau_2)x(t-\tau_3)d\tau_1 d\tau_2\tau_3. \quad (12)$$

The three first weight functions $w_n(\tau_1,\tau_2,...,\tau_n)$ for the given object are:

$$w_1(\tau_1)=e^{-\alpha\tau_1},\quad w_2(\tau_1,\tau_2)=\frac{\beta}{\alpha}(e^{-\alpha(\tau_1+\tau_2)}-e^{-\alpha\tau_2}),\quad \tau_1\le\tau_2,$$

$$w_3(\tau_1,\tau_2,\tau_3)=\frac{1}{3}\left(\frac{\beta}{\alpha}\right)^2\cdot(e^{a(\tau_1-\tau_2-\tau_3)}+3e^{-a(\tau_1+\tau_2+\tau_3)}-$$

$$-4e^{-\alpha(\tau_2+\tau_3)}-2e^{-\alpha(\tau_1+\tau_3)}+2e^{-\alpha\tau_3}),\quad \tau_1\le\tau_2\le\tau_3. \tag{13}$$

Setting $\tau_1=\tau_2=\tau_3=t$, we obtain the diagonal sections of the Volterra kernels of the 2nd and 3rd orders:

$$w_2(t,t)=\frac{\beta}{\alpha}(e^{-2\alpha t}-e^{-\alpha t}),$$

$$w_3(t,t,t)=\left(\frac{\beta}{\alpha}\right)^2\cdot(e^{-3at}-2e^{-2\alpha t}+e^{-\alpha t}). \tag{14}$$

In estimating the errors of modeling of the diagonal sections of the Volterra kernels we used the root-mean-square error criterion:

$$\varepsilon=\sqrt{\frac{1}{p}\sum_{t=1}^{p}(w_t-\hat{w}_t)^2} \tag{15}$$

where p is the number of counts in the observation time interval, w_t is the exact value of the Volterra kernel and $\hat{w}_t$ is the value of the Volterra kernel estimation obtained by processing experimental data (system responses) at discrete instants t's.

In reality the target output signal is measured with some error, and one can consider it as a superposition of the target signal itself and white noise (errors of measurements, scaled as 1, 3, and 5% of the maximal value of the response).

Table 1 contains the optimal areas (i.e. minimizing the identification error ε) of signals under identification of the Volterra kernels of the second and third order.

Table 1: Optimal areas of input pulse actions (*S*)

n	Optimal areas of input pulse actions (*S*) at various response measurement errors (*eps*):		
	1 %	3 %	5 %
2	0.70	0.9	1.1
3	1.02	1.30	1.38

Figs. 1,2 show the dependences of the identification error (ε) on the area of the input pulse actions (*S*) in determination of the diagonal sections of the Volterra kernels of the second and third orders, respectively, at different errors of measurements of the response (*eps*).

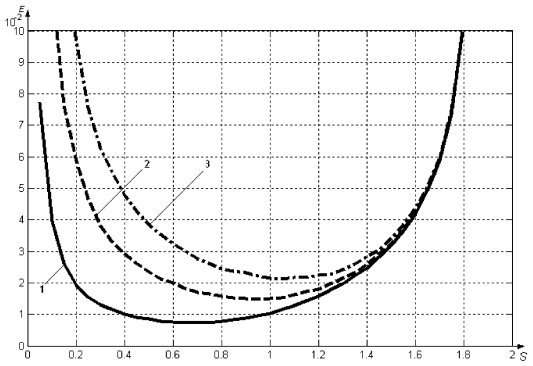

Figure 1: The dependence of the identification error (ε) on the area of the input pulse actions (*S*) in determination of the diagonal sections of the Volterra kernels of the second order. *1,2,3* – 1%, 3%, 5% measurement errors, respectively.

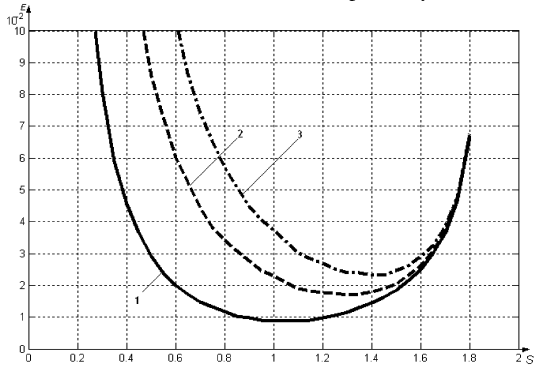

Figure 2: The dependence of the identification error (ε) on the area of the input pulse actions *(S)* in determination of the diagonal sections of the Volterra kernels of the third order. *1,2,3* – 1%, 3%, 5% measurement errors, respectively.

Figs. 3, 4, 5 represent the results of identification of the diagonal section of the Volterra kernels of the second order (*n=2*) at response measurement errors (*eps*) of 1, 3, 5%, respectively, with the areas of the input pulses taken from Table 1. Fig. 6 shows the same for *n=3* and *eps*=1%.

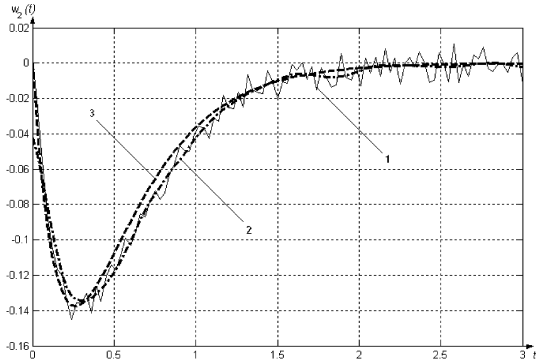

Figure 3: The result of identification of the diagonal sections of the Volterra kernels of the second order. *1* – results of identification, *2* – application of wavelet transforms, *3* – exact value of the Volterra kernel; *eps*=1%.

In Table 2 the identification errors for n=2, 3 are given.

Table 2: Identification errors (ε) for n=2, 3

n	Identification errors (ε) at various measurement errors					
	1 %	3 %	5 %	1 %	3 %	5 %
	without application of wavelet transform			with application of wavelet transform		
2	0.0085	0.0140	0.0219	0.0055	0.0077	0.0094
3	0.0096	0.0174	0.0235	0.0061	0.0096	0.0112

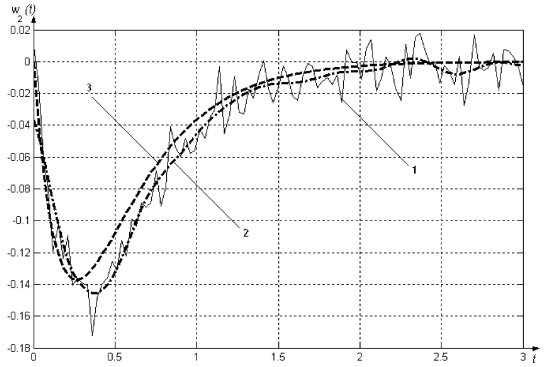

Figure 4: The result of identification of the diagonal sections of the Volterra kernels of the second order. *1* – results of identification, *2* – application of wavelet transforms, *3* – exact value of the Volterra kernel; *eps*=3%.

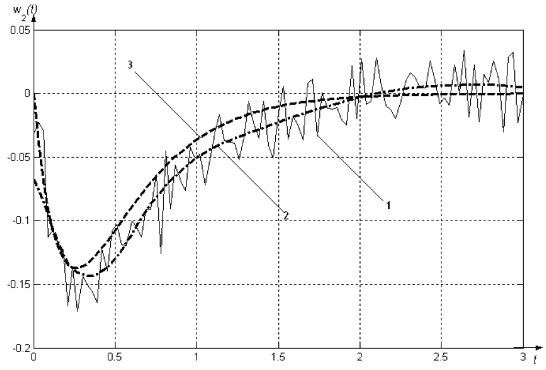

Figure 5: The result of identification of the diagonal sections of the Volterra kernels of the second order. *1* – results of identification, *2* – application of wavelet transforms, *3* – exact value of the Volterra kernel; *eps*=5%.

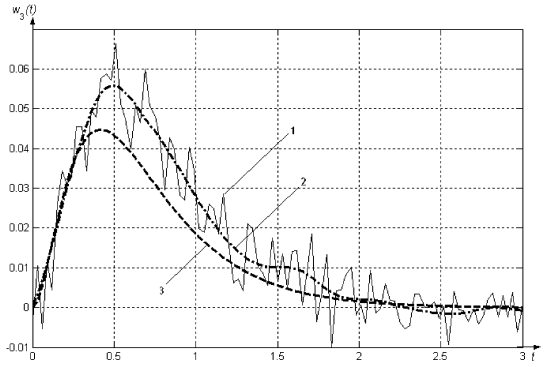

Figure 6: The result of identification of the diagonal sections of the Volterra kernels of the third order. *1* –results of identification, *2* – application of wavelet transforms, *3* – exact value of the Volterra kernel; *eps*=1%.

4. Identification of the Electric Motor

Offered methods of black-box diagnostics for nonlinear dynamic object are analyzed on example of the switched reluctance motor [8].

During long work the rotor of the electric drive has air friction and eventually an air backlash between a rotor and stator in electric drive increases. It is typical for high-speed electric drives. An air backlash increasing brings to power parameters decreasing and greater losses of energy. But direct measurements of air backlash are impossible. Therefore, engineering of diagnostic system of electric drive air backlash using indirect measurements is impotent today.

The electric drive is described by the system of nonlinear differential equations [8]:

$$U_\Phi = I_\Phi R_\Phi + \frac{d\Psi_\Phi}{dt} \tag{16}$$

$$\Psi_\Phi = f_1(I_\Phi, \Theta) \tag{17}$$

here $U_\Phi(t)$ – voltage (entrance variable); $I_\Phi(t)$ –current (measured response); R_Φ – resistance, Ψ_Φ – flux linkage; Θ–rotor angle. Function of flux linkage from a current is illustrated on Fig.7.

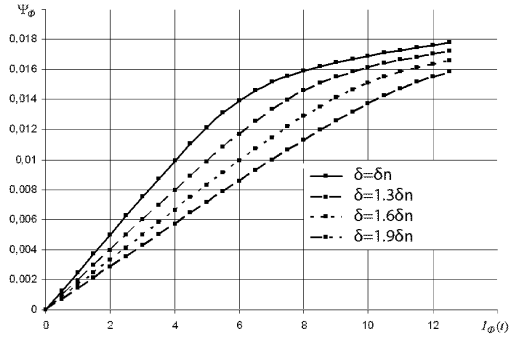

Figure 7: Function of flux linkage from a current for $\Theta = 30^0$ for a nominal value of air backlash $\delta=\delta_n$ and for a cases $\delta=1.3\delta_n$, $\delta=1.6\delta_n$, $\delta=1.9\delta_n$.

Using a nonparametric identification method for electric drive, the estimations of Volterra kernels of first order $w_1(t)$

and the main section of Volterra kernels of second order $w_2(t,t)$ for a cases $\delta=\delta_n$, $\delta=1.3\delta_n$, $\delta=1.6\delta_n$ and $\delta=1.9\delta_n$ are taken (Fig. 8, 9).

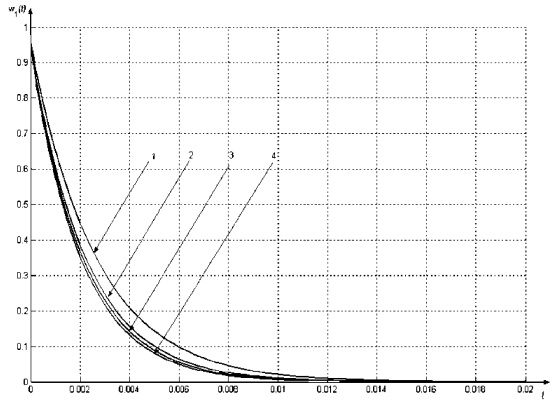

Figure 8: Volterra kernels of first order $w_1(t)$: 1 - for a nominal value of air backlash $\delta=\delta_n$; 2, 3, 3 - for a cases $\delta=1.3\delta_n$, $\delta=1.6\delta_n$, $\delta=1.9\delta_n$ accordingly.

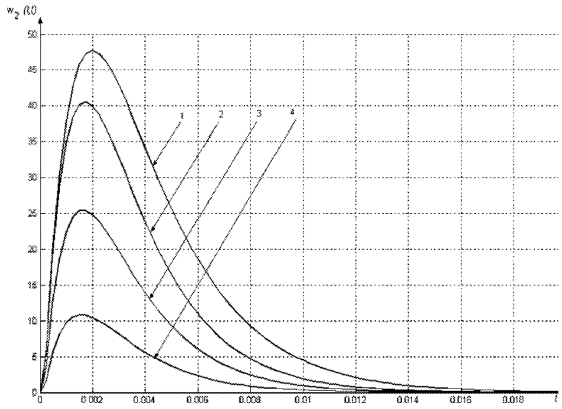

Figure 9: The main section of Volterra kernels of second order $w_2(t,t)$: 1 - for a nominal value of air backlash $\delta=\delta$; 2, 3, 3 - for a cases $\delta=1.3\delta_n$, $\delta=1.6\delta$, $\delta=1.9\delta_n$ accordingly.

For diagnostics of the electric drive conditions Volterra kernels of first order and the main section of Volterra kernels of second order are used.

5. Conclusion

The use of the mathematical models based on the Volterra integro-power series for identification of nonlinear dynamic systems is one of the long-standing problems of the control theory. When determining the multidimensional weight functions (Volterra kernels), however, the problems arise in separating the n-th order partial components from the measured system response to a given perturbation and then in determining the n-dimensional Volterra kernel. Solving these problems is computationally unstable, and this leads to significant identification errors even at small deviations (measurement noises) of initial input data.

We have investigated the errors of identification of a nonlinear system in the form of the Volterra series with the use of testing pulse signals, basing on the separation of the partial components by differentiation of the system response with respect to the parameter-amplitude. Computer experiments (within MATLAB) on the choice of the test signal amplitude are performed and the results of identification of the Volterra kernels of the 1st, 2nd and 3rd orders are presented.

Application of the noise suppression procedure based on the wavelet transformation to estimations of the Volterra kernels allows us to obtain smooth solutions and to lower the identification error 1.5÷3 times. The presented dependences of identification errors on the area of testing actions in determining the diagonal sections of the Volterra kernels allow us to specify the range of optimal amplitudes of pulse actions for different levels of response measurement errors which correspond to the minimal errors of identification of the Volterra kernels.

6. References

[1] Giannakis G.B. and Serpedin E.A., "Bibliography on Nonlinear System Identification and its Applications in Signal Processing, Communications and Biomedical Engineering", *Signal Processing EURASIP*, Vol.81, No.3, 2001, pp. 533-580.

[2] Schetzen M., *The Volterra and Wiener Theories of Nonlinear Systems.* Wiley, New York., 1980.

[3] Apartsyn A.S., Sidorov D.N. and Solodusha S.V., "To Identification of Integral Models of Nonlinear Dynamic Systems", *Proceedings of III International Conference "Identification of Dynamical systems and Inverse problems"*, Moscow-St.Petersburg, 1998, p.167-175.

[4] Pavlenko V.D. and Cherevatiy V.V., "Method of Identification of Nonlinear Continuous Dynamic Objects for the Decision of Problems of Diagnostic Check", *Proc. of the VII All–Ukrainian International Conference*, October 11-15, 2004, Kyjiv, Ukraine, pp. 277–280.

[5] Zinoviev A.A. and Pavlenko V.D., "Increase of Accuracy of Identification of Nonlinear Systems by the Way Integral-Power Series," *Proceedings of the III International Conference "System Identification and Control Problems"*, Institute of Control Sciences, Moscow, January 28-30, 2004, pp. 899-918, ISBN 5-201-14966-9, www.sicpro.org.

[6] Teolis A., *Computational Signal Processing with Wavelets*, Publishing Birkhauser, 1998.

[7] Pavlenko V.D., Cherevatiy V.V., "Identification on Nonlinear Systems as Volterra Kernels with the Help of Differentiation of Responses on Amplitude of Test Signals", *Proc. of the V International Conference "System Identification and Control Problems"*, Moscow, January 30 – February 2, 2006, V.A. Trapeznikov Institute of Control Sciences , pp.203–216,CD ISBN 5–201–14984–7, www.sicpro.org

[8] Miller T.J.E. *Switched Reluctance Motors and their Control,* Magna Physics Publishing and Clarendon Oxford Press, 1993.

Name: **PAVLENKO Vitaliy Danilovich**

Address: Ap. 47, 16, I. Rabina, Odessa 65076, Ukraine.
Tel.:+3(8-048)762-84-79;
+3(8-063)461-74-72. E-mail:pavlenko_vitalij@mail.ru

Present employer: Associated Professor at the Department of Computerized control systems Odessa National Polytechnic University

Duties or Job: Reading lecture on course "Modeling dynamic systems" and "Systems intellectual data processing" and "Software modern computer".

Highlights about your present work: Scientific studies and development in the field of Modeling and Simulation for Industrial Applications, Non-parametric Identification of Nonlinear Systems, Theory of the Volterra series, Statistic Classification, Neural nets for simulation, Diagnostic, Fault detection, Forecasting, Computers Information Technologies, High-performance computing, including parallel and distributed computing.

Past employment: Associate Professor from 1989. Published more 160 papers in Ukrainian, Russian and International Journals and Conference Proceedings.

Education: University of Polytechnical in Odessa, 1964-1970. Post graduate Student at the Computers Department of Odessa Polytechnical University, 1970-73. Studies: Certificate of the scientific degree Doctor of Philosophy - Computer Sciences and Certificate of the scientific rank Senior research associate - Computer Sciences at Highest Certificate Commission of USSR, Moscow, 1987, 1989.

Civic and professional activities, awards, etc.: Participant of the Fifth and Sixth All-Ukrainian International Conference "Signal/Image Processing and Pattern Recognition", UkrOBRAZ'2000/2002/2004/2006 (Nov 27-Dec 1, 2000; Oct 8-12, 2002; Oct 11-15, 2004; Aug 28–31,2006), Kyjiv, Ukraine; International Conference on Control AUTOMATICS-2000/2001/2002 (Sep 11-15, 2000, Lviv; Sep 11-15, 2001, Odessa; Sep 11-15, 2002, Donetck; Ukraine); Second International Conference on Control Problems, Moscow, Institute of Control Sciences, Russian Academy Sciences, Jun 17–19, 2003; III International Conference "System Identification and Control Problems" SICPRO'04, Institute of Control Sciences, Moscow, January 28 – 30, 2004; MESM'2004, September 14 -16, 2004, Philadelphia University, Amman, Jordan; V International Conference "System Identification and Control Problems" SICPRO'06, Institute of Control Sciences, Moscow, Jan 30 – Febr. 2, 2006; III International Conference "Parallel Computations and Control Problems" PACO'2006. Moscow, October 2 – 4, 2006. V.A. Trapeznikov Institute of Control Sciences, 2006; 6th International Conference ISTA'2007, May 23–25, 2007, Kharkiv, Ukraine; IEEE EAST–WEST DESIGN & TEST INTERNATIONAL SYMPOSIUM (EWDTS'07). Yerevan, Armenia on 7–10 September 2007.

Massri Muhannad born in Homs (Syria).
Education:
2003-2007 bachelor at the Department of Computer Control Systems of Odessa National Polytechnic University.
2007-2009 studant of master at the Department of Computer Control Systems of Odessa National Polytechnic University.
Languages: English good ,Russian perfect , and Arabic native.
Tel.:+3(8-093)750-12-00.
E-mail:mohannad_massri@hotmail.com .

AUTHOR LISTING

AUTHOR LISTING